Role of Tissue Plasminogen Activator in Central Nervous System Physiology and Pathology

by

Tamara Kato Stevenson

A dissertation submitted in partial fulfillment
of the requirement for the degree of
Doctor of Philosophy
(Molecular and Integrative Physiology)
in the University of Michigan
2018

Doctoral Committee:

Professor Daniel A. Lawrence, Chair
Professor David A. Antonetti
Professor Geoffrey G. Murphy
Associate Professor Jordan A. Shavit
Professor Edward L. Stuenkel

“Writing is like driving at night in the fog. You can only see as far as your headlights, but you can make the whole trip that way.”

- E.L. Doctorow

“I am fortunate because I have been able to spend my life in study of the world…I have never felt the need to invent a world beyond this world, for this world has always seemed large and beautiful enough for me. I have wondered why it is not large and beautiful enough for others – why they must dream up new and marvelous spheres, or long to live elsewhere, beyond this dominion… All I ever wanted was to know this world. I can say now, as I reach my end, that I know quite a bit more of it than I knew when I arrived. Moreover, my little bit of knowledge has been added to all the other accumulated knowledge of history – added to the great library, as it were…Anyone who can say such a thing has lived a fortunate life.”

- Elizabeth Gilbert, *The Signature of All Things*

Tamara Kato Stevenson

tamaraks@umich.edu

ORCID: 0000-0003-4306-1164

DEDICATION

To Mitch and Edie who have been with me from the start, and to Emi and Luna who have joined me at the finish.

ACKNOWLEDGEMENTS

"There are always a few people in this life who think that you can do more than you think you can do" – Mr. Rogers

It seems obligatory to acknowledge one's thesis advisor; this implicit requirement, however, does not detract from the sentiments behind the obligation. Dan has been a constant and continual source of support throughout my graduate studies. He has trained me to be a better scientist and he has advocated for me in all things related to my career development. Throughout my time in the lab Dan has given me the freedom in my project to follow the data, but also to make mistakes. Importantly, he has been there to provide intellectual guidance and troubleshoot, and to offer encouragement when mistakes or experimental hurdles seemed insurmountable. At the beginning of my graduate studies I probably thought that the trials of research and graduate school would in-and-of-itself foster expertise and confidence, however, I now recognize and appreciate that those qualities are strongly influenced and nurtured by the guidance provided by one's mentor.

I also need to acknowledge the support that I have received from Dan outside the lab. Graduate school is long. And the years that encompass graduate school in one's life coincide with significant life events. While in Dan's lab I have gotten married, moved to Japan for fourteen months, and I have both lost and had a baby. Dan has allowed me the time to enjoy the good, but also grieve the bad, and for that, I am so very grateful.

A special acknowledgment also needs to be extended to Dr. Geoffrey Murphy. When Dan went on sabbatical my second year of graduate school, Geoff gave me a home in his lab and was instrumental in fostering my budding interest in neuroscience. Geoff supported me through a critical period in my graduate career and being in his lab was a really transformative time intellectually. Geoff is also one of the few professors I know that still work in the lab. While you wouldn't trust other professors to even pipette, Geoff is the one you call when instrumentation or experiments aren't working….or if you need to put an e-phys rig together. When I first started working in Geoff's lab I didn't envision my thesis project being "neuro-centric" nor did I think of myself as a neuroscientist, but Geoff made neuroscience fun and exciting, and I think I've been trying to make my way back to his lab ever since, which is why I am thrilled to officially join his lab for my post-doctoral studies.

In addition to Dan and Geoff, I would like to thank the other members of my thesis committee: Dr. David Antonetti, Dr. Jordan Shavit, and Dr. Edward Stuenkel. I was apprehensive before every committee meeting, but I always came away feeling encouraged and more motivated with their helpful suggestions about experiments to perform or how to focus my project.

I would also like to acknowledge the following current and former Lawrence Lab members that have been instrumental to this dissertation: Cody Barlow, David Bushart, Kris Mann, Dr. Ashley Reinke, Dr. Gerald Shielke, Dr. Enming Su, Daniel Torrente, and Mark Warnock. Each of my fellow Lawrence Lab mates has been incredibly helpful; from taking care of my transgenic mouse colonies and helping with experiments to

intellectual discussions and critical feedback, the research in my dissertation would not have been possible without their support.

It is also imperative that I acknowledge the following current and former Murphy Lab members that have been critical to the completion of my dissertation: Dr. Ali Althaus, Dr. Victor Cazares, Grace Fisher, Dr. Kasia Glanowska, Dr. Shannon Moore, Rachel Parent, Dr. Stephanie Temme, and Dr. Aislin Williams. These women (and Victor) have been fundamental in my development as a neuroscientist. They are inspiring for their work ethic, their intellect, and their collaborative spirit. Their camaraderie has helped to cultivate a working environment that is both intellectually stimulating, but also enjoyable.

A special thanks needs to go to Shannon. Without hyperbole, I can say that any success I've had as a graduate student is partly due to Shannon's guidance. She is not only fiercely bright, but she is a patient teacher; whether it be related to troubleshooting a noise problem on an e-phys rig, formatting graphs in Prism, or discussing the neurophysiology of synaptic transmission, Shannon avails herself to help. I feel extremely fortunate to not only call Shannon my mentor, but my friend.

To all the other women who have believed in me: Dr. Sharlene Day – thank you. Thank you for hiring me when I was an undergrad even though I had absolutely no lab experience and didn't even know what a protein was. Dr. Jennifer Davis – thank you for cultivating my independence by giving me my first project in the Metzger Lab. Dr. Margaret Westfall – thank you for encouraging me to go to graduate school. Clearly, you saw something in me before I did. Dr. Elizabeth Rust – thank you for being such an amazing teacher and helping me to become a better teacher as well.

I would also like to acknowledge Dr. Junichi Nabekura and members of the Nabekura Lab at the National Institute for Physiological Sciences (NIPS) in Okazaki, Japan, including Dr. Tatsuya Ishikawa; Dr. Kei Eto; Dr. Hiroaki Wake, Dr. Hiroyuki Inada, Dr. Ryohei Akiyoshi, Dr. Akiko Miyamoto Dr. Yasuyo Tanaka, and Dr. Kayo Nakamura. I was so very fortunate to be able to join the Nabekura Lab while my husband was working on an assignment in Japan. Everybody was so welcoming and I learned so much from them culturally as well as scientifically. My time at NIPS was integral to my research and to the completion of this dissertation, as much of what I learned about microscopy and image processing was from my training in the Nabekura Lab.

It's also important to acknowledge the support that I have received from the Department of Molecular and Integrative Physiology. In particular, Michele Boggs, the graduate student coordinator, has been indispensable. From helping navigate the University bureaucracy to planning events/meetings, Michele is an inexhaustible source of institutional knowledge. A special thanks to the former department chair, Dr. Bishr Omary. Even though Bishr was/is always incredibly busy, he would take the time to talk about basically anything. He would ask about my research, he would help me raise money for the Graduate Education Fund, he would help me plan for post-graduate opportunities, and he would inquire about my life outside the lab. He made you feel important. And, it's also imperative that I thank all my former Graduate Student advisors: Dr. Ormand MacDougald, Dr. Scott Pletcher, Dr. Suzanne Moentor, and Dr. Daniel Michele. All have been incredibly supportive and their academic and career advice has always been steadying during the rough times that inevitably arise during graduate school.

I must also acknowledge the University of Michigan Transgenic Animal Model Core and the Microscopy and Imaging Analysis (MIL) Core. In particular, Dr. Thom Saunders and Michael Zeidler from the Transgenic Animal Model Core were critical in helping design the genetic strategy for my Bacterial Artificial Chromosome (BAC) transgenic mice, and in answering any subsequent questions I had regarding those mice. Sasha Meshinchi from the MIL trained me on the Leica SP5X confocal/two-photon microscope and was always helpful in answering my imaging questions.

To my graduate school friends, Joanne Garbincius, Francisco Alvarado, Surojit Sural, Keita Uchida, Kristoffer Sugg, Johhny Saldate, and Sam Slocum. Sometimes, I wish I didn't get pregnant so that we could have enjoyed a few more beers together.

I need to thank my family. I feel fortunate to have parents whom I get to thank not only for their parental duties, but for their help in my research. My mother, Junko Stevenson, helped me when I was first starting to learn how to code in Matlab and while I was taking my first computer programming class during graduate school. My mother has also been extremely helpful in her role as an おばあちゃん(grandmother) for my daughter, Emmeline (Emi). From 6-weeks post-partum, my mother has helped care for Emi part-time. Her support has not only helped me to finish my dissertation, but it has given me the space/time to enjoy in life-things extraneous to work and home. It's also important for me to thank my father, Dr. Randy Stevenson, was hired on as an applied physicist to model blood flow and I've been fortunate to work with him on a project that is partly written-into the fourth chapter of my dissertation. My father has truly done some novel work and I am in awe of his brilliance. And, of course, a special thanks goes to my

sister, Dr. Michelle Medley, my best friend who is infinitely a wiser and better person than me.

Lastly, I need to acknowledge my husband, Mitch Gerczak. What else is there to say other than, you da best!

TABLE OF CONTENTS

LIST OF FIGURES

CHAPTER 1

CHAPTER 2

CHAPTER 3

LIST OF TABLES

CHAPTER 1

CHAPTER 2

CHAPTER 4

ABSTRACT

Tissue plasminogen activator (tPA) is a serine protease classically known for its endogenous activity promoting fibrinolysis and for its clinical role as a thrombolytic agent for treating ischemic stroke. This singular function for tPA in the vasculature contrasts with the numerous reported actions of tPA in the central nervous system (CNS); including, synaptic plasticity, neurodegeneration, and blood-brain barrier (BBB) permeability. Within each of these processes a variety of substrates and receptors have been implicated in mediating tPA's effects, suggesting that tPA is a pleiotropic mediator whose actions are restricted in space and time. The specific localization of tPA, therefore, can provide useful information about its function.

Accordingly, we utilized two new transgenic reporter mice – PlatBetaGAL and tPA^{BAC}-Cer – to provide a detailed characterization of tPA expression in the adult murine brain. The PlatBetaGAL reporter mouse houses the beta-galactosidase gene in the tPA locus and the tPA^{BAC}-Cer mouse has a cerulean-fluorescent protein fused in-frame to the tPA C-terminus. A comparison of these reporter mice demonstrates that neuronal tPA is primarily trafficked away from its somatic site of synthesis to nerve fibers in limbic brain structures, such as the hippocampus, amygdala, and basal ganglia. This differential expression pattern is most apparent in the hippocampus where tPA-

BetaGAL expression is present in the dentate gyrus, while tPA-Cer is localized to giant mossy fiber boutons (MFBs) in the mossy fiber pathway.

To understand the functional implications of tPA in the MFBs we assessed synchronous activity in the CA3 hippocampal subfield using a “no magnesium/high potassium” model of “seizure-like” activity. As previous work from our lab implicated tPA in mediating seizure progression *in vivo* via its role regulating BBB permeability, we dissected the BBB component to seizure progression and specifically tested tPA’s effect on neuronal communication. We found brain slices from tPA deficient mice to have an enhanced synchronous activity onset time, suggesting that the “seizure-resistance” observed in tPA deficient mice *in vivo* is likely a result of improved barrier function, not tPA’s role in modulating synaptic transmission.

Lastly, in this dissertation, using sophisticated imaging and analytical tools we provide a rigorous assessment of vascular morphometry in wild-type mice, the original Carmeliet-tPA null mice, and in newly-generated tPA deficient mice on a pure C57BL/6J background (Szabo-tPA null mice). Through this examination we report that the lognormal distribution is a good model for cerebral vessel diameter and length and that there is a weak negative correlation between vessel diameter and length. We also find that the increased vascular density in Carmeliet-tPA null mice is possibly a compound result of constitutive loss of tPA and/or some strain-dependent modifier genes.

Cumulatively, our data supports a model whereby tPA acts a pleiotropic mediator in the CNS whose actions are highly spatially and temporally compartmentalized. This compartmentalized localization is appreciable in the differential expression pattern seen for tPA between the PlatBetaGAL and tPA^{BAC}-Cer transgenic mice; and functionally, we

show that in *ex vivo* hippocampal slices tPA modulates synchronous activity, but in an *in vivo* model of seizure, the dominant effect of tPA is on regulating BBB permeability. Our vascular morphometry data also suggests a possible developmental effect of tPA on cerebrovascular patterning. Future work using the models developed here should help to clarify the relative contribution of the various substrates and pathways associated with tPA in CNS physiology and pathology.

CHAPTER 1

Introduction

1.1 Abstract

Tissue plasminogen activator's (tPA) fibrinolytic function in the vasculature is well-established. This specific role for tPA in the vasculature, however, contrasts with its pleiotropic activities in the nervous system. Numerous physiological and pathological functions have been attributed to tPA in the central and peripheral nervous system: including, neurite outgrowth and regeneration; synaptic and spine plasticity; neurovascular coupling; and neurodegeneration, microglial activation, and blood-brain barrier permeability. A variety of substrates, plasminogen-dependent and plasminogen-independent, and receptors have been reported to mediate tPA's actions in these processes, including pro-hepatocyte growth factor (pro-HGF), N-methyl-D-aspartate receptor (NMDAR), platelet-derived growth factor-CC (PDGF-CC), low-density lipoprotein (LDL) receptor-related protein (LRP1), pro-brain derived neurotrophic factor (pro-BDNF).

Given the varied reports on tPA roles in the central and peripheral nervous system and the different substrates implicated in effectuating tPA's actions, it's likely that tPA's functions are spatially and temporally restricted. This review of the literature aims to dissect these different roles and the different molecular mechanisms attributed

to tPA. In addition, it aims to contextualize some of the original research on tPA with what is currently known about tPA's function and localization in the nervous system.

1.2 Introduction

Tissue plasminogen activator (tPA) is a serine protease with a well-established role in fibrinolysis. It is released from endothelial cells and mediates clot resolution by specifically catalyzing the conversion of the zymogen plasminogen into the active enzyme plasmin. Plasmin, in turn, proteolyzes the fibrin network of a blood clot. Mechanistic understanding of tPA's endogenous fibrinolytic function led to the development of recombinant tPA (rtPA) as a thrombolytic agent for the treatment of ischemic stroke. However, tPA's usage is limited, especially if given outside its prescribed time window (< 3 – 4.5 hrs), due to reduced efficacy and an increased risk of hemorrhagic conversion (Ahmed et al., 2010; group et al., 2012; Prabhakaran et al., 2015). Efforts to understand the molecular mechanism for this phenomenon have shown that the increased risk for hemorrhage are due, in part, from exogenously administered rtPA crossing the ischemic blood-brain barrier (BBB) and acting through endogenous tPA-mediated signaling pathways on the abluminal side of the vasculature to induce further opening of the barrier (Su et al., 2008). Indeed, in addition to its role in regulating BBB permeability, tPA has been shown to be involved in multiple processes in the central and peripheral nervous system (CNS and PNS), including, neurite outgrowth and regeneration; synaptic and spine plasticity; neurovascular coupling; and neurodegeneration and microglial activation. In addition, numerous molecular mechanisms implicating a variety of substrates, both plasminogen-dependent and -

independent, have been proposed to be responsible for tPA's action in the CNS. This review summarize the foundational studies on tPA function and how those studies have led to and informed more recent work on tPA in the CNS and PNS.

1.3 Role of tPA in CNS development and nerve regeneration

1.3.1 Neuritogenesis and neurite outgrowth

Neuritogenesis and neurite outgrowth during development and regeneration (Table 1.1) involves the complex interplay between the actin-cytoskeletal network of the growing neurite and its surrounding extracellular environment (da Silva and Dotti, 2002; Kiryushko et al., 2004). Proteases and their cognate inhibitors have long been implicated in regulating neurite outgrowth via remodeling of the extracellular matrix (ECM) (Monard, 1988; Pittman et al., 1989; Pittman and Williams, 1989). Krystosek and Seeds were the first to demonstrate a possible role for the plasminogen activation (PA) system (tissue plasminogen activator, tPA; and urokinase plasminogen activator, uPA) in neurite outgrowth (Krystosek and Seeds, 1981a). PAs were shown to be released from the growth cones of cerebellar granule neurons (Krystosek and Seeds, 1981b; Verrall and Seeds, 1988), peripheral neurons and Schwann cells (Krystosek and Seeds, 1984), and neuroblastoma cells (Krystosek and Seeds, 1981a). Specifically, tPA's release was found to strongly correlate with ECM degradation in migration and regeneration assays (Pittman and DiBenedetto, 1995), supporting a functional role for tPA in structurally modifying the cell-matrix interactions of migrating neurons.

Mechanistic studies examining PA-mediated neuritogenesis suggested a role for the membrane-associated protein annexin II (Jacovina et al., 2001). Similar to its role in

the vasculature promoting fibrinolysis by acting as a scaffolding cofactor for plasminogen and tPA, annexin II facilitates plasmin generation in pheochromocytoma PC-12 cels and, in turn, supports nerve growth factor (NGF) - induced neurite outgrowth (Figure 1.1 A). The PA system and annexin II were specifically implicated since treatment of PC-12 cells with neutralizing antibodies against uPA, tPA, plasmin, and annexin II blocked neurite outgrowth.

Yet. other studies have demonstrated tPA-mediated neurite outgrowth independent of plasminogen activation (Shi et al., 2009; Lee et al., 2014). Using a proteolytically inactive mutant of tPA, Shi et al. (2009) showed that mutant tPA was able to transactivate Trk-receptors via the endocytic and signaling receptor low-density lipoprotein (LDL) receptor-related protein (LRP1) in PC-12 cells and granule cell neurons (Figure 1.1 B). Subsequent activation of Akt and ERK1/2 signaling pathways downstream of Trk was shown to promote neurite outgrowth, which could be blocked by pharmacological inhibitors of LRP1 or Trk.

In addition to LRP1, another member of the LDL receptor-related family of proteins, LRP5/6, was implicated in tPA-mediated signaling and neurite outgrowth (Lee et al., 2014). Though plasminogen-dependence wasn't tested *per se*, activation of the Wnt-LRP5/6-GSK3β-β-catenin canonical signaling pathway, which is known to induce transcription of genes involved in neuritogenesis (Endo and Rubin, 2007), was shown to be upregulated by tPA treatment in primary neural progenitor cell (NPC) cultures (Figure 1.1 C). Increased neurite outgrowth was also measured upon application of tPA to primary neuronal cultures, which could be inhibited by siRNAs individually knocking-down expression of LRP5/6, GSK3β, and β-catenin. Two possible mechanisms for tPA-

induced activation of β-catenin signaling were demonstrated: 1) tPA increased release of Wnt7a from the ECM of cultured NPCs and 2) direct tPA binding to LRP5/6. The Wnt-LRP5/6-GSK3β-β-catenin signaling pathway is also critical for vasculogenesis and BBB differentiation in the CNS (Quaegebeur et al., 2011). Interestingly, $tPA^{-/-}$ mice were recently reported to have an altered cerebrovascular architecture, including an increase in the capillary bed density, and an increase in endothelial cell and tight-junction (ZO-1) content (Stefanitsch et al., 2015) (*See also Chapter 4*). A direct connection between tPA and Wnt signaling and vasculogenesis, however, has yet to be investigated.

1.3.2 Neuronal migration

With the generation of mice deficient in the tPA gene (Carmeliet et al., 1994), it became possible to directly assess tPA's functional role in regulating neuritogenesis *in vivo*. As cultured cerebellar granule neurons were previously shown to store and release tPA (Krystosek and Seeds, 1981b; Verrall and Seeds, 1988) cerebellar granule neuron migration was examined in developing brains of $tPA^{-/-}$ mice (Seeds et al., 1999). Granule cells were found to migrate from their germination zone in the external granule cell layer through the molecular layer and in to the internal granule cell layer at a slower rate in $tPA^{-/-}$ mice, compared to wild-type controls. Despite the slower migration rate, however, at the end of the granule cell migratory phase, there was no detectable difference in granule cell layer number or thickness.

tPA has also been implicated in mediating neuronal migration through its activation of hepatocyte growth factor (HGF). tPA was shown to cleave single-chain HGF, a potent mitogen that shares high homology with plasminogen (though HGF

doesn't have proteolytic activity), into its mitogenic active two-chain form (Mars et al., 1993). HGF is highly expressed in the brain (Jung et al., 1994) and acts as a pleiotropic mediator of cell proliferation and differentiation, neuronal outgrowth and chemoattraction, and survival (Maina and Klein, 1999). Moreover, the expression pattern of HGF and its receptor c-met is coincident with tPA expression in the rostral migratory stream (RMS), a well-established route that neuroblasts from the striatal subventricular zone (SVZ) of the lateral ventricles traverse on their way to the olfactory bulb (Thewke and Seeds, 1996). As deficiency in HGF or c-met cause embryonic lethality, $tPA^{-/-}$ mice were used as a model of partial HGF deficiency to assess tPA/HGF's role in proliferation, migration, and differentiation (Wang et al., 2011).

Indeed, in the postnatal mouse brain (P2 to P14) $tPA^{-/-}$ mice were found to have decreased expression of HGF in the RMS (Wang et al., 2011). In addition, neuroblasts from the SVZ of $tPA^{-/-}$ mice were shown to have an accelerated, but dispersed and ectopic, migratory path; and immunostaining for Ki67+ and doublecortin demonstrated $tPA^{-/-}$ mice to have diminished cell proliferation and neurogenesis, respectively, in the SVZ (Figure 1.2). These data are in keeping with previously reported roles for HGF in cell proliferation, neurogenesis, and chemoattraction (Maina and Klein, 1999). Since gross aberrant neuronal patterning in adult $tPA^{-/-}$ mice has not been observed (Carmeliet et al., 1994; Frey et al., 1996; Huang et al., 1996), these *in vivo* results suggest that tPA may be playing a more supportive, but not an essential, role in neuritogenesis and neuronal migration during development in the cerebellum, forebrain, and olfactory bulb.

Differences in cerebroventricular morphology and ependymal lining molecular composition, however, have been reported in adult tPA$^{-/-}$ mice, when compared to their wild-type littermate controls. Two groups have independently observed mice deficient in tPA to have enlarged ventricles (Wang et al., 2011; Stefanitsch et al., 2015) and an ependymal lining that has enhanced GLUT-1 and ZO-1 expression (Stefanitsch et al., 2015). It is unclear if the developmental consequence of enlarged ventricles in tPA$^{-/-}$ mice is biologically significant and how such morphological and molecular differences in the ventricles might influence the functions attributed to tPA in the adult murine brain.

1.3.3 Nerve Regeneration

While tPA may have a more subtle role in neuritogenesis during development, it has been shown to be a critical player in models of nerve regeneration in the adult mouse PNS (Akassoglou et al., 2000; Siconolfi and Seeds, 2001a, b; Zou et al., 2006). Following sciatic nerve crush, Wallerian degeneration occurs (Waxman, 2005) whereby the axon disintegrates along with the myelin sheath. In addition, Wallerian degeneration is accompanied by infiltrating macrophages and proliferating Schwann cells and by regenerating peripheral neurons that migrate through the lesion to reinnervate their synaptic targets (Figure 1.3 A). The *in vitro* observation that peripheral neurons and Schwann cells release tPA was supported by spatial correlational evidence demonstrating upregulation of the serine protease *in vivo* around the sciatic nerve following injury (Akassoglou et al., 2000). This increase in plasminogen-dependent proteolytic activity after nerve injury appeared to be primarily driven by tPA, not uPA, as *in situ* zymography of the sciatic nerve after injury from uPA$^{-/-}$ mice and wild-type mice

treated with the uPA inhibitor, amiloride, still showed increased proteolysis. SDS-PAGE gel zymography of sciatic nerve homogenates, however, showed increases in both tPA and uPA proteolytic activity following sciatic nerve injury (Siconolfi and Seeds, 2001a).

Overall, though, tPA was found to have a protective effect in sciatic nerve injury, as axonal degeneration and demyelination and functional recovery were deleteriously exacerbated in $tPA^{-/-}$ mice (Akassoglou et al., 2000; Ling et al., 2006) (Figure 1.3 B and C). Given the *in vitro* data suggesting a role for tPA in neurite outgrowth, it was hypothesized that tPA is acting to promote axonal regrowth. However, while axonal regeneration was assessed using GAP-43, a marker of regeneration, in injured versus sham-treated sciatic nerves, axonal regeneration was never reported in $tPA^{-/-}$ or $uPA^{-/-}$ mice (Siconolfi and Seeds, 2001a). To more directly test the effect of loss of tPA on axonal regrowth, therefore, these studies should be repeated in $tPA^{-/-}$ mice.

It's also possible that tPA-mediated fibrinolysis is responsible, as fibrin(ogen) deposition correlated with axonal degeneration and demyelination and as pharmacological depletion of fibrinogen reduced axonal damage and muscle atrophy in $tPA^{-/-}$ mice (Akassoglou et al., 2000). Reduced macrophage migration has also been implicated (Ling et al., 2006). After sciatic nerve injury, $tPA^{-/-}$ mice were found to have significantly fewer infiltrating macrophages compared to wild-type controls (Figure 1.3 B and C), and it was suggested that this was due to decreased macrophage expression of the ECM degradation enzyme MMP9. Other studies, however, have shown that tPA can directly promote macrophage migration through its interaction with the integrin MAC-1 (Cao et al., 2006). These reported beneficial effects of tPA appear to be PNS specific, supporting a tPA-mediated role involving infiltrating macrophages and Schwann cells,

which are unique to PNS regeneration, as overexpression of tPA appears to have no effect in CNS models of axonal degeneration (Moon et al., 2006).

1.4 Role of tPA in synaptic transmission and synaptic plasticity

1.4.1 Upregulation of tPA following activity-dependent events

Contemporaneous to the early studies investigating tPA's involvement in neurite outgrowth was a report demonstrating that tPA is an immediate-early gene that is induced by neuronal activity (Qian et al., 1993). In this study tPA was identified in a differential screen of 30,000 clones from a cDNA library; using three activity-dependent paradigms - seizure, long-term potentiation (LTP), and kindling - tPA gene expression was found to be upregulated *in vivo* by 1 hr in the granule and pyramidal cell layers of the hippocampus in the adult rat brain (Figure 1.4 A). tPA's upregulation following increased neuronal activity suggested a novel role for tPA in synaptic plasticity. Consistent with these data, tPA was found to be induced in the cerebellum of rats after learning a complex motor task (Seeds et al., 1995). Using a pegged runway of regular and irregular patterning to test cerebellar-dependent motor learning, Seeds et al. (1995) found tPA mRNA expression upregulated in Purkinje cells during the most active phase of learning (Figure 1.4 B). This spatial and temporal evidence demonstrating upregulation of tPA expression in both hippocampal and cerebellar learning paradigms suggested that tPA may have a role in regulating neuronal plasticity.

1.4.2 Modulation of basal synaptic transmission by tPA

Further studies deconstructing tPA's role in hippocampal plasticity *ex vivo*, however, have yielded somewhat varied results (Table 1.2). While some groups have observed defects in basal synaptic transmission (Frey et al., 1996) and the early (Calabresi et al., 2000) and late phase of LTP (L-LTP) in the hippocampal CA1 region of $tPA^{-/-}$ mice, others have not (Huang et al., 1996; Zhuo et al., 2000) (Figure 1.5 A). Frey and colleagues were the first to report deficits in synaptic efficacy at the Schaffer collateral-to-CA1 synapse in $tPA^{-/-}$ mice under basal conditions (Frey et al., 1996). In $tPA^{-/-}$ mice, a larger stimulus was needed to evoke a pop-spike of similar amplitude to that seen in wild-type mice, and when measuring paired-pulse behavior of the pop-spike, $tPA^{-/-}$ mice displayed significant reductions in paired-pulse facilitation (Figure 1.5 B and C). These results suggest that $tPA^{-/-}$ mice are under enhanced GABAergic inhibition, especially since increased facilitation was observed when slices were treated with the $GABA_A$ receptor competitive antagonist bicuculline. Consistent with the hypothesis that $tPA^{-/-}$ mice have altered GABAergic transmission, Frey et al. (1996) found no differences in L-LTP between $tPA^{-/-}$ mice and wild-type mice, but significant differences when GABAergic transmission was blocked with the noncompetitive $GABA_A$ channel blocker picrotoxin (Figure 1.5 D).

Alternatively, Wu and colleagues proposed that tPA modulates synaptic transmission through its effects on synaptic vesicle cycling (Wu et al., 2015). From immunoblots of cortical neuron membrane extracts and isolated synaptic fractions from synaptoneurosomes, tPA was found to recruit βII-spectrin, a cytoskeletal protein implicated in synaptic vesicle release, to the active zone and induce the binding of

synaptic vesicles to βII-spectrin. tPA also induced phosphorylation of synapsin I, a synaptic vesicle membrane protein, presumably via tPA-mediated increases in voltage-gated calcium channels expression. In keeping with these expression and localization studies indicating that tPA facilitates synaptic vesicle release, tPA treatment was shown to increase miniature excitatory post-synaptic currents (mEPSCs) in CA1 pyramidal neurons from rat brain slices. Further mechanistic studies investigating whether tPA increases the release probability of individual synaptic vesicle or increases the number of synaptic vesicles released were not performed. Moreover, it is unclear if this increase in mEPSCs is due to tPA-mediated increases in the expression/recruitment of synaptic vesicle cycling proteins to the active zone. Further studies, therefore, need to be done to determine if these reported effects of tPA are linked and if they are responsible for the defects in basal synaptic transmission first reported by Frey et al. (1996).

1.4.3 Effects of tPA on long-term potentiation

Still others, however, have reported no differences in basal synaptic transmission in the CA1 hippocampal region of $tPA^{-/-}$ mice, but significant defects in L-LTP, with or without blocking GABAergic transmission (Huang et al., 1996; Calabresi et al., 2000; Zhuo et al., 2000) (Figure 1.6 A). It has also been shown that L-LTP can be blocked at the Schaffer collateral-to-CA1 synapse with application of the protease inhibitor tPA-Stop (Baranes et al., 1998), while potentiation can be enhanced when tentanization is coupled with either pharmacologic or genetic increases in tPA (Baranes et al., 1998; Madani et al., 1999; Zhuo et al., 2000). It was further demonstrated that this potentiation in CA1 is due to activation of a cAMP/PKA- mediated pathway (Huang et al., 1996;

Baranes et al., 1998), as analogs to cAMP and activators of cAMP/PKA-dependent signaling cascades (Sp-cAMPS and 6-Br-APB) can induce L-LTP in wild-type, but not tPA$^{-/-}$ mice (Figure 1.6 B). Consistent with this, the tPA gene, *Plat*, has previously been shown to house a functional cAMP responsive element (CRE) in its promoter (Medcalf et al., 1990).

It is still unclear if the differences in hippocampal plasticity between wild-type and tPA$^{-/-}$ mice are biologically related to tPA or the result of variations in experimental technique, or to differences in genetic background. The background strain of the tPA$^{-/-}$ mice used in the initial LTP experiments (Frey et al., 1996; Huang et al., 1996) was not reported; and, while Zhuo et al. used tPA$^{-/-}$ mice on a pure C57BL/6J background, L-LTP experiments comparing wild-type and tPA$^{-/-}$ mice were not performed (Zhuo et al., 2000). Rescue experiments - where tPA protein is infused over hippocampal slices from tPA$^{-/-}$ mice - were done, though, and showed potentiation from tPA treatment. Given that we now understand the importance of controlling for genetic background it would useful to repeat these experiments in the recently described tPA$^{-/-}$ mouse that was generated directly in the C57BL/6J background using zinc-finger nuclease genome editing technology. These mice are not on a mixed background and unlike the original tPA$^{-/-}$ mice they do not harbor any remnant DNA from the 129/Sv embryonic stem (ES) cells flanking the tPA allele (Szabo et al., 2016).

There is also conflicting evidence on whether or not tPA directly or indirectly, through plasmin generation, mediates the induction and maintenance of L-LTP. Several lines of evidence suggest that tPA's role in L-LTP is independent of plasminogen. 1) Mice deficient in uPA (uPA$^{-/-}$) show no defect in L-LTP (Huang et al., 1996)*;* 2) Mice

that overexpress uPA display impaired learning (Meiri et al., 1994); and 3) Deficits in step-down avoidance learning in $tPA^{-/-}$ mice are not rescued by hippocampal infusions of uPA (Pawlak et al., 2002). As uPA is also a specific activator of plasminogen, these data implicate tPA, and not plasmin, as being directly responsible for the observed L-LTP phenotype. Moreover, Zhuo et al. demonstrated that tPA could be acting directly through LRP1 (Zhuo et al., 2000), an endocytic receptor for tPA in neurons (Bu et al., 1994), to induce L-LTP. Blocking LRP with an inhibitor, receptor-associated protein (RAP), caused deficits in L-LTP that were similar to what was reported previously for $tPA^{-/-}$ mice (Figure 1.6 C). And RAP blocked Schaffer collateral-to-CA1 synaptic potentiation in $tPA^{-/-}$ hippocampal slices that had been treated with tPA. PKA, a kinase known to play a key role in the induction and maintenance of L-LTP (Abel et al., 1997), was also shown to be activated upon tPA binding to LRP. Together, these data support a plasminogen-independent mechanism of action for tPA in L-LTP (Figure 1.6 D). In addition, they suggest that tPA's protease activity is not necessary for the full expression of L-LTP, as proteolytically active tPA is not required to interact with and signal through LRP (Hu et al., 2006).

While LRP's involvement in tPA-mediated L-LTP implicates tPA as having a plasminogen-independent mechanism of action, tPA/plasmin-induced cleavage of BDNF has also been demonstrated to be essential for long-term hippocampal plasticity (Pang et al., 2004). Previously, genetic or pharmacologic ablation of BDNF or its receptor TrkB was shown to inhibit L-LTP (Korte et al., 1995; Korte et al., 1998; Xu et al., 2000; Minichiello et al., 2002). It was also previously demonstrated that secreted proBDNF can be cleaved extracellularly by plasmin (Lee et al., 2001). It was not known,

however, if the tPA/plasmin/mBDNF pathway formed a common pathway important for hippocampal L-LTP.

Through a series of L-LTP experiments using $tPA^{-/-}$ mice, plasminogen deficient ($Plg^{-/-}$) mice, and mice heterozygous for BDNF ($BDNF^{+/-}$), Pang and colleagues (2004) demonstrated that tPA/plasmin-mediated cleavage of proBDNF is critical for the full expression of L-LTP in the CA1 region of the mouse hippocampus (Figure 1.7). Subcellular localization studies support these functional findings. In cultured hippocampal neurons transfected with BDNF-mCherry and tPA-EYFP vectors, BDNF and tPA were shown to be co-packaged in presynaptic dense core vesicles (Scalettar et al., 2012), suggesting that tPA and BDNF are proximally localized and likely concomitantly released to act through a common pathway.

Interestingly, while these experiments were looking at long-term plasticity in the CA1 region, both BDNF and tPA have been shown to be most highly expressed in giant mossy fiber boutons (MFB) in the mossy fiber pathway of the hippocampus (Figure 1.8) (Stevenson and Lawrence, 2018; Conner et al., 1997; Yan et al., 1997; Danzer and McNamara, 2004). Giant MFBs are one of three - in addition to *en passant* terminals and filipodial extensions - identified presynaptic specializations that emanate from the mossy fiber axons of dentate granule neurons (Acsady et al., 1998; Rollenhagen and Lubke, 2010). The subcellular localization of both BDNF and tPA to giant MFBs, therefore, not only indicates that these two proteins are proximally localized to act in concert, but that their role in synaptic plasticity is highly compartmentalized and possibly unique to mossy fiber-to-CA3 synaptic plasticity. However, while deficits in L-LTP have been reported in $tPA^{-/-}$ mice at the mossy fiber-to-CA3 cell synapse (Huang et al., 1996;

Baranes et al., 1998), functional consequences of tPA/plasmin-mediated mBDNF generation have not been tested in the CA3 region specifically. Therefore, it remains to be seen if this protease-induced neurotrophin cascade is involved in regulating plasticity at the mossy fiber-to-CA3 synapse.

High-resolution, confocal microscopy of plasminogen in adult murine brain, however, has yet to be done. Though widefield microscopy has shown plasminogen immunoreactivity in the hippocampus, plasminogen was not expressed in the mossy fiber pathway (Tsirka et al., 1997; Taniguchi et al., 2011). Rather, plasminogen appeared to be localized to scattered cell bodies in the pyramidal cell layers of CA1 - CA3, the hilus, and the stratum oriens and stratum radiatum lamina. tPA-expressing inhibitory interneurons have also been reported to have a scattered localization in stratum oriens (Stevenson and Lawrence, 2018). It has not been investigated if this population of neurons co-expresses plasminogen and tPA.

In addition to tPA being highly expressed in the hippocampus, tPA protein is also present in other subcortical regions of the adult murine brain (Figure 1.9). In a transgenic fusion reporter mouse that has a cerulean fluorescent protein tagged to the C-terminus of tPA, it was shown that tPA-protein is primarily expressed in blood vessels throughout the murine brain and in nerve fibers emanating or innervating brain regions associated with the limbic system (Stevenson and Lawrence, 2018). When compared with the gene expression pattern of tPA, an uncoupling between tPA's sites of synthesis and its trafficked localization becomes apparent (Sappino et al., 1993; Yu et al., 2001; Salles and Strickland, 2002; Louessard et al., 2016).

1.5 Functional behavioral consequences of tPA deficiency

1.5.1 Mice deficient in tPA display defects in avoidance behavior

Given the deficits in hippocampal L-LTP in $tPA^{-/-}$ mice (Huang et al., 1996; Calabresi et al., 2000; Zhuo et al., 2000) it was thought that mice lacking tPA would exhibit comparable behavioral deficits in hippocampal-dependent learning and memory tasks. Deletion of the tPA gene, however, does not appear to cause overt cognitive defects (Huang et al., 1996; Calabresi et al., 2000; Pawlak et al., 2002). Mice deficient in tPA, however, have been consistently found to have impairments in avoidance tests (Huang et al., 1996; Calabresi et al., 2000; Pawlak et al., 2002). Avoidance tests require the mouse to learn to avoid an adverse stimulus, usually foot shock. Depending on the experimental design avoidance tests can reveal differences in acquisition, working memory, consolidation, and long-term recall (Rodriguiz and Wetsel, 2006). In addition, how the adverse stimulus is presented to the mouse - in an active or passive way - can alter the cognitive difficulty, and affect the type of learning being tested and brain structures involved (Rodriguiz and Wetsel, 2006).

Mice lacking the tPA gene have been tested in both two-way shuttlebox active avoidance (Huang et al., 1996; Calabresi et al., 2000) and step-down passive avoidance (Pawlak et al., 2002) (Figure 1.10 A and B). In a two-way shuttlebox active avoidance test, mice are trained to avoid a foot shock upon the presentation of a light cue. Mice are said to have successfully learned the task if they associate the light cue with the oncoming foot shock and avoid the shock by moving to the neighboring compartment. Using this paradigm, $tPA^{-/-}$ mice were found to have significant defects in their ability to avoid the aversive stimulus. Similarly, in a step-down passive avoidance

test, mice are placed on a raised platform and learn to not step-down onto the lower platform/electrical grid, thereby avoiding a foot shock. In the step-down passive avoidance test, $tPA^{-/-}$ mice had significantly shorter latencies to step-down than wild-type mice. Though these data suggest that $tPA^{-/-}$ mice have deficits in acquisition or working memory to aversive or associative learning, this interpretation is complicated by the role tPA has been shown to have in the amygdala function.

1.5.2 Key role for tPA in anxiety-like behavior

Mice deficient in tPA have been found to be resistant to stress-induced anxiety (Matys and Strickland, 2003; Pawlak et al., 2003). Anxiety was tested in an elevated-plus maze, which takes advantage of a rodent's natural aversion to open spaces and preference for closed spaces. And, while $tPA^{-/-}$ mice were initially found to not have altered basal levels of anxiety when assessed in an elevated-plus maze, further evaluation, in which wild-type and $tPA^{-/-}$ mice were first subjected to bouts of chronic restraint, demonstrated a lack of stress-induced anxiety in the absence of tPA. This increased anxiety in wild-type mice correlated with increased tPA activity in the central (CeA) and medial (MeA) amygdala, but not the basolateral amygdala. In line with this phenotype and in-keeping with tPA promoting anxiety-like behavior, intraventricular injections of the stress hormone, corticotropin-releasing factor, were found to upregulate tPA activity in the CeA and MeA.

The molecular mechanism for tPA's role in facilitating anxiety-like behavior points to plasminogen-independent neuronal remodeling, with evidence showing that: 1) $Plg^{-/-}$ mice do not phenocopy $tPA^{-/-}$ mice, 2) signaling cascades implicated in spine plasticity

(ERK 1/2 and GAP-43) are upregulated in wild-type, but not $tPA^{-/-}$ mice (Pawlak et al., 2003; Thomas and Huganir, 2004), and 3) $tPA^{-/-}$ mice have significantly attenuated stress-induced spine retraction in the MeA compared to wild-type mice (Bennur et al., 2007). Given the behavioral data demonstrating $tPA^{-/-}$ mice to have diminished stress-induced anxiety, it's possible that the impairments observed in $tPA^{-/-}$ mice in avoidance tasks are due to tPA's effect on stress-induced neuronal plasticity in the amygdala and not any effect of tPA on hippocampal-dependent learning and memory. Future studies that employ task-independent stressors to test learning and memory (Moore et al., 2013) would be informative in discriminating between tPA's role in stress versus learning and memory.

1.6 Consequences of dysregulated tPA expression and activity

1.6.1 Excitotoxicity-induced neuronal degeneration

In addition to stress, other pathological perturbations - such as excitotoxicity, seizures, stroke, and traumatic brain injury (TBI) - have revealed tPA to be a pleiotropic mediator of numerous neurological processes, such as neuronal degeneration and blood-brain barrier permeability (Table 1.3). tPA was first implicated in having a role in neuronal degeneration when Tsirka et al. demonstrated tPA deficient mice to be resistant to cell death following excitotoxic intrahippocampal injections of kainate (KA) (Tsirka et al., 1995) (Figure 1.11 A). Plasminogen deficient mice and mice treated with α_2-antiplasmin, a plasmin inhibitor, were also found to be resistant to excitotoxic neuronal degeneration (Tsirka et al., 1997). Subsequent studies demonstrated that degradation of the ECM protein laminin - not fibronectin or collagen IV - by plasmin

plays a critical role in promoting neuronal degeneration (Chen and Strickland, 1997) (Figure 1.11 B).

1.6.2 Microglial activation

Microglia cells have also been implicated in tPA-mediated neuronal degeneration. In a transgenic tPA/LacZ reporter mouse that has the mouse tPA promoter driving expression of the bacterial LacZ gene (Carroll et al., 1994), extant tPA/LacZ-expression was observed in the CA1 pyramidal cell layer after excitotoxic injury, despite complete neuronal cell loss (Tsirka et al., 1995). The remaining tPA/LacZ expression was presumed to be from microglia cells. Evidence for the existence of tPA-expressing microglial cells *in vivo*, however, is still tenuous (Louessard et al., 2016). While more than one group has reported microglia to express tPA (Rogove and Tsirka, 1998; Rogove et al., 1999; Yu et al., 2001), these conclusions were based on results from *in vitro* culture studies or widefield microscopy of immunohistochemical stains. To date, high resolution confocal microscopy and coexpression analysis has yet to demonstrate microglia cells expressing tPA *in vivo*.

Regardless of the cellular source of tPA, *in vitro* studies have shown that tPA is necessary for lipopolysaccharide (LPS)-induced activation of microglia cells (Rogove et al., 1999; Siao and Tsirka, 2002) and $tPA^{-/-}$ mice have attenuated microglial activation following excitotoxic injury (Tsirka et al., 1995) (Figure 1.11 A). The correlation between tPA-mediated microglial activation and tPA/plasmin-mediated neuronal degeneration strongly suggested a pathway by which activated microglial cells cause degeneration. However, $Plg^{-/-}$ mice, unlike $tPA^{-/-}$ mice, do not show attenuated KA-induced microglial

activation (Tsirka et al., 1997) (Figure 1.11 A). Moreover, intrahippocampal injections of tPA into $tPA^{-/-}$ mice were shown to cause neuronal degeneration and microglial activation, but intrahippocampal injections of proteolytically inactive tPA only induced microglial activation, with no corresponding neuronal degeneration (Rogove et al., 1999) (Figure 1.11 C). Therefore, it appears two separate pathways - a proteolytically-dependent and a proteolytically-independent tPA pathway - are responsible for excitotoxicity-induced neuronal degeneration and microglial activation, respectively.

1.6.3 Alzheimer's disease

The tPA/plasmin system has also been implicated in amyloid β (Aβ)-induced neuronal degeneration in Alzheimer's disease (AD) (Van Nostrand and Porter, 1999; Ledesma et al., 2000; Tucker et al., 2000a; Tucker et al., 2000b; Melchor et al., 2003; Liu et al., 2011; Oh et al., 2014). One of the hallmark pathologies of AD is the deposition of Aβ plaques in the brain parenchyma; the neuroinflammation that accompanies Aβ accumulation is also now thought to contribute to AD progression (Heppner et al., 2015). Multiple groups have demonstrated the importance of the tPA/plasmin system in the degradation of Aβ and how regulation of tPA by its inhibitor plasminogen activator inhibitor-1 (PAI-1) decreases tPA activity and increases Aβ burden. Indeed, in both mouse AD models and human patients, Aβ accumulation correlates with increased PAI-1 expression and decreased activity of the tPA/plasmin system (Sutton et al., 1994; Mari et al., 1996; Melchor et al., 2003; Liu et al., 2011). In contrast, knocking out the PAI-1 gene from the Aβ precursor protein/presenilin 1 (APP/PS1) transgenic AD mouse increases tPA/plasmin activity and Aβ degradation (Liu et al., 2011). Interestingly,

ablation of the tPA gene in AD mice overexpressing the amyloid precursor protein (Tg2576) is lethal; Tg2576 mice heterozygous for the tPA gene also have reduced survival rates and a more severe AD pathology than tPA wild-type Tg2576 mice (Oh et al., 2014). It is unknown if dysregulation of the tPA/plasmin system is a contributing factor to AD or a consequence of disease progression. It also remains to be seen if tPA's proteolytically-independent role in microglial activation and tPA's proteolytically-dependent role in neurodegeneration intersect in AD.

1.6.4 NMDA receptor function

Though Chen and Strickland (1997) demonstrated the extracellular importance of laminin in tPA/plasmin-mediated neuronal degeneration, the downstream signaling events leading to cell death were not known. Since tPA in-and-of itself does not induce cell death, but potentiates the excitotoxicity of KA (Tsirka et al., 1996), Nicole et al. explored the possibility that tPA was modulating excitatory glutamatergic drive via the NMDA receptor (NMDAR) (Nicole et al., 2001). From both mixed cortical cultures and intra-striatal injections of tPA and NMDA, catalytically active tPA was shown to enhance NMDA-induced neuronal death. Though $Plg^{-/-}$ mice weren't used to demonstrate an *in vivo* plasminogen-independent effect of tPA on NMDA excitotoxicity, tPA's actions appeared not to require plasmin in *in vitro* excitotoxicity studies. From co-immunoprecipitation analysis and calcium imaging, tPA was found to interact with and cleave the NR1 subunit of the NMDAR to potentiate intracellular calcium influx. It is via this Ca^{2+} overload mechanism that tPA's neurotoxic effects were postulated to occur.

The direct interaction between tPA and the NR1 subunit of the NMDAR (Nicole et al., 2001; Reddrop et al., 2005), however, has been debated (Matys and Strickland, 2003; Kvajo et al., 2004; Liu et al., 2004; Pawlak et al., 2005; Samson et al., 2008). While other groups have observed downstream tPA-mediated activation of the NMDAR, it was not through interaction with the NR1 subunit, but indirect interaction via a LDL receptor (LDLR) family member (Samson et al., 2008) or the NR2B subunit of the NMDAR (Pawlak et al., 2005; Park et al., 2008) (Figure 1.12). In well-controlled *in vitro* model systems Samson et al. persuasively demonstrated that 1) plasmin, but not tPA, can cleave the NR1 subunit, 2) a LDLR family member is required for tPA-mediated potentiation of NMDA-induced Ca^{2+} transients, and 3) NMDA-induced changes in Ca^{2+} is dependent on proteolytically active tPA, but independent of plasminogen (Samson et al., 2008).

Activation of the NMDAR via tPA signaling through the NR2B subunit has been shown to be important for regulating neurovascular coupling (Park et al., 2008) and seizure severity in a model of ethanol withdrawal (Pawlak et al., 2005) (Figure 1.12). Park et al. (2008) demonstrated that mice deficient in tPA, but not plasminogen, have a reduced functional hyperemia response in the whisker barrel cortex following whisker stimulation. This response in $tPA^{-/-}$ mice could be restored with application of rtPA. As the NR2B subunit is functionally coupled to nNOS it was hypothesized that modulation of the NMDAR by tPA altered nNOS-dependent NO synthesis and, in turn, cerebral perfusion. To test if this mechanism is responsible for tPA's effects on blood flow, the cell permeable peptide inhibitor NR2B9c was used to uncouple NMDAR activity from NO production. With NR2B9c application, wild-type mice had an attenuated cerebral

blood flow response to whisker stimulation and rtPA no longer rescued the functional hyperemia response in $tPA^{-/-}$ mice.

Pawlak et al. (2005) also demonstrated a role for tPA/NMDAR-signaling via the NR2B subunit in a model of ethanol withdrawal (Figure 1.12). Using *in situ* zymography and co-immunoprecipitation assays, tPA was found to be temporally upregulated with the NR2B subunit in the amygdala during ethanol treatment and ethanol withdrawal, and to directly bind the NR2B subunit. Moreover, activation of the NMDAR signaling pathway, as evidenced by phosphorylation of NR2B and ERK1/2, was specifically and significantly downregulated in $tPA^{-/-}$ mice during ethanol withdrawal. Mice deficient in tPA that received an intracerebroventricular injection of tPA also had much more severe seizures than mice that received a vehicle injection. The NR2B subunit was specifically implicated in this process as seizure severity could be attenuated by the NR2B-specific NMDAR antagonist ifenprodil. This tPA-mediated effect on signaling and seizures appears to be via a non-proteolytic, plasminogen-independent mechanism, as the tPA protease inhibitor, tPA-STOP, had no effect on seizure severity and plasmin completely degraded NR2B. Cumulatively, these data demonstrate that tPA can signal through the NMDAR, as Nicole et al. (2001) first speculated, but its interaction is likely more complex than a one-to-one/protease-to-substrate cleavage mechanism.

And while Samson et al. (2008) and Pawlak et al. (2005) implicated different subunits of the NMDAR, their results are not mutually exclusive. Samson and colleagues (2008) specifically demonstrated that the NR1 subunit is not a direct substrate of tPA and that tPA potentiates Ca^{2+} influx in cultured cortical neurons and oocytes transfected to express NR1A- and NR2A-containing NMDARs. The isoform

composition of the NMDARs present in cortical cultures was not reported and any specific effect of tPA on NMDARs comprising NR2B subunits was not interrogated. Interestingly, though, a time-dependent effect of culture day (DIV 5 vs DIV12) was observed for tPA-mediated NMDA Ca^{2+} transients; larger Ca^{2+} transients were seen in cortical cultures at DIV12, suggesting that an additional co-factor present at DIV12 was facilitating tPA's modulation of the NMDAR. The authors pointed to protease nexin-1 (PN-1), as a previous report (Kvajo et al., 2004) implicated this protease:inhibitor pair in regulating NMDAR function, and the fact that PN-1 expression at DIV5 vs DIV12 correlated with increased tPA-mediated NMDA Ca^{2+} influx.

It's possible, however, that this difference in the NMDA Ca^{2+} response between DIV 5 and DIV12 was not due to some extrinsic co-factor, but an intrinsic change in NMDAR subunit composition. For, NMDARs have been shown to be dynamically regulated during development and in response to activity (Lau and Zukin, 2007). And, given that NMDARs comprised of different subunits (NR1, NR2, and NR3) display differences in their biophysical and pharmacological properties (Lau and Zukin, 2007), the enhanced Ca^{2+} signal observed in cortical cell cultures at DIV12 could be due to a change in molecular composition of the NMDARs. Indeed, evidence for differential cleavage based on the neuronal culture system (hippocampal vs cortical) and the maturity of the culture system can be found for another protease, the calcium-activated protease calpain (Li et al., 1998; Sans et al., 2000; Dong et al., 2004; Wu et al., 2005; Dong et al., 2006). In younger and acutely dissociated cortical cultures calpain proteolyzes intracellular cleavage sites of both the NR2A and NR2B subunits of the NMDAR (Wu et al., 2005). However, in more mature hippocampal neuronal cultures

(DIV 17 or older) NR2A's association with the PSD-95 protein hinders calpain-mediated cleavage (Li et al., 1998; Sans et al., 2000; Dong et al., 2004). Therefore, it remains to be seen whether the reported differences in tPA/NMDAR signaling are experimental or part of the biological complexity of these two molecules in the central nervous system.

1.6.5 Mitochondrial dysfunction – the Nervous (nr) mutant mouse

Other models of neuronal degeneration, however, have pointed to different mechanisms of action for tPA in this pathological process. In two unrelated mutant mouse models that present with cerebellar Purkinje cell loss - *Lurcher* (*Lc*) and *Nervous* (*nr*) (Lu and Tsirka, 2002; Li et al., 2006) tPA mRNA and protein/activity are significantly upregulated and correlated with cell death. One of the most striking features of the *nr* mutant mice, whose Purkinje neurons (PN) selectively degenerate by P35, is their altered PN mitochondrial morphology. Starting from P9, PN mitochondria balloon; this spherical swelling is accompanied by partial or complete disintegration of the outer mitochondrial membrane. Intracerebellar injections of tPA into wild-type mice reproduce the mitochondrial phenotype observed in *nr* mice, and the *nr mice* express elevated levels of tPA (Li et al., 2013).

VDAC, a voltage-dependent anion channel, is a major pore-forming protein on the outer membrane of mitochondria that is involved in regulating ATP release and cell volume. VDAC's role in contributing to the mitochondrial pathology observed in mice was investigated as biochemical analysis showed VDAC to act as a cofactor for tPA and plasminogen to promote plasmin generation (Gonzalez-Gronow et al., 2013). Not only does VDAC act as a cofactor, like fibrin(ogen), to enhance tPA's catalytic activity, but

VDAC also acts as a receptor for the Kringle 5 domain of plasmin(ogen) (Gonzalez-Gronow et al., 2003). Functional downstream effects of plasmin(ogen) binding to VDAC include intracellular acidification and mitochondrial membrane hyperpolarization (Gonzalez-Gronow et al., 2003; Li et al., 2013), processes associated with apoptosis (Gottlieb et al., 1996; Vander Heiden et al., 1999).

Indeed, in cerebellar cell cultures treated with tPA/plasminogen, decrements in mitochondrial membrane potential, as well as increases in mitochondrial diameter and cell death, were measured (Li et al., 2013). While cell death was not found to be mediated by caspase-3, apoptosis-inducing factors (AIFs) have been shown to be released through VDACs to initiate apoptosis (Madamanchi and Runge, 2007; Shoshan-Barmatz et al., 2017). Whether or not this caspase-independent mitochondrial apoptotic pathway was involved in mediating tPA's effects was not investigated. Moreover, when *nr* mutant mice were crossed with $tPA^{-/-}$ mice (*nr;*$tPA^{-/-}$), these doubly mutant mice had significant reductions in PN death and enhanced motor coordination. Despite the protection conferred by tPA deficiency, *nr*;$tPA^{-/-}$ mice had only partial PN preservation, suggesting that other pathways are also responsible for PN degeneration in the *nr* mutant mice. Nonetheless, a VDAC-mediated pathway responsible for tPA/plasmin-induced mitochondrial dysfunction and cell death is intriguing, especially given the *in vitro* evidence demonstrating VDAC expression on endothelial cells (Gonzalez-Gronow et al., 2003; Madamanchi and Runge, 2007) and tPA's role in regulating blood-brain barrier permeability (*as discussed below*).

1.6.6 Apoptosis - the Lurcher (Lc) mutant mouse

In a separate model of cerebellar neuronal degeneration, Lu and Tsirka also demonstrated a link between tPA and PN cell loss in the *Lc* mutant mouse (Lu and Tsirka, 2002). Sequencing revealed an alanine to threonine gain-of-function mutation in the δ2 glutamate receptor (GluRδ2), which are predominantly expressed on PN, to be the genetic cause of the *Lc* mouse. The molecular mechanism bridging genotype to phenotype, however, is still debated and likely highly factorial. While both the *nr* and *Lc* mutant mice display ataxia cerebellar degeneration, the *Lc* mice have a more severe phenotype in that homozygous *Lc* mice die soon after birth (Vogel et al., 2007). Heterozygous *Lc* mice (+/*Lc*), however, are viable, and they are outwardly characterized by their “lurching” gait and inwardly by the complete degeneration of PN by 3 months post-birth. While this degeneration reaches its apex at 3 months, necrotic PN are noticeable by P4 (Caddy and Biscoe, 1979).

tPA appears to be more highly involved in the earlier phase of degeneration as both tPA mRNA and tPA protein/activity are significantly upregulated in the +/*Lc* mice at P12, but comparably normal at P30 (Lu and Tsirka, 2002). tPA’s role in degeneration was further demonstrated when doubly mutant +/*Lc*:tPA$^{-/-}$ mice were found to have an attenuation in PN cell death. This partial preservation appears to be due to decreased activation of apoptotic caspase-8 mediated signaling (at P12 and P30) in +/*Lc*:tPA$^{-/-}$ mice compared to +/*Lc* mice. Despite this reduction in caspase-8, caspase-9 was still elevated in both +/LC and +/*Lc*:tPA$^{-/-}$ mice (at P30, but not P12). These data suggest that while tPA may play a role in receptor-mediated apoptosis (caspase-8) in the +/Lc

mouse, tPA-independent mitochondrial-mediated apoptotic (caspase-9) pathways are also at work.

Given more recent data, however, that demonstrate mitochondrial caspase-independent apoptosis (Madamanchi and Runge, 2007; Gupta et al., 2009) and tPA's involvement in mitochondrial dysfunction in the *nr* mouse (Li et al., 2006; Li et al., 2013), tPA's role in mitochondrial-mediated apoptosis in the +/*Lc* mouse shouldn't be excluded. Moreover, it was not investigated if tPA/plasmin-induced cleavage of laminin in the *Lc* mice enhances receptor-mediated caspase-8 PN cell death. As extracellular matrix proteins, including laminin, have been shown to be important players in neuronal survival and death, in both development and disease states (Hagg et al., 1989; Coucouvanis and Martin, 1995), it's possible that the KA-induced degeneration in adult mice and degeneration in *Lc* mutant mice are part of a common tPA/plasmin/laminin-mediated apoptosis signaling pathway.

1.7 Stroke and tPA

1.7.1 Effects of endogenous and exogenous tPA in models of cerebral ischemia

Efforts to elucidate tPA-mediated signaling pathways that promote excitotoxicity and neuronal degeneration have largely been driven by the fact that rtPA is still the only FDA-approved pharmacologic treatment of ischemic stroke. Further, understanding these pathways could lead to the development of adjuvant therapies that block tPA's harmful effects in the brain parenchyma, while preserving its thrombolytic action, which could extend the efficacy of rtPA in the clinical setting. This would be especially beneficial as the hemorrhagic complications that can arise from rtPA treatment limit its

administration, despite strong endorsements from the American Heart Association and the American Stroke Association (Powers et al., 2018).

Early reports on tPA-mediated excitotoxicity (Tsirka et al., 1995) suggested that additional studies were necessary to understand all of the implications of the use of tPA for the treatment of ischemic stroke. Wang et al. (1998) was the first to discriminate between tPA's beneficial role in the vasculature and its harmful role in the brain parenchyma in a model of cerebral ischemia (Wang et al., 1998). Using an intravascular filament to transiently occlude the middle cerebral artery, $tPA^{-/-}$ mice were found to have smaller infarct volumes and hippocampal neuronal preservation compared to wild-type controls (Figure 1.13 A). Since the $tPA^{-/-}$ mice used were generated from 129/Sv ES cells and crossed onto a C57BL/6J background (Doetschman et al., 1985; Carmeliet et al., 1993; Carmeliet et al., 1994), both C57BL/6J and 129/Sv wild-type mice were separately used as controls.

Contradicting these results, however, was a study showing $tPA^{-/-}$ mice to have larger, not smaller, stroke volumes than wild-type mice (Tabrizi et al., 1999). In this study Tabrizi et al. (1999) followed the same transient ischemia/reperfusion model as Wang et al. (1998); however, in an effort to control for the mixed genetic background of the $tPA^{-/-}$ mice (Carmeliet et al., 1993; Carmeliet et al., 1994) these authors compared $tPA^{-/-}$ mice to wild-type mice on a mixed 129/Sv and C57BL/6J background. The breeding strategy employed to generate the mixed C57BL/6J and 129/Sv control mice, however, was not an appropriate way to control for strain differences. The control mice and $tPA^{-/-}$ mice were genetically unique, containing a mix of genes from the C57BL/6J

and 129/Sv strains but in a random configuration that was different between the two (Flurkey et al., 2009).

Since these early studies (Wang et al., 1998; Tabrizi et al., 1999) that utilized knockout mice, there is a better appreciation for the phenotypic differences between strains and the importance of controlling for genetic background. Szabo et al. (2016) recently described new $tPA^{-/-}$ mice (NIH-$tPA^{-/-}$) that were generated using zinc-finger nuclease genome editing technology, and these mice are not on a mixed background. Unlike the original $tPA^{-/-}$ mice they are on a pure C57BL/6J background and do not harbor any 129/Sv genomic DNA (Szabo et al., 2016). Using these newly created NIH-$tPA^{-/-}$ mice and the original $tPA^{-/-}$ mice that have been extensively backcrossed into C57BL/6J, we have now validated the results from the original publication by Wang colleagues. In a photothrombotic middle cerebral artery occlusion (MCAO) stroke model, we show that both the original and NIH-$tPA^{-/-}$ mice have significantly smaller infarct volumes than their pure C57BL/6J wild-type controls (Su and Lawrence, personal communication). Importantly, these data strongly indicate that endogenous tPA, and not strain-dependent modifier genes, is directly responsible for stroke severity in response to cerebral ischemia.

In addition to examining the effects of parenchymal brain tPA on cerebral ischemia, Wang and colleagues (1998) investigated the impact of exogenous rtPA on stroke outcome. Accordingly, rtPA was injected via the femoral vein 2 hrs after vascular occlusion of either 2 or 3 hrs in wild-type and $tPA^{-/-}$ mice. Following thrombolysis, both tPA deficient mice and wild-type mice had significantly larger infarct volumes compared to their saline-injected control mice. *In situ* zymography revealed tPA activity in the

ischemic core of $tPA^{-/-}$ mice, suggesting that exogenous rtPA crossed the ischemic, compromised BBB and exacerbated neuronal degeneration.

Using a similar intraluminal filament ischemic stroke model, but in contrast to Wang et al. (1998), Zhang and colleagues (2017) observed reduced infarct volume and improved neurological score in C57BL/6J wild-type mice after intravenous rtPA thrombolysis administered 2 hrs after 1 hour of vascular occlusion (Zhang et al., 2017). The disparity in stroke outcome between these studies is likely related to the initial stroke severity (2 or 3 hrs occlusion time in Wang vs only 1 hr in Zhang), since a well-established correlation is known to exists between occlusion time and infarct volume (Stoll et al., 2008). Thus, even after recanalization, the prolonged occlusion time likely provoked a pathological state that promoted secondary thrombosis (Pham et al., 2010) and greater BBB damage (Liu et al., 2018), allowing exogenous rtPA to enter the brain parenchyma and worsen stroke outcome. In agreement with tPA's efficacious use as a thrombolytic agent, other studies using models of thrombotic (Su et al., 2008) or thromboembolic stroke (Zivin et al., 1988; Orset et al., 2016) have shown that, as in humans, early rtPA treatment following stroke onset is beneficial for restoring blood flow and reducing ischemic damage to the brain.

1.7.2 BBB opening by tPA mediates neuronal degeneration in models of cerebral ischemia

How tPA promotes neuronal degeneration, however, is still controversial. Yepes and colleagues (2003) advanced a novel hypothesis in 2003 when they showed that tPA induces opening of the blood-brain barrier (BBB) in a model of stroke. Following

MCAO, $tPA^{-/-}$ mice and wild-type mice treated with an intraventricular injection of a specific tPA inhibitor, neuroserpin (Nsp), had significantly less leakage of Evan's blue dye from the vasculature into the brain parenchyma (Yepes et al., 2003), while in a related study rats treated with intracerebral Nsp had less neurodegeneration (Yepes et al., 2000) (Figure 1.13 B). In contrast, mice lacking uPA and Plg were not protected from MCAO-induced leakage of Evan's blue dye (Yepes et al., 2003). Moreover, when active tPA was injected into the cerebral ventricles of wild-type mice and $Plg^{-/-}$ mice, there was a significant increase in BBB permeability. This increase in tPA-induced BBB permeability was not blocked by treatment with MK-801, an antagonist of the NMDAR. However, intraventricular co-injections of tPA with RAP or tPA with an anti-LRP1 antibody did protect against tPA-induced BBB opening. Conversely, intraventricular injections of inactive tPA or uPA did not induce opening of the BBB. Cumulatively, these results demonstrate that 1) active tPA is required for inducing opening of the BBB, 2) tPA-mediated BBB opening is plasminogen- and NMDAR-independent, 3) the substrate involved in BBB opening is specific to tPA, not uPA, and 4) tPA-induced BBB opening is mediated by activation of a signaling pathway involving LRP1.

As previous studies also implicated matrix metalloproteinase 9 (MMP9) in stroke-induced neuronal degeneration (Asahi et al., 2000; Asahi et al., 2001), BBB permeability was assessed after MCAO in $MMP9^{-/-}$ mice. MMP9 is a member of the MMP family of zinc-dependent endopeptidases that proteolyzes components of the ECM. Despite earlier studies demonstrating a reduction in infarct volume and BBB leakage in $MMP^{-/-}$ mice (Asahi et al., 2000; Asahi et al., 2001), when Yepes et al. (2003) assessed BBB permeability after MCAO, deficiency in MMP9 did not confer protection. MMP9 activity,

however, was increased in brain extracts from both rats and wild-type mice that underwent cerebral ischemia. And, this increase in MMP9 appeared to be dependent on proteolytic tPA (Lapchak et al., 2000; Wang et al., 2003; Cheng et al., 2006), as MMP9 activity was blunted in rats treated with Nsp and in mice lacking tPA.

Experimental differences in the circulating time of Evan's blue dye may be responsible for the differential reports on MMP9's involvement in stroke-induced BBB opening. Asahi et al. infused Evan's blue dye at the onset of reperfusion 2 hrs after transient focal ischemia and the dye circulated for 18-20 hrs before the brains were harvested (Asahi et al., 2001), while Yepes et al. (2003) delivered an intravenous injection of Evan's blue immediately after MCAO, without reperfusion, and allowed the dye to circulate for 6 hrs before harvesting the brains. As BBB opening following stroke is thought to follow a biphasic progression, it's likely that MMP9 is involved in the later, second phase of BBB disruption (Sandoval and Witt, 2008), which was not captured at the earlier experimental time-point used by Yepes and colleagues (2003). Though the mechanism and cellular source of MMP9 in stroke and BBB damage is still controversial (Turner and Sharp, 2016), numerous studies have demonstrated that neutrophils infiltrating the brain parenchyma are the main source of MMP9 in the later stages of stroke and BBB damage (Justicia et al., 2003; Gidday et al., 2005).

1.7.3 Tissue plasminogen activator induces opening of the BBB via activation of the PDGFRα.

Since tPA-induced upregulation of MMP9 expression and MMP9-mediated ECM degradation appears to be more involved during the later stages of BBB breakdown, it

was unclear how tPA was signaling to increase BBB permeability. Earlier studies already precluded plasminogen as a potential substrate of mediating tPA's actions on the barrier (Yepes et al., 2003). Coincidental but independent of efforts to elucidate tPA's effector molecule in stroke, Fredriksson et al.(2004) found tPA to be a potent activator of platelet-derived growth factor C (PDGF-CC). It was unknown, though, if PDGF-CC was the downstream substrate of tPA in the neurovascular unit responsible for inducing BBB opening.

PDGF-CC belongs to the VEGF/PDGF family of growth factors (Andrae et al., 2008). The VEGF/PDGF family can be subdivided into two classes: class I family members house basic retention motifs (PDGF-AA and PDGF-BB) and class II family members house CUB domains (PDGF-CC and PDGF-DD). As a class II family member, structurally, PDGF-CC is characterized by two C-terminal disulfide-linked growth factor domains and their associated N-terminal CUB (for complement C1r/C1s, Uegf, Bmp1) domains. Unlike PDGF-AA and PDGF-BB, which are secreted in their active forms, PDGF-CC and PDGF-DD are secreted as inactive growth factors and processed extracellularly into their active forms via proteolysis. Both the growth factor and CUB domains of PDGF-CC are required for tPA to interact; upon binding, tPA's cleaves the CUB domains of latent PDGF-CC to form active PDGF-CC (Fredriksson et al., 2004). Binding of active PDGF-CC induces homodimerization and activation of downstream signaling of the PDGF receptor α (PDGFRα), a receptor tyrosine kinase.

Subsequent immunohistochemical analysis has demonstrated tPA, PDGF-CC, and the PDGFRα to be expressed by perivascular cells on the abluminal side of the vasculature in the adult mouse brain (Su et al., 2008; Fredriksson et al., 2015).

Moreover, both tPA and PDGF-CC independently, and to similar degrees, induce BBB opening when injected intraventricularly. Co-injections of the two are not additive and tPA's actions on the barrier can be blocked by anti-PDGF-CC antibodies. And, while RAP does not block PDGF-CC-induced opening, LRP1 was shown to significantly facilitate cleavage of latent PDGF-CC into active PDGF-CC by tPA. Together, these data indicate that tPA, PDGF-CC, and the PDGFRα are proximally situated to act on the vasculature; tPA and PDGF-CC work through a common pathway to induce opening; and tPA and LRP1 are upstream mediators of PDGF-CC activation.

These *in vivo* mechanistic studies were then extrapolated to a model of photothrombotic stroke to see if blocking the tPA/PDGF-CC/PDGFRα signaling pathway could reduce BBB permeability and neuronal damage after MCAO. PDGFRα activation was inhibited with the tyrosine kinase inhibitor Imatinib or with anti-PDGF-CC antibodies. With either inhibitor there was a significant decrease in Evan's blue extravasation into the brain parenchyma and Imatinib treatment (200 mg/kg, p.o.; 1 hr and 8 hr after MCAO) improved stroke outcome by significantly decreasing infarct size, presumably due to preserved barrier function (Figure 1.13 B). Imatinib treatment was also shown to significantly reduce intracerebral hemorrhage following photothrombotic MCAO and late (5 hrs post-MCAO) thrombolytic treatment with tPA.

1.7.4 MAC-1-expressing microglia enhance tPA-mediated cleavage of PDGF-CC and downstream BBB opening in models of cerebral ischemia

Additional insights into the molecular mechanism underlying activation of the tPA/PDGF-CC/PDGFRα signaling pathway were made when it was shown that the

integrin MAC-1 (also known as αMβ2 and CD11b/CD18) acts as a co-factor for tPA to accelerate cleavage of PDGF-CC (Su et al., 2017). Earlier biochemical work had shown tPA to be an inefficient enzyme, compared to other serine proteases (Fredriksson et al., 2004). tPA's activity, however, can be greatly enhanced by co-factors, like fibrinogen. Insights from the biophysical attributes of tPA in the vasculature and tPA's inefficient activation of PDGF-CC *in vitro* led Su et al. to hypothesize that there existed some unknown co-factor in the neurovascular unit that was facilitating tPA's cleavage of PDGF-CC (Su et al., 2017). Previous work by numerous groups had already demonstrated the importance of LRP1, but more recent studies also indicated that MAC-1 on microglial cells might be involved.

Using a combination of well-controlled *in vitro* and *in vivo* model systems, Su et al. demonstrated that both LRP1 and MAC-1 are necessary and sufficient to facilitate activation of PDGF-CC by tPA (Su et al., 2017). In a sequential cell culture system with PAE-α cells that stably express PDGFRα, but not PDGFRβ, both immortalized (Line BV2) and primary microglial cells were shown enhance tPA-mediated activation of PDGF-CC from latent PDGF-CC. This effect from microglial cells appeared to be specific to MAC-1, as primary microglial cells cultured from MAC-1 deficient mice (MAC-$1^{-/-}$) were not able to facilitate tPA-mediated activation of PDGF-CC. To more directly assess the contribution of MAC-1 and LRP1 to PDGF-CC activation, PDGFRα phosphorylation was monitored after PAEα and BV2 co-cultures were treated with specific antagonists and small hairpin RNAs against MAC-1 and LRP1. These studies demonstrated that independently blocking MAC-1 or LRP1 reduced PDGF-CC activation to similar degrees.

In agreement with these *in vitro* data indicating that MAC-1 is upstream of PDGF-CC activation, intracerebroventricular injections of either tPA or active PDGF-CC induced BBB opening in wild-type mice, but only active PDGF-CC and not tPA, increased Evan's blue extravasation in MAC-$1^{-/-}$ mice (Figure 1.13 B). This decrease in PDGF-CC activation in MAC-$1^{-/-}$ mice translates to preserved BBB function, as MAC-1 deficient mice had significantly less BBB leakage than wild-type mice following MCAO. These functional data are supported by immunohistochemical stains showing CD11b (the alpha chain of MAC-1), LRP1, and the PDGFRα to be localized to the neurovascular unit. Immunohistochemical analysis of the neurovascular unit also showed PDGFRα activation to be elevated in wild-type mice 6 hrs post-MCAO compared to MAC-1 null mice.

Taking advantage of the CX3CR1-GFP/CCR2-RFP (R/G) transgenic mouse line (Jung et al., 2000; Saederup et al., 2010) Su et al. (2017) were also able to show that resident microglial cells, not infiltrating monocytes, are the likely source of the MAC-1 co-factor (Figure 1.14). In R/G mice, GFP expression is driven by the CX3CR1 promoter and selectively labels microglia and macrophages, while RFP is driven by the CCR2 promoter and is expressed in monocytes and macrophages. With these mice, green resident microglial cells are easily distinguishable from red circulating monocytes and yellow monocyte-derived macrophages. At 6 hrs post-MCAO, when immunohistochemical analysis showed increased PDGFRα activation, there was little evidence of infiltrating RFP+ monocytes, but high levels of resident GFP+ microglia in the neurovascular unit of the ischemic penumbra (Figure 1.14). Infiltrating RFP+ monocytes are not observed till later (24 hrs) time-points of stroke development. The

presence of GFP+ microglia and not RFP+ monocytes suggests that microglial MAC-1 is facilitating tPA-mediated activation of PDGF-CC and PDGFRα downstream signaling.

To further validate that resident microglia and not infiltrating monocytes are the source of MAC-1, wild-type and MAC-$1^{-/-}$ mice underwent bone marrow transplantation. Lethally irradiated wild-type mice received bone marrow transplants from MAC-$1^{-/-}$ mice (MAC-$1^{-/-}$ -> WT), while irradiated MAC-$1^{-/-}$ received transplants from wild-type mice (WT -> MAC-$1^{-/-}$). Unlike circulating monocytes, microglial cells in the brain are not replenished by peripheral hematopoietic stem cells after BBB formation (Ginhoux and Prinz, 2015; Reu et al., 2017). Following irradiation and transplantation, therefore, the resident microglial population in wild-type and MAC-$1^{-/-}$ mice will be unchanged; monocytes in wild-type mice, however, will be MAC-1 deficient while monocytes in MAC-$1^{-/-}$ mice will express MAC-1. If MAC-1 from infiltrating monocytes is responsible for activating the tPA/PDGF-C/PDGFRα signaling pathway and inducing BBB opening, then wild-type mice transplanted with MAC-$1^{-/-}$ bone-marrow cells should phenocopy un-irradiated MAC-$1^{-/-}$ mice after MCAO. Following ischemia and assessment of BBB leakage, however, there was no difference in wild-type or MAC-1 deficient mice with or without irradiation, indicating that MAC-1-mediated BBB permeability in the first 24 hrs after MCAO is independent of infiltrating monocytes.

1.7.5 Imatinib treatment improves outcome in murine models of cerebral ischemia and in human stroke patients

Importantly, in agreement with these results, other groups have reported similar benefits to blocking the tPA/PDGF-CC/PDGFRα pathway in stroke. In a rat

endovascular perforation subarachnoid hemorrhage model, Imatinib was found to ameliorate BBB leakage and edema 24 hrs after hemorrhage (Zhan et al., 2015). This preservation of BBB integrity was in conjunction with improved neurological function. Imatinib has also been shown to improve stroke outcome in an ischemia/reperfusion injury model (Merali et al., 2015). Following transient MCAO and Imatinib treatment, BBB permeability was assessed using MRI by analyzing Gadolinium leakage, and again, with this method, Imatinib preserved BBB integrity, which in turn, led to a decrease in infarct volume, edema, and improved neurologic function. In humans, elevated plasma levels of PDGF-CC in stroke patients with hemorrhagic transformation after tPA treatment have also been observed (Rodriguez-Gonzalez et al., 2013). Based on all of these studies a phase II randomized clinical trial of Imatinib's efficacy as an adjuvant therapy for tPA-mediated thrombolysis was assessed (Wahlgren et al., 2016). From this study, Imatinib was found to be safe and tolerable, and importantly, Imatinib treatment correlated with improved neurological outcome. A phase III trial is now currently being planned to further test the efficacy of Imatinib as an adjuvant therapy for tPA-mediated thrombolysis.

1.8 Regulation of BBB permeability and seizure progression by tPA

In the course of the original KA-induced neuronal degeneration experiments by Tsirka and colleagues (Tsirka et al., 1995; Tsirka et al., 1997) the authors made an intriguing observation: They noticed that following intrahippocampal KA injections wild-type mice developed seizures, but $tPA^{-/-}$ mice did not. To more systematically test and quantify this observation, wild-type and $tPA^{-/-}$ mice were behaviorally evaluated for

seizure progression following intraperitoneal injections of metrazol (a known convulsant) or KA. Indeed, for both seizure-inducing drugs, $tPA^{-/-}$ mice had significantly less severe seizures. And while $tPA^{-/-}$ mice were also protected from KA-induced neuronal loss and microglia activation, it was unclear how, if at all, these events were related to seizure susceptibility. Given that proteolytically-active tPA and proteolytically-inactive tPA appear to effectuate divergent outcomes - neuronal degeneration and microglial activation, respectively - it was also unclear if the discrepancy between active and inactive tPA pertained to seizure progression.

Subsequent investigations have since shown that proteolytically-active tPA is an important mediator of acute KA-induced seizures and that tPA's role in seizure progression is, in part, due to regulating BBB permeability. These actions of tPA were revealed in studies using intra-amygda injections of KA to induce seizure. In this acute seizure model, $tPA^{-/-}$ mice were again found to have a delayed seizure onset time compared to wild-type mice (Yepes et al., 2002). Moreover, neuroserpin (Nsp), not plasminogen activator inhibitor-1 (PAI1), the principal inhibitor of tPA in the vasculature, was demonstrated to be the critical regulator of tPA activity in seizure. To determine if tPA's role in seizure spreading is mediated by plasmin, the behavioral seizures of $Plg^{-/-}$ mice were assessed. Given the plasminogen-dependence of tPA in KA-induced models of neuronal degeneration, it was surprising, therefore, when the seizure behavior of $Plg^{-/-}$ mice phenocopied wild-type mice, not $tPA^{-/-}$ mice, which is not what would be expected if tPA and plasmin were working through a common pathway. As studies examining tPA's role in stroke suggested that PDGF-CC was a candidate effector molecule, Fredriksson et al. (2015) tested if the tPA/PDGF-CC/PDGFRα signaling

pathway responsible for promoting BBB permeability and worse stroke outcome was also responsible for seizure severity.

Using a combination of *in vitro* and *in vivo* approaches, Fredriksson and colleagues (2015) demonstrated a clear link between tPA/PDGF-CC/PDGFRα-induced BBB opening and seizure progression. It was also shown that this pathway could be opposed at the level of tPA by Nsp or through genetic or pharmacologic inhibition of the PDGFRα. Similar to what was previously reported for $tPA^{-/-}$ mice in an intra-amygdala KA-induced seizure model (Yepes et al., 2002) mice lacking tPA had delayed seizure progression. Conversely, mice deficient in Nsp ($Nsp^{-/-}$) had enhanced seizure progression, compared to wild-type and $tPA^{-/-}$ mice. And, as hypothesized, mice doubly deficient in tPA and Nsp ($Nsp:tPA^{-/-}$) phenocopied $tPA^{-/-}$ with their attenuated seizure onset and generalization times. PAI-1 deficient mice behaved like wild-type mice, demonstrating that in this seizure model, Nsp is the primary inhibitory of tPA activity.

Using Evan's blue to evaluate BBB leakage after KA-induced seizure, seizure severity was found to correlate with BBB permeability, with "seizure resistant" $tPA^{-/-}$ mice showing significant barrier protection at 4 hrs post seizure induction (Fredriksson et al., 2015). In contrast, by 2 hrs post seizure induction, "seizure prone" $Nsp^{-/-}$ mice already had significant levels of Evan's blue extravasation into the parenchymal space. The BBB component to the *in vivo* seizure phenotype observed in these mice was further assessed in a no Mg^{2+}/high K^{+} ex vivo model that induces synchronous (or "seizure-like") activity. In an *ex vivo* preparation, a brain slice is bathed in oxygenated artificial cerebrospinal fluid (aCSF) and not subject to alterations of the BBB. As such, a "seizure-like" phenotype can be evaluated independent of the BBB. If the *in vivo* seizure

phenotype in wild-type, tPA$^{-/-}$, and Nsp$^{-/-}$ mice is related to the BBB, then in an *ex vivo* slice preparation there should be no phenotypic difference between these mice. Using this approach, latency to synchronous activity was evaluated. While brain slices from Nsp$^{-/-}$ mice showed no significant difference in onset time, brain slices from tPA$^{-/-}$ mice actually showed an enhanced onset time (We have since increased our "n" for these experiments and now find no significant difference between wild-type and Nsp$^{-/-}$ mice or wild-type and tPA$^{-/-}$ mice. We do, however, find a significant difference between tPA$^{-/-}$ and Nsp$^{-/-}$ mice, with tPA$^{-/-}$ mice developing synchronous activity earlier than Nsp$^{-/-}$ mice. Further details of these experiments are provided in Chapter 3 of this thesis). This more hyperexcitable phenotype in brain slices of tPA$^{-/-}$ mice, however, is opposite the "seizure resistant" phenotype observed *in vivo*. Therefore, despite tPA$^{-/-}$ mice being more excitable *ex vivo*, these data suggest that a significant component of the *in vivo* seizure phenotype in wild-type, tPA$^{-/-}$, and Nsp$^{-/-}$ mice is due to dysregulation of the BBB.

Pharmacologic and genetic blockade of the PDGFRα activation further demonstrated the tPA/PDGF-CC/PDGFRα signaling cascade as being an important pathway regulating BBB permeability and seizure progression. Consistent with tPA being an upstream activator of PDGFRα signaling, Imatinib treatment had no effect on seizure onset or generalization in tPA$^{-/-}$ mice, but it significantly delayed seizure progression in Nsp$^{-/-}$ and wild-type mice. Moreover, conditional ablation of the PDGFRα in perivascular astrocytes, which show high expression of the α-receptor, significantly delayed time to seizure generalization. Together, these results strongly support a mechanism whereby activation of the tPA/PDGF-CC/PDGFRα signaling pathway induces opening of the BBB and contributes to seizure progression.

1.9 Role for tPA in mediating BBB dysregulation in other CNS pathologies

The tPA/PDGF-CC/PDGFRα pathway regulating BBB permeability doesn't appear to be unique to stroke or seizures (Figure 1.15). Blocking PDGFRα activation with Imatinib also improved barrier function and cognition after traumatic brain injury (Su et al., 2015); and it improved recovery after spinal cord injury (Abrams et al., 2012). Preserving BBB function with Imatinib has been shown to be therapeutically beneficial in neurodegenerative and neuroinflammatory mouse models as well. In a model of amyotrophic lateral sclerosis (ALS) Imatinib treatment restored integrity of the brain spinal cord barrier and delayed ALS onset (Lewandowski et al., 2016), while rats with autoimmune encephalomyelitis (EAE), a model of multiple sclerosis, had improved barrier function and EAE symptoms after Imatinib treatment (Adzemovic et al., 2013). The congruity of the tPA/PDGF-CC/PDGFRα pathway across disease model systems suggests that this pathway is a conserved, common regulator of BBB permeability. Targeting this pathway to preserve barrier integrity, therefore, could have therapeutic benefit for numerous pathologies associated with BBB dysfunction.

References

Abel T, Nguyen PV, Barad M, Deuel TA, Kandel ER, Bourtchouladze R (1997) Genetic demonstration of a role for PKA in the late phase of LTP and in hippocampus-based long-term memory. Cell 88:615-626.

Abrams MB, Nilsson I, Lewandowski SA, Kjell J, Codeluppi S, Olson L, Eriksson U (2012) Imatinib enhances functional outcome after spinal cord injury. PLoS One 7:e38760.

Acsady L, Kamondi A, Sik A, Freund T, Buzsaki G (1998) GABAergic cells are the major postsynaptic targets of mossy fibers in the rat hippocampus. J Neurosci 18:3386-3403.

Adzemovic MV, Zeitelhofer M, Eriksson U, Olsson T, Nilsson I (2013) Imatinib ameliorates neuroinflammation in a rat model of multiple sclerosis by enhancing blood-brain barrier integrity and by modulating the peripheral immune response. PLoS One 8:e56586.

Ahmed N, Wahlgren N, Grond M, Hennerici M, Lees KR, Mikulik R, Parsons M, Roine RO, Toni D, Ringleb P, investigators S (2010) Implementation and outcome of thrombolysis with alteplase 3-4.5 h after an acute stroke: an updated analysis from SITS-ISTR. Lancet Neurol 9:866-874.

Akassoglou K, Kombrinck KW, Degen JL, Strickland S (2000) Tissue plasminogen activator-mediated fibrinolysis protects against axonal degeneration and demyelination after sciatic nerve injury. J Cell Biol 149:1157-1166.

Andrae J, Gallini R, Betsholtz C (2008) Role of platelet-derived growth factors in physiology and medicine. Genes Dev 22:1276-1312.

Asahi M, Asahi K, Jung JC, del Zoppo GJ, Fini ME, Lo EH (2000) Role for matrix metalloproteinase 9 after focal cerebral ischemia: effects of gene knockout and enzyme inhibition with BB-94. J Cereb Blood Flow Metab 20:1681-1689.

Asahi M, Wang X, Mori T, Sumii T, Jung JC, Moskowitz MA, Fini ME, Lo EH (2001) Effects of matrix metalloproteinase-9 gene knock-out on the proteolysis of blood-brain barrier and white matter components after cerebral ischemia. J Neurosci 21:7724-7732.

Baranes D, Lederfein D, Huang YY, Chen M, Bailey CH, Kandel ER (1998) Tissue plasminogen activator contributes to the late phase of LTP and to synaptic growth in the hippocampal mossy fiber pathway. Neuron 21:813-825.

Bennur S, Shankaranarayana Rao BS, Pawlak R, Strickland S, McEwen BS, Chattarji S (2007) Stress-induced spine loss in the medial amygdala is mediated by tissue-plasminogen activator. Neuroscience 144:8-16.

Bu G, Maksymovitch EA, Nerbonne JM, Schwartz AL (1994) Expression and function of the low density lipoprotein receptor-related protein (LRP) in mammalian central neurons. J Biol Chem 269:18521-18528.

Caddy KW, Biscoe TJ (1979) Structural and quantitative studies on the normal C3H and Lurcher mutant mouse. Philos Trans R Soc Lond B Biol Sci 287:167-201.

Calabresi P, Napolitano M, Centonze D, Marfia GA, Gubellini P, Teule MA, Berretta N, Bernardi G, Frati L, Tolu M, Gulino A (2000) Tissue plasminogen activator controls multiple forms of synaptic plasticity and memory. Eur J Neurosci 12:1002-1012.

Cao C, Lawrence DA, Li Y, Von Arnim CA, Herz J, Su EJ, Makarova A, Hyman BT, Strickland DK, Zhang L (2006) Endocytic receptor LRP together with tPA and PAI-1 coordinates Mac-1-dependent macrophage migration. EMBO J 25:1860-1870.

Carmeliet P, Kieckens L, Schoonjans L, Ream B, van Nuffelen A, Prendergast G, Cole M, Bronson R, Collen D, Mulligan RC (1993) Plasminogen activator inhibitor-1 gene-deficient mice. I. Generation by homologous recombination and characterization. J Clin Invest 92:2746-2755.

Carmeliet P, Schoonjans L, Kieckens L, Ream B, Degen J, Bronson R, De Vos R, van den Oord JJ, Collen D, Mulligan RC (1994) Physiological consequences of loss of plasminogen activator gene function in mice. Nature 368:419-424.

Carroll PM, Tsirka SE, Richards WG, Frohman MA, Strickland S (1994) The mouse tissue plasminogen activator gene 5' flanking region directs appropriate expression in development and a seizure-enhanced response in the CNS. Development 120:3173-3183.

Chen ZL, Strickland S (1997) Neuronal death in the hippocampus is promoted by plasmin-catalyzed degradation of laminin. Cell 91:917-925.

Cheng T, Petraglia AL, Li Z, Thiyagarajan M, Zhong Z, Wu Z, Liu D, Maggirwar SB, Deane R, Fernandez JA, LaRue B, Griffin JH, Chopp M, Zlokovic BV (2006) Activated protein C inhibits tissue plasminogen activator-induced brain hemorrhage. Nat Med 12:1278-1285.

Conner JM, Lauterborn JC, Yan Q, Gall CM, Varon S (1997) Distribution of brain-derived neurotrophic factor (BDNF) protein and mRNA in the normal adult rat CNS: evidence for anterograde axonal transport. J Neurosci 17:2295-2313.

Coucouvanis E, Martin GR (1995) Signals for death and survival: a two-step mechanism for cavitation in the vertebrate embryo. Cell 83:279-287.

da Silva JS, Dotti CG (2002) Breaking the neuronal sphere: regulation of the actin cytoskeleton in neuritogenesis. Nat Rev Neurosci 3:694-704.

Danzer SC, McNamara JO (2004) Localization of brain-derived neurotrophic factor to distinct terminals of mossy fiber axons implies regulation of both excitation and feedforward inhibition of CA3 pyramidal cells. J Neurosci 24:11346-11355.

Doetschman TC, Eistetter H, Katz M, Schmidt W, Kemler R(1985) The in vitro development of blastocyst-derived embryonic stem cell lines: formation of visceral yolk sac, blood islands and myocardium. Journal of embryology and experimental medicine 87:18.

Dong YN, Waxman EA, Lynch DR (2004) Interactions of postsynaptic density-95 and the NMDA receptor 2 subunit control calpain-mediated cleavage of the NMDA receptor. J Neurosci 24:11035-11045.

Dong YN, Wu HY, Hsu FC, Coulter DA, Lynch DR (2006) Developmental and cell-selective variations in N-methyl-D-aspartate receptor degradation by calpain. J Neurochem 99:206-217.

Echeverry R, Wu J, Haile WB, Guzman J, Yepes M (2010) Tissue-type plasminogen activator is a neuroprotectant in the mouse hippocampus. J Clin Invest 120:2194-2205.

Endo Y, Rubin JS (2007) Wnt signaling and neurite outgrowth: insights and questions. Cancer Sci 98:1311-1317.

Flurkey K, Currer JM, Leiter EH, Witham B (2009) The Jackson Laboratory Handbook on Genetically Standardized Mice, Sixth Edition, Sixth Edition Edition. Bar Harbor, ME 04609 USA: The Jackson Laboratory.

Fredriksson L, Li H, Fieber C, Li X, Eriksson U (2004) Tissue plasminogen activator is a potent activator of PDGF-CC. EMBO J 23:3793-3802.

Fredriksson L, Stevenson TK, Su EJ, Ragsdale M, Moore S, Craciun S, Schielke GP, Murphy GG, Lawrence DA (2015) Identification of a neurovascular signaling pathway regulating seizures in mice. Ann Clin Transl Neurol 2:722-738.

Frey U, Muller M, Kuhl D (1996) A different form of long-lasting potentiation revealed in tissue plasminogen activator mutant mice. J Neurosci 16:2057-2063.

Gidday JM, Gasche YG, Copin JC, Shah AR, Perez RS, Shapiro SD, Chan PH, Park TS (2005) Leukocyte-derived matrix metalloproteinase-9 mediates blood-brain

barrier breakdown and is proinflammatory after transient focal cerebral ischemia. Am J Physiol Heart Circ Physiol 289:H558-568.

Ginhoux F, Prinz M (2015) Origin of microglia: current concepts and past controversies. Cold Spring Harb Perspect Biol 7:a020537.

Gonzalez-Gronow M, Ray R, Wang F, Pizzo SV (2013) The voltage-dependent anion channel (VDAC) binds tissue-type plasminogen activator and promotes activation of plasminogen on the cell surface. J Biol Chem 288:498-509.

Gonzalez-Gronow M, Kalfa T, Johnson CE, Gawdi G, Pizzo SV (2003) The voltage-dependent anion channel is a receptor for plasminogen kringle 5 on human endothelial cells. J Biol Chem 278:27312-27318.

Gottlieb RA, Nordberg J, Skowronski E, Babior BM (1996) Apoptosis induced in Jurkat cells by several agents is preceded by intracellular acidification. Proc Natl Acad Sci U S A 93:654-658.

group ISTc et al. (2012) The benefits and harms of intravenous thrombolysis with recombinant tissue plasminogen activator within 6 h of acute ischaemic stroke (the third international stroke trial [IST-3]): a randomised controlled trial. Lancet 379:2352-2363.

Gualandris A, Jones TE, Strickland S, Tsirka SE (1996) Membrane depolarization induces calcium-dependent secretion of tissue plasminogen activator. J Neurosci 16:2220-2225.

Gupta S, Kass GE, Szegezdi E, Joseph B (2009) The mitochondrial death pathway: a promising therapeutic target in diseases. J Cell Mol Med 13:1004-1033.

Hagg T, Muir D, Engvall E, Varon S, Manthorpe M (1989) Laminin-like antigen in rat CNS neurons: distribution and changes upon brain injury and nerve growth factor treatment. Neuron 3:721-732.

Heppner FL, Ransohoff RM, Becher B (2015) Immune attack: the role of inflammation in Alzheimer disease. Nat Rev Neurosci 16:358-372.

Hu K, Yang J, Tanaka S, Gonias SL, Mars WM, Liu Y (2006) Tissue-type plasminogen activator acts as a cytokine that triggers intracellular signal transduction and induces matrix metalloproteinase-9 gene expression. J Biol Chem 281:2120-2127.

Huang YY, Bach ME, Lipp HP, Zhuo M, Wolfer DP, Hawkins RD, Schoonjans L, Kandel ER, Godfraind JM, Mulligan R, Collen D, Carmeliet P (1996) Mice lacking the gene encoding tissue-type plasminogen activator show a selective interference

with late-phase long-term potentiation in both Schaffer collateral and mossy fiber pathways. Proc Natl Acad Sci U S A 93:8699-8704.

Jacovina AT, Zhong F, Khazanova E, Lev E, Deora AB, Hajjar KA (2001) Neuritogenesis and the nerve growth factor-induced differentiation of PC-12 cells requires annexin II-mediated plasmin generation. J Biol Chem 276:49350-49358.

Jung S, Aliberti J, Graemmel P, Sunshine MJ, Kreutzberg GW, Sher A, Littman DR (2000) Analysis of fractalkine receptor CX(3)CR1 function by targeted deletion and green fluorescent protein reporter gene insertion. Mol Cell Biol 20:4106-4114.

Jung W, Castren E, Odenthal M, Vande Woude GF, Ishii T, Dienes HP, Lindholm D, Schirmacher P (1994) Expression and functional interaction of hepatocyte growth factor-scatter factor and its receptor c-met in mammalian brain. J Cell Biol 126:485-494.

Justicia C, Panes J, Sole S, Cervera A, Deulofeu R, Chamorro A, Planas AM (2003) Neutrophil infiltration increases matrix metalloproteinase-9 in the ischemic brain after occlusion/reperfusion of the middle cerebral artery in rats. J Cereb Blood Flow Metab 23:1430-1440.

Kiryushko D, Berezin V, Bock E (2004) Regulators of Neurite Outgrowth: Role of Cell Adhesion Molecules. Annals of the New York Academy of Sciences 1014:140-154.

Korte M, Kang H, Bonhoeffer T, Schuman E (1998) A role for BDNF in the late-phase of hippocampal long-term potentiation. Neuropharmacology 37:553-559.

Korte M, Carroll P, Wolf E, Brem G, Thoenen H, Bonhoeffer T (1995) Hippocampal long-term potentiation is impaired in mice lacking brain-derived neurotrophic factor. Proc Natl Acad Sci U S A 92:8856-8860.

Krystosek A, Seeds NW (1981a) Plasminogen activator release at the neuronal growth cone. Science 213:1532-1534.

Krystosek A, Seeds NW (1981b) Plasminogen activator secretion by granule neurons in cultures of developing cerebellum. Proc Natl Acad Sci U S A 78:7810-7814.

Krystosek A, Seeds NW (1984) Peripheral neurons and Schwann cells secrete plasminogen activator. J Cell Biol 98:773-776.

Kvajo M, Albrecht H, Meins M, Hengst U, Troncoso E, Lefort S, Kiss JZ, Petersen CC, Monard D (2004) Regulation of brain proteolytic activity is necessary for the in vivo function of NMDA receptors. J Neurosci 24:9734-9743.

Lapchak PA, Chapman DF, Zivin JA (2000) Metalloproteinase inhibition reduces thrombolytic (tissue plasminogen activator)-induced hemorrhage after thromboembolic stroke. Stroke 31:3034-3040.

Lau CG, Zukin RS (2007) NMDA receptor trafficking in synaptic plasticity and neuropsychiatric disorders. Nat Rev Neurosci 8:413-426.

Ledesma MD, Da Silva JS, Crassaerts K, Delacourte A, De Strooper B, Dotti CG (2000) Brain plasmin enhances APP alpha-cleavage and Abeta degradation and is reduced in Alzheimer's disease brains. EMBO Rep 1:530-535.

Lee R, Kermani P, Teng KK, Hempstead BL (2001) Regulation of cell survival by secreted proneurotrophins. Science 294:1945-1948.

Lee SH, Ko HM, Kwon KJ, Lee J, Han SH, Han DW, Cheong JH, Ryu JH, Shin CY (2014) tPA regulates neurite outgrowth by phosphorylation of LRP5/6 in neural progenitor cells. Mol Neurobiol 49:199-215.

Lewandowski SA, Nilsson I, Fredriksson L, Lonnerberg P, Muhl L, Zeitelhofer M, Adzemovic MZ, Nichterwitz S, Lawrence DA, Hedlund E, Eriksson U (2016) Presymptomatic activation of the PDGF-CC pathway accelerates onset of ALS neurodegeneration. Acta Neuropathol 131:453-464.

Li J, Ma Y, Teng YD, Zheng K, Vartanian TK, Snyder EY, Sidman RL (2006) Purkinje neuron degeneration in nervous (nr) mutant mice is mediated by a metabolic pathway involving excess tissue plasminogen activator. Proc Natl Acad Sci U S A 103:7847-7852.

Li J, Yu L, Gu X, Ma Y, Pasqualini R, Arap W, Snyder EY, Sidman RL (2013) Tissue plasminogen activator regulates Purkinje neuron development and survival. Proc Natl Acad Sci U S A 110:E2410-2419.

Li JH, Wang YH, Wolfe BB, Krueger KE, Corsi L, Stocca G, Vicini S (1998) Developmental changes in localization of NMDA receptor subunits in primary cultures of cortical neurons. Eur J Neurosci 10:1704-1715.

Ling C, Zou T, Hsiao Y, Tao X, Chen ZL, Strickland S, Song H (2006) Disruption of tissue plasminogen activator gene reduces macrophage migration. Biochem Biophys Res Commun 349:906-912.

Liu D, Cheng T, Guo H, Fernandez JA, Griffin JH, Song X, Zlokovic BV (2004) Tissue plasminogen activator neurovascular toxicity is controlled by activated protein C. Nature Medicine 10:5.

Liu P, Zhang R, Liu D, Wang J, Yuan C, Zhao X, Li Y, Ji X, Chi T, Zou L (2018) Time-course investigation of blood-brain barrier permeability and tight junction protein changes in a rat model of permanent focal ischemia. J Physiol Sci 68:121-127.

Liu RM, van Groen T, Katre A, Cao D, Kadisha I, Ballinger C, Wang L, Carroll SL, Li L (2011) Knockout of plasminogen activator inhibitor 1 gene reduces amyloid beta peptide burden in a mouse model of Alzheimer's disease. Neurobiol Aging 32:1079-1089.

Louessard M, Lacroix A, Martineau M, Mondielli G, Montagne A, Lesept F, Lambolez B, Cauli B, Mothet JP, Vivien D, Maubert E (2016) Tissue Plasminogen Activator Expression Is Restricted to Subsets of Excitatory Pyramidal Glutamatergic Neurons. Mol Neurobiol 53:5000-5012.

Lu W, Tsirka SE (2002) Partial rescue of neural apoptosis in the Lurcher mutant mouse through elimination of tissue plasminogen activator. Development 129:2043-2050.

Madamanchi NR, Runge MS (2007) Mitochondrial dysfunction in atherosclerosis. Circ Res 100:460-473.

Madani R, Hulo S, Toni N, Madani H, Steimer T, Muller D, Vassalli JD (1999) Enhanced hippocampal long-term potentiation and learning by increased neuronal expression of tissue-type plasminogen activator in transgenic mice. EMBO J 18:3007-3012.

Maina F, Klein R (1999) Hepatocyte growth factor, a versatile signal for developing neurons. Nat Neurosci 2:213-217.

Mari D, Parnetti L, Coppola R, Bottasso B, Reboldi GP, Senin U, Mannucci PM (1996) Hemostasis abnormalities in patients with vascular dementia and Alzheimer's disease. Thromb Haemost 75:216-218.

Mars WM, Zarnegar R, Michalopoulos GK (1993) Activation of hepatocyte growth factor by the plasminogen activators uPA and tPA. Am J Pathol 143:949-958.

Matys T, Strickland S (2003) Tissue plasminogen activator and NMDA receptor cleavage. Nat Med 9:371-372; author reply 372-373.

Medcalf RL, Ruegg M, Schleuning WD (1990) A DNA motif related to the cAMP-responsive element and an exon-located activator protein-2 binding site in the human tissue-type plasminogen activator gene promoter cooperate in basal expression and convey activation by phorbol ester and cAMP. J Biol Chem 265:14618-14626.

Meiri N, Masos T, Rosenblum K, Miskin R, Dudai Y (1994) Overexpression of urokinase-type plasminogen activator in transgenic mice is correlated with impaired learning. Proc Natl Acad Sci U S A 91:3196-3200.

Melchor JP, Pawlak R, Strickland S (2003) The tissue plasminogen activator-plasminogen proteolytic cascade accelerates amyloid-beta (Abeta) degradation and inhibits Abeta-induced neurodegeneration. J Neurosci 23:8867-8871.

Merali Z, Leung J, Mikulis D, Silver F, Kassner A (2015) Longitudinal assessment of imatinib's effect on the blood-brain barrier after ischemia/reperfusion injury with permeability MRI. Transl Stroke Res 6:39-49.

Minichiello L, Calella AM, Medina DL, Bonhoeffer T, Klein R, Korte M (2002) Mechanism of TrkB-mediated hippocampal long-term potentiation. Neuron 36:121-137.

Monard D (1988) Cell-derived proteases and protease inhibitors as regulators of neurite outgrowth. Trends Neurosci 11:541-544.

Moon LD, Madani R, Vassalli JD, Bunge MB (2006) Neuronal overexpression of tissue-type plasminogen activator does not enhance sensory axon regeneration or locomotor recovery following dorsal hemisection of adult mouse thoracic spinal cord. J Neurosci Res 84:1245-1254.

Moore SJ, Deshpande K, Stinnett GS, Seasholtz AF, Murphy GG (2013) Conversion of short-term to long-term memory in the novel object recognition paradigm. Neurobiol Learn Mem 105:174-185.

Nicole O, Docagne F, Ali C, Margaill I, Carmeliet P, MacKenzie ET, Vivien D, Buisson A (2001) The proteolytic activity of tissue-plasminogen activator enhances NMDA receptor-mediated signaling. Nat Med 7:59-64.

Oh SB, Byun CJ, Yun J-H, Jo D-G, Carmeliet P, Koh J-Y, Lee J-Y (2014) Tissue plasminogen activator arrests Alzheimer's disease pathogenesis. Neurobiology of Aging 35:9.

Orset C et al. (2016) Efficacy of Alteplase in a Mouse Model of Acute Ischemic Stroke: A Retrospective Pooled Analysis. Stroke 47:1312-1318.

Pang PT, Teng HK, Zaitsev E, Woo NT, Sakata K, Zhen S, Teng KK, Yung WH, Hempstead BL, Lu B (2004) Cleavage of proBDNF by tPA/plasmin is essential for long-term hippocampal plasticity. Science 306:487-491.

Park L, Gallo EF, Anrather J, Wang G, Norris EH, Paul J, Strickland S, Iadecola C (2008) Key role of tissue plasminogen activator in neurovascular coupling. Proc Natl Acad Sci U S A 105:1073-1078.

Parmer RJ, Mahata M, Mahata S, Sebald MT, O'Connor DT, Miles LA (1997) Tissue plasminogen activator (t-PA) is targeted to the regulated secretory pathway. Catecholamine storage vesicles as a reservoir for the rapid release of t-PA. J Biol Chem 272:1976-1982.

Pawlak R, Magarinos AM, Melchor J, McEwen B, Strickland S (2003) Tissue plasminogen activator in the amygdala is critical for stress-induced anxiety-like behavior. Nat Neurosci 6:168-174.

Pawlak R, Melchor JP, Matys T, Skrzypiec AE, Strickland S (2005) Ethanol-withdrawal seizures are controlled by tissue plasminogen activator via modulation of NR2B-containing NMDA receptors. Proc Natl Acad Sci U S A 102:443-448.

Pawlak R, Nagai N, Urano T, Napiorkowska-Pawlak D, Ihara H, Takada Y, Collen D, Takada A (2002) Rapid, specific and active site-catalyzed effect of tissue-plasminogen activator on hippocampus-dependent learning in mice. Neuroscience 113:995-1001.

Pham M, Kleinschnitz C, Helluy X, Bartsch AJ, Austinat M, Behr VC, Renne T, Nieswandt B, Stoll G, Bendszus M (2010) Enhanced cortical reperfusion protects coagulation factor XII-deficient mice from ischemic stroke as revealed by high-field MRI. Neuroimage 49:2907-2914.

Pittman RN, Williams AG (1989) Neurite penetration into collagen gels requires Ca2+-dependent metalloproteinase activity. Dev Neurosci 11:41-51.

Pittman RN, DiBenedetto AJ (1995) PC12 cells overexpressing tissue plasminogen activator regenerate neurites to a greater extent and migrate faster than control cells in complex extracellular matrix. J Neurochem 64:566-575.

Pittman RN, Ivins JK, Buettner HM (1989) Neuronal plasminogen activators: cell surface binding sites and involvement in neurite outgrowth. J Neurosci 9:4269-4286.

Powers Wj, Rabinstein AA, Ackerson T,Adeoye OM, Bambakidis NC, Becker K, Biller J, Brown M, Demaerschalk BM, Hoh B, Jauch EC, Kidwell CS, Leslie-Mazwi TM, Ovbiagele B, Scott PA, Sheth KN, Southerland AM, Summers DV, Tirschwell DL (2018) 2018 Guidelines for the Early Management of Patients With Acute Ischemic Stroke: A Guideline for Healthcare Professionals From the American Heart Association/American Stroke Association. Stroke 49:64.

Prabhakaran S, Ruff I, Bernstein RA (2015) Acute stroke intervention: a systematic review. Journal of the American Medical Association 313:12.

Qian Z, Gilbert ME, Colicos MA, Kandel ER, Kuhl D (1993) Tissue-plasminogen activator is induced as an immediate-early gene during seizure, kindling and long-term potentiation. Nature 361:453-457.

Quaegebeur A, Lange C, Carmeliet P (2011) The neurovascular link in health and disease: molecular mechanisms and therapeutic implications. Neuron 71:406-424.

Reddrop C, Moldrich RX, Beart PM, Farso M, Liberatore GT, Howells DW, Petersen KU, Schleuning WD, Medcalf RL (2005) Vampire bat salivary plasminogen activator (desmoteplase) inhibits tissue-type plasminogen activator-induced potentiation of excitotoxic injury. Stroke 36:1241-1246.

Reu P, Khosravi A, Bernard S, Mold JE, Salehpour M, Alkass K, Perl S, Tisdale J, Possnert G, Druid H, Frisen J (2017) The Lifespan and Turnover of Microglia in the Human Brain. Cell Rep 20:779-784.

Rodriguez-Gonzalez R, Blanco M, Rodriguez-Yanez M, Moldes O, Castillo J, Sobrino T (2013) Platelet derived growth factor-CC isoform is associated with hemorrhagic transformation in ischemic stroke patients treated with tissue plasminogen activator. Atherosclerosis 226:165-171.

Rodriguiz RM, Wetsel WC (2006) Assessments of Cognitive Deficits in Mutant Mice. In: Animal Models of Cognitive Impairment (Levin ED, Buccafusco JJ, eds). Boca Raton (FL).

Rogove AD, Tsirka SE (1998) Neurotoxic responses by microglia elicited by excitotoxic injury in the mouse hippocampus. Curr Biol 8:19-25.

Rogove AD, Siao C, Keyt B, Strickland S, Tsirka SE (1999) Activation of microglia reveals a non-proteolytic cytokine function for tissue plasminogen activator in the central nervous system. J Cell Sci 112 (Pt 22):4007-4016.

Rollenhagen A, Lubke JH (2010) The mossy fiber bouton: the "common" or the "unique" synapse? Front Synaptic Neurosci 2:2.

Saederup N, Cardona AE, Croft K, Mizutani M, Cotleur AC, Tsou CL, Ransohoff RM, Charo IF (2010) Selective chemokine receptor usage by central nervous system myeloid cells in CCR2-red fluorescent protein knock-in mice. PLoS One 5:e13693.

Salles FJ, Strickland S (2002) Localization and regulation of the tissue plasminogen activator-plasmin system in the hippocampus. J Neurosci 22:2125-2134.

Samson AL, Nevin ST, Croucher D, Niego B, Daniel PB, Weiss TW, Moreno E, Monard D, Lawrence DA, Medcalf RL (2008) Tissue-type plasminogen activator requires a co-receptor to enhance NMDA receptor function. J Neurochem 107:1091-1101.

Sandoval KE, Witt KA (2008) Blood-brain barrier tight junction permeability and ischemic stroke. Neurobiol Dis 32:200-219.

Sans N, Petralia RS, Wang YX, Blahos J, 2nd, Hell JW, Wenthold RJ (2000) A developmental change in NMDA receptor-associated proteins at hippocampal synapses. J Neurosci 20:1260-1271.

Sappino AP, Madani R, Huarte J, Belin D, Kiss JZ, Wohlwend A, Vassalli JD (1993) Extracellular proteolysis in the adult murine brain. J Clin Invest 92:679-685.

Scalettar BA, Jacobs C, Fulwiler A, Prahl L, Simon A, Hilken L, Lochner JE (2012) Hindered submicron mobility and long-term storage of presynaptic dense-core granules revealed by single-particle tracking. Dev Neurobiol 72:1181-1195.

Seeds NW, Williams BL, Bickford PC (1995) Tissue plasminogen activator induction in Purkinje neurons after cerebellar motor learning. Science 270:1992-1994.

Seeds NW, Basham ME, Haffke SP (1999) Neuronal migration is retarded in mice lacking the tissue plasminogen activator gene. Proc Natl Acad Sci U S A 96:14118-14123.

Shi Y, Mantuano E, Inoue G, Campana WM, Gonias SL (2009) Ligand binding to LRP1 transactivates Trk receptors by a Src family kinase-dependent pathway. Sci Signal 2:ra18.

Shoshan-Barmatz V, Krelin Y, Shteinfer-Kuzmine A, Arif T (2017) Voltage-Dependent Anion Channel 1 As an Emerging Drug Target for Novel Anti-Cancer Therapeutics. Front Oncol 7:154.

Siao CJ, Tsirka SE (2002) Tissue plasminogen activator mediates microglial activation via its finger domain through annexin II. J Neurosci 22:3352-3358.

Siconolfi LB, Seeds NW (2001a) Mice lacking tPA, uPA, or plasminogen genes showed delayed functional recovery after sciatic nerve crush. J Neurosci 21:4348-4355.

Siconolfi LB, Seeds NW (2001b) Induction of the plasminogen activator system accompanies peripheral nerve regeneration after sciatic nerve crush. J Neurosci 21:4336-4347.

Stefanitsch C, Lawrence AL, Olverling A, Nilsson I, Fredriksson L (2015) tPA Deficiency in Mice Leads to Rearrangement in the Cerebrovascular Tree and Cerebroventricular Malformations. Frontiers in cellular neuroscience 9:456.

Stevenson TK and Lawrence AL (2018) Characerization of tissue plasminogen activator expression and trafficking in the adult murine brain. eNeuro (in press).

Stoll G, Kleinschnitz C, Nieswandt B (2008) Molecular mechanisms of thrombus formation in ischemic stroke: novel insights and targets for treatment. Blood 112:3555-3562.

Su EJ, Fredriksson L, Geyer M, Folestad E, Cale J, Andrae J, Gao Y, Pietras K, Mann K, Yepes M, Strickland DK, Betsholtz C, Eriksson U, Lawrence DA (2008) Activation of PDGF-CC by tissue plasminogen activator impairs blood-brain barrier integrity during ischemic stroke. Nat Med 14:731-737.

Su EJ, Cao C, Fredriksson L, Nilsson I, Stefanitsch C, Stevenson TK, Zhao J, Ragsdale M, Sun YY, Yepes M, Kuan CY, Eriksson U, Strickland DK, Lawrence DA, Zhang L (2017) Microglial-mediated PDGF-CC activation increases cerebrovascular permeability during ischemic stroke. Acta Neuropathol 134:585-604.

Su EJ, Fredriksson L, Kanzawa M, Moore S, Folestad E, Stevenson TK, Nilsson I, Sashindranath M, Schielke GP, Warnock M, Ragsdale M, Mann K, Lawrence AL, Medcalf RL, Eriksson U, Murphy GG, Lawrence DA (2015) Imatinib treatment reduces brain injury in a murine model of traumatic brain injury. Frontiers in cellular neuroscience 9:385.

Sutton R, Keohane ME, VanderBerg SR, Gonias SL (1994) Plasminogen activator inhibitor-1 in the cerebrospinal fluid as an index of neurological disease. Blood Coagulation and Fibrinolysis 5:5.

Szabo R, Samson AL, Lawrence DA, Medcalf RL, Bugge TH (2016) Passenger mutations and aberrant gene expression in congenic tissue plasminogen activator-deficient mouse strains. J Thromb Haemost 14:1618-1628.

Tabrizi P, Wang L, Seeds N, McComb JG, Yamada S, Griffin JH, Carmeliet P, Weiss MH, Zlokovic BV (1999) Tissue plasminogen activator (tPA) deficiency exacerbates cerebrovascular fibrin deposition and brain injury in a murine stroke model: studies in tPA-deficient mice and wild-type mice on a matched genetic background. Arterioscler Thromb Vasc Biol 19:2801-2806.

Taniguchi Y, Inoue N, Morita S, Nikaido Y, Nakashima T, Nagai N, Okada K, Matsuo O, Miyata S (2011) Localization of plasminogen in mouse hippocampus, cerebral cortex, and hypothalamus. Cell Tissue Res 343:303-317.

Thewke DP, Seeds NW (1996) Expression of hepatocyte growth factor/scatter factor, its receptor, c-met, and tissue-type plasminogen activator during development of the murine olfactory system. J Neurosci 16:6933-6944.

Thomas GM, Huganir RL (2004) MAPK cascade signalling and synaptic plasticity. Nat Rev Neurosci 5:173-183.

Tsirka SE, Rogove AD, Strickland S (1996) Neuronal cell death and tPA. Nature 384:123-124.

Tsirka SE, Gualandris A, Amaral DG, Strickland S (1995) Excitotoxin-induced neuronal degeneration and seizure are mediated by tissue plasminogen activator. Nature 377:340-344.

Tsirka SE, Rogove AD, Bugge TH, Degen JL, Strickland S (1997) An extracellular proteolytic cascade promotes neuronal degeneration in the mouse hippocampus. J Neurosci 17:543-552.

Tucker HM, Kihiko-Ehmann M, Wright S, Rydel RE, Estus S (2000a) Tissue plasminogen activator requires plasminogen to modulate amyloid-beta neurotoxicity and deposition. J Neurochem 75:2172-2177.

Tucker HM, Kihiko M, Caldwell JN, Wright S, Kawarabayashi T, Price D, Walker D, Scheff S, McGillis JP, Rydel RE, Estus S (2000b) The plasmin system is induced by and degrades amyloid-beta aggregates. J Neurosci 20:3937-3946.

Turner RJ, Sharp FR (2016) Implications of MMP9 for Blood Brain Barrier Disruption and Hemorrhagic Transformation Following Ischemic Stroke. Frontiers in cellular neuroscience 10:56.

Van Nostrand WE, Porter M (1999) Plasmin cleavage of the amyloid beta-protein: alteration of secondary structure and stimulation of tissue plasminogen activator activity. Biochemistry 38:7.

Vander Heiden MG, Chandel NS, Schumacker PT, Thompson CB (1999) Bcl-xL prevents cell death following growth factor withdrawal by facilitating mitochondrial ATP/ADP exchange. Mol Cell 3:159-167.

Verrall S, Seeds NW (1988) Tissue plasminogen activator binding to mouse cerebellar granule neurons. J Neurosci Res 21:420-425.

Vogel MW, Caston J, Yuzaki M, Mariani J (2007) The Lurcher mouse: fresh insights from an old mutant. Brain Res 1140:4-18.

Wahlgren N, Thoren M, Hojeberg B, Kall TB, Laska AC, Sjostrand C, Hoijer J, Almqvist H, Holmin S, Lilja A, Fredriksson L, Lawrence D, Eriksson U, Ahmed N (2016) Randomized assessment of imatinib in patients with acute ischaemic stroke treated with intravenous thrombolysis. J Intern Med 281:273-283.

Wang TW, Zhang H, Gyetko MR, Parent JM (2011) Hepatocyte growth factor acts as a mitogen and chemoattractant for postnatal subventricular zone-olfactory bulb neurogenesis. Mol Cell Neurosci 48:38-50.

Wang X, Lee SR, Arai K, Lee SR, Tsuji K, Rebeck GW, Lo EH (2003) Lipoprotein receptor-mediated induction of matrix metalloproteinase by tissue plasminogen activator. Nat Med 9:1313-1317.

Wang YF, Tsirka SE, Strickland S, Stieg PE, Soriano SG, Lipton SA (1998) Tissue plasminogen activator (tPA) increases neuronal damage after focal cerebral ischemia in wild-type and tPA-deficient mice. Nat Med 4:228-231.

Waxman SG (2005) Multiple sclerosis as a neuronal disease. Burlington, MA: Elsevier Academic Press.

Wu F, Torre E, Cuellar-Giraldo D, Cheng L, Yi H, Bichler EK, Garcia PS, Yepes M (2015) Tissue-type plasminogen activator triggers the synaptic vesicle cycle in cerebral cortical neurons. J Cereb Blood Flow Metab 35:1966-1976.

Wu HY, Yuen EY, Lu YF, Matsushita M, Matsui H, Yan Z, Tomizawa K (2005) Regulation of N-methyl-D-aspartate receptors by calpain in cortical neurons. J Biol Chem 280:21588-21593.

Xu B, Gottschalk W, Chow A, Wilson RI, Schnell E, Zang K, Wang D, Nicoll RA, Lu B, Reichardt LF (2000) The role of brain-derived neurotrophic factor receptors in the mature hippocampus: modulation of long-term potentiation through a presynaptic mechanism involving TrkB. J Neurosci 20:6888-6897.

Yan Q, Rosenfeld RD, Matheson CR, Hawkins N, Lopez OT, Bennett L, Welcher AA (1997) Expression of brain-derived neurotrophic factor protein in the adult rat central nervous system. Neuroscience 78:431-448.

Yepes M, Sandkvist M, Moore EG, Bugge TH, Strickland DK, Lawrence DA (2003) Tissue-type plasminogen activator induces opening of the blood-brain barrier via the LDL receptor-related protein. J Clin Invest 112:1533-1540.

Yepes M, Sandkvist M, Wong MK, Coleman TA, Smith E, Cohan SL, Lawrence DA (2000) Neuroserpin reduces cerebral infarct volume and protects neurons from ischemia-induced apoptosis. Blood 96:569-576.

Yepes M, Sandkvist M, Coleman TA, Moore E, Wu JY, Mitola D, Bugge TH, Lawrence DA (2002) Regulation of seizure spreading by neuroserpin and tissue-type plasminogen activator is plasminogen-independent. J Clin Invest 109:1571-1578.

Yu H, Schleuning WD, Michl M, Liberatore G, Tan SS, Medcalf RL (2001) Control elements between -9.5 and -3.0 kb in the human tissue-type plasminogen activator gene promoter direct spatial and inducible expression to the murine brain. Eur J Neurosci 14:799-808.

Zhan Y, Krafft PR, Lekic T, Ma Q, Souvenir R, Zhang JH, Tang J (2015) Imatinib preserves blood-brain barrier integrity following experimental subarachnoid hemorrhage in rats. J Neurosci Res 93:94-103.

Zhang B, Xu X, Chu X, Yu X, Zhao Y (2017) Protective effects of angiopoietin-like 4 on the blood-brain barrier in acute ischemic stroke treated with thrombolysis in mice. Neurosci Lett 645:113-120.

Zhuo M, Holtzman DM, Li Y, Osaka H, DeMaro J, Jacquin M, Bu G (2000) Role of tissue plasminogen activator receptor LRP in hippocampal long-term potentiation. J Neurosci 20:542-549.

Zivin JA, Lyden PD, DeGirolami U, Kochhar A, Mazzarella V, Hemenway CC, Johnston P (1988) Tissue plasminogen activator. Reduction of neurologic damage after experimental embolic stroke. Arch Neurol 45:387-391.

Zou T, Ling C, Xiao Y, Tao X, Ma D, Chen ZL, Strickland S, Song H (2006) Exogenous tissue plasminogen activator enhances peripheral nerve regeneration and functional recovery after injury in mice. J Neuropathol Exp Neurol 65:78-86.

Table 1.1. Studies supporting a role for tPA in CNS development and nerve regeneration

Process	Biological Effect and/or Mechanism of Action	References
Neurite outgrowth	(*in vitro*) Plasminogen activators (tPA and uPA) are released from growth cones of cerebellar granule neurons, peripheral neurons and Schwann cells, and neuroblastoma cells. Implications for neurite outgrowth.	Krystosek and Seeds, 1981a, b, 1984; Verrall and Seeds, 1988
	(*in vitro*) PC12 cells overexpressing tPA regenerate neurites and migrate faster than control cells in a complex extracellular matrix	Pittman and DiBenedetto, 1995
	(*in vitro*) Plasma membrane-related protein annexin II on PC12 cells supports tPA-mediated plasmin generation and NGF-induced neurite outgrowth	Jacovina et al., 2001
	(*in vitro*) Inactive tPA transactivates Trk-receptor signaling via LRP1, promoting NGF-induced neurite outgrowth in cultured PC12 cells and primary cerebellar neurons	Shi et al., 2009
	(*in vitro*) Upregulation of the Wnt-LRP5/6-GSK3beta-beta-catenin canonical signaling pathway and neurite outgrowth following tPA treatment in primary neural progenitor cells	Lee et al., 2014
Neuronal migration	(*in vivo*) Delayed migration of cerebellar granule neurons during development (P7 – P13) in $tPA^{-/-}$ mice, but similar granule cell patterning at the end of the granule cell migratory period (P16)	Seeds et al., 1999
	(*in vivo*) Reduced tPA-mediated generation of HGF in $tPA^{-/-}$ mice leads to accelerated, but ectopic, neuroblasts in the rostral migratory stream and decreased cell proliferation and neurogenesis in the sub-ventricular zone in the developing mouse brain (P2 – P14)	Mars et al., 1993; Jung et al., 1994; Thewke and Seeds, 1996; Wang et al., 2011
Nerve Regeneration	(*in vivo*) Mice deficient in tPA have exacerbated axonal degeneration and demyelination and impaired functional recovery following sciatic nerve injury. Exogenous tPA treatment enhances nerve regeneration and functional recovery.	Akassoglou et al., 2000; Siconolfi and Seeds, 2001a, b; Ling et al., 2006; Zou et al., 2006
Cerebro-vascular architecture	(*in vivo*) Increased capillary density, decreased number of large diameter (>10 µm), smooth-muscle covered vessels, and enhanced ZO-1 staining in $tPA^{-/-}$ mice.	Stefanitsch et al., 2015
Cerebro-ventricular morphology	(*in vivo*) Enlarged ventricles and altered molecular composition of ependymal lining in $tPA^{-/-}$ mice.	Wang et al., 2011; Stefanitsch et al., 2015

Table 1.2. Studies demonstrating a role for tPA in synaptic transmission and plasticity

Process	Biological Effect and/or Mechanism of Action	References
Synaptic plasticity	(*in vivo*) Gene expression of tPA is upregulated in the hippocampus and cerebellum following activity-dependent events. Implications for tPA in synaptic plasticity.	Qian et al., 1993; Seeds et al., 1995
	(*in vivo*) No difference in the late phase of LTP between wild-type and $tPA^{-/-}$ mice in the CA1 hippocampal region, but a significant difference when GABAergic transmission is blocked.	Frey et al., 1996
	(*in vivo*) Defects in the late phase of LTP in the CA1 hippocampal region in $tPA^{-/-}$ mice with and without GABAergic transmission blocked. A post-synaptic mechanism of action for tPA involving the endocytic receptor LRP1 and cAMP/PKA signaling is proposed.	Huang et al., 1996; Baranes et al., 1998; Calabresi et al., 2000; Zhuo et al., 2000
	(*in vivo*) tPA/plasmin-mediated cleavage of pro-BDNF is critical for the full expression of the late phase of LTP in the CA1 hippocampal region.	Pang et al., 2004
Synaptic transmission	(*in vivo*) A larger stimulus is required to evoke a population-spike of similar amplitude in $tPA^{-/-}$ mice compared to wild-type controls and $tPA^{-/-}$ mice display deficits in paired-pulse facilitation.	Frey et al., 1996
	(*in vivo*) tPA treatment of rat brain slices increases mEPSCs in CA1 hippocampal pyramidal neurons.	Wu et al., 2015

Table 1.3. Pathological consequences of dysregulated tPA expression and activity

Process	Biological Effect and/or Mechanism of Action	References
Excitotoxicity-induced neuronal degeneration	(*in vivo*) $tPA^{-/-}$ mice are resistant to KA-induced excitotoxic neuronal degeneration in the hippocampus. tPA/plasmin-mediated degradation of the extracellular matrix protein laminin promotes cell death.	Carroll et al., 1994; Tsirka et al., 1995; Chen and Strickland, 1997; Tsirka et al., 1997
Purkinje neuron degeneration	(*in vivo* and *in vitro*) In two unrelated mutant mouse models - Lurcher (*Lc*) and Nervous (*nr*) - tPA mRNA and protein/activity are significantly upregulated and correlated with Purkinje neuron cell death. Crossing the *Lc* or *nr* mutant mice with $tPA^{-/-}$ mice reduced PN cell death.	Lu and Tsirka, 2002; Li et al., 2006; Li et al., 2013
Microglial activation	(*in vitro* and *in vivo*) Microglia in mixed cortical cultures from $tPA^{-/-}$ mice and microglia in the hippocampal region of $tPA^{-/-}$ mice show attenuated endotoxin-induced or excitotoxin-induced activation, respectively. Treatment with tPA restores microglial activation. Proteolytically active tPA is not necessary for microglial activation.	Tsirka et al., 1995; Rogove and Tsirka, 1998; Rogove et al., 1999; Siao and Tsirka, 2002
Alzheimer's disease	(*in vivo*) Amyloid β accumulation correlates with increased PAI-1 expression and decreased activity of the tPA/plasmin system in mouse AD models and human AD patients. Ablation of the tPA gene in the mouse Tg2576 AD model is lethal.	Sutton et al., 1994; Mari et al., 1996; Melchor et al., 2003; Liu et al., 2011; Oh et al., 2014
BBB permeability	(*in vivo*) The tPA/PDGF-CC/PDGFRα pathway regulates BBB permeability in animal models of stroke, seizures, and TBI. Blocking PDGFRα activation with Imatinib reduced BBB permeability.	Su et al., 2008; Fredriksson et al., 2015; Merali et al., 2015; Su et al., 2015; Zhan et al., 2015; Su et al., 2017
	(*in vivo*) Imatinib treatment improves barrier function and neurologic outcome in progressive neurodegenerative and neuroinflammatory animal models of ALS and EAE.	Adzemovic et al., 2013; Lewandowski et al., 2016
	Stroke patients have elevated plasma levels of PDGF-CC and Imatinib treatment correlates with improved neurological outcome after stroke.	Rodriguez-Gonzalez et al., 2013; Wahlgren et al., 2016

Figure 1.1

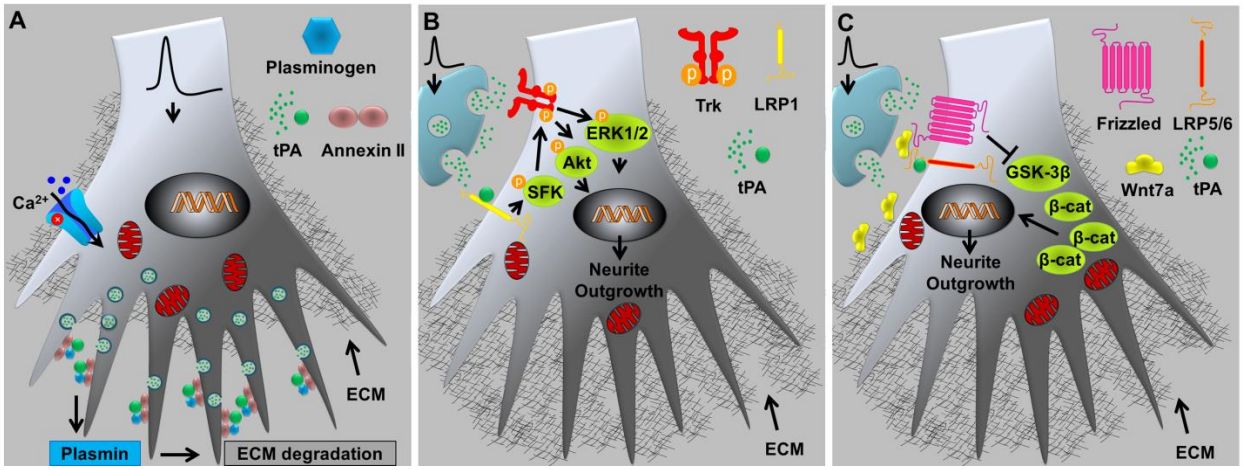
A
Plasminogen
tPA
Annexin II
Ca2+
ECM
Plasmin
ECM degradation
B
Trk
LRP1
ERK1/2
Akt
SFK
tPA
Neurite Outgrowth
ECM
C
Frizzled
LRP5/6
GSK-3β
Wnt7a
tPA
β-cat
β-cat
β-cat
Neurite Outgrowth
ECM

Figure 1.1. Proposed models for tPA-mediated neurite outgrowth. (A) The membrane-associated protein annexin II acts as a scaffolding cofactor for plasminogen and tPA, promoting plasmin generation by pheochyromocytoma PC-12 cells (Jacovina et al., 2001). Neurite outgrowth was attenuated by ε-aminocaproic acid, a lysine analog that inhibits plasminogen binding to annexin II and plasmin generation. Previous studies found a correlation between tPA-mediated extracellular matrix degradation and neuronal migration (Pittman and DiBenedetto, 1995). **(B)** Proteolytically inactive tPA transactivated Trk receptors via tPA binding to LRP1 and SFK-dependent phosphorylation of Trk (Shi et al., 2009). Activation of Akt and ERK1/2 signaling pathways downstream of Trk promoted neurite outgrowth in PC-12 cells and granule neurons. **(C)** Activation of the Wnt-LRP5/6-GSK3β-β-catenin canonical signaling pathway was upregulated by tPA treatment of primary NPCs. The Wnt-LRP5/6-GSK3 β-β-catenin signaling pathway is involved in regulating the transcription of genes that promote neurite outgrowth. tPA was shown to activate β-catenin signaling via the release of Wnt7a from the extracellular matrix of cultured NPCs and direct binding to LRP5/6 (Lee et al., 2014). Abbreviations: SFK – Src family kinase; ERK1/2 – extracellular regulated kinase, LRP – low-density lipoprotein (LDL) receptor-related protein; GSK-3β – glyocogen synthase kinase-3β; β-cat – β-catenin.

Figure 1.2

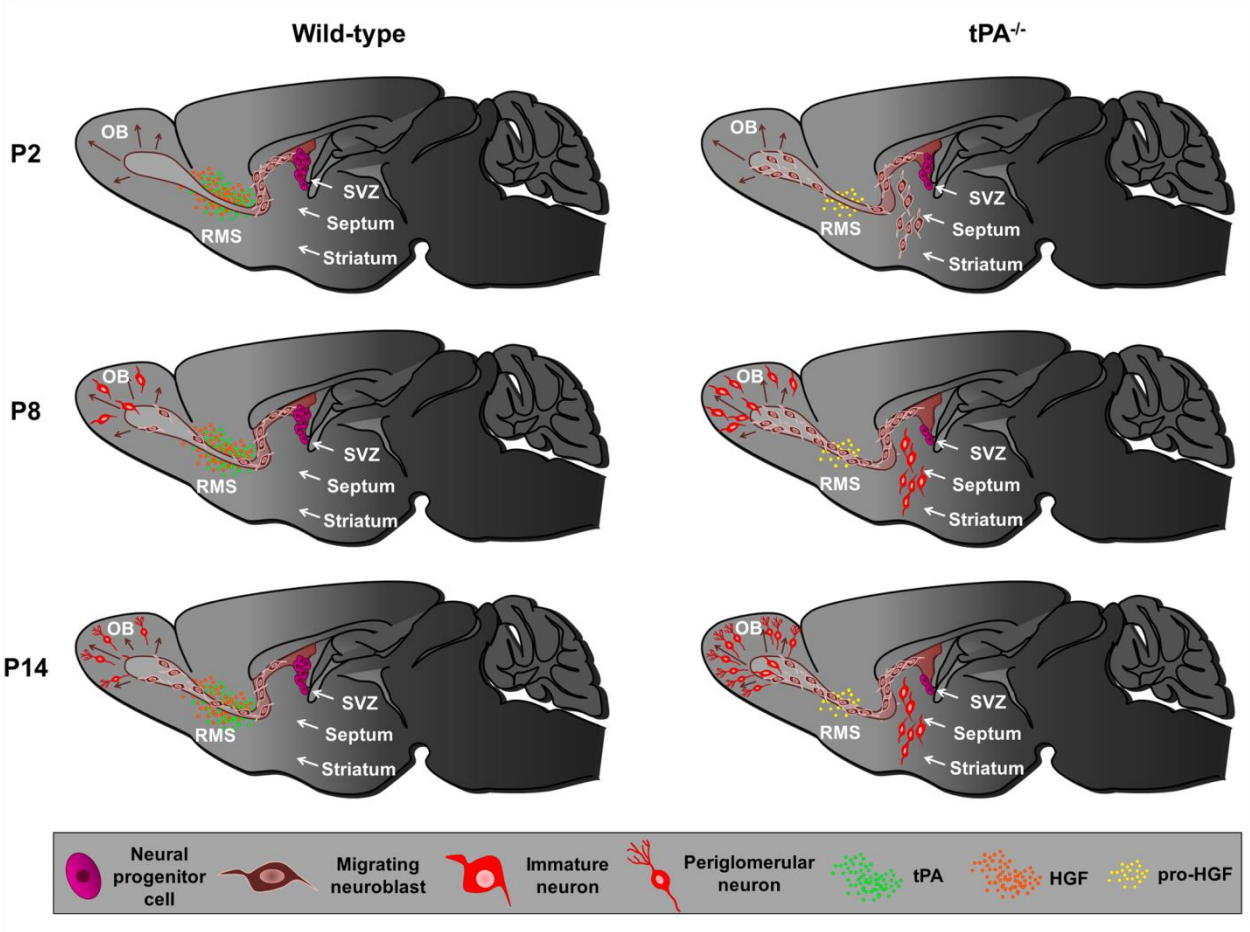
Wild-type
tPA-/-
P2
P8
P14
OB
RMS
SVZ
Septum
Striatum
Neural progenitor cell
Migrating neuroblast
Immature neuron
Periglomerular neuron
tPA
HGF
pro-HGF

Figure 1.2. Reduced HGF expression in tPA$^{-/-}$ mice leads to altered neuronal migration, neurogenesis, and proliferation. Compared to wild-type mice, at post-natal day 2 (P2) migrating neuroblasts from the SVZ in tPA$^{-/-}$ mice had an accelerated, but ectopic, migratory path into the striatum. Immunostaining for Ki67+ and doublecortin also demonstrated tPA$^{-/-}$ mice to have diminished cell proliferation and neurogenesis in the SVZ. In addition, enhanced neurogenesis in the olfactory bulb, as evidenced by increased BrdU labeling, was apparent at P8 and P14 in tPA$^{-/-}$ mice (Wang et al., 2011).

Figure 1.3

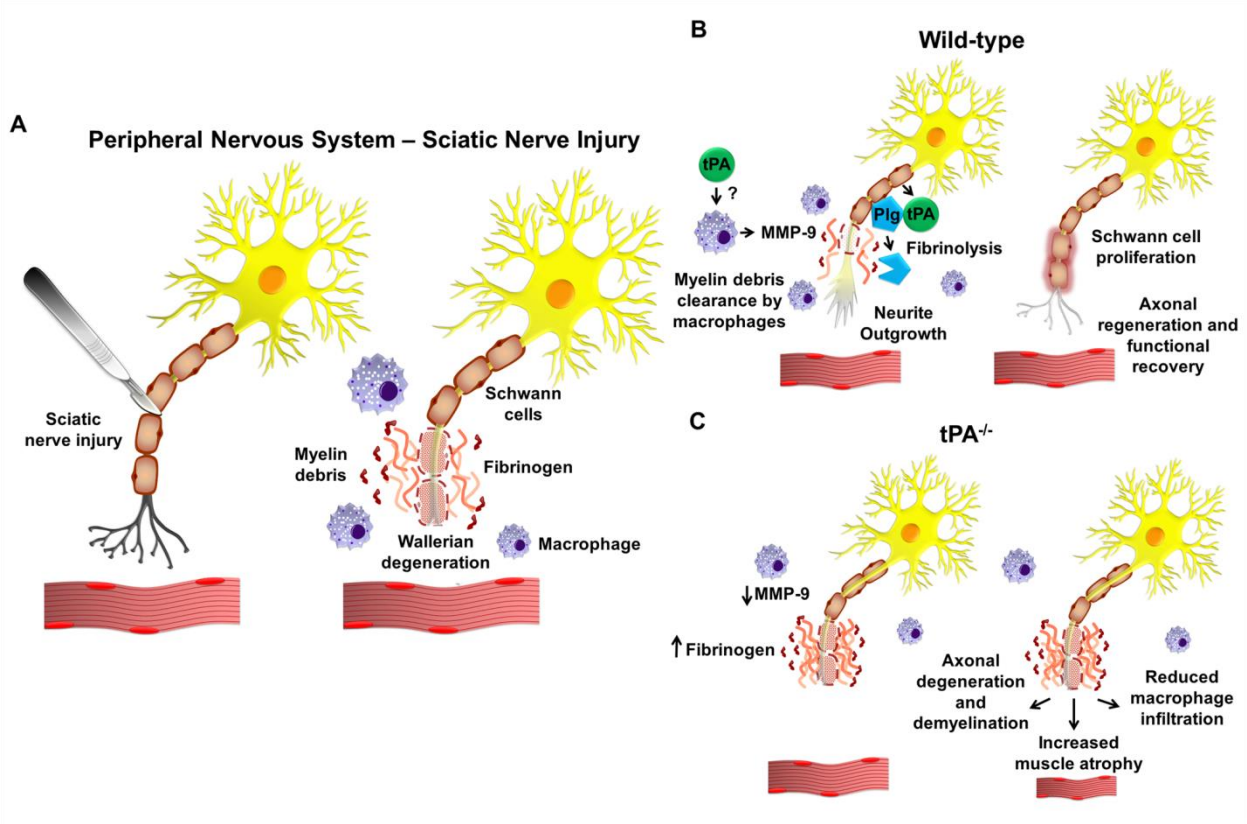
A
Peripheral Nervous System – Sciatic Nerve Injury
Sciatic nerve injury
Schwann cells
Myelin debris
Fibrinogen
Wallerian degeneration
Macrophage
B
Wild-type
tPA
?
MMP-9
Plg
tPA
Fibrinolysis
Myelin debris clearance by macrophages
Neurite Outgrowth
Schwann cell proliferation
Axonal regeneration and functional recovery
C
tPA-/-
↓MMP-9
↑Fibrinogen
Axonal degeneration and demyelination
Reduced macrophage infiltration
Increased muscle atrophy

Figure 1.3. Axonal degeneration and demyelination are exacerbated in tPA$^{-/-}$ mice after sciatic nerve injury. (A) Following peripheral nerve injury, such as in a model of sciatic nerve crush, Wallerian degeneration, whereby the distal axonal process of the injured neuron degenerates, occurs. Wallerian degeneration is accompanied by degradation of the myelin sheath and infiltration of macrophages. Macrophages and proliferating Schwann cells help to promote an environment that favors axonal regeneration. **(B)** Release of tPA from Schwann cells and subsequent tPA/plasmin-mediated fibrinolysis appears to be important for axonal regeneration and functional recovery, as **(C)** fibrinogen deposition correlates with axonal degeneration and demyelination and increased muscle atrophy in tPA$^{-/-}$ mice (Akassoglou et al., 2000). Following sciatic nerve injury, tPA$^{-/-}$ mice have also been shown to have reduced macrophage infiltration. Decreased macrophage expression of the extracellular matrix degradation enzyme MMP-9, of which tPA may directly or indirectly upregulate, was found to attenuate macrophage migration (Ling et al., 2006). Though other studies have shown that tPA can directly stimulate macrophage migration through its interaction with the integrin MAC-1 (Cao et al., 2006).

Figure 1.4

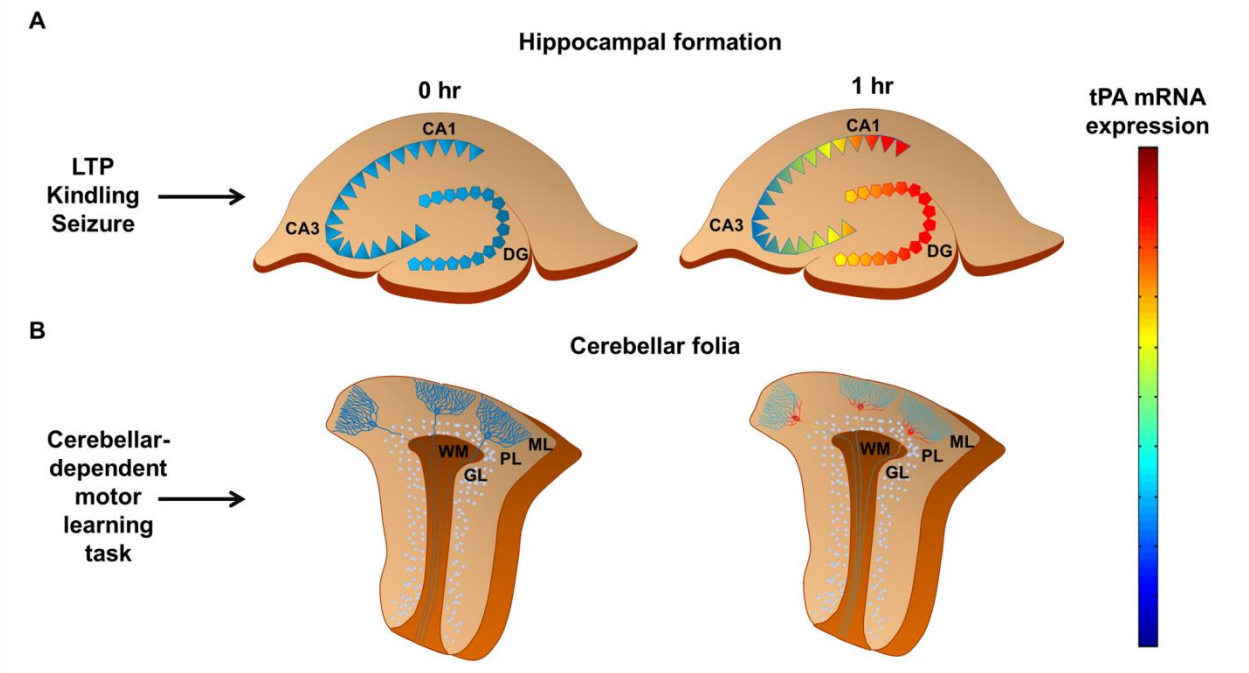
A
Hippocampal formation
0 hr
1 hr
tPA mRNA expression
LTP Kindling Seizure
CA1
CA3
DG
B
Cerebellar folia
Cerebellar-dependent motor learning task
WM
GL
PL
ML

Figure 1.4. Expression of tPA mRNA is upregulated by neuronal activity. (A) A differential screen of ~ 30,000 clones from a hippocampal complementary DNA library identified tPA as an immediate-early gene whose expression is elevated in the rat brain following three activity-dependent events: long-term potentiation (LTP), seizures, and kindling. LTP-induced increases in tPA mRNA expression were restricted to the granule cell layers of the dentate gyrus, while seizures and kindling induced tPA mRNA in both the granule and pyramidal cell layers of the hippocampus. Increased tPA mRNA levels were detectable by 1 hr following neuronal activity and remained elevated for at least 4 hrs (Qian et al., 1993). **(B)** In situ hybridization of tPA mRNA in rat cerebella also demonstrated induction of tPA mRNA expression in the Purkinje cell layers after rats learned a complex motor task. Levels of tPA mRNA were elevated 1 hr after performing a cerebellar-dependent motor learning test, and remained elevated for at least 4 hrs (Seeds et al., 1995). These studies by **(A)** Qian et al. (1993) and **(B)** Seeds et al. (1995) demonstrating upregulation of tPA mRNA expression following activity-dependent events implicated tPA in having a role in regulating neuronal plasticity.

Figure 1.5

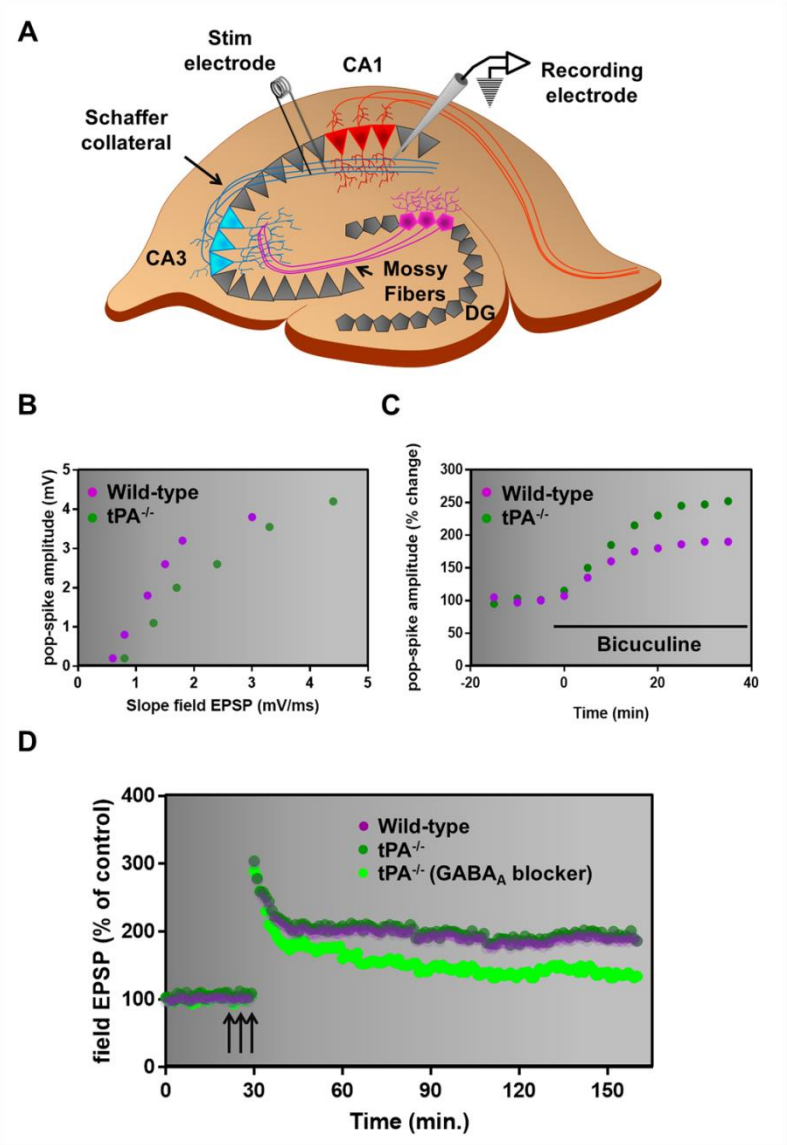
A
Stim electrode
CA1
Recording electrode
Schaffer collateral
CA3
Mossy Fibers
DG
B
Wild-type
tPA-/-
pop-spike amplitude (mV)
Slope field EPSP (mV/ms)
C
Wild-type
tPA-/-
pop-spike amplitude (% change)
Bicuculine
Time (min)
D
Wild-type
tPA-/-
tPA-/- (GABAA blocker)
field EPSP (% of control)
Time (min.)

Figure 1.5. Mice lacking the tPA gene display deficits in basal synaptic transmission in the CA1 hippocampal region. (A) In field potential recordings from hippocampal brain slices, Frey et al. (1996) performed some of the initial electrophysiological experiments of basal synaptic transmission and long-term potentiation in $tPA^{-/-}$ mice. **(B)** EPSP-pop spike relationship in stratum radiatum gathered from increasing stimulus intensities. EPSP-pop spike curve from $tPA^{-/-}$ mice displayed a rightward shift, indicating that in $tPA^{-/-}$ mice a larger stimulus is needed to evoke a pop-spike of similar amplitude to that seen in wild-type mice. **(C)** As paired-pulse behavior of the pop-spike in $tPA^{-/-}$ mice showed reduced facilitation, which can be suggestive of increased feedback inhibition, GABAergic transmission was examined. When blocking GABAergic transmission with the $GABA_A$receptor blocker bicuculine $tPA^{-/-}$ mice displayed increased facilitation. **(D)** Consistent with $tPA^{-/-}$ mice being under enhanced GABAergic transmission, no differences in the late phase of LTP between $tPA^{-/-}$ mice and wild-type mice were found. However, significant differences were seen when GABAergic transmission was blocked with the noncompetitive $GABA_A$ channel blocker picrotoxin.

Figure 1.6

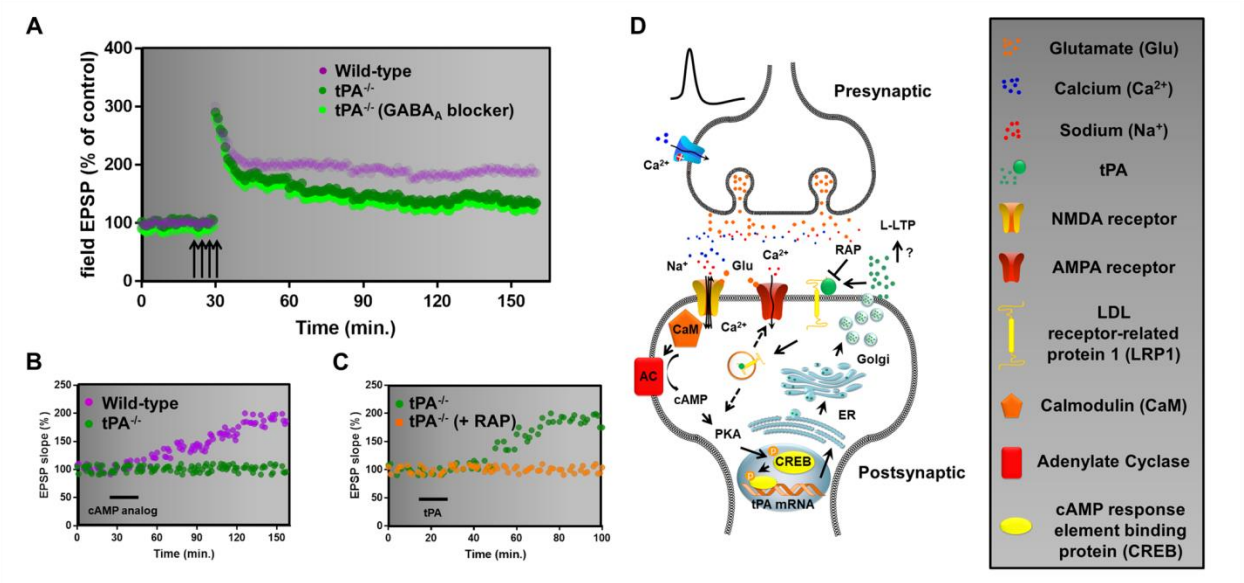
A
field EPSP (% of control)
Time (min.)
Wild-type
tPA-/-
tPA-/- (GABAA blocker)
B
EPSP slope (%)
Time (min.)
Wild-type
tPA-/-
cAMP analog
C
EPSP slope (%)
Time (min.)
tPA-/-
tPA-/- (+ RAP)
tPA
D
Presynaptic
Postsynaptic
Ca2+
Na+
Glu
L-LTP
RAP
CaM
AC
cAMP
PKA
CREB
tPA mRNA
Golgi
ER
Glutamate (Glu)
Calcium (Ca2+)
Sodium (Na+)
tPA
NMDA receptor
AMPA receptor
LDL receptor-related protein 1 (LRP1)
Calmodulin (CaM)
Adenylate Cyclase
cAMP response element binding protein (CREB)

Figure 1.6. Mice lacking the tPA gene display deficits in L-LTP in the CA1 hippocampal region. (A) In contrast to Frey et al. (1996) deficits in L-LTP at the Schaffer collateral-to-CA1 synapse of $tPA^{-/-}$ mice have been found by other groups (Huang et al., 1996; Calabresi et al., 2000; Zhuo et al., 2000). This deficit in L-LTP was apparent in $tPA^{-/-}$ mice with or without blocking GABAergic transmission. **(B)** The tPA gene, *Plat*, has a cAMP response element in its promoter and was shown to be a downstream effector gene important for L-LTP when activators of the cAMP/PKA-signaling pathway, such as the cAMP analog Sp-cAMP, induced synaptic potentiation in wild-type mice, but not $tPA^{-/-}$ mice. Sp-cAMP was previously shown to induce a L-LTP. **(C)** The endocytic signaling receptor LRP1 was also implicated in mediating tPA's role in L-LTP (Zhuo et al., 2000). While pharmacologic treatment of tPA induced synaptic potentiation in stratum radiatum of $tPA^{-/-}$ mice, this effect could be blocked when hippocampal slices were pretreated with the LRP1 inhibitor RAP. **(D)** Proposed model for upstream mediators of tPA gene transcription and post-synaptic release of tPA in L-LTP.

Figure 1.7

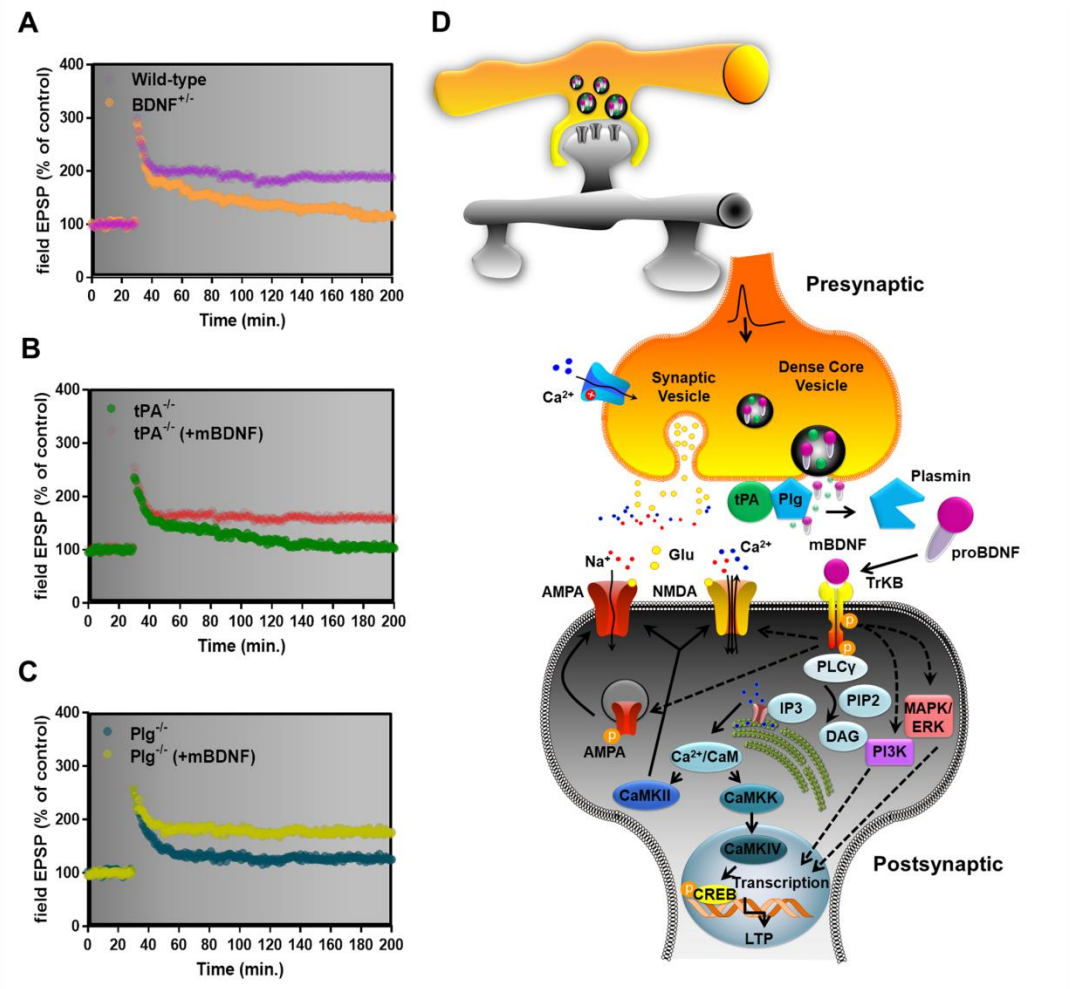
A
field EPSP (% of control)
Time (min.)
Wild-type
BDNF+/-
B
tPA-/-
tPA-/- (+mBDNF)
C
Plg-/-
Plg-/- (+mBDNF)
D
Presynaptic
Synaptic Vesicle
Dense Core Vesicle
Ca2+
tPA
Plg
Plasmin
proBDNF
mBDNF
TrkB
Na+
Glu
AMPA
NMDA
PLCγ
IP3
PIP2
DAG
MAPK/ ERK
PI3K
Ca2+/CaM
CaMKII
CaMKK
CaMKIV
Transcription
CREB
LTP
Postsynaptic

Figure 1.7. Cleavage of proBDNF by tPA/plasmin is critical for the full expression of L-LTP. (A) Previous work demonstrated that the neruotrophin BDNF plays an important role in L-LTP as hippocampal slices from heterozygous $BDNF^{+/-}$ mice have defects in L-LTP in the CA1 region. Mature BDNF (mBDNF) rescues L-LTP impairments in both $tPA^{-/-}$ **(B)** and $Plg^{-/-}$ mice **(C)**. Proposed model of presynaptic tPA/plasmin-mediated cleavage of proBDNF and mBDNF activated signaling pathways through its receptor TrKB. Three main pathways are known to be activated upon mBDNF binding to TrkB: the MAPK/ERK and PI3K pathways that induce transcription of genes important for neuronal survival and growth and the PLCgamma signaling cascade which regulates the transcription of genes involved in LTP. PLCgamma cleaves PIP2 into IP3 and DAG. IP3 stimulates Ca^{2+} release from the ER and elevated Ca2+ levels activate Ca^{2+}/Camodulin-dependent protein kinses (CamKII, CamKK and CamKIV). Subcellular localization studies using cultured hippocampal neurons demonstrated that BDNF and tPA are co-packaged in presynaptic dense core vesicles (Scalettar et al., 2012). Abbreviations: MAPK - Ras-mitogen-activated protein kinase; ERK - extracellular signal-regulated kinase; PLCγ – phospholipase Cγ; PIP_2 – phosphatidylinositol 4,5-bisphosphate (PtdIns(4,5)P2); Ca^{2+}/CaM - Ca2+/Calmodulin; CaMK - (Ca^{2+}/CaM)-dependent protein kinases; IP3 – inositol-1,4,5-trisphosphate (Ins(1,4,5)P3); DAG – diacylglycerol; PI3K – phosphatidylinositol 3-kinase.

Figure 1.8

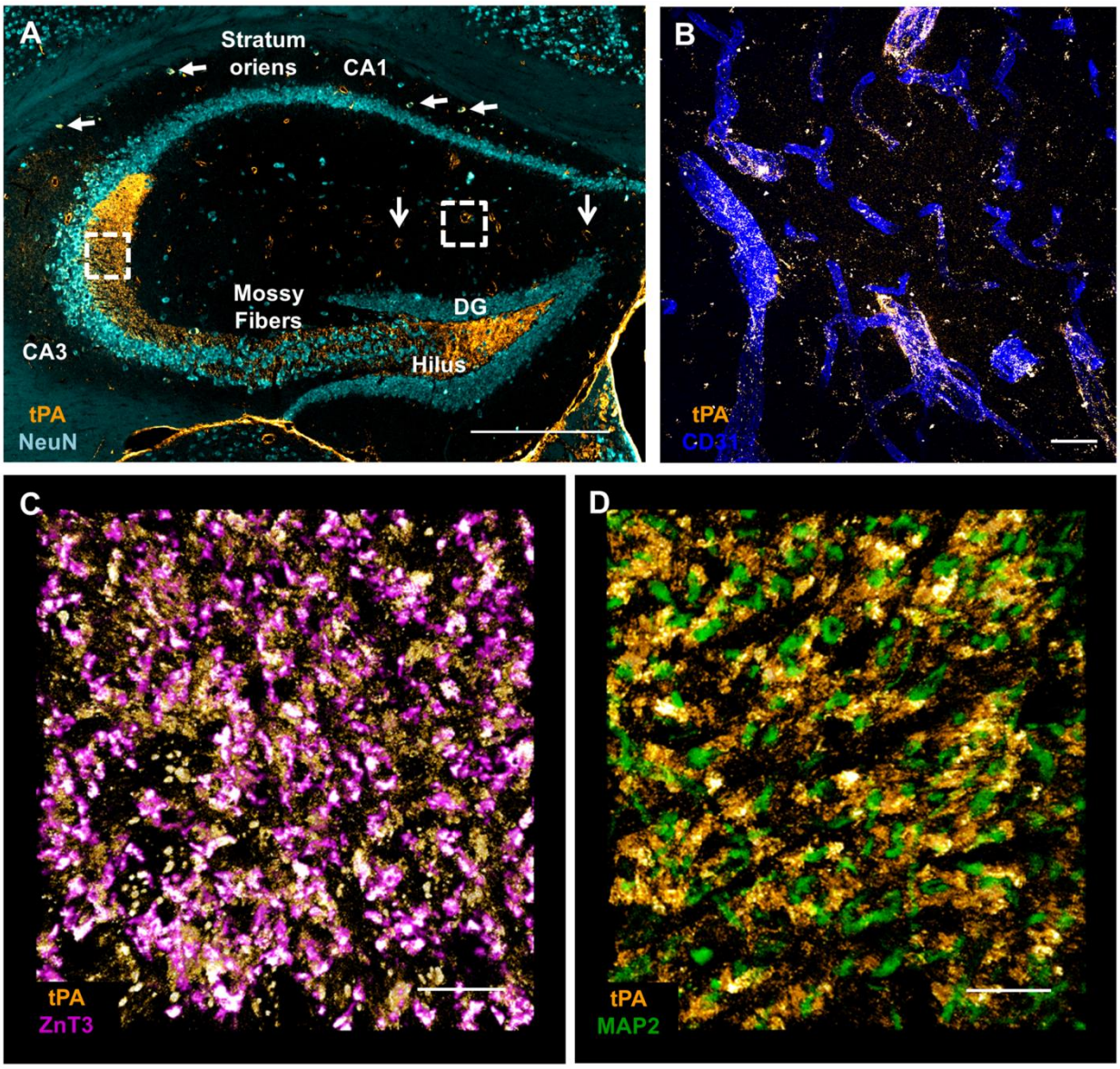
A
Stratum
oriens
CA1
Mossy
Fibers
DG
CA3
Hilus
tPA
NeuN
B
tPA
CD31
C
tPA
ZnT3
D
tPA
MAP2

Figure 1.8. Tissue plasminogen activator is highly expressed in blood vessels and in the hippocampus of the adult murine brain. (A) Coronal hippocampal section from a transgenic fusion reporter mouse that expresses a cerulean fluorescent protein tagged to tPA (Stevenson and Lawrence, 2018). Image has been pseudocolored so that tPA protein is in orange and the neuronal marker NeuN is in cyan. tPA protein is most apparent in the hilus and mossy fiber pathway, but also in blood vessels (open arrows) and neuronal cell bodies in the stratum oriens lamina (closed arrows). **(B)** Confocal 20 µm max projection (63x) of blood vessels in the hippocampal fissure showing that tPA protein is highly expressed in blood vessels stained with the endothelial cell marker CD31 (blue). **(C)** 3D max projection of a 5 µm z-stack from the stratum lucidum lamina of the hippocampus demonstrating colocalization of tPA-protein (orange) and the zinc transporter-3 (ZnT3, magenta), which is exclusively expressed in giant mossy fiber boutons. Areas of colocalization are seen in white. **(D)** 3D max projection of a 5 µm z-stack from the stratum lucidum lamina of the hippocampus demonstrating that tPA (orange) does not colocalize with the dendritic marker MAP2 (green), which detects the dendritic thorny excrescences of CA3 pyramidal neurons and are the post-synaptic partner to the mossy fiber boutons. Scale bars: A – 500 µm; B – 25 µm; C,D – 10 µm.

Figure 1.9

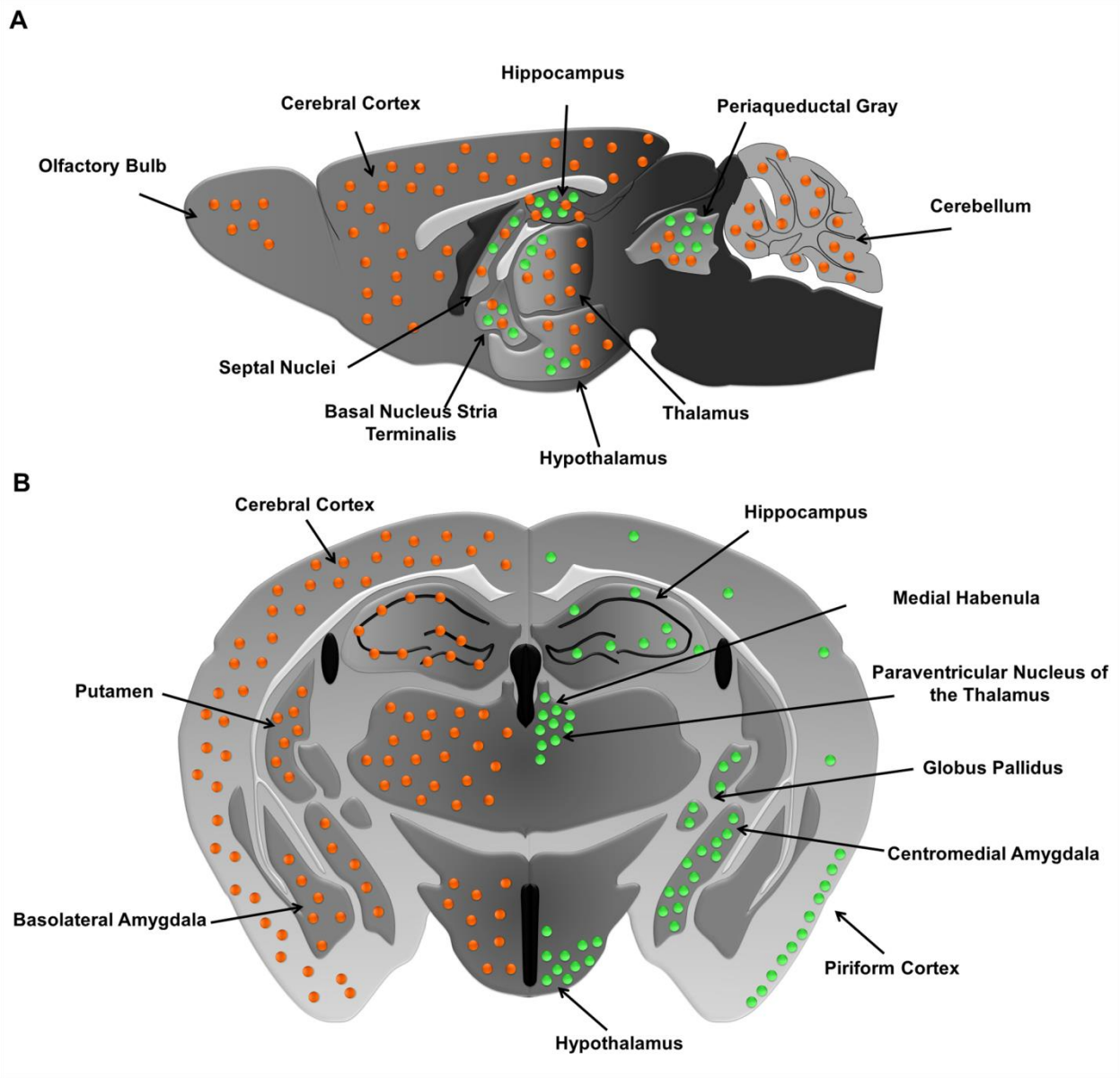
A
Hippocampus
Cerebral Cortex
Periaqueductal Gray
Olfactory Bulb
Cerebellum
Septal Nuclei
Basal Nucleus Stria Terminalis
Thalamus
Hypothalamus
B
Cerebral Cortex
Hippocampus
Medial Habenula
Putamen
Paraventricular Nucleus of the Thalamus
Globus Pallidus
Centromedial Amygdala
Basolateral Amygdala
Piriform Cortex
Hypothalamus

Figure 1.9. Schematic summary of tPA gene and protein expression in the adult murine brain. (**A**) Sagittal and (**B**) coronal sections illustrating the gene and protein expression pattern of tPA compiled from published reports. Orange dots represent gene expression of tPA from transgenic reporter mice (Stevenson and Lawrence, 2018; Yu et al., 2001) and *in situ* mRNA hybridization studies (Sappino et al., 1993), and green dots represent the expression pattern of somatic or trafficked tPA protein (Stevenson and Lawrence, 2018; Salles and Strickland, 2002; Louessard et al., 2016). While the tPA gene (orange) is highly expressed in the olfactory system, cerebellum, cortex, and subcortical brain structures, tPA protein (green) is more restricted and concentrated in nerve fibers in subcortical regions of or associated with the limbic system. Immunohistochemistry has revealed sparsely populated tPA-positive cell bodies in the somatosensory and piriform cortex as well as the stratum oriens layer of the hippocampus. Primarily, though, tPA protein is expressed in the mossy fiber pathway of the hippocampus, the globus pallidus nuclei of the basal ganglia, the centromedial nucleus of the amygdala, the hypothalamus and paraventricular nucleus of the thalamus, the medial habenula, the septal nuclei, the bed nucleus of the stria terminalis, and the periaqueductal (Stevenson and Lawrence, 2018).

Figure 1.10

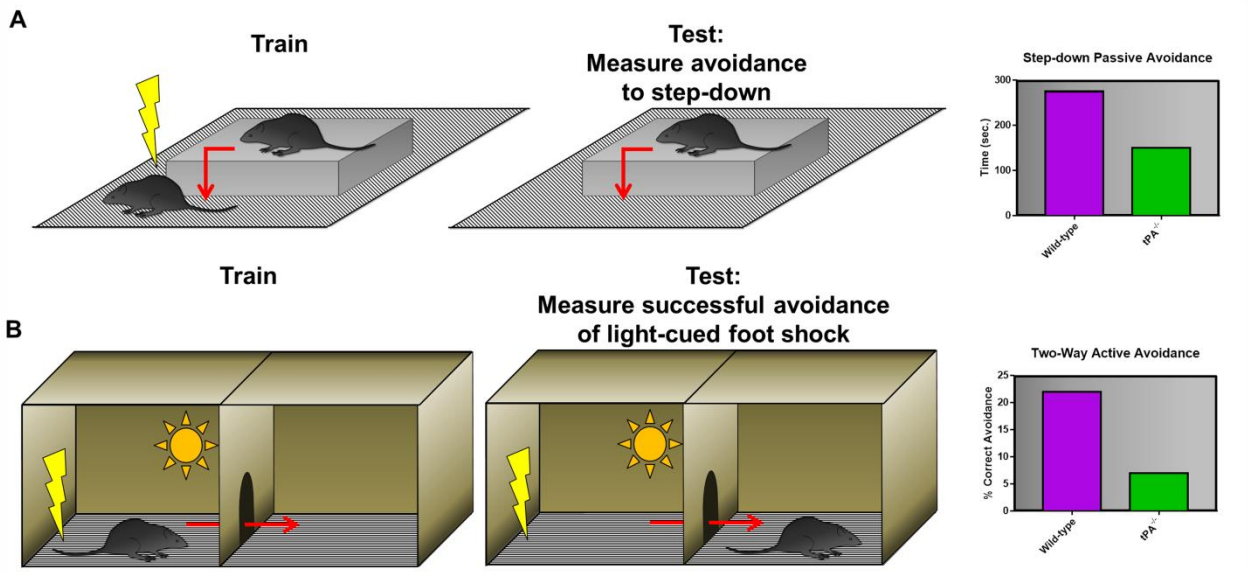
A
Train
Test:
Measure avoidance
to step-down
Step-down Passive Avoidance
Time (sec.)
300
200
100
0
Wild-type
tPA-/-
B
Train
Test:
Measure successful avoidance
of light-cued foot shock
Two-Way Active Avoidance
% Correct Avoidance
25
20
15
10
5
0
Wild-type
tPA-/-

Figure 1.10. Mice deficient in tPA have impairments in avoidance tests. In passive and active avoidance behavioral assessments, $tPA^{-/-}$ mice have been shown to have deficits in avoiding behaviors that increase anxiety and engaging in behaviors that decrease anxiety, respectively (Huang et al., 1996; Calabresi et al., 2000; Pawlak et al., 2002). **(A)** In a step-down passive avoidance task, during the training sessions, mice are placed on a raised platform and receive a foot shock if they step-down to the lower platform. To test if mice have learned to associate the lower electrical grid platform with foot shock, their latency to step-down time is measured during test trials. Compared to wild-type mice, $tPA^{-/-}$ mice were found to have significantly shorter latencies to step-down (Pawlak et al., 2002) . **B)** In an active two-way shuttle box avoidance task, during the training sessions, mice are presented with a light cue that precedes a foot shock. They are taught to move, upon presentation of that light, to the neighboring compartment to avoid the foot shock. Similar to the passive avoidance task, compared to wild-type mice, $tPA^{-/-}$ mice displayed impairments in their ability to correctly avoid the foot shock (Huang et al., 1996; Calabresi et al., 2000). These data indicated that mice lacking the tPA gene might have deficits in hippocampal-dependent earning. Subsequent studies demonstrating high expression of tPA in the centromedial amygdala and that $tPA^{-/-}$ mice are resistant to stress-induced anxiety, however, have complicated that interpretation (Pawlak et al., 2003). Indeed, the work by Pawlak et al. suggests that tPA's role in the amygdala and anxiety (Pawlak et al., 2003), not the hippocampus and learning, may be influencing the phenotypic behavioral output in these avoidance tasks.

Figure 1.11

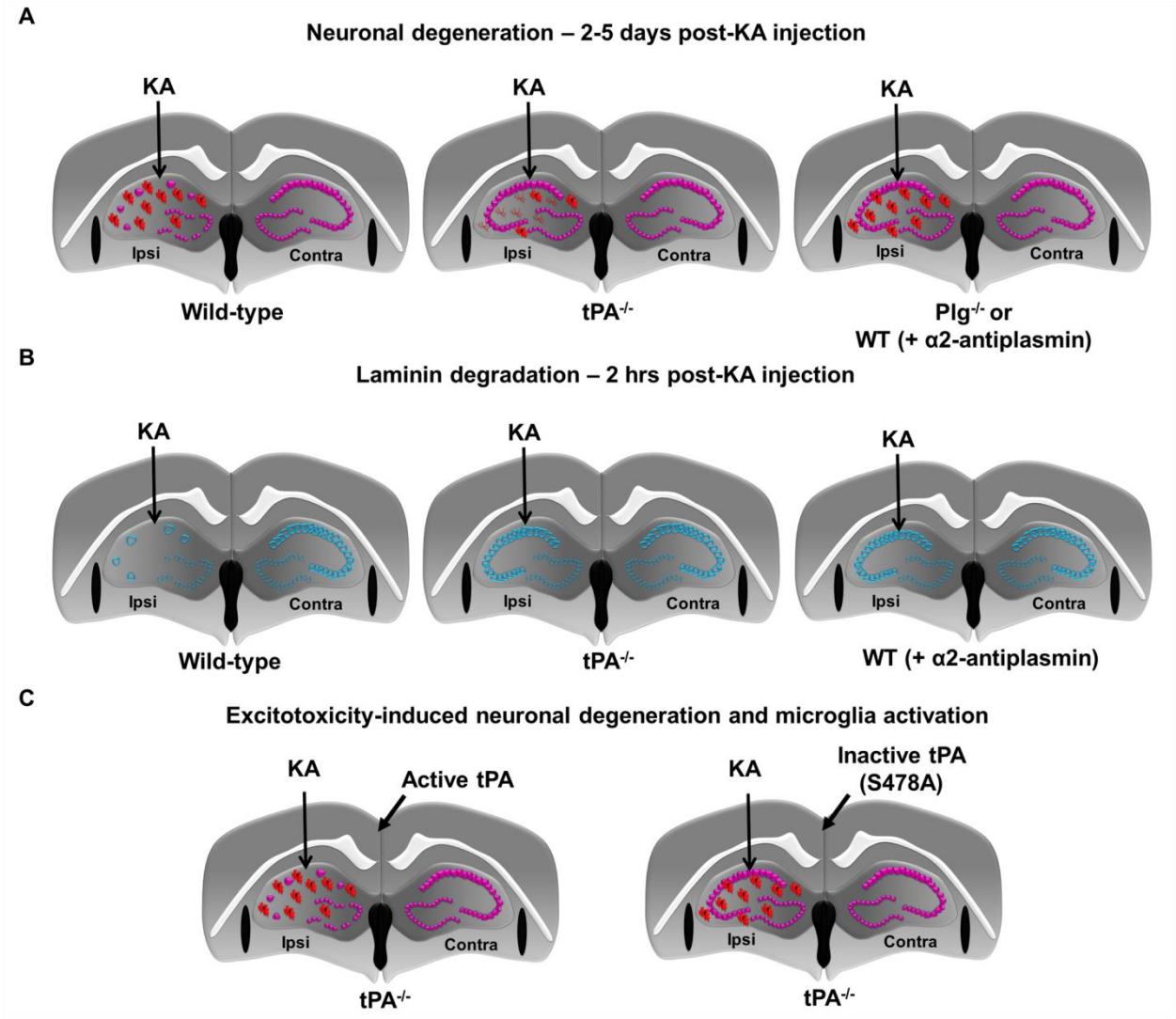
A
Neuronal degeneration – 2-5 days post-KA injection
KA
Ipsi
Contra
Wild-type
tPA-/-
Plg-/- or
WT (+ α2-antiplasmin)
B
Laminin degradation – 2 hrs post-KA injection
KA
Ipsi
Contra
Wild-type
tPA-/-
WT (+ α2-antiplasmin)
C
Excitotoxicity-induced neuronal degeneration and microglia activation
KA
Active tPA
Ipsi
Contra
tPA-/-
KA
Inactive tPA
(S478A)
Ipsi
Contra
tPA-/-

Figure 1.11. Tissue plasminogen activator mediates neuronal degeneration and microglial activation. (A) In a kainate (KA) – induced model of excitotoxicity, $tPA^{-/-}$ mice were protected against neuronal degeneration and they had reduced microglia activation. Mice deficient in plasminogen (Plg), the putative substrate of tPA, or wild-type mice treated with α2-antiplasmin, a serine protease inhibitor of plasmin, were also resistant to KA-induced neuronal degeneration, but had wild-type levels of microglia activation (Tsirka et al., 1995; Tsirka et al., 1997). **(B)** tPA/plasmin-mediated degradation of the extracellular matrix protein laminin, which is expressed perisomatically in the pyramidal and granule cell layers of the adult murine brain, was shown to precede and correlate with neuronal degeneration (Chen and Strickland, 1997). **(C)** Differential microglia activation in response to KA injections following Intrahippocampal infusions of active tPA or inactive tPA (S478A) into $tPA^{-/-}$ mice. Proteolytically active tPA was shown to be responsible for neuronal degeneration, while proteolytically inactive tPA mediates microglial activation (Rogove et al., 1999).

Figure 1.12

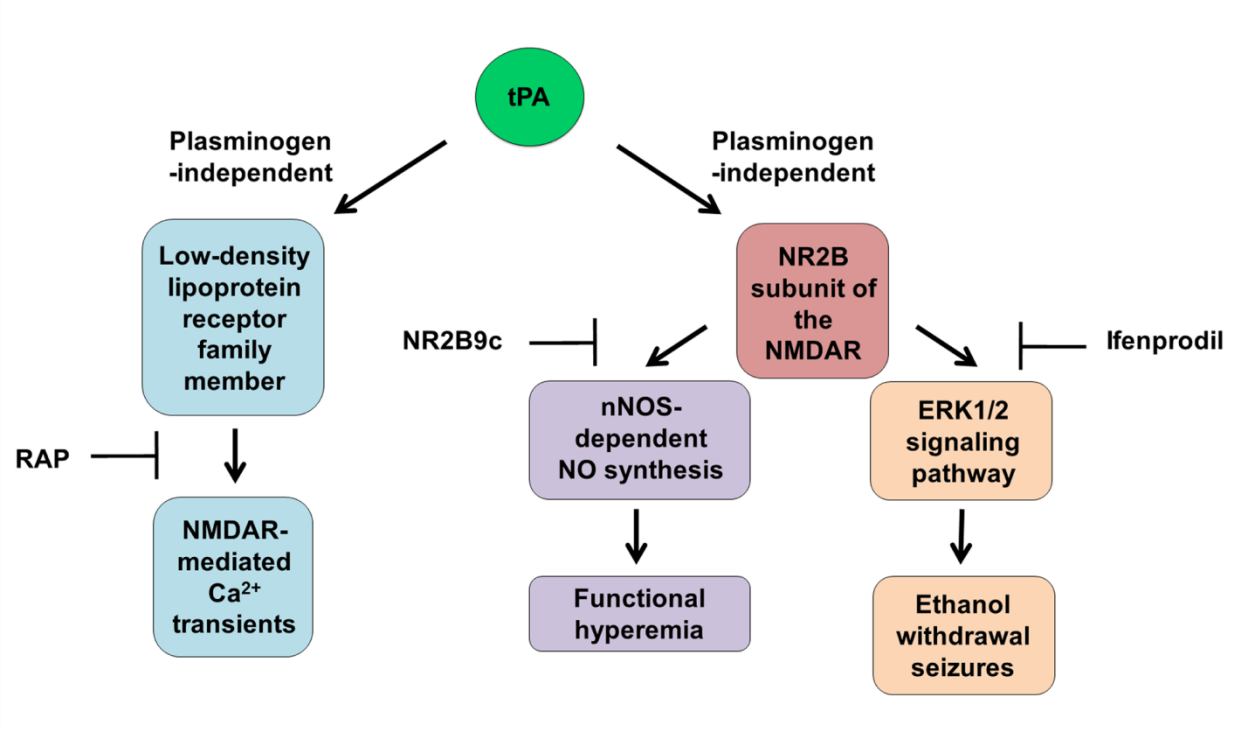
tPA
Plasminogen -independent
Plasminogen -independent
Low-density lipoprotein receptor family member
NR2B subunit of the NMDAR
NR2B9c
Ifenprodil
RAP
nNOS-dependent NO synthesis
ERK1/2 signaling pathway
NMDAR-mediated Ca^{2+} transients
Functional hyperemia
Ethanol withdrawal seizures

Figure 1.12. Modulation of NMDA receptor function by tPA. Using well-controlled *in vitro* model systems, Samson et al. (2008) demonstrated that a low-density lipoprotein receptor (LDLR) family member is required for tPA-mediated potentiation of NMDA-induced Ca^{2+} transients. tPA-induced potentiation of NMDAR-mediated Ca^{2+} transients can be blocked by the LDLR inhibitor RAP. This signaling was independent of plasminogen, but it required proteolytically active tPA. Functional hyperemia and ethanol withdrawal seizures have also been shown to be regulated by tPA signaling through the NMDAR, specifically via the NR2B subunit (Pawlak et al., 2005; Park et al., 2008). The NR2B subunit of the NMDAR is functionally coupled to nNOS. The cell permeable peptide inhibitor NR2B9c uncouples NMDAR activity from NO production. Using this inhibitor, Park et al. (2008) showed that wild-type mice had an attenuated neurovascular coupling response and that rtPA no longer rescued the functional hyperemia response in $tPA^{-/-}$ mice. tPA/NMDAR-signaling via the NR2B subunit has also been shown in a model of ethanol withdrawal seizures. Pawlak et al. demonstrated that tPA directly binds to the NR2B subunit and that activation of the NMDAR, as seen by downstream activation of ERK1/2, is downregulated in $tPA^{-/-}$ mice during ethanol withdrawal (Pawlak et al., 2005). $tPA^{-/-}$ mice have less severe ethanol withdrawal seizures than wild-type mice and injections of tPA into $tPA^{-/-}$ mice during ethanol withdrawal increases seizure severity. The NR2B inhibitor Ifenprodil blocks this tPA-mediated increase in seizure severity. Abbreviations: ERK1/2 – extraceulluar signal-regulated kinase; NMDAR – *N*-methyl-D-aspartate Receptor; nNOS – neuronal nitric oxide synthase; NO – nitric oxide; NR2B - *N*-methyl-D-aspartate Receptor subtype 2B; RAP – receptor-associated protein.

Figure 1.13

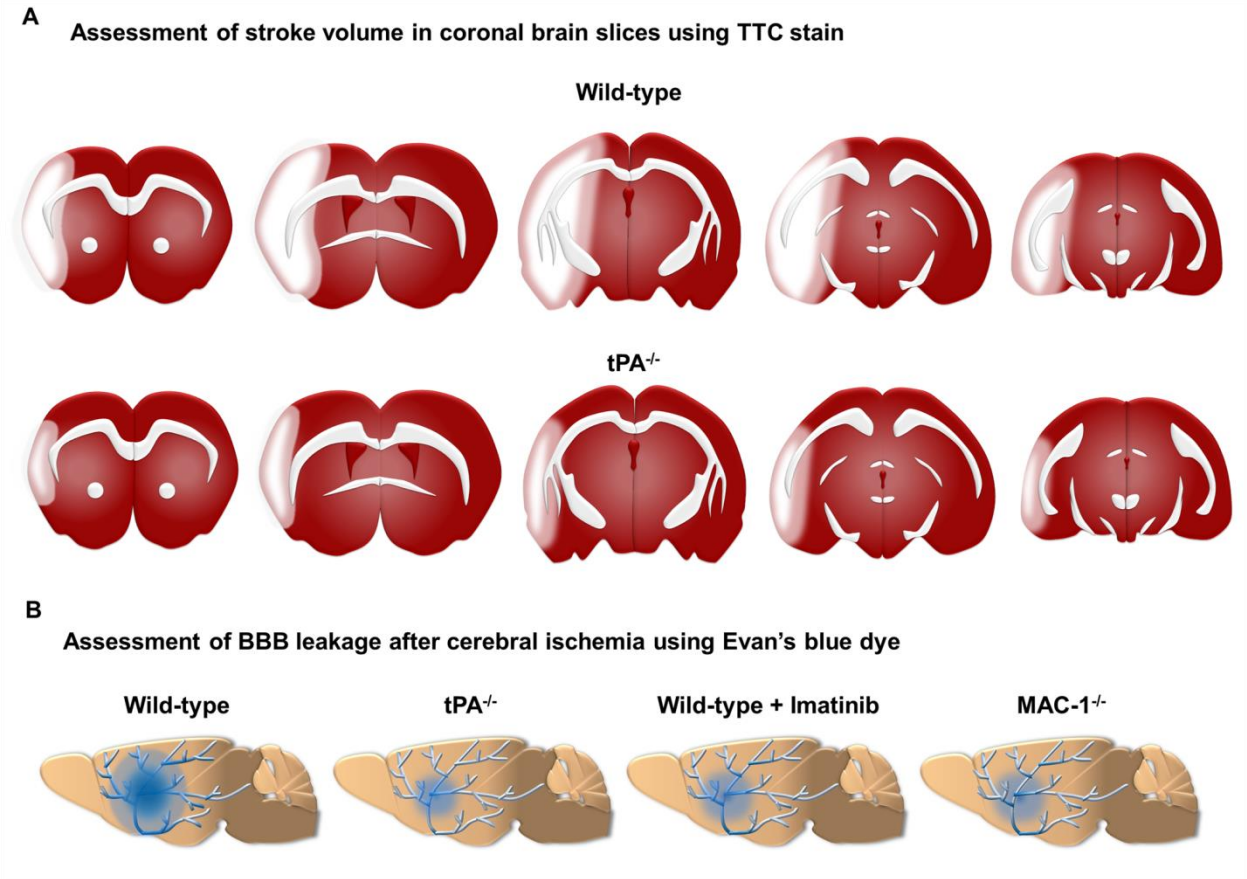
A
Assessment of stroke volume in coronal brain slices using TTC stain
Wild-type
tPA-/-
B
Assessment of BBB leakage after cerebral ischemia using Evan's blue dye
Wild-type
tPA-/-
Wild-type + Imatinib
MAC-1-/-

Figure 1.13. Mice deficient in tPA are protected during cerebral ischemia. (A) In a transient intravascular filament stroke model, Wang et al. (1998) was the first the demonstrate the $tPA^{-/-}$ mice have smaller infarct volumes and neuronal preservation following cerebral ischemia when compared to their wild-type controls. Stroke volume was quantified using a 2,3,5-triphenyltetrazolium chloride (TTC) stain that differentiates between metabolically active (red) and inactive (white) tissue. Though not tested, the role tPA plays in excitotoxicity-induced neuronal degeneration – via plasmin generation and laminin degradation – was suggested to play a part in promoting cell death in wild-type mice. **(B)** Subsequent studies, however, have also pointed to the role that tPA plays in regulating BBB leakage (Yepes et al., 2003; Su et al., 2008; Su et al., 2017). Following occlusion of the middle cerebral artery, $tPA^{-/-}$ mice have significantly less Evan's blue extravasation than wild-type mice. Blocking tPA-mediated signaling through the PDGFRα receptor using the tyrosine kinase inhibitor Imatinib and/or attenuating tPA-mediated generation of active PDGF-CC from latent PDGF-CC in MAC-1 null mice also decreases BBB leakage.

Figure 1.14

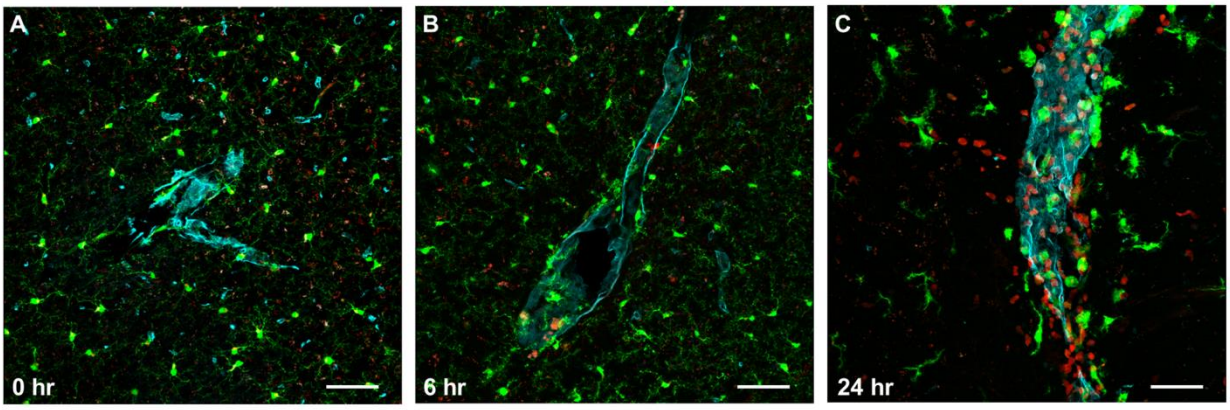

Figure 1.14. Time course of monocyte infiltration in the pneumbra after cerebral ischemia in R/G mice. Representative confocal images (20x) stained for the blood vessel marker podocalyxin (cyan) from the pneumbra of RFP+ (monocytes/macrophages) and GFP+ (microglia) brain sections 6 hrs and 24 hrs after MCAO (Su et al., 2017). At 0 hr (**A**, sham mice) and 6 hr (**B**) there is no or minimal detectable RFP+ monocytes in the parenchyma, but by 24 hr (**C**) there is a significant increase in infiltrating RFP+ monocytes in and around the blood vessels. These data indicate that resident microglia, not infiltrating monocytes/macrophages, are the source of MAC-1 and that microglial MAC-1 is responsible for mediating activation of PDGF-CC by tPA. Abbreviations: R/G – CX3CR1-GFP/CCR2-RFP; MCAO – middle cerebral artery occlusion. Scale bars: 50 μm.

Figure 1.15

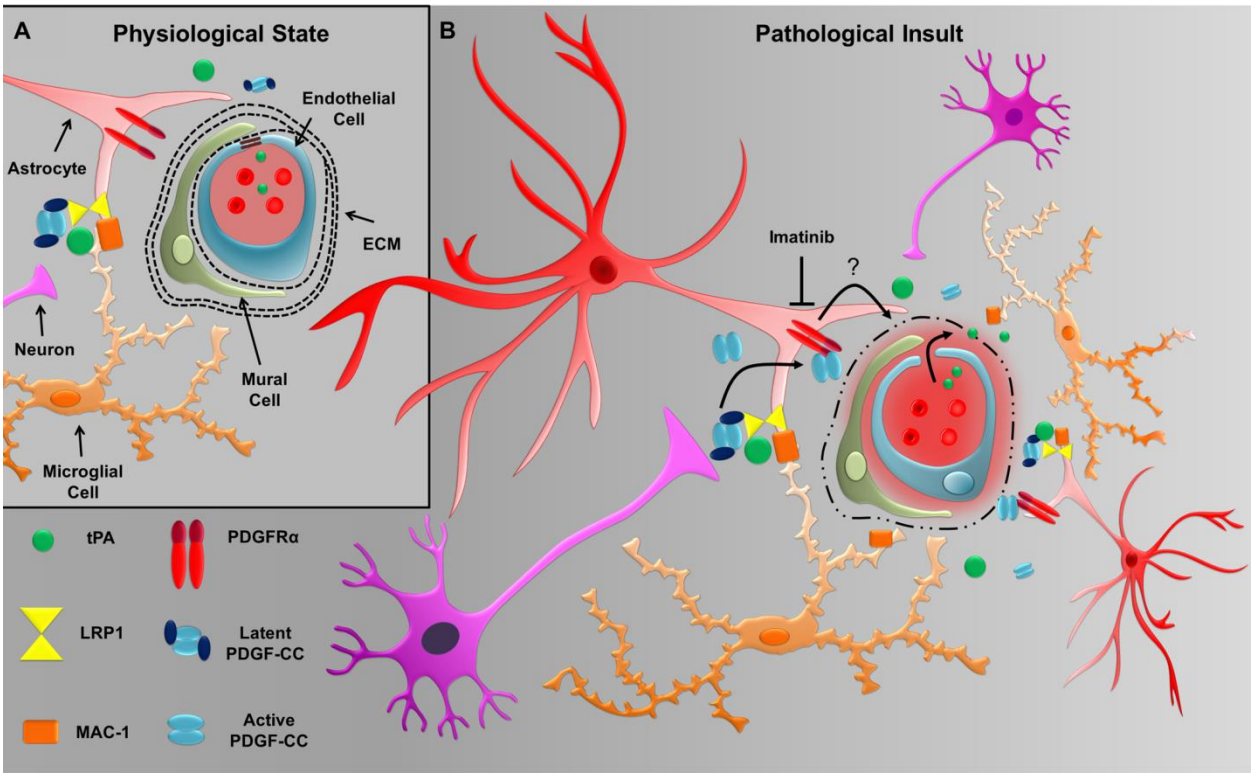
A
Physiological State
Endothelial Cell
Astrocyte
ECM
Neuron
Mural Cell
Microglial Cell
B
Pathological Insult
Imatinib
?
tPA
PDGFRα
LRP1
Latent PDGF-CC
MAC-1
Active PDGF-CC

Figure 1.15. Proposed model for tPA-mediated activation of PDGF-CC and BBB leakage. (A) The neurovascular unit is comprised of endothelial cells, mural cells (pericytes and smooth muscle cells), astrocytes, microglia and neurons. Immunohistochemistry and high-resolution confocal microscopy have demonstrated that the PDGFRα, LRP1, and MAC-1 are localized to the neurovascular unit (Fredriksson et al., 2015; Su et al., 2017). Potassium chloride (KCl)-induced membrane depolarization and oxygen glucose deprivation have been shown to stimulate the release of tPA *in vitro* from primary hippocampal and cortical neurons and clonal neuroendocrine cells (Gualandris et al., 1996; Parmer et al., 1997; Echeverry et al., 2010). It is unclear if the tPA/PDGF-CC/PDGFRα signaling pathway is activated under physiological conditions. **(B)** During pathological conditions, however, such as cerebral ischemia, microglial MAC-1 and LRP1 facilitate tPA-mediated activation of latent PDGF-CC into active PDGF-CC (Su et al., 2017). Binding of active PDGF-CC induces homodimerization and activation of downstream signaling of the PDGFRα that results in BBB leakage. Treatment with the tyrosine kinase inhibitor Imatinib preserves barrier integrity and reduces hemorrhagic bleeding after MCAO and late thrombolysis in mice (Su et al., 2008). The molecular mechanism by which PDGFRα activation leads to BBB disruption is unknown. With late thrombolysis, rtPA can cross the compromised barrier and exacerbate leakage by acting on endogenous tPA signaling pathways. Activation of the tPA/PDGF-CC/PDGFRα signaling pathway appears to be involved in the early loss of BBB integrity (Su et al., 2008; Su et al., 2017), while MMP9 from infiltrating neutrophils is responsible for ECM breakdown in the later stage of stroke and BBB damage (Justicia et al., 2003; Gidday et al., 2005). Moreover, the tPA/PDGF-CC/PDGFRα signaling pathway that regulates BBB has been implicated in other pathologies, including seizures, traumatic brain injury, amyotrophic lateral sclerosis, and experimental autoimmune encephalomyelitis (Su et al., 2008; Adzemovic et al., 2013; Rodriguez-Gonzalez et al., 2013; Fredriksson et al., 2015; Merali et al., 2015; Su et al., 2015; Zhan et al., 2015; Lewandowski et al., 2016; Wahlgren et al., 2016; Su et al., 2017). Abbreviations: PDGFRα – platelet derived growth factor receptor α; PDGF-CC – platelet derived growth factor-CC; LRP1 – low-density lipoprotein (LDL) receptor-related protein-1; MAC-1 – macrophage-1 antigen.

Chapter 2

Characterization of tissue plasminogen activator expression and trafficking in the adult murine brain

2.1 Abstract

Tissue plasminogen activator (tPA) is an immediate-early gene important for regulating physiological processes like synaptic plasticity and neurovascular coupling. It has also been implicated in several pathological processes including blood-brain barrier permeability, seizure progression, and stroke. These varied reports suggest that tPA is a pleiotropic mediator whose actions are highly compartmentalized in space and time. The specific localization of tPA, therefore, can provide useful information about its function. Accordingly, the goal of this study was to provide a detailed characterization of tPA's regional, cellular, and subcellular localization in the brain. To achieve this, two new transgenic mouse lines were utilized: (1) a PlatβGAL reporter mouse, which houses the β-galactosidase gene in the tPA locus and (2) a tPA^{BAC}-Cerulean mouse, which has a cerulean-fluorescent protein fused in-frame to the tPA C-terminus. Using these two transgenic reporters, we show that while tPA is expressed throughout most regions of the adult murine brain, it appears to be preferentially targeted to fiber tracts

---

This chapter represents a published article: Stevenson TK and Lawrence DA (2018) Characterization of tissue plasminogen activator expression and trafficking in the adult murine brain. eNeuro (in press).

in the limbic system. In the hippocampus, confocal microscopy revealed tPA-Cerulean (tPA-Cer) puncta localized to giant mossy fiber boutons and astrocytes in stratum lucidum. With amplification of the tPA-Cer signal, somatically localized tPA was also observed in the stratum oriens/alveus layer of both CA1 and CA3 subfields. Co-immunostaining of tPA-Cer and interneuronal markers indicates that these tPA-positive cell bodies belong to a subclass of somatostatin/oriens-lacunosum moleculare interneurons. Together, these data imply that tPA's localization is differentially regulated, suggesting that its neuromodulatory effects may be compartmentalized and specialized to cell-type.

2.2 Significance Statement

The serine protease tissue plasminogen activator (tPA) has been shown to modulate numerous neurological processes including synaptic plasticity and neurodegeneration. Many of the functional conclusions drawn about tPA activity, however, have not been affirmed by high-resolution, imaging analysis of tPA localization. To address these shortcomings, we utilized two new transgenic reporter mice to provide a detailed characterization of tPA expression in the adult murine brain. A comparison of these reporter mice demonstrates a differential expression pattern between where tPA is synthesized and where it is trafficked in the hippocampus, amygdala, and basal ganglia. Moreover, colocalization and co-expression analysis reveals that tPA is primarily trafficked to pre-synaptic structures and that it's predominant somatic and/or axonal localization is cell-type specific.

2.3 Introduction

Tissue plasminogen activator (tPA) is a serine protease expressed in vascular endothelial cells with a well-established role in fibrinolysis. Biomechanistic understanding of tPA's fibrinolytic function led to the development of recombinant tPA (rtPA) as a thrombolytic agent, and the current standard of care for moderate to severe ischemic stroke is thrombolytic therapy with rtPA (Prabhakaran et al., 2015). However, beyond 3-4.5 hrs following stroke onset, thrombolytic efficacy is diminished and there is an increased risk of hemorrhagic conversion, limiting the therapeutic window for rtPA administration (Ahmed et al., 2010; group et al., 2012). The molecular mechanisms responsible for the increased risk of hemorrhage are thought, in part, to occur from exogenously administered rtPA crossing the ischemic, compromised blood-brain barrier (BBB) and acting through endogenous tPA-mediated signaling pathways on the abluminal side of the vasculature in the central nervous system (CNS) to induce BBB opening (Su et al., 2008).

In addition to BBB regulation (Fredriksson et al., 2015) parenchymal brain tPA has been reported to be involved in other processes in the CNS, including neurite outgrowth (Krystosek and Seeds, 1981), regeneration (Akassoglou et al., 2000; Zou et al., 2006) synaptic transmission and synaptic plasticity (Frey et al., 1996; Huang et al., 1996; Wu et al., 2015), excitotoxic injury (Tsirka et al., 1995; Nicole et al., 2001; Siao and Tsirka, 2002), and neurovascular coupling (Park et al., 2008). One of the earliest studies implicating tPA in a non-fibrinolytic function found the serine protease to be an immediate-early gene that is upregulated in the hippocampus following seizures, kindling, and long-term potentiation (Qian et al., 1993), suggesting a proteolytic

mechanism for activity-dependent structural changes at the synapse. Subsequent *in situ* hybridization studies showed tPA mRNA expression predominantly in hippocampal pyramidal and granule cell layers, and the granule cell layer of the cerebellum (Sappino et al., 1993).

While gross anatomical localization studies of tPA protein and protease activity have consistently shown tPA in the hilus and stratum lucidum layer of the hippocampus (Sappino et al., 1993; Salles and Strickland, 2002), more detailed cellular localization studies of tPA protein expression have been inconsistent (Fredriksson et al., 2015; Louessard et al., 2016). tPA-immunoreactivity, following colchicine treatment to block axo-dendritic transport, has been reported in glutamatergic cortical neurons and in the pyramidal and granule cell layers of the hippocampus (Louessard et al., 2016). In contrast, Fredriksson et al. (2015) primarily detected tPA-immunoreactivity in endothelial cells and a subset of perivascular interneurons. At the subcellular level, tPA appears to have a polarized distribution, as it has been localized to dense core vesicles in both pre- (Silverman et al., 2005; Scalettar et al., 2012) and post-synaptic (Lochner et al., 1998; Shin et al., 2004; Lochner et al., 2006) compartments; though these studies were done *in vitro* using clonal neuroendocrine cell lines or primary hippocampal neurons.

These disparate findings on localization of tPA have complicated and contributed to the multivariate hypotheses that exist regarding tPA's function in the CNS. To address some of these discrepancies, we have utilized two transgenic mouse strategies: (1) a PlatβGAL reporter mouse, which has the β-galactosidase gene knocked-in to the tPA gene, *Plat*, and (2) a tPA^{BAC}-Cerulean (tPA^{BAC}-Cer) fusion mouse,

which has a cerulean-fluorescent protein fused to tPA. The tPA^{BAC}-Cer mice were generated using bacterial artificial chromosome (BAC) technology. Critically, large transgene vectors, like BACs, are more likely than smaller plasmids to produce copy-number dependent transgene expression, and thereby, recapitulate endogenous gene expression patterns (Van Keuren et al., 2009). In parallel analysis of coronal sections from PlatβGAL and tPA^{BAC}-Cer mice, our results demonstrate that tPA's protein localization is uncoupled from its site of synthesis. This differential expression pattern is most prominent in the hippocampus, but it is also pronounced in the amygdala and basal ganglia. Moreover, using high-resolution confocal microscopy, in the hippocampus we found tPA to be localized to giant mossy fiber boutons and astrocytes in stratum lucidum and somatically localized to interneurons in stratum oriens/alveus. Co-expression analysis indicates that these tPA-positive cell bodies in the hippocampus belong to a subset of somatostatin/oriens-lacunosum moleculare inhibitory interneurons. These results suggest that tPA is differently trafficked and positioned to have diverse modulatory effects on synaptic efficacy based on cell-type and subcellular localization.

2.4 Materials and Methods

2.4.1 Transgenic mice

2.4.1.1 tPA^{BAC}-Cerulean transgenic mice. Founder lines (863 and 876) for tPA^{BAC}-Cer transgenic mice were generated using BAC technology. To generate tPA^{BAC}-Cer transgenic mice, exon 14 of the tPA gene, *Plat*, on a 162.524 kb BAC acquired from chori.org (RP23-259A10) was replaced with a cerulean fluorescent gene fused to the carboxy terminal of exon 14 of the murine tPA gene (NM_008872.2) followed by a

bovine growth hormone polyadenylation signal sequence. The tPA-Cer fusion gene is under control of the endogenous regulatory elements contained in the *Plat* locus. BAC DNA integrity was verified by restriction enzyme analysis via pulse field gel electrophoresis and exon sequencing prior to pronuclear microinjection of supra-ovulated eggs from (C57BL/6 x SJL)F1/TAC female mice. Transgenic mice were genotyped by PCR using primers that were specific to a remnant of the sub-cloning PGKneo vector and the tPA-Cer fusion gene (FWD 5' – CAT GAA GCA AGG ATC CAT GG – 3', and REV 5' – GGA ACT TCG CGG CCG CAG C – 3'); and tPA protein expression was confirmed by analysis of brain homogenates from the founder lines. After PCR analysis of the cerulean fusion gene confirmed stable, germline transmission in F1 pups two founder lines - lines 863 and 876 - were propagated; these mice were then backcrossed at least 8 generations onto a C57BL/6J genetic background. Transgenic mice displayed normal gross anatomy and a Mendelian inheritance pattern.

2.4.1.2 PlatβGAL reporter mice. The PlatβGAL mice were acquired from the UC Davis Knockout Mouse Project (KOMP) Repository (Project ID: VG15085) on a C57BL/6NTac background. PlatβGAL mice were then backcrossed onto a C57BL/6J background for at least 10 generations. Per the KOMP Repository, PlatβGAL mice were generated by inserting a *LacZ*-containing targeting vector between exon 2 and 14 to produce a null allele. The insertion sites of the PlatβGAL mice were sequenced to confirm the appropriate insertion of the *LacZ* gene in the *Plat* locus.

All animals were housed in a controlled environment and were provided with food and water *ad libitum*. All animal experiments were approved by the Institutional Animal

Care and Use Committee at the University of Michigan, USA, and the studies were conducted in accordance with the United States Public Health Services Policy on Humane Care and Use of Laboratory Animals.

2.4.2 Protein expression analysis

2.4.2.1 Sample preparation. Total tPA protein and enzymatic activity were analyzed using whole brain homogenates from tPA^{BAC}-Cer mice. The total and active tPA values from tPA^{BAC}-Cer transgene positive mice were normalized to transgene negative littermate controls for each experimental run. Two independent experiments were carried out for a combined total of 6-7 mice per transgenic line. Briefly, brains were harvested into ice-cold extraction buffer (0.4 M HEPES, 0.1 M NaCl, pH 7.4, 1% Triton X-100), homogenized for 1 min. (2 x 30 sec) and centrifuged at 10,000 x g for 10 min The supernatant was removed to a new, chilled 1.5 mL microcentrifuge tube and centrifuged again at 10,000 x g for 10 min. The supernatant was again removed to a new, chilled 1.5 mL microcentrifuge tube and used for ELISA, Luminex, and SDS-PAGE zymography assays.

2.4.2.2 Enzyme-linked immunosorbent assay (ELISA). An ELISA was performed to measure tPA activity from brain tissue extracts. Briefly, avidin-coated microtiter plates (Molecular Innovations, AVI-PLATE) were incubated with a biotin-conjugated PAI-1 capture (1 µg/ml; Molecular Innovations, NTBIOCPAI) for 30 min at room temperature. After which, 100uL of brain extract samples were loaded onto the plate and incubated for 1hr. at room temperature. A Rabbit anti-human tPA (3 µg/mL; Molecular Innovations,

ASHTPA-GF) was used as the primary antibody and a Donkey anti-rabbit HRP (1:5000; Jackson ImmunoResearch, 711-036-152) was used as the secondary. All sample and antibody incubations were followed by 3 washes of PBS-0.05% Tween-20. After the final wash, 3,3',5,5'-Tetramethylbenzidine (TMB) substrate (Molecular Innovations, TMB) was added to each sample for 3 min at room temperature. H_2SO_4 (1 N) was then added and the plate read on a spectrophotometer at 450 nm.

2.4.2.3 Luminex. To measure total murine tPA protein from tPA^{BAC}-Cer brain extracts, 50 µg of Rabbit anti-murine tPA (mtPA; Molecular Innovations, ASMTPA-GF-HT) was coupled to Luminex carboxylated beads for mtPA capture. Standards of known concentration of murine tPA (Molecular Innovations, MTPA) and brain extract samples (diluted in 0.4 M HEPES, 0.1 M NaCl pH7.4, 1.0% Triton X-100) were loaded onto a 96 well filter plate (Millipore) and incubated with 5000 beads (PBS – 1.0% Bovine Serum Albumin, BSA) for 2 hrs at room temperature in the dark. The solution from was removed from each well and washed twice with PBS - 0.05% Tween-20. The beads were then mixed with continuous shaking in the dark at room temperature for 1 hour with 2 µg/mL biotin-labeled Rabbit anti-mouse tPA-high titer (Molecular Innovations, ASHTPA-HT), after which 10 µg/mL of Streptavidin, R-Phycoerythrin (ThermoFisher Scientific, S866) was added to each well for 1 hour. The solution was removed from each well and the beads were washed three times with PBS-0.05% Tween-20 and, lastly, sheath fluid was added for 5-10 mins. The beads were then read with the Luminex 100 (medium setting; 10 µL sample size; 100 events/bead).

2.4.2.4 SDS-PAGE zymographies. Gel electrophoresis and zymography were performed as previously described (Huarte et al., 1985). Briefly, 1 µg of protein from homogenized whole brain tissue extracts from transgene positive and transgene negative tPA^{BAC}-Cer mice were loaded onto an in-house prepared 10% polyacrylamide gel with plasminogen ($[10.0\ \mu g/ml]_{FINAL}$) and casein ($[1.0\ mg/ml]_{FINAL}$). Samples were run for 30 min at 100 V through the stacking gel and 200 V for 40 min through the running gel. Gel was washed 4x30 min in 2.5% Tx-100 (dH_2O) and then briefly washed for 5 min. in 0.1 M Tris buffer (pH 8.1) before developing in 0.1 M Tris buffer at 37 °C for 4 hrs. Gels were stained with Bio-Safe Coomasie (Bio-Rad, 1610786); bands devoid of stain indicate areas of proteolytic activity.

2.4.3 Immunofluorescence and histochemical analysis

2.4.3.1 Sample preparation. Mice were anesthetized with isoflurane and sacrificed by transcardiac perfusion for 3 min with PBS followed by perfusion for 5 min with 4% paraformaldehyde (PFA). Brains were harvested and post-fixed in 4% PFA for 1hr at 4 C, then overnight in PBS. The brains were then moved to a 30% sucrose solution and kept at 4 C till submerged. Subsequently, dorsal hippocampal sections (14 µm and 50 µm) and serial sections (14 µm, bregma +1.0 to bregma -8.0) were cut coronally for immunofluorescence analysis of tPA expression. When using the Rabbit anti-mtPA antibody, sections underwent antigen retrieval (DAKO, S1700); the additional antigen retrieval step was not necessary for other antibodies. Sections were permeabilized with 0.50% Triton X-100 (PBS) for 20 min at room temperature and blocked in 3% BSA (PBS) for 1 hr at room temperature. The sections were then incubated with primary

antibodies in 2% BSA (PBS) overnight at 4 C, followed by incubation with secondary antibodies in 2% BSA (PBS) for 1 hr at room temperature. When using biotin-conjugated primary antibodies and their respective streptavidin-conjugated secondary was used, a biotin-blocking kit was used to reduce background (ThermoFisher Scientific, E21390) and for amplification using the Tyramide SuperBoost Kit (ThermoFisher Scientific, B40932) detection protocols were followed according to the manufacturer's instructions.

2.4.3.2 Primary and secondary antibodies. The primary antibodies used were as follows: calbindin D28K (Rabbit anti-Calbindin, 1:500; Synaptic Systems, 214002; Lot# 214002/3), microtubule-associated protein 2 (Rabbit anti-MAP2, 1:1000; Millipore, AB5622; Lot# 2624211), zinc transporter 3 (Guinea Pig anti-ZnT3, 1:500; Synaptic Systems, 197004; Lot# 197004/4), excitatory amino acid transporter 2 (Rabbit anti-EAAT2, 1:500; Synaptic Systems, 250203; Lot# 250203/3), GFP (Chicken anti-GFP, 1:1000; abcam, ab13970; Lot# GR236651-7 and GR236651-14), NeuN (Guinea Pig anti-NeuN, 1:400; Synaptic Systems 266004; Lot# 266004/2-14 and 266004/7), GAD65 (Guinea Pig anti-GAD65, 1:500; Synaptic Systems 198104; Lot# 198104/7), murine tissue plasminogen activator (Rabbit anti-mtPA, 12µg/mL; Molecular Innovations, ASMTPA-GF-HT; Lot# 804 and 914), metabotropic glutamate receptor type 1a (Rabbit anti-mGluR1a, 1:200; Sigma, G9665; Lot# SLBL4165V), somatostatin (Rat anti-SST, 1:100; Millipore, MAB354; Lot# 2885355, 3005269), CD31 (Rat anti-mCD31, 1:100; BD Biosciences, 550274; Lot # 21055). The secondary antibodies used were as follows: Biotin-conjugated Goat anti-Chicken IgY H&L (1:100; abcam, ab6876), Goat anti-

Guinea Pig IgG (H+L) 568 (1:500; ThermoFisher Scientific, A-11075), Donkey anti-Rabbit IgG (H+L) 568 (1:500; ThermoFisher Scientific, A-10042), Donkey anti-Guinea Pig IgG (H+L) 594 (1:500; Jackson ImmunoResearch, 706-585-148), Donkey anti-Rat IgG (H+L) 594 (1:500; ThermoFisher Scientific, A-21209), Donkey anti-Rabbit IgG (H+L) 594 (1:500; ThermoFisher Scientific, A-21207), Tyramide-conjugated Alexa Fluor 488 (ThermoFisher Scientific, B40953). The sections were mounted using VectaShield anti-fade mounting medium (Vector Laboratories, H-1000).

2.4.3.3 5-Bromo-4-Chloro-3-Indolyl-β-D-Galactoside. Heterozygous, homozygous, and wildtype PlatβGAL mice (mice, n = 3 – 5 per genotype) were used to examine the regional somatic expression of tPA. Homozygous PlatβGAL mice, which are null for tPA with two copies of the β-Gal gene, served as control mice for immunohistochemical stains that used an antibody directed against mtPA. PlatβGAL mice were anesthetized with isoflurane and sacrificed by transcardiac perfusion for 3 min with PBS and 1 min with 2% PFA, and post-fixed in 2% PFA for 1 hr at 4 C. Brains were then cryopreserved and sectioned by microtome. Dorsal hippocampal sections and serial sections (50 µm, bregma +1.0 to bregma -8.0) were stained and analyzed for LacZ reporter gene expression using the β-Galactosidase Reporter Gene Staining Kit (Sigma, GALS).

2.4.4 Image acquisition, processing, and analysis

2.4.4.1 Widefield and confocal microscopy. For PlatβGAL and tPA^{BAC}-Cer transgenic mice, low-resolution images were acquired on an inverted Nikon Te2000 widefield microscope equipped with a MicroPublisher 5.0 RTV color camera and a CoolSNAP

HQ2 CCD camera or an inverted Ti Nikon widefield microscope with an ANDOR Zyla sCMOS camera. High-resolution fluorescent images of the dorsal hippocampus in tPA^{BAC}-Cer transgenic mice were taken using an upright confocal laser scanning microscope (Leica SP5X). The SP5X is equipped with an acousto-optical beam splitter (AOBS) and a tunable white-light laser; accordingly, the following Ex/Em combinations were used: Cerulean (458/468-558) and Alexa Fluor 568 (568/578-720); and Alexa Fluor 488 (488/498-584) and Alexa Fluor 594 (594/604-750). Images were acquired with a 20x multi-immersion objective or a 63x oil objective (Plan-Apo, 1.4 numerical aperture, NA) at a scanning rate of 200 Hz with 4x line averaging at 2x or 4x optical zoom. Each frame consists of 512 x 512 pixels or 1024 x 1024 pixels. Z-stacks were collected at 0.5 µm or 1 µm increments, ranging in total thickness from 5.0 µm to 35 µm, respectively, with the pinhole set to 1 Airy unit.

2.4.4.2 Image processing and colocalization analysis. Widefield images (4x, 10x, 20x, or 40x objectives) of hippocampal and serial sections from PlatβGAL mice and tPA^{BAC}-Cer transgene positive and transgene negative mice were stitched using MetaMorph Image Analysis software or Nikon's NIS-Elements Advanced Research software package, respectively. Further processing was done using the open source image processing package FIJI (Schindelin et al., 2012). Confocal images are presented as either maximum intensity projections, orthongonal slices, or 3D maximum projections using FIJI's 3D viewer (Schmid et al., 2010).

Subcellular colocalization analysis of tPA-Cer puncta in stratum lucidum was performed using the JACoP (Just Another Colocalization Plugin) analysis software in

FIJI (Bolte and Cordelieres, 2006). Images were concatenated from 5 µm z-stacks (Δz = 0.5 µm) that were independently acquired 2 – 4 times (ZnT3: mice n = 10, lines 863 and 876; EAAT2: mice n = 6 - 8, lines 863 and 876, respectively; MAP2: mice n = 4, lines 863 and 876). Manders coefficient and Costes randomization control were used to quantify tPA-Cer colocalization (Costes et al., 2004; Bolte and Cordelieres, 2006; Dunn et al., 2011). The Manders coefficient was chosen because it is a more sensitive measure of colocalization for partial colocalization events and when there are large differences in fluorescent intensity between fluorophores (Bolte and Cordelieres, 2006; Dunn et al., 2011). The Manders coefficient, which doesn't mathematically take into account average fluorophore intensity values, ranges from 0 to 1, with 0 corresponding to no overlap and 1 to complete overlap. Two coefficients are given: M1 and M2, where M1 is the summed intensities of fluorophore 1 that are coincident with fluorophore 2, divided by the total intensity of fluorophore 1; M2 is calculated the same but for fluorophore 2. Costes randomization control provides a statistical assessment of whether or not observed colocalization events could be expected to occur by chance. It is calculated by comparing the coincidence of colocalization in an original image against the coincidence of colocalization in a randomized imaged of shuffled pixels (200 times). Costes approach is expressed as a percentage; a Probability (*P*)-value of ≥ 95% suggests that colocalization is significant and not random (Costes et al., 2004).

Cell count of tPA-Cer and somatostatin (SST)-positive cell bodies was performed in the dorsal hippocampus of tPA^{BAC}-Cer transgenic mice over an approximate 500 µm range from -2.0 to -2.5 bregma. tPA-Cer and SST-positive cells were counted manually using the ROI Manager in FIJI. Cells were deemed positive if their mean pixel intensity

was 1 standard deviation (SD) above the mean pixel intensity for the image (Liao et al., 2016). Cell count data was gathered from 2 - 4 hippocampal sections per mouse (mice, n = 8) for each of tPA^{BAC}-Cer transgenic lines and their transgene negative littermate controls. Cell count data was averaged per mouse and statistics were generated using GraphPad Prism, version 7.0. Data are presented as the mean ± 95% confidence interval ($CI_{(0.95)}$) of tPA-Cer expressing cells from stratum oriens/alveus (CA1 and CA3, respectively) and stratum radiatum/stratum pyramidale (CA1 and CA3). The percentage mean ± $CI_{(0.95)}$ of tPA-Cer cells that co-express SST and the percentage mean ± $CI_{(0.95)}$ of SST-positive cells that co-express tPA-Cer is also given. Immunohistochemical analysis of tPA-Cer cell bodies that co-express markers of oriens-lacunosum moleculare (O-LM) interneurons was gathered from stainings from 4-8 mice per co-expression marker.

2.4.5 Experimental design and statistical analysis

Experimental design, including all critical variables for independent replication, is described in detail in the *Materials and Methods* for each experiment. Briefly, for all analysis using PlatβGAL and tPA^{BAC}-Cer transgenic mice, a mixture of adult male and female mice were used (age 12 – 45 weeks). Wildtype PlatβGAL littermates were used as controls for β-Gal stains, while homozygous PlatβGAL littermates were used as controls for immunoreactivity against tPA. When evaluating global protein expression or using antibodies directed against GFP, tPA^{BAC}-Cer transgene negative littermates were used as controls. Brightness and contrast were adjusted over the entire image and applied equally to control images from transgene negative samples for figure display. All

image processing and statistical analysis of colocalization was preformed using the JACoP software in FIJI and described in detail in the *Materials and Methods*. Statistical *t* tests were performed in GraphPad Prism, version 7.0, and a significance criterion of $p < 0.05$ was adopted. All other graphs and statistics (including mean, standard error of the mean, and 95% confidence interval) were also generated using GraphPad Prism.

2.5 Results

2.5.1 Global and regional expression pattern of tPA in the adult murine brain

PlatβGAL reporter mice were utilized to characterize the global expression pattern of tPA in the adult murine brain. Serial coronal sections (50 µm) from heterozygous PlatβGAL mice were stained for β-Gal to assess regional patterning of somatic tPA expression. Prominent staining is present in layers 2-6 of the cortex (Fig. 1 A - F), with an especially strong β-Gal signal highlighting the compact granule cell layer of the dentate gyrus and the pyramidal cell layer of the dorsal hippocampal CA3 subfield (Fig. 1 D). Though less concentrated, the pyramidal cell layer of the CA1 and CA2 subfields in the dorsal hippocampus also demonstrates tPA/β-Gal expression (Fig. 2 A). In addition, β-Gal staining is apparent in blood vessels throughout the adult murine brain, as illustrated in the hippocampal formation (filled arrows, Fig. 2 A). More diffuse reporter gene expression is present in subcortical regions, like the medial (Fig. 1 B) and lateral (Fig. 1 C) septal nuclei, the bed nucleus of the stria terminalis (Fig. 1 C), the thalamus and hypothalamus (Fig. 1, D, E), caudate/putamen (Fig. 1 D), and the basolateral and centromedial nuclei of the amygdala (Fig.1 D), while intense β-Gal staining populates the molecular and granular layers of the cerebellum (Fig. 1 G-H). There is also

noticeable β-Gal staining in the midbrain, pons, and medulla (Fig. 1 E-H); specifically there is a cluster of reporter gene expression in the interpeduncular nucleus (Fig. 1 F). The interpeduncular nucleus is an integral group of cells involved in limbic midbrain circuitry and has been implicated in active avoidance behavior (Hammer and Klingberg, 1990). Interestingly, multiple groups have demonstrated a role for tPA in avoidance behavioral tasks (Huang et al., 1996; Calabresi et al., 2000; Pawlak et al., 2002), though interpeduncular tPA has never been explicitly examined. Also, in the pontine central gray (Fig. 1 G) there is a small area devoid of β-Gal staining that appears to correspond to the locus coeruleus, which is known for its high concentration of neuroserpin, the neuronal inhibitor of tPA (Krueger et al., 1997). The regional patterning of tPA in the PlatβGAL mice is largely consistent with previous reports examining tPA expression using [^{P}32]-labeled tPA cRNA probes (Sappino et al., 1993) and transgenic mice with tPA promoter-directed expression of β-Gal (Carroll et al., 1994; Yu et al., 2001). However, some differences were observed, such as strong tPA expression in the CA3 subfield and blood vessels (Fig. 2 A), suggesting that the earlier studies lacked either the resolution or specific regulatory elements important for regional and cell specific expression.

2.5.2 Differential expression pattern between where tPA is synthesized and where it is trafficked in the dorsal hippocampus

Immunohistochemical analysis of heterozygous PlatβGAL mice, which have one functional copy of the tPA gene and one copy of the LacZ gene, reveals tPA to have a differential expression pattern. Using an antibody directed against tPA, there is a distinct

uncoupling between the sites of tPA synthesis and sites of tPA trafficking. This is most apparent in the dorsal hippocampus where the granule cell layer of the dentate gyrus is brightly positive for β-Gal, but devoid of tPA-immunoreactivity (Fig. 2 A, B-B'). Conversely, the mossy fiber axonal tracts of the granule cells that project into the hilus (Fig. 2 B') and traverse along stratum lucidum (Fig. 2 B'') are strongly immunoreactive against anti-tPA antibodies. Though strongly expressing β-Gal, no tPA-immunoreactivity is detectable in the granule cell layer or CA3 pyramidal layer (Fig. 2 B – B'').

Given the disparate expression profiles of where tPA is synthesized and where it is trafficked, a more targeted strategy for visualizing tPA is needed. To achieve this, bacterial artificial chromosome (BAC) technology was utilized to generate transgenic fusion reporter mice that have a fluorescent cerulean protein tagged to the carboxy terminal of tPA (Fig. 3 A). Compared to a reporter gene approach, the tPA-Cer fusion reporter approach facilitates a more precise analysis of the regional, cellular, and subcellular expression pattern of tPA in the adult murine brain. And, it can lead to greater functional insights about the dynamic nature of tPA in the brain, including cellular packaging and transport, cellular communication, and regional connectivity.

2.5.3 Global tPA protein expression profile in tPA^{BAC}-Cerulean transgenic mice

Prior to a detailed characterization of tPA localization in tPA^{BAC}-Cer mice, global tPA protein expression levels were measured. Brains from transgene positive and transgene negative adult tPA^{BAC}-Cer mice (mice, n = 6-7) were harvested and homogenized for total and active protein levels using a bead-based Luminex assay (Fig. 3 B) and ELISA (Fig. 3 C). tPA^{BAC}-Cer mice were found to have an approximate 5-6 fold

change in total tPA levels from transgene negative mice (Fig. 3 B), and an approximate 6 fold change in active tPA levels from transgene negative mice (Fig. 3 C). No statistical difference in total or active tPA was noted between the two transgenic lines. To more specifically discriminate between endogenous tPA protein and that which is from the BAC, whole brain homogenates from transgenic tPA^{BAC}-Cer mice (lines 863 and 876) and their respective transgene negative littermate controls were run on a zymography gel (Fig. 3 D). Transgene positive tPA^{BAC}-Cer mice showed enzymatic activity from both endogenous tPA (~60kDa) and the tPA-Cer protein (~75kDa). Samples from transgene negative mice did not display the higher molecular weight band that is indicative of tPA protein with the added cerulean fluorescent protein.

2.5.4 tPA-Cerulean fusion protein is prominently expressed in limbic structures and blood vessels in the adult murine brain

In a global survey of tPA-Cer fluorescence in tPA^{BAC}-Cer transgenic mice, tPA-Cer puncta appear to be primarily restricted to two pools: nerve fibers (Fig. 4 A-G, I-M) and vascular endothelial cells (Fig. 4 N). No observable cerulean fluorescence was detected in transgene negative littermate controls (Fig. 5 A-F, H). In the brain parenchyma, faint tPA-Cer cell bodies are noticeable in the piriform and entorhinal cortex (Fig. 4 A–E), while more predominant and intense tPA-Cer fluorescence is seen in nerve fibers in hippocampal and subcortical regions of the brain. Juxtaposed to the somatic neuronal marker NeuN, tPA-Cer fluorescence is clearly not localized to the cell body; rather, it appears to be expressed in nerve fibers emanating or innervating brain structures associated with the limbic system, including the medial and lateral septal

nuclei (Fig. 4 B),the bed nucleus of the stria terminalis (Fig. 4 C, I), the paraventricular nucleus of the thalamus (Fig. 4 C), hypothalamus (Fig. 4 C–D), the mossy fiber pathway of the hippocampus (Fig. 4 D–F; Fig. 5 G), the centromedial nucleus of the amygdala (Fig. 4 D, J), the external and internal globus pallidus nuclei of the basal ganglia (Fig. 4 D, M), the substantia nigra pars reticulata (Fig. 4 E), the periaqueductal gray (Fig. 4 F, K), and the parabrachical nucleus (Fig. 4 G, L).

In situ zymography previously demonstrated tPA activity in the mossy fiber pathway and hypothalamus (Sappino et al., 1993), the bed nucleus stria terminalis (Matys et al., 2005), and the centromedial, but not basolateral, nucleus of the amygdala (Pawlak et al., 2003). To our knowledge, though, we are the first to report on tPA expression in the paraventricular nucleus of the thalamus, the periaqueductal gray, and the parabrachial nucleus. These regions, in addition to the bed nucleus stria terminalis and the hypothalamus, are connected via afferent and/or efferent projections to the centromedial amygdalar nucleus (Janak and Tye, 2015; Penzo et al., 2015; Tasan et al., 2016; Babaev et al., 2018). Neurons in the basolateral nucleus also send projections to the centromedial nucleus. And, while β-Gal expression was detected in both the basolateral and centromedial nuclei, given the complex circuitry of the amygdala, it is unclear if the tPA-Cer fluorescence in the centromedial nucleus is trafficked tPA from basolateral nerve projections or trafficked tPA in afferent/efferent nerve fibers to/from other brain regions.

We also report, for the first time, on tPA expression in the external (GPe) and internal (GPi) globus pallidus nuclei of the basal ganglia. Indeed, the differential expression of somatic tPA/β-Gal and trafficked tPA-Cer is appreciable when comparing

tPA expression in the PlatβGAL (Fig. 1 D) and tPA^{BAC}-Cer (Fig. 4 D) transgenic mice. While β-Gal staining is present in the caudate/putamen nucleus, it is devoid in both the GPe and GPi nuclei in the PlatβGAL reporter mice (Fig. 1 D). In contrast, tPA-Cer fluorescence is absent in the caudate/putamen, but present in the GPe, GPi, and substantia nigra pars reticulata (SNr) (Fig. 4 D–E). The GPi and SNr are equivalent anatomical structures, both embryologically and functionally (Purves et al., 2001), as they are the output nuclei of the basal ganglia. Given that tPA-Cer, but not β-Gal, is present in the GPe, it's likely that the observed tPA-Cer is part of the direct loop through the basal ganglia. The circuitry of the direct loop involves GABAergic neurons that project from caudate/putamen through the GPe to the GPi or GABAergic neurons from caudate/putamen that travel through the strionigral fibers to SNr (Purves et al., 2001; Gilman and Newman, 2002). In turn, both the GPi and SNr send GABAergic projections to the thalamus. The direct loop is known to increase thalamocortical excitation and it is important for the selection of desired behaviors. Together, the high expression of tPA-Cer fluorescence in cell bodies and nerve fibers in limbic structures, especially amygdalar-associated brain regions, strongly support a role for tPA in affective, motivational, and anxiety-like behavior (Pawlak et al., 2002; Pawlak et al., 2003; Matys et al., 2004). And, while tPA has yet to be studied in the basal ganglia, more recent evidence has suggested that, functionally, the basal ganglia is more than an "organ of habit" in the brain, as it plays a role in perception, cognition, and emotional behaviors (Jahanshahi et al., 2015).

2.5.5 tPA-Cerulean puncta are localized to large mossy fiber boutons in the stratum lucidum CA3 subregion of the hippocampus

Our previous results established that tPA-Cer fluorescence is highly enriched in the mossy fiber pathway (Fig. 4 D, Fig. 5 G). These findings are consistent with immunohistochemical analysis and *in situ* zymography which also report high levels of tPA localization and proteolytic activity in the mossy fiber pathway (Sappino et al., 1993; Salles and Strickland, 2002; Louessard et al., 2016). As mossy fiber axons are known to have morphologically and functionally distinct presynaptic terminals we leveraged the use of the tPA^{BAC}-Cer mice, combined with high-resolution confocal imaging, to establish tPA's subcellular distribution in the hippocampus. Confocal z-stacks were captured of both tPA-Cer and putative co-localization markers. Dorsal hippocampal sections from tPA^{BAC}-Cer mice were first probed for zinc transporter-3 (ZnT3), which is the protein correlate underlying the Timm's histochemical stain to visualize the mossy fiber pathway (Frotscher et al., 1994). ZnT3 was used based on previous electron microscopy immunocytochemistry of ZnT3 in the murine brain which revealed the exclusive localization of ZnT3 to large mossy fiber boutons (MFB) (Wenzel et al., 1997). An analysis of orthogonal YZ and XZ sections from a 5 µm z-stack (Δz = 0.5 µm) suggests that tPA-Cer puncta colocalize with ZnT3 (Fig. 6 A). Further, 3-dimensional projection confirms that tPA-Cer puncta reside in ZnT3-positive MFB (Fig. 6 A'). As shown in Fig. 6 D–E, quantification of colocalization between tPA and ZnT3 from 5 µm concatenated image stacks (mice, n = 10), shows that tPA-Cer has a high degree of overlap with ZnT3 (M1 coefficient: 0.704 and 0.649 for lines 863 and 876, respectively; Costes Probability (*P*)-value ≥ 95%). There was no observable detection of cerulean

fluorescence in transgene negative littermate controls (Fig. 5 H). Conversely, ZnT3 shows only partial overlap with tPA-Cer (M2 coefficient: 0.426 and 0.352 for lines 863 and 876, respectively). The lack of a one-to-one relationship between the M1 and M2 coefficients is possibly due to the zinc transporter being a synaptic, not dense core, vesicle marker. Though dense core vesicles are sporadically found in MFBs (Wenzel et al., 1997; Rollenhagen et al., 2007), synaptic vesicles are much more abundant. ZnT3 staining, therefore, likely illuminates a larger area of the MFB, while the tPA-Cer signal, presumably in dense core vesicles, appears more punctate (Silverman et al., 2005; Lochner et al., 2008; Scalettar et al., 2012). Lastly, these data indicate that while the vast majority of tPA is localized to giant MFBs there is also a population that occupies another locale.

As astrocytes are known to wrap fine processes around mossy fiber boutons (Rollenhagen and Lubke, 2010) and as tPA has been shown to be taken-up by astrocytes (Casse et al., 2012), tPA^{BAC}-Cer hippocampal sections were stained for the astrocytic glutamate transporter EAAT2 (excitatory amino acid transporter 2). While a strong visual colocalization was difficult to ascertain from orthogonal YZ and XZ slices (Fig. 6 B) and 3D projections (Fig. 6 B'), image quantification (Fig. 6 D–E) did demonstrate lower levels of colocalization (M1 coefficient: 0.183 and 0.198 for lines 863 and 876, respectively; Costes Probability (*P*)-value ≥ 95%). To further validate our results, tPA^{BAC}-Cer sections were stained for the dendritic marker MAP2 (microtubule associated protein 2) as a negative control. In stratum lucidum, MAP2 detects the dendritic thorny excrescences of CA3 pyramidal neurons which are the post-synaptic partner to the MFBs. As predicated, orthogonal YZ and XZ slices of tPA-Cer and MAP2

showed no visual overlap (Fig. 6 C) and a 3D projection (Fig. 6 C') showed that tPA-Cer puncta encapsulate the MAP2-positive dendritic thorny excrescences. Moreover, when quantified (Fig. 6 D–E), no colocalization was found (M1 coefficient: 0.032 and 0.060 for lines 863 and 876, respectively; Costes Probability (*P*)-value = 0%).

2.5.6 tPA is expressed in a subset of SST-positive inhibitory interneurons in stratum oriens/alveus of CA1 and CA3 hippocampal subfields

The presence of sporadic β-Gal puncta in stratum oriens (SO), stratum radiatum (SR), and the hilus (Fig. 2 A) of the hippocampus in PlatβGAL reporter mice suggested that other cell types, in addition to the granule and pyramidal cells, express tPA. In an effort to visualize and identify these cells in the tPA^{BAC}-Cer transgenic mice, the cerulean signal was magnified using a GFP antibody in conjunction with Tyramide signal amplification. With amplification, tPA-Cer positive cell bodies were revealed in the CA1 and CA3 hippocampal subfields of transgene positive mice (Fig. 7 A, E). CA3 pyramidal cells became visible, but more strikingly were the sparsely-populated tPA-Cer expressing cell somas in SO, SP, and SR, though most were strongly localized to the SO/alveus lamina of the CA1 and CA3 subfields (Table 2.1). To quantify strata localization of tPA-Cer cell bodies, 2-4 hippocampal sections per mouse (mice, n = 8) for each of the transgenic lines were analyzed. Our results show that for a hippocampal section there were, on average, 11.68±1.53 (n = 301 cells) and 10.90±2.06 (n = 238 cells) tPA-Cer cells bodies in the CA1 SO/alveus region and approximately 5.58±1.14 (n = 141 cells) and 5.34±1.98 (n = 115 cells) tPA-Cer cell bodies in the CA3 SO/alveus region for lines 863 and 876, respectively. Less frequently, on average, 3.32±1.15 (n =

78 cells) and 2.28± 1.06 (n = 52 cells) tPA-Cer cells bodies were found in SR and SP for lines 863 and 876, respectively. No statistical difference was noted between lines 863 and 876.

The sporadic nature of tPA-Cer positive cell bodies is consistent with that of GABAergic interneurons (Oliva et al., 2000). To test if tPA-Cer positive cells are indeed GABAergic interneurons, various immuno-markers for SO/alveus-interneurons were used to neurochemically identify the subpopulation of tPA-Cer positive cells in the hippocampus (Somogyi and Klausberger, 2005). tPA-Cer positive cells were found to strongly co-express the interneuronal marker somatostatin (SST) in the SO/alveus lamina of hippocampal regions CA1 and CA3 (Table 2.1 and Fig. 7). Widefield images of the hippocampus show prominent tPA-expression in stratum luciudum (Fig. 7 E), but also in SST-positive interneurons scattered throughout SO/alveus (Fig. 7 A). Immunostaining for SST and GFP with Tyramide signal amplification in transgene negative controls only revealed SST-positive interneurons (Fig. 7 I,J). Confocal images from CA1 (Fig. 7 B–D) and CA3 (Fig. 7 F–H) show tPA-Cer cells (green) that clearly overlap with SST-positive (magenta) interneurons. When quantified, for a given hippocampal section, approximately 54.35±6.32% (n = 520 cells) and 58.90±6.74% (n = 405 cells) of tPA-Cer cells were found to co-express SST, while 53.89±8.82% (n = 520 cells) and 44.66±9.45% (n = 540 cells) of SST-positive cells were found to co-express tPA-Cer, for lines 863 and 876, respectively. No statistical difference was noted between lines 863 and 876.

Since oriens-lacunosum moleculare (O-LM) interneurons, whose cell bodies reside in stratum oriens and send axonal projections to stratum lacunosum-moleculare,

are known to express SST (Fig. 8 A), other neurochemical markers of O-LM interneurons were probed for to see if tPA-Cer cells can be immunocytochemically classified as O-LM interneurons. tPA-Cerulean cells were found to co-express the calcium-binding protein calbindin (Fig. 8 C), which has previously been reported to comprise roughly 32% of SST/O-LM interneurons (Oliva et al., 2000); they were also found to co-express the metabotropic glutamate receptor 1 (mGlur1a; Fig. 8 B), which is highly expressed in SST/O-LM interneurons (Klausberger et al., 2003; Somogyi and Klausberger, 2005; Sylwestrak and Ghosh, 2012). Interestingly, tPA mRNA polyadenylation and translation has previously been shown to be dependent on mGluR1 activation (Shin et al., 2004). To confirm the inhibitory nature of these cells, immunohistochemistry against GAD65 (glutamic acid decarboxylase 65) in tPA^{BAC}-Cer mice was performed (Fig. 8 D). In agreement with the localization and cytochemical profile of SST/O-LM interneurons, tPA-Cer puncta were observed in structures reminiscent of axonal processes in SR (Fig. 8 E). These data strongly suggest that at least a portion of tPA-Cer cells can be categorized as O-LM interneurons.

2.6 Discussion

In the present study we have confirmed and extended our understanding of the expression of tPA in the adult murine brain. Using both a PlatβGAL reporter mouse and a BAC transgenic mouse expressing a tPA-Cer fusion protein, we have provided a detailed characterization of the regional, cellular, and sub-cellular localization of tPA. While largely complimenting the expression pattern observed in transgenic mice that harbored a 9.5kb segment of the human tPA promoter to drive expression of LacZ (Yu

et al., 2001), PlatβGAL reporter mice displayed differences that provide insight into the transcriptional regulation of tPA. In contrast to the PlatβGal reporter mice, in the human 9.5kb tPA^{LacZ} reporter mouse, β-Gal staining was only weakly observed in the CA3 subfield and there was no detection of β-Gal in blood vessels, a well-established site of tPA expression (Fredriksson et al., 2015; Louessard et al., 2016). In addition, Yu *et al*. (2001) observed high tPA/LacZ expression in the medial habenula, which was not the case for the PlatβGAL reporter mice. These discrepancies suggest that regulatory elements important for the regional and cellular expression patterning of tPA are not encompassed in the 9.5kb human promoter segment or that there are differences between the human and murine promoter sequences that do not completely recapitulate species specific expression of tPA.

When comparing the PlatβGAL reporter mice and the tPA^{BAC}-Cer transgenic mice, there is a clear uncoupling between where tPA is synthesized and where it is trafficked, which is in agreement with previous *in situ* expression studies examining tPA mRNA and tPA-catalyzed proteolysis (Sappino et al., 1993). And, while the laminar, tri-synaptic circuitry of the hippocampus illustrates this uncoupling most distinctly, tPA's differential expression pattern is also apparent in the amygdala and the basal ganglia. In addition, there is a stark dichotomy between β-Gal expression and tPA-Cer fluorescence in the cortex and cerebellum. Though β-Gal is abundant throughout the cortex and cerebellum in PlatβGAL reporter mice, other than faintly positive cell bodies in the piriform and entorhinal cortex, there is no detectable tPA-Cer fluorescence in the cortex and cerebellum of tPA^{BAC}-Cer transgenic mice. Tracing experiments of cortical and cerebellar projections, which are beyond the scope of this paper, would help

address this discrepancy. For, if tPA is primarily trafficked as our data suggests, then it's possible that tPA-Cer is localized along cortical descending pathways or in efferent targets in the cerebellum, the basal ganglia, the brain stem, and spinal cord. Similarly, more detailed tracing studies would be required to assess if tPA-Cer is localized to cerebellar efferents, like the vestibulocerebellum, spinocerebellum, and cerebrocerebellum pathways, and their target nuclei. Given that tPA's site of action is removed from its site of synthesis, the tPA^{BAC}-Cer transgenic mice, when analyzed in conjunction with the PlatβGAL reporter mice, provide a more informative expression profile of tPA in the adult murine brain.

Taking advantage of the tPA-Cer fusion construct, therefore, we report for the first time tPA's subcellular localization to giant MFBs in stratum lucidum of CA3. Previous studies have only generally described tPA expression in the mossy fiber pathway, without examining its specific compartmentalization. The specific structural localization can potentially provide meaningful insight into tPA's function. This is especially true since mossy fiber axons of DGCs display two other morphologically distinct presynaptic terminals - small *en passant* boutons and filipodial extensions that emanate from the MFBs (Acsady et al., 1998; Rollenhagen and Lubke, 2010). Moreover, these structurally distinct terminals have divergent post-synaptic targets; MFBs synapse with hilar mossy cells and the apical dendritic spines or "thorny excrescences" of CA3 pyramidal cells, while *en passant* boutons and filipodial extensions preferentially target GABAergic interneurons in the hilus and stratum lucidum (Frotscher et al., 1994; Acsady et al., 1998). The mossy fiber-to-CA3 pyramidal cell synapse also has a different synaptic physiology; compared to the mossy fiber-to-interneuron synapse, the

mossy fiber-to-CA3 pyramidal cell synapses shows marked paired-pulse facilitation and long-term potentiation (LTP) (Salin et al., 1996; Henze et al., 2000; Toth et al., 2000; Nicoll and Schmitz, 2005).

Thus, the specific localization of tPA-Cer puncta to giant MFBs suggests that it may have a role in regulating synaptic efficacy at the mossy fiber-to-CA3 pyramidal cell synapse. Consistent with this model, functional studies demonstrate $tPA^{-/-}$ mice have deficits in LTP in the mossy fiber pathway (Huang et al., 1996). Further interrogations into the mechanism underlying deficits in LTP have focused on a post-synaptic locus of expression. Mice deficient in tPA, which carries a cAMP response element in its promoter, exhibit reduced potentiation by cAMP analogs (Huang et al., 1996); blocking tPA's non-proteolytic interaction with the post-synaptically expressed low-density lipoprotein receptor-related protein (LRP) causes deficits in synaptic potentiation (Bu et al., 1994; Zhuo et al., 2000); and tPA-mediated cleavage of proBDNF was found to be essential for the full expression of LTP (Korte et al., 1995; Korte et al., 1998; Pang et al., 2004). These mechanistic studies, however, presumed post-synaptic tPA expression and were performed in the hippocampal CA1 region, not at the mossy fiber-to-CA3 pyramidal cell synapse, where we have shown tPA to be most highly expressed in the giant MFBs. Additionally, while amplification of the tPA-Cer signal was able to reveal tPA expression in the soma of CA3 pyramidal cells, high-resolution colocalization analysis did not uncover tPA in the post-synaptic thorny excrescences of CA3 pyramidal cells. In fact, no colocalization was observed between tPA-Cer puncta and the dendritic marker MAP2. Though *in vitro* studies have shown activity-dependent release of tPA from both pre- and post-synaptic compartments (Gualandris et al., 1996; Lochner et al.,

1998; Lochner et al., 2006; Scalettar et al., 2012), our *in situ* expression data demonstrates that tPA's localization is largely pre-synaptic and suggests that potential pre-synaptic neuromodulatory effects at the mossy fiber-to-CA3 synapse may have been overlooked.

Interestingly, tPA-Cer puncta were also observed to partially co-localize with astrocytes. It is unclear, however, if the tPA present is endogenous to astrocytes, as transcriptome analysis has shown astrocytes to express tPA mRNA *in vitro (Zhang et al., 2014)*, or if tPA is endocytosed by astrocytes in an LRP-dependent fashion (Casse et al., 2012). The mossy fiber-to-CA3 pyramidal cell synapse appears unique with respect to its trisynaptic cytoarchitecture. Previous studies indicate that astrocytes completely insulate the synapse, cordoning off the active zone and synaptic cleft from the surrounding parenchyma, but not physically encroaching into the cleft (Rollenhagen et al., 2007). And, while there is no *in vivo* functional evidence demonstrating the effects of tPA release from astrocytes on synaptic function, *in vitro* evidence has pointed to tPA acting as a gliotransmitter that is released and recycled by astrocytes (Casse et al., 2012). The lack of perisynaptic astrocytic processes making contact with axon-spine interfaces (Rollenhagen et al., 2007), however, possibly indicates that, at least at the mossy fiber-to-CA3 pyramidal cell synapse, diffusion-limited gliotransmitter tPA may have reduced effects on synaptic function. Moreover, if tPA is released in an activity-dependent manner (Gualandris et al., 1996; Robert J. Parmer, 1997) from giant MFBs, the configuration of the mossy fiber-to-CA3 pyramidal cell synapse suggests that it is not geared toward immediate clearance and uptake, but rather, toward potentiating the effects of tPA and presumably enhancing synaptic efficacy.

In this study we also identify tPA expression in a subset of SST-positive interneurons in the hippocampal stratum oriens/alveus lamina. We provide a detailed distribution of tPA-Cer positive cell bodies in both the CA1 and CA3 subfields and their quantified co-expression with SST-positive interneurons. While enhancement of the tPA-Cer protein, with anti-GFP Tyramide amplification, was necessary to distinctly visualize these cell bodies, we believe this somatic expression of tPA is physiological as (1) no signal was observed in littermate transgene negative controls, (2) the recapitulation of tPA expression in the mossy fiber pathway indicates that tPA-Cer is appropriately targeted to its cellular and subcellular locale, and (3) β-GAL puncta in the PlatβGAL reporter mice are noticeable in stratum oriens/alveus and stratum radiatum (Figure 2.2). Presumably, the increase in tPA expression, due to extra copy number from the BAC transgene, allowed for the detection of a previously unrecognized and specific population of tPA-expressing cells. It is unclear, though, why tPA is differentially localized to the soma or axonal projection and if such differential trafficking is functionally significant. For, tPA appears to be largely localized to the soma of inhibitory interneurons (Fredriksson et al., 2015) and to the axons of excitatory neurons (Louessard et al., 2016). While knowledge about dense core vesicle trafficking is still nascent compared to synaptic vesicle trafficking, there is evidence which demonstrates regionally-specific, differential trafficking of the neuropeptide NPY to dendrites and axons (Ramamoorthy et al., 2011) and that excitatory and inhibitory neurons in the hippocampus exhibit different dense core vesicle molecular machinery (Ramirez-Franco et al., 2016).

In the CA1 hippocampal region alone more than a dozen different types of interneurons have been classified based on their morphological, neurochemical and physiological properties (Freund and Buzsaki, 1996; Somogyi and Klausberger, 2005). And, while no one single marker is indicative of a specific type of interneuron, tPA-Cer positive cells appear to share a very similar somatic distribution (Oliva et al., 2000) and immunocytochemical profile with O-LM interneurons ((Somogyi and Klausberger, 2005; Minneci et al., 2007; Sylwestrak and Ghosh, 2012). As tPA-expressing neurons have never been described in SST/O-LM interneurons before, it is unclear how tPA may be exerting its effects. Morphologically, the axonal projections of O-LM interneurons ramify at the distal apical dendrites of CA1 pyramidal cells, where perforant path fibers from the entorhinal cortex terminate. Functionally, O-LM interneurons are known to fire rhythmically at the trough of theta (4-8 Hz) oscillations in the hippocampus (Klausberger et al., 2003), and they have been shown to facilitate LTP in the Schaffer collateral-to-CA1 pathway. Though deficiency in tPA has been previously implicated in defects in the late-phase of LTP in the hippocampal CA1 region (Huang et al., 1996; Calabresi et al., 2000), the contribution of tPA from O-LM interneurons has not been specifically tested in this paradigm. Plasticity of glutamatergic CA1 synapses onto O-LM interneurons has also been investigated, as changes in synaptic efficacy may have an important role in modulating network excitability (Nicholson and Kullmann, 2014). To date, though, it is unknown if tPA is involved in these events.

Taken together, the regional, cellular, and subcellular characterization of tPA expression presented here provides a primer on tPA's role in the central nervous system. Many of the foundational experiments on tPA's function in the brain were

performed prior to a detailed description of its protein localization, this is especially confounding in the case of tPA as its site of synthesis is uncoupled from it targeted site of action. With the generation of the tPA^{BAC}-Cer transgenic mice and its appropriately targeted tPA-Cer fusion protein, however, future mechanistic studies to elucidate tPA's function are now possible.

Acknowledgments: We would like to thank Kris Mann and Mark Warnock for excellent technical assistance and the University of Michigan Transgenic Core for their expertise in the generation of BAC transgenic animals. We would also like to thank Geoffrey Murphy, Edward Stuenkel, Shannon Moore, Kasia Glanowska, and Victor Cazares for their critical reading of the manuscript. This work was supported by National Institutes of Health Grants HL055374, and NS079639 (to D.A. L.), and T32-HL125242 and T32 - GM008322 (T.K.S.).

References

Acsady L, Kamondi A, Sik A, Freund T, Buzsaki G (1998) GABAergic cells are the major postsynaptic targets of mossy fibers in the rat hippocampus. J Neurosci 18:3386-3403.

Ahmed N, Wahlgren N, Grond M, Hennerici M, Lees KR, Mikulik R, Parsons M, Roine RO, Toni D, Ringleb P, investigators S (2010) Implementation and outcome of thrombolysis with alteplase 3-4.5 h after an acute stroke: an updated analysis from SITS-ISTR. Lancet Neurol 9:866-874.

Akassoglou K, Kombrinck KW, Degen JL, Strickland S (2000) Tissue plasminogen activator-mediated fibrinolysis protects against axonal degeneration and demyelination after sciatic nerve injury. J Cell Biol 149:1157-1166.

Babaev O, Piletti Chatain C, Krueger-Burg D (2018) Inhibition in the amygdala anxiety circuitry. Exp Mol Med 50:18.

Bolte S, Cordelieres FP (2006) A guided tour into subcellular colocalization analysis in light microscopy. J Microsc 224:213-232.

Bu G, Maksymovitch EA, Nerbonne JM, Schwartz AL (1994) Expression and function of the low density lipoprotein receptor-related protein (LRP) in mammalian central neurons. J Biol Chem 269:18521-18528.

Calabresi P, Napolitano M, Centonze D, Marfia GA, Gubellini P, Teule MA, Berretta N, Bernardi G, Frati L, Tolu M, Gulino A (2000) Tissue plasminogen activator controls multiple forms of synaptic plasticity and memory. Eur J Neurosci 12:1002-1012.

Carroll PM, Tsirka SE, Richards WG, Frohman MA, Strickland S (1994) The mouse tissue plasminogen activator gene 5' flanking region directs appropriate expression in development and a seizure-enhanced response in the CNS. Development 120:3173-3183.

Casse F, Bardou I, Danglot L, Briens A, Montagne A, Parcq J, Alahari A, Galli T, Vivien D, Docagne F (2012) Glutamate controls tPA recycling by astrocytes, which in turn influences glutamatergic signals. J Neurosci 32:5186-5199.

Costes SV, Daelemans D, Cho EH, Dobbin Z, Pavlakis G, Lockett S (2004) Automatic and quantitative measurement of protein-protein colocalization in live cells. Biophys J 86:3993-4003.

Dunn KW, Kamocka MM, McDonald JH (2011) A practical guide to evaluating colocalization in biological microscopy. Am J Physiol Cell Physiol 300:C723-742.

Fredriksson L, Stevenson TK, Su EJ, Ragsdale M, Moore S, Craciun S, Schielke GP, Murphy GG, Lawrence DA (2015) Identification of a neurovascular signaling pathway regulating seizures in mice. Ann Clin Transl Neurol 2:722-738.

Freund TF, Buzsaki G (1996) Interneurons of the hippocampus. Hippocampus 6:347-470.

Frey U, Muller M, Kuhl D (1996) A different form of long-lasting potentiation revealed in tissue plasminogen activator mutant mice. J Neurosci 16:2057-2063.

Frotscher M, Soriano E, Misgeld U (1994) Divergence of hippocampal mossy fibers. Synapse 16:148-160.

Gilman S, Newman S (2002) Manter and Gatz's Essentials of Clinical Neuroanatomy and Neurophysiology, 10th edition Edition. Philadelphia, PA: F.A. Davis Company.

group ISTc et al. (2012) The benefits and harms of intravenous thrombolysis with recombinant tissue plasminogen activator within 6 h of acute ischaemic stroke (the third international stroke trial [IST-3]): a randomised controlled trial. Lancet 379:2352-2363.

Gualandris A, Jones TE, Strickland S, Tsirka SE (1996) Membrane depolarization induces calcium-dependent secretion of tissue plasminogen activator. J Neurosci 16:2220-2225.

Hammer KH, Klingberg F (1990) Active avoidance is permanently abolished after lesions of the nucleus interpeduncularis in rat. Biomed Biochim Acta 49:489-497.

Henze DA, Urban NN, Barrionuevo G (2000) The multifarious hippocampal mossy fiber pathway: a review. Neuroscience 98:407-427.

Huang YY, Bach ME, Lipp HP, Zhuo M, Wolfer DP, Hawkins RD, Schoonjans L, Kandel ER, Godfraind JM, Mulligan R, Collen D, Carmeliet P (1996) Mice lacking the gene encoding tissue-type plasminogen activator show a selective interference with late-phase long-term potentiation in both Schaffer collateral and mossy fiber pathways. Proc Natl Acad Sci U S A 93:8699-8704.

Jahanshahi M, Obeso I, Rothwell JC, Obeso JA (2015) A fronto-striato-subthalamic-pallidal network for goal-directed and habitual inhibition. Nat Rev Neurosci 16:719-732.

Janak PH, Tye KM (2015) From circuits to behaviour in the amygdala. Nature 517:284-292.

Klausberger T, Magill PJ, Marton LF, Roberts JD, Cobden PM, Buzsaki G, Somogyi P (2003) Brain-state- and cell-type-specific firing of hippocampal interneurons in vivo. Nature 421:844-848.

Korte M, Kang H, Bonhoeffer T, Schuman E (1998) A role for BDNF in the late-phase of hippocampal long-term potentiation. Neuropharmacology 37:553-559.

Korte M, Carroll P, Wolf E, Brem G, Thoenen H, Bonhoeffer T (1995) Hippocampal long-term potentiation is impaired in mice lacking brain-derived neurotrophic factor. Proc Natl Acad Sci U S A 92:8856-8860.

Krueger SR, Ghisu GP, Cinelli P, Gschwend TP, Osterwalder T, Wolfer DP, Sonderegger P (1997) Expression of neuroserpin, an inhibitor of tissue plasminogen activator, in the developing and adult nervous system of the mouse. J Neurosci 17:8984-8996.

Krystosek A, Seeds NW (1981) Plasminogen activator release at the neuronal growth cone. Science 213:1532-1534.

Liao MC, Muratore CR, Gierahn TM, Sullivan SE, Srikanth P, De Jager PL, Love JC, Young-Pearse TL (2016) Single-Cell Detection of Secreted Abeta and sAPPalpha from Human IPSC-Derived Neurons and Astrocytes. J Neurosci 36:1730-1746.

Lochner JE, Kingma M, Kuhn S, Meliza CD, Cutler B, Scalettar BA (1998) Real-time imaging of the axonal transport of granules containing a tissue plasminogen activator/green fluorescent protein hybrid. Mol Biol Cell 9:2463-2476.

Lochner JE, Honigman LS, Grant WF, Gessford SK, Hansen AB, Silverman MA, Scalettar BA (2006) Activity-dependent release of tissue plasminogen activator from the dendritic spines of hippocampal neurons revealed by live-cell imaging. J Neurobiol 66:564-577.

Lochner JE, Spangler E, Chavarha M, Jacobs C, McAllister K, Schuttner LC, Scalettar BA (2008) Efficient copackaging and cotransport yields postsynaptic colocalization of neuromodulators associated with synaptic plasticity. Dev Neurobiol 68:1243-1256.

Louessard M, Lacroix A, Martineau M, Mondielli G, Montagne A, Lesept F, Lambolez B, Cauli B, Mothet JP, Vivien D, Maubert E (2016) Tissue Plasminogen Activator Expression Is Restricted to Subsets of Excitatory Pyramidal Glutamatergic Neurons. Mol Neurobiol 53:5000-5012.

Matys T, Pawlak R, Strickland S (2005) Tissue plasminogen activator in the bed nucleus of stria terminalis regulates acoustic startle. Neuroscience 135:715-722.

Matys T, Pawlak R, Matys E, Pavlides C, McEwen BS, Strickland S (2004) Tissue plasminogen activator promotes the effects of corticotropin-releasing factor on the amygdala and anxiety-like behavior. Proc Natl Acad Sci U S A 101:16345-16350.

Minneci F, Janahmadi M, Migliore M, Dragicevic N, Avossa D, Cherubini E (2007) Signaling properties of stratum oriens interneurons in the hippocampus of transgenic mice expressing EGFP in a subset of somatostatin-containing cells. Hippocampus 17:538-553.

Nicholson E, Kullmann DM (2014) Long-term potentiation in hippocampal oriens interneurons: postsynaptic induction, presynaptic expression and evaluation of candidate retrograde factors. Philos Trans R Soc Lond B Biol Sci 369:20130133.

Nicole O, Docagne F, Ali C, Margaill I, Carmeliet P, MacKenzie ET, Vivien D, Buisson A (2001) The proteolytic activity of tissue-plasminogen activator enhances NMDA receptor-mediated signaling. Nat Med 7:59-64.

Nicoll RA, Schmitz D (2005) Synaptic plasticity at hippocampal mossy fibre synapses. Nat Rev Neurosci 6:863-876.

Oliva AA, Jr., Jiang M, Lam T, Smith KL, Swann JW (2000) Novel hippocampal interneuronal subtypes identified using transgenic mice that express green fluorescent protein in GABAergic interneurons. J Neurosci 20:3354-3368.

Pang PT, Teng HK, Zaitsev E, Woo NT, Sakata K, Zhen S, Teng KK, Yung WH, Hempstead BL, Lu B (2004) Cleavage of proBDNF by tPA/plasmin is essential for long-term hippocampal plasticity. Science 306:487-491.

Park L, Gallo EF, Anrather J, Wang G, Norris EH, Paul J, Strickland S, Iadecola C (2008) Key role of tissue plasminogen activator in neurovascular coupling. Proc Natl Acad Sci U S A 105:1073-1078.

Pawlak R, Magarinos AM, Melchor J, McEwen B, Strickland S (2003) Tissue plasminogen activator in the amygdala is critical for stress-induced anxiety-like behavior. Nat Neurosci 6:168-174.

Pawlak R, Nagai N, Urano T, Napiorkowska-Pawlak D, Ihara H, Takada Y, Collen D, Takada A (2002) Rapid, specific and active site-catalyzed effect of tissue-plasminogen activator on hippocampus-dependent learning in mice. Neuroscience 113:995-1001.

Penzo MA, Robert V, Tucciarone J, De Bundel D, Wang M, Van Aelst L, Darvas M, Parada LF, Palmiter RD, He M, Huang ZJ, Li B (2015) The paraventricular thalamus controls a central amygdala fear circuit. Nature 519:455-459.

Prabhakaran S, Ruff I, Bernstein RA (2015) Acute stroke intervention: a systematic review. Journal of the American Medical Association 313:12.

Purves D, Augustine G, Fitzpatrick D, Katz L, LaMantia A, McNamara J, Williams S (2001) Modulation of movement by the basal ganglia, 2nd edition Edition. Sunderland, MA: : Sinauer Associates.

Qian Z, Gilbert ME, Colicos MA, Kandel ER, Kuhl D (1993) Tissue-plasminogen activator is induced as an immediate-early gene during seizure, kindling and long-term potentiation. Nature 361:453-457.

Ramamoorthy P, Wang Q, Whim MD (2011) Cell type-dependent trafficking of neuropeptide Y-containing dense core granules in CNS neurons. J Neurosci 31:14783-14788.

Ramirez-Franco JJ, Munoz-Cuevas FJ, Lujan R, Jurado S (2016) Excitatory and Inhibitory Neurons in the Hippocampus Exhibit Molecularly Distinct Large Dense Core Vesicles. Frontiers in cellular neuroscience 10:202.

Robert J. Parmer MM, Sushil Mahata, Matthew T. Sebald, Daniel T. O'Connor, and Lindsey A. Miles (1997) Tissue Plasminogen Activator (t-PA) Is Targeted to the Regulated Secretory Pathway. The Journal of Biological Chemistry 272:1976-1982.

Rollenhagen A, Lubke JH (2010) The mossy fiber bouton: the "common" or the "unique" synapse? Front Synaptic Neurosci 2:2.

Rollenhagen A, Satzler K, Rodriguez EP, Jonas P, Frotscher M, Lubke JH (2007) Structural determinants of transmission at large hippocampal mossy fiber synapses. J Neurosci 27:10434-10444.

Salin PA, Scanziani M, Malenka RC, Nicoll RA (1996) Distinct short-term plasticity at two excitatory synapses in the hippocampus. Proc Natl Acad Sci U S A 93:13304-13309.

Salles FJ, Strickland S (2002) Localization and regulation of the tissue plasminogen activator-plasmin system in the hippocampus. J Neurosci 22:2125-2134.

Sappino AP, Madani R, Huarte J, Belin D, Kiss JZ, Wohlwend A, Vassalli JD (1993) Extracellular proteolysis in the adult murine brain. J Clin Invest 92:679-685.

Scalettar BA, Jacobs C, Fulwiler A, Prahl L, Simon A, Hilken L, Lochner JE (2012) Hindered submicron mobility and long-term storage of presynaptic dense-core granules revealed by single-particle tracking. Dev Neurobiol 72:1181-1195.

Schindelin J, Arganda-Carreras I, Frise E, Kaynig V, Longair M, Pietzsch T, Preibisch S, Rueden C, Saalfeld S, Schmid B, Tinevez JY, White DJ, Hartenstein V, Eliceiri K, Tomancak P, Cardona A (2012) Fiji: an open-source platform for biological-image analysis. Nat Methods 9:676-682.

Schmid B, Schindelin J, Cardona A, Longair M, Heisenberg M (2010) A high-level 3D visualization API for Java and ImageJ. BMC Bioinformatics 11:274.

Shin CY, Kundel M, Wells DG (2004) Rapid, activity-induced increase in tissue plasminogen activator is mediated by metabotropic glutamate receptor-dependent mRNA translation. J Neurosci 24:9425-9433.

Siao CJ, Tsirka SE (2002) Tissue plasminogen activator mediates microglial activation via its finger domain through annexin II. J Neurosci 22:3352-3358.

Silverman MA, Johnson S, Gurkins D, Farmer M, Lochner JE, Rosa P, Scalettar BA (2005) Mechanisms of transport and exocytosis of dense-core granules containing tissue plasminogen activator in developing hippocampal neurons. J Neurosci 25:3095-3106.

Somogyi P, Klausberger T (2005) Defined types of cortical interneurone structure space and spike timing in the hippocampus. J Physiol 562:9-26.

Su EJ, Fredriksson L, Geyer M, Folestad E, Cale J, Andrae J, Gao Y, Pietras K, Mann K, Yepes M, Strickland DK, Betsholtz C, Eriksson U, Lawrence DA (2008) Activation of PDGF-CC by tissue plasminogen activator impairs blood-brain barrier integrity during ischemic stroke. Nat Med 14:731-737.

Sylwestrak EL, Ghosh A (2012) Elfn1 regulates target-specific release probability at CA1-interneuron synapses. Science 338:536-540.

Tasan RO, Verma D, Wood J, Lach G, Hormer B, de Lima TC, Herzog H, Sperk G (2016) The role of Neuropeptide Y in fear conditioning and extinction. Neuropeptides 55:111-126.

Toth K, Suares G, Lawrence JJ, Philips-Tansey E, McBain CJ (2000) Differential mechanisms of transmission at three types of mossy fiber synapse. J Neurosci 20:8279-8289.

Tsirka SE, Gualandris A, Amaral DG, Strickland S (1995) Excitotoxin-induced neuronal degeneration and seizure are mediated by tissue plasminogen activator. Nature 377:340-344.

Van Keuren ML, Gavrilina GB, Filipiak WE, Zeidler MG, Saunders TL (2009) Generating transgenic mice from bacterial artificial chromosomes: transgenesis efficiency, integration and expression outcomes. Transgenic Res 18:769-785.

Wenzel HJ, Cole TB, Born DE, Schwartzkroin PA, Palmiter RD (1997) Ultrastructural localization of zinc transporter-3 (ZnT-3) to synaptic vesicle membranes within mossy fiber boutons in the hippocampus of mouse and monkey. Proc Natl Acad Sci U S A 94:12676-12681.

Wu F, Torre E, Cuellar-Giraldo D, Cheng L, Yi H, Bichler EK, Garcia PS, Yepes M (2015) Tissue-type plasminogen activator triggers the synaptic vesicle cycle in cerebral cortical neurons. J Cereb Blood Flow Metab 35:1966-1976.

Yu H, Schleuning WD, Michl M, Liberatore G, Tan SS, Medcalf RL (2001) Control elements between -9.5 and -3.0 kb in the human tissue-type plasminogen activator gene promoter direct spatial and inducible expression to the murine brain. Eur J Neurosci 14:799-808.

Zhang Y, Chen K, Sloan SA, Bennett ML, Scholze AR, O'Keeffe S, Phatnani HP, Guarnieri P, Caneda C, Ruderisch N, Deng S, Liddelow SA, Zhang C, Daneman R, Maniatis T, Barres BA, Wu JQ (2014) An RNA-sequencing transcriptome and splicing database of glia, neurons, and vascular cells of the cerebral cortex. J Neurosci 34:11929-11947.

Zhuo M, Holtzman DM, Li Y, Osaka H, DeMaro J, Jacquin M, Bu G (2000) Role of tissue plasminogen activator receptor LRP in hippocampal long-term potentiation. J Neurosci 20:542-549.

Zou T, Ling C, Xiao Y, Tao X, Ma D, Chen ZL, Strickland S, Song H (2006) Exogenous tissue plasminogen activator enhances peripheral nerve regeneration and functional recovery after injury in mice. J Neuropathol Exp Neurol 65:78-86.

Table 2.1. Localization and coexpression of tPA-Cerulean positive soma in hippocampus of tPA^{BAC}-Cer mice

	Localization of tPA-Cerulean positive soma			Coexpression of tPA-Cerulean positive soma	
	CA1 SO Alveus	CA3 SO Alveus	CA1 and CA3 SP/SR	tPA-Cerulean positive neurons expressing SST (%)	SST-positive interneurons expressing tPA (%)
Line 863	11.68 ± 1.53 (n=301)	5.58 ± 1.14 (n=141)	3.32 ± 1.15 (n=78)	54.35 ± 6.32 (n=520)	53.89 ± 8.82 (n=520)
Line 876	10.90 ± 2.06 (n=238)	5.34 ± 1.98 (n=115)	2.28 ± 1.06 (n=52)	58.90 ± 6.74 (n=405)	44.66 ± 9.45 (n=540)

Results are presented as the mean ± $CI_{(0.95)}$ for a given hippocampal section. Cell count data was gathered from stratum oriens/alveus (SO/Alveus), stratum pyramidale (SP), and stratum radiatum (SR). "n" refers to the total number of cells counted from 2-4 hippocampal sections per tPA^{BAC}-Cer transgenic mouse (lines 863 and 876; mice = 8 per line).

Figure 2.1

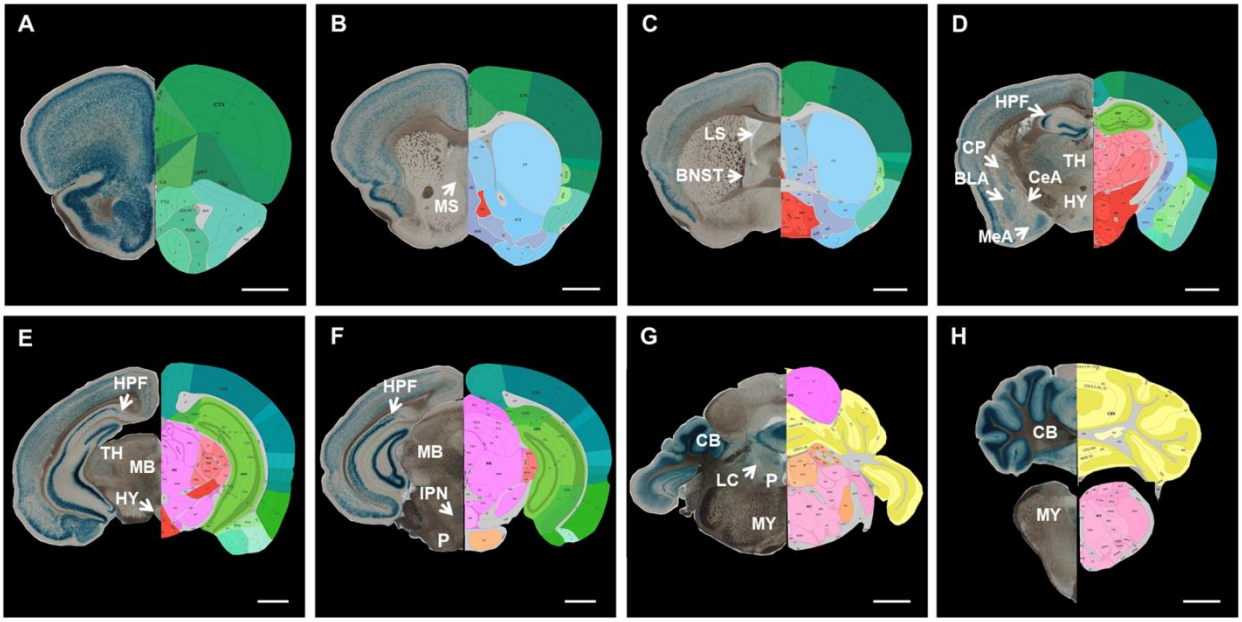
A
B
MS
C
LS
BNST
D
HPF
CP
BLA
CeA
TH
HY
MeA
E
HPF
TH
MB
HY
F
HPF
MB
IPN
P
G
CB
LC
P
MY
H
CB
MY

Figure 2.1. 5-Bromo-4-Chloro-3-Indolyl-β-D-Galactoside analysis of tPA expression in PlatβGAL reporter mice. Representative images (10x) from a heterozygous PlatβGAL reporter mouse (mice, n = 5) stained for β-Gal. Sections (50 µm) were cut coronally starting from the frontal cortex around bregma +2.5 and progressing caudally to the cerebellum around bregma -8.0. tPA/β-Gal activity is strongly present in the cortex (**A - F**), in the granule and pyramidal cell layers of the hippocampus (**D - F**), and in the molecular and granular layers of the cerebellum (**G - H**). More diffuse tPA/β-Gal staining is observable in subcortical regions, such as the medial (**B**) and lateral septal nuclei (**C**), the bed nucleus of the stria terminalis (**C**), caudate/putamen (**D**), the basolateral and centromedial nuclei of the amygdala (**D**), and thalamus and hypothalamus (**D,E**). The locus coeruleus, where neuroserpin, the neuronal inhibitor of tPA is highly concentrated, is largely devoid of tPA/β-Gal staining (**G**). There are also distinct β-Gal clusters in midbrain-, pontine-, and medulla structures (**F,G**), such as the interpeduncular nucleus (**F**). Coronal reference atlas images (were taken from the Allen Developing Mouse Brain Atlas (http://mouse.brain-map.org/static/atlas). From **A**-**H**, the following thumbnails were used: 32, 47, 53, 71, 82, 89, 109, and 123, respectively. Abbreviations: MS – medial septal nuclei; LS – lateral septal nuclei; BNST – bed nucleus of the stria terminalis; HPF – hippocampal formation; TH – thalamus; CP – caudate/putamen; BLA – basolateral nucleus of the amygdala; CeA – central nucleus of the amygdala; MeA – medial nucleus of the amygdala; HY – hypothalamus; MB – midbrain; IPN – interpeduncular nucleus; P – pons; LC – locus coeruleus; CB – cerebellum; MY - medulla. Scale bars: 1 mm. Reference atlas images credit: Allen Institute.

Figure 2.2

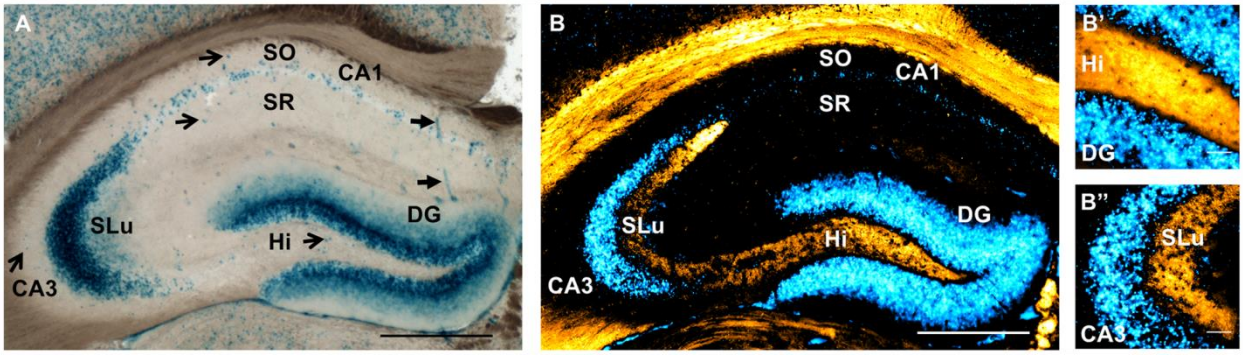

Figure 2.2. Immunohistochemical analysis of tPA protein expression in the hippocampus of PlatβGAL reporter mice reveals a differential expression pattern between the sites of tPA synthesis and tPA trafficking. (**A**) Representative image (10x) of a 50 µm hippocampal section from a heterozygous PlatβGAL reporter mouse (mice, n = 5). tPA is shown to be strongly expressed in the granule cell layer of the dentate gyrus and the pyramidal cell layer of hippocampal regions CA1 - CA3. There are also scattered β-Gal puncta (*arrows*) in the hilus, stratum radiatum, and stratum oriens; β-Gal staining is also present in blood vessels in the hippocampus (*filled arrows*). (**B**) Immunohistochemical analysis of a representative image (10x) from a 50 µm hippocampal section from a heterozygous PlatβGAL reporter mouse (mice, n = 5) using antibodies directed against murine tPA (*orange*). In contrast to the β-Gal stain (*cyan*), tPA is not expressed in the cell body layers, but in the mossy fiber axons of dentate granule cells in the hilus and stratum lucidum lamina (**B'** and **B"**, 40x). To visualize the colored β-Gal stain in the immunofluorescent image captured showing tPA-immunoreactivity, a negative of the fluorescent image was generated and pseudo-colored cyan. Abbreviations: SLu – stratum lucidum; Hi – hilus; DG – dentate gyrus; SR – stratum radiatum; SO – stratum oriens. Scale bars: A and B, 500 µm; B' and B'', 50 µm.

Figure 2.3

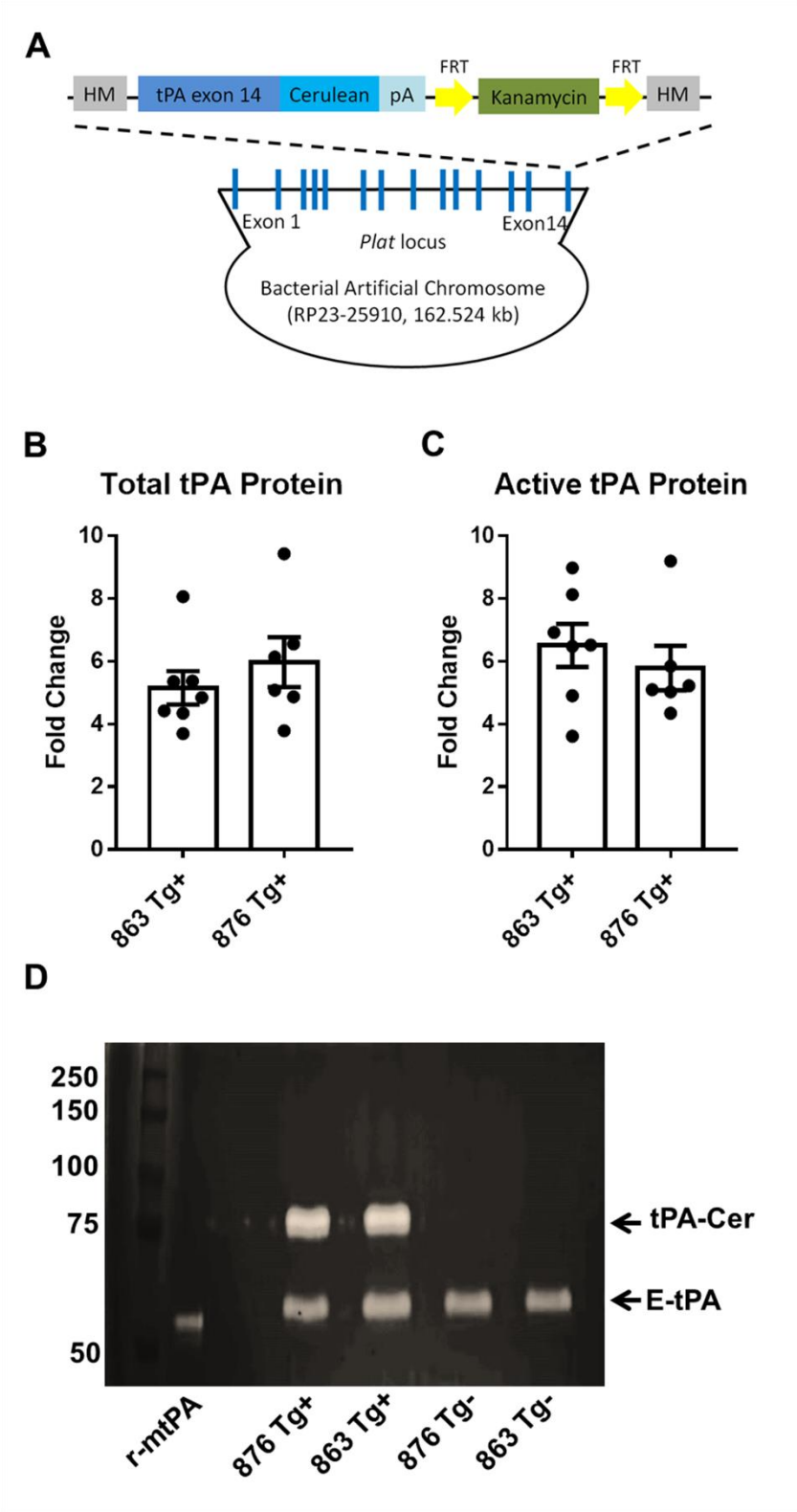
A
HM
tPA exon 14
Cerulean
pA
FRT
Kanamycin
FRT
HM
Exon 1
Exon14
Plat locus
Bacterial Artificial Chromosome
(RP23-25910, 162.524 kb)
B
Total tPA Protein
Fold Change
10
8
6
4
2
0
863 Tg+
876 Tg+
C
Active tPA Protein
Fold Change
10
8
6
4
2
0
863 Tg+
876 Tg+
D
250
150
100
75
50
tPA-Cer
E-tPA
r-mtPA
876 Tg+
863 Tg+
876 Tg-
863 Tg-

Figure 2.3. Generation and global tPA protein characterization of tPA^{BAC}-Cerulean transgenic mice. (**A**) Founder lines for tPA^{BAC}-Cer transgenic mice (863 and 876) were generated using Bacterial Artificial Chromosome (BAC) technology. To generate tPA^{BAC}-Cer transgenic mice, a kanamycin-resistance recombineering cassette containing a cerulean fluorescent gene fused to the carboxy terminal of exon 14 of the tPA gene was recombineered into a BAC. The tPA-Cer fusion gene is under control of endogenous regulatory elements contained in the *Plat* locus. (**B**–**D**) Protein expression profile of tPA^{BAC}-Cer transgenic mice. Brains from transgene positive and transgene negative adult tPA^{BAC}-Cer mice were harvested and homogenized for total and active protein quantification using a bead-based Luminex assay (**B**) and ELISA (**C**). Data are presented as the mean ± SEM fold change from tPA protein levels in transgene negative littermate controls (mice n = 6-7). No statistical difference was noted in total and active tPA protein levels between line 863 and 876. (**D**) Zymographic analysis of whole brain homogenates from tPA^{BAC}-Cer transgene positive and negative mice (lines 863 and 876) visually delineates endogenous tPA (lower molecular weight bands, E-tPA) and the tPA-Cer from the BAC (higher molecular weight bands, tPA-Cer). Not only is there increased levels of tPA protein in both tPA^{BAC}-Cer transgenic lines, but the tPA-Cer protein is proteolytically active. Abbreviations: FRT – flippase recognition target; HM - homology arms; r-mtPA, recombinant-murine tPA; E-tPA, endogenous-tPA.

Figure 2.4

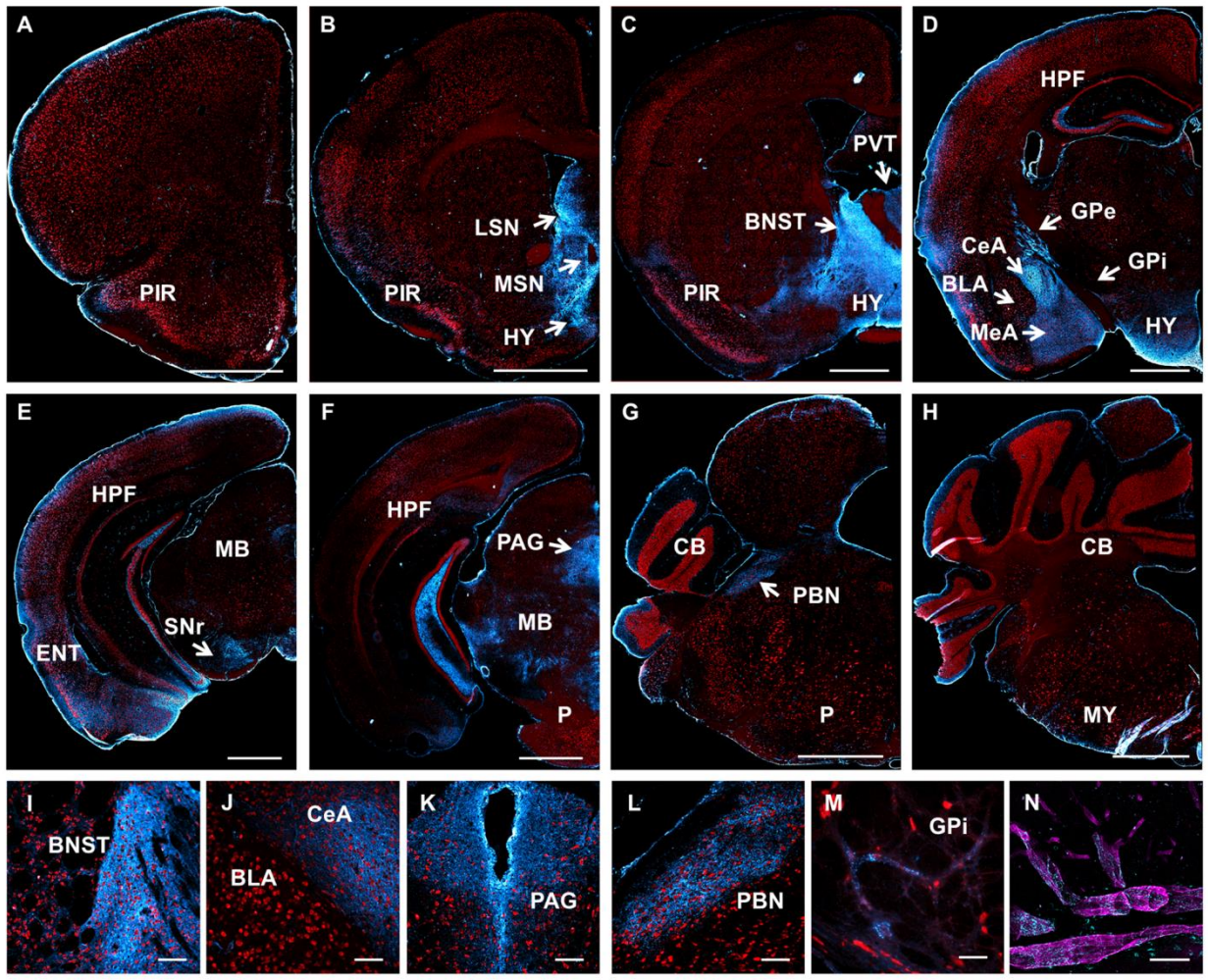
A
PIR
B
LSN
MSN
PIR
HY
C
PVT
BNST
PIR
HY
D
HPF
GPe
CeA
GPi
BLA
MeA
HY
E
HPF
MB
SNr
ENT
F
HPF
PAG
MB
P
G
CB
PBN
P
H
CB
MY
I
BNST
J
CeA
BLA
K
PAG
L
PBN
M
GPi
N

Figure 2.4. tPA-Cerulean fusion protein is prominently expressed in limbic structures and blood vessels in the adult murine brain. Images shown are representative of stitched serial coronal sections from tPA^{BAC}-Cer transgenic mice (n = 3) captured on a widefield microscope (**A**–**H**, 10x; **I**–**L**, 20x; **M**, 40x) or confocal microscope (**N**, 63x). Cryosections stained for the neuronal marker NeuN (*red*) clearly distinguishes the faint tPA-Cer (*cyan*) cells bodies observed in the piriform (**A**–**D**) and entorhinal cortex (**E**), and the tPA-Cer fluorescent nerve fibers found in the medial and lateral septal nuclei (**B**), the bed nucleus of the stria terminals (**C**,**I**), the paraventricular nucleus of the thalamus (**C**) and hypothalamus (**D**), the central (**D**, **J**) and medial (**D**) nuclei of the amygdala, the external (**D**) and internal (**M**) globus pallidus of the basal ganglia, substantia nigra pars reticulata (**E**), the periaqueductal gray (**F**, **K**), and the parabrachial nucleus (**G**, **L**).tPA is also robustly expressed in the hilus and mossy fiber pathway of the hippocampus (**D**–**F**). (**G**, **H**) In contrast to the PlatβGAL reporter mice, tPA expression is not observable in the cerebellum. (**N**) Brightly positive tPA-Cer puncta are noticeable throughout all brain regions in blood vessels using the endothelial cell marker, CD31 (*magenta*). Abbreviations: PIR – piriform cortex; ENT – entorhinal cortex; LS – lateral septal nuclei; MS – medial septal nuclei; BNST – bed nucleus of the stria terminalis; PVT –paraventricular nucleus of the thalamus; HY – hypothalamus; HPF – hippocampal formation; CeA – central nucleus of the amygdala; MeA – medial nucleus of the amygdala; BLA – basolateral nucleus of the amygdala; GPe – globus pallidus external segment; GPi – globus pallidus internal segment; SNr – substantia nigra pars reticulata; PAG – periaqueductal gray; PBN – parabrachial nucleus; MB – midbrain; P – pons; CB – cerebellum; MY – medulla. Scale bars: A - H, 1mm; I–M, 100 µm; K, N, 50 µm.

Figure 2.5

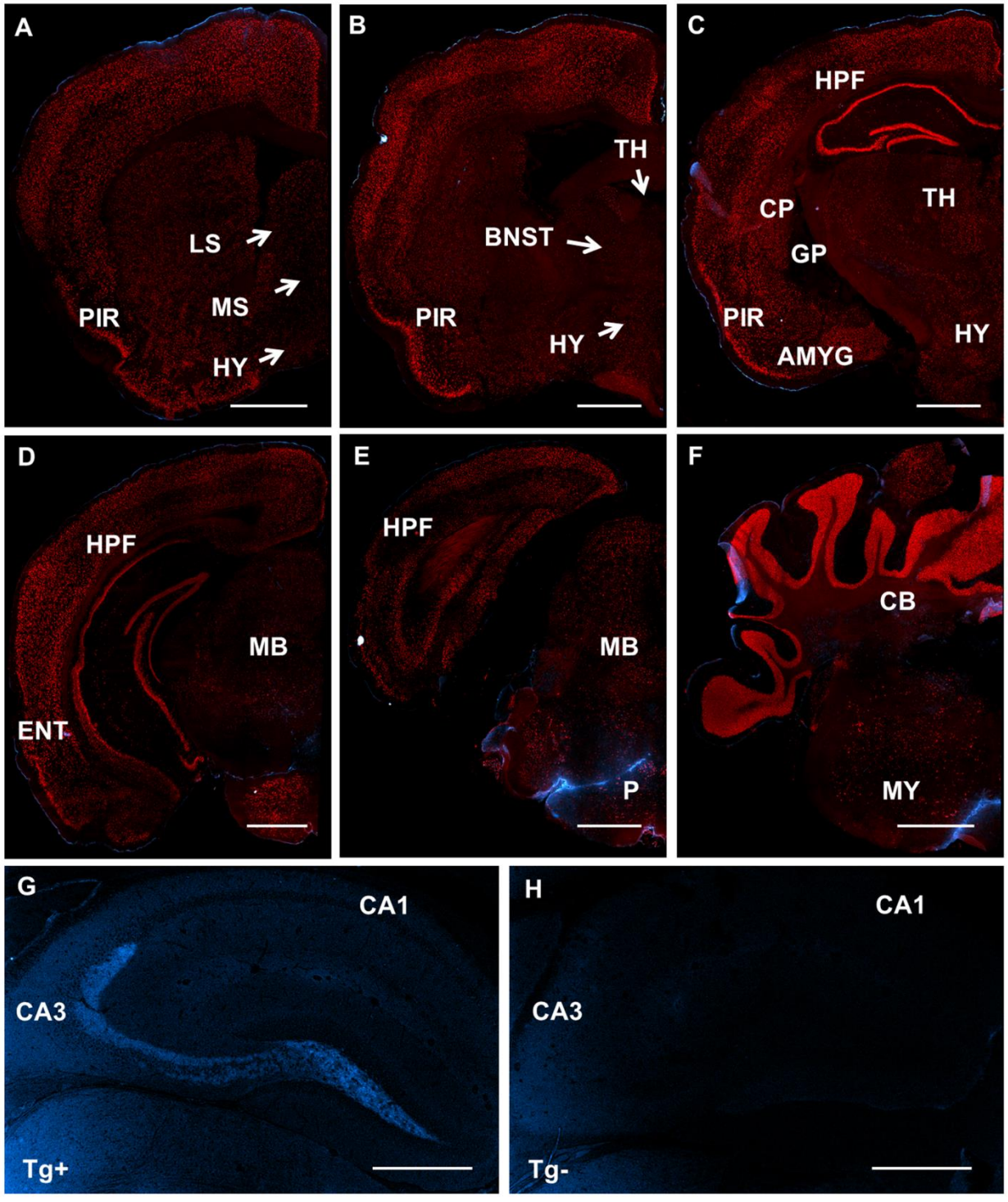
A
LS
MS
PIR
HY
B
TH
BNST
PIR
HY
C
HPF
TH
CP
GP
PIR
AMYG
HY
D
HPF
MB
ENT
E
HPF
MB
P
F
CB
MY
G
CA1
CA3
Tg+
H
CA1
CA3
Tg-

Figure 2.5. tPA-Cerulean fluorescence is not observed in tPA^{BAC}-Cer transgene negative littermate controls. (**A**–**D**) Images shown are representative of stitched serial coronal sections from tPA^{BAC}-Cer transgene negative littermate mice (n = 2) captured on a widefield microscope (10x). Cyrosections (14 µm) stained for the neuronal marker NeuN (*red*) show no cerulean fluorescence in cell bodies in the piriform (**A**–**C**) or entorhinal cortex (**D**). Cerulean fluorescence is also not observable in the medial and lateral septal nuclei (**B**), the bed nucleus of the stria terminals (**B**), the amygdala (**C**), globus pallidus (**C**), or the thalamus and hypothalamus (**B**, **C**). Midbrain and pontine brain structures are devoid of any cerulean fluorescence (**D**–**E**), as are the medulla and cerebellum (**F**). (**G**, **H**) Representative images from widefield microscopy (4x) of the hippocampus from a tPA^{BAC}-Cer transgene positive (Tg+) mouse and its transgene negative (Tg-) littermate. Cerulean fluorescence is clearly observable in the mossy fiber pathway of a tPA^{BAC}-Cer transgene positive mouse, but completely absent in the transgene negative control. Cerulean fluorescent artifacts from edge effects or folds are apparent in panels **C**, **E**, and **F**. Abbreviations: PIR – piriform cortex; ENT – entorhinal cortex; LS – lateral septal nuclei; MS – medial septal nuclei; BNST – bed nucleus of the stria terminalis; TH – thalamus; HPF – hippocampal formation; AMYG – amygdala; HTH – hypothalamus; CP – caudate/putamen; GP – globus pallidus; MB – midbrain; P – pons; CB – cerebellum; MY - medulla. Scale bars: A - F, 1mm; G-H, 500 µm.

Figure 2.6

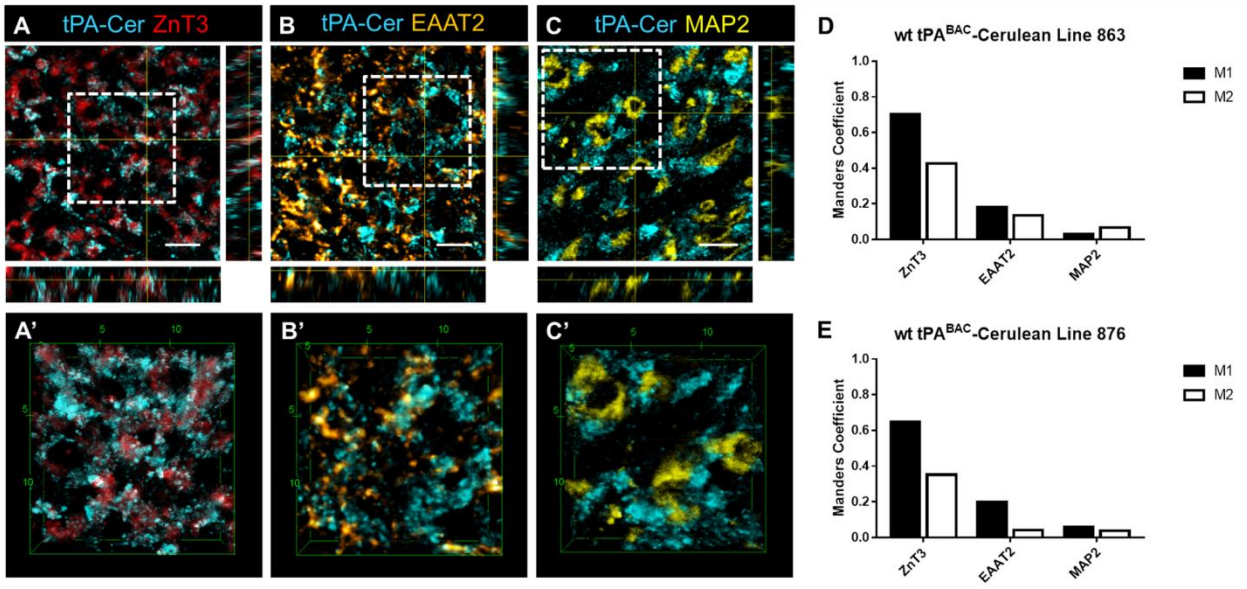
A tPA-Cer ZnT3
B tPA-Cer EAAT2
C tPA-Cer MAP2
A'
B'
C'
D
wt tPA^BAC-Cerulean Line 863
Manders Coefficient
1.0
0.8
0.6
0.4
0.2
0.0
ZnT3
EAAT2
MAP2
M1
M2
E
wt tPA^BAC-Cerulean Line 876
Manders Coefficient
1.0
0.8
0.6
0.4
0.2
0.0
ZnT3
EAAT2
MAP2
M1
M2

Figure 2.6. tPA-Cerulean is localized to large mossy fiber boutons and astrocytes in the CA3 stratum lucidum lamina of the hippocampus. Subcellular colocalization of tPA in stratum lucidum of the hippocampus was investigated using high-resolution confocal microscopy. Images (63x) are representative regions of interest from the stratum lucidum lamina of tPA^{BAC}-Cer transgenic mice and are presented as 5 µm z-stacks (Δz = 0.5 µm) visualized in orthogonal YZ and XZ slices (**A**–**C,**) and magnified 3D maximum intensity projections (**A'**–**C'**), for each of the respective colocalization markers. For quantification of colocalization using the Manders coefficient (**D**, **E**) entire images were concatenated from 5 µm z-stacks (512 pixels x 512 pixels; Δz = 0.5 µm) that were independently acquired 2 – 4 times (ZnT3: mice n = 10, lines 863 and 876; EAAT2: mice n = 6 - 8, lines 863 and 876, respectively; MAP2: mice n = 4, lines 863 and 876). tPA-Cer puncta was found to colocalize with the zinc transporter-3 (ZnT3, *red*), which has previously been observed exclusively in mossy fiber boutons, as indicated visually by the white overlay in the orthogonal sections and 3D max projection (Manders M1: 0.704 and 0.649 for lines 863 and 876, respectively; Costes Probability (P)-value ≥ 95%) (**D**, **E**). Partial colocalization was weakly observed in astrocytes visualized with the astrocytic glutamate transporter EAAT2 (*orange*; **B**, **B'**), which is in agreement with the lower quantified colocalization coefficient (Manders M1: 0.183 and 0.198 for lines 863 and 876, respectively; Costes Probability (P)-value ≥ 95%) (**D**, **E**). To confirm the pre-synaptic localization of tPA to mossy fiber boutons, sections were also stained for the dendritic marker MAP2, which detects the dendritic thorny excrescences of CA3 pyramidal neurons that mossy fiber boutons encase. Orthogonal YZ and XZ slices and 3D max projections of tPA-Cer and MAP2 (*yellow;* **C**, **C'**) showed no colocalization (Manders M1: 0.032 and 0.060 for lines 863 and 876, respectively; Costes Probability (P)-value = 0.0% (**D**, **E**). Abbreviations: ZnT3 - zinc-transporter 3; EAAT2 - excitatory amino acid transporter 2; MAP2 - microtubule associated protein 2. Scale bars: A – C, 5 µm; A' – C', µm.

Figure 2.7

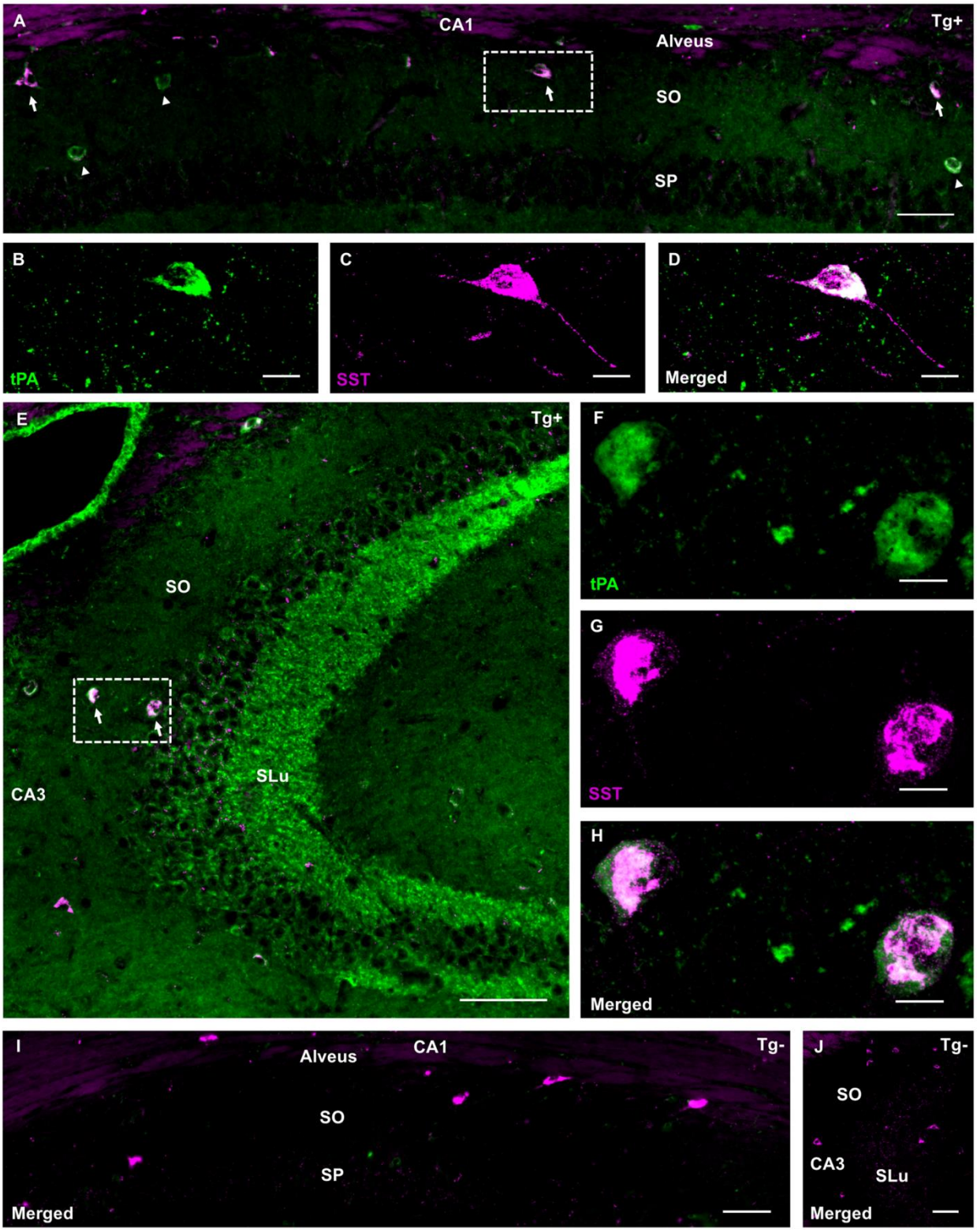
A
CA1
Alveus
Tg+
SO
SP
B
tPA
C
SST
D
Merged
E
Tg+
SO
SLu
CA3
F
tPA
G
SST
H
Merged
I
Alveus
CA1
Tg-
SO
SP
Merged
J
Tg-
SO
CA3
SLu
Merged

Figure 2.7. Amplification of tPA-Cerulean signal reveals a population of cells in stratum oriens/alveus of the hippocampal CA1 and CA3 regions that co-express somatostatin. Representative images of hippocampal CA1 (**A**) and CA3 (**E**) subfields from tPA^{BAC}-Cer transgenic mice (mice, n = 8) exemplifying the localization and distribution of tPA-Cer cell bodies (tPA, *green*) that co-express the inhibitory interneuronal marker somatostatin (SST, *magenta*) – see Table 2.1 for localization and distribution statistics. With GFP Tyramide signal amplification, somatic tPA is also detectable in the pyramidal cell layer of the CA3 subfield (**E**), though it is still largely absent in the CA1 pyramidal cell layer (**A**). Confocal (63x) maximum intensity projections focused on a region of interest (dashed box) highlighting tPA-Cer positive cells (tPA, *green*) that co-express SST (*magenta*) from the CA1 (**B**–**D**) and CA3 (**F**–**H**) stratum oriens/alveus lamina. Unlike the punctate nature of tPA in axonal projections, tPA's somatic expression appears more diffuse. (**I**–**J**) Immunostaining for SST and GFP with Tyramide signal amplification in transgene negative controls only revealed SST-positive interneurons in the SO/alveus lamina of hippocampal CA1 (**I**) and CA3 (**J**). Abbreviations: SO – stratum oriens; SP – stratum pyramidale; and SLu – stratum lucidum. Scale bars: A, 50 µm; C – D, 10 µm; E, 100 µm; F – H, 10 µm; I, 50 µm; J, 100 µm.

Figure 2.8

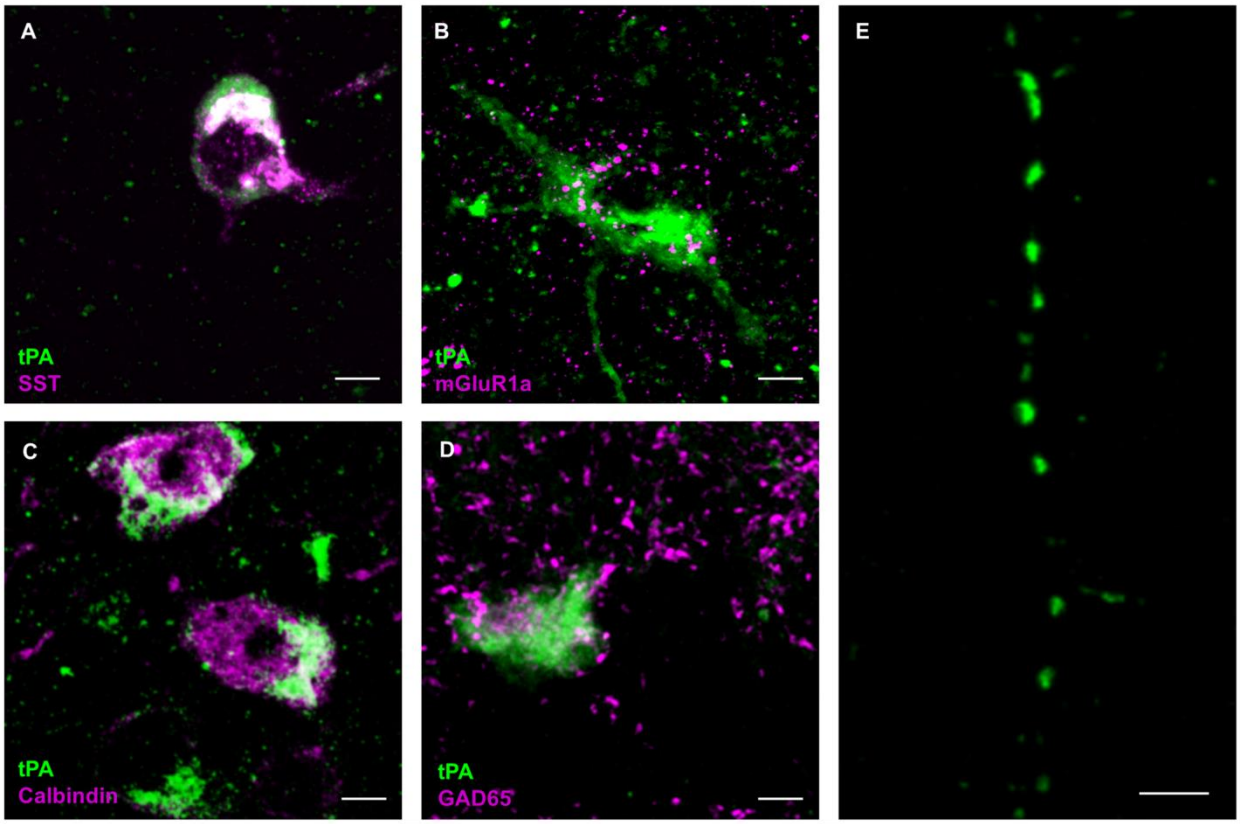

Figure 2.8. tPA-Cerulean cells are positive for immunocytochemical markers of oriens-lacunosum moleculare (O-LM) inhibitory interneurons. Dorsal hippocampal sections from tPA^{BAC}-Cer transgenic mice were probed for previously confirmed immunocytochemical markers of O-LM inhibitory interneurons. While O-LM interneurons are known for expressing SST (**A**), other morphologically distinct interneuron subgroups have been shown to stain positive for the neuropeptide. O-LM interneurons, though, have been shown to be strongly decorated with the metabotropic glutamate receptor 1a, mGluR1a, and they have been shown to express the calcium-binding protein calbindin. High-resolution, confocal images (63x) of 10 µm thick z-stack maximum intensity projections demonstrate that tPA-Cer positive cells bodies in SO/alveus co-express both mGluR1a (**B**) and calbindin (**C**). Sections were also stained for GAD65, confirming the GABAergic nature of the tPA-Cer expressing cells (**D**). In agreement with this O-LM immunocytochemical profile was the observation of axonal-like projections in stratum radiatum, as axons of O-LM interneurons extend to stratum lacunosum moleculare (**E**). Pictures are representative images from stratum oriens/alveus of stainings from at least 4 transgenic mice (n = 4–8) per interneuronal marker. Abbreviations: SST-somatostatin; mGluR1a – metabotropic glutamate receptor 1a; GAD 65 – glutamic acid decarboxylase 65. Scale bars: A – E, 5 µm.

CHAPTER 3

Ex vivo synchronous activity in brain slices from tPA$^{-/-}$ and Nsp$^{-/-}$ mice does not phenocopy the *in vivo* seizure behavior of tPA$^{-/-}$ and Nsp$^{-/-}$ mice

3.1 Abstract

Seizures are episodes of abnormal brain activity and are characterized by hyper-excitable neurons and the synchronous propagation of electrical activity. They are a significant health and economic burden in the U.S., with 200,000 new cases reported each year and 17.6 billion spent annually to treat and care for patients. Proteolytic activity in the CNS has been shown to play a role in seizure severity. Indeed, following injection of kainate into the amygdala, our lab has shown that mice lacking the serine protease tissue plasminogen activator (tPA$^{-/-}$) have a delayed seizure onset time compared to wild-type mice; and, mice lacking the serine protease inhibitor (serpin) neuroserpin (Nsp$^{-/-}$), a specific inhibitor of tPA, have an enhanced seizure onset time. Electroencephalography recordings agree with this behavioral seizure scoring data. In contrast, we have shown that in *ex vivo* electrophysiological recordings of synchronous (or "seizure-like") activity in brain slices from each genotype do not show this phenotype.

Parts of this chapter were published in: Fredriksson L, Stevenson TK, Su EJ, Ragsdale M, Moore S, Craciun S, Schielke GP, Murphy GG, Lawrence DA (2015) Identification of a neurovascular signaling pathway regulating seizures in mice. Ann Clin Transl Neurol 2:722-738.

Instead, our data suggests that the onset time and severity of seizures in $Nsp^{-/-}$ and $tPA^{-/-}$ mice correlate with increases in blood-brain barrier (BBB) permeability. In our previously published study we focused on the role of the BBB in seizure progression (Fredriksson et al., 2015), whereas in this chapter we focus on the electrophysiological consequences of Nsp and tPA deficiency.

3.2 Introduction

Epilepsy is a neurological disorder characterized by hyperactive, excitable neurons and the synchronous propagation of electrical activity, resulting in seizure behavior. It comes from the Greek word “epikgqia,” which originates from the verb “epilambanein” – to seize, possess, or afflict (Magiorkinis et al., 2010). The Ancient Greeks attributed seizures to a form of spiritual possession. With recent advances in genetic sequencing, however, epilepsy has shifted from becoming an idiopathic disease to a genetic one. Even the International League Against Epilepsy proposed language that would label epilepsy to be of genetic etiology and not idiopathic in nature (Berg et al., 2010; Lascano et al., 2016). Not all seizures result from genetic defects, though, as there are still about 40% of cases of epilepsy that fall into a “cryptogenic” classification because a cause cannot be identified (Shorvon, 2011). Moreover, roughly 30-40% of patients with epilepsy has what is known as refractory epilepsy and fails to respond to currently available antiepileptic drugs (Laxer et al., 2014). Therefore, there is still a large, unmet need for understanding the diverse etiology and complicated pathophysiology of epilepsy.

Dramatic insults to the cerebrovasculature from stroke, traumatic brain injury (TBI), or infection are known to be causal in the development of symptomatic epilepsy (Herman, 2002; Friedman et al., 2009). Furthermore, accumulating evidence suggests that dysregulation of the blood-brain barrier (BBB) can be a significant contributing factor to the pathophysiology of seizures (Oby and Janigro, 2006; Daneman, 2012). This has led to the recognition that the BBB is a druggable target for the treatment of seizures (Friedman et al., 2009). The serine protease tissue plasminogen activator (tPA), which is more commonly known for its role promoting fibrinolysis in the vasculature, is also highly expressed in the central nervous system (CNS) (Sappino et al., 1993; Yu et al., 2001) and has been implicated in regulating BBB permeability in models of stroke, seizures, and TBI (Yepes et al., 2003; Su et al., 2008; Fredriksson et al., 2015; Su et al., 2015; Su et al., 2017). Mice deficient in tPA ($tPA^{-/-}$) have been shown to have delayed seizure progression as well (Tsirka et al., 1995; Yepes et al., 2002; Pawlak et al., 2005; Fredriksson et al., 2015). It is unclear if the seizure phenotype in $tPA^{-/-}$ mice is related to tPA's role in regulating BBB permeability or in modulating synaptic transmission, as tPA expression and activity is specifically upregulated in the hippocampus following seizure induction (Qian et al., 1993; Tsirka et al., 1995; Yepes et al., 2002).

It is also unclear if proteolytically active tPA or inactive tPA is responsible for modulating seizure progression. For, in both rats and wild-type mice treated with the serine protease inhibitor neuroserpin (Nsp), a specific inhibitor of tPA in the brain, seizure progression of kainic acid (KA)-induced seizures is delayed (Yepes et al., 2002). Moreover, Nsp deficient mice ($Nsp^{-/-}$) have enhanced seizure onset time following KA-

injection, while tPA$^{-/-}$ mice have an attenuated seizure onset time, suggesting that dysregulation of tPA activity promotes seizure progression (Fredriksson et al., 2015). This “seizure-resistant” phenotype observed in tPA$^{-/-}$ mice is thought, in part, to occur from tPA’s role in regulating BBB integrity. For, seizure progression and severity in Nsp$^{-/-}$ and tPA$^{-/-}$ mice correlate with increases in BBB permeability.

In contrast, in a model of ethanol withdrawal seizures, treatment with the tPA-inhibitor, tPA-STOP, had no effect on seizure severity (Pawlak et al., 2005). Rather, it was shown that tPA’s non-proteolytic interaction with NR2B subunit of the NMDA receptor was responsible for seizure severity after ethanol withdrawal. As there is evidence for active tPA and inactive tPA mediating independent pathways in neuronal degeneration and microglial activation, respectively (Rogove et al., 1999), it’s possible that the experimental seizure paradigms revealed differential roles for active and inactive tPA in seizure progression. Further studies, however, are needed to specifically test and dissect the contribution of active tPA and inactive tPA to seizures.

In an effort to begin to address 1) the BBB component to the observed seizure phenotype in tPA$^{-/-}$ mice and Nsp$^{-/-}$ mice and 2) the effect of unregulated tPA activity in synaptic transmission and synchronous activity, an *ex vivo* electrophysiological approach was taken in our studies. In an *ex vivo* preparation, a brain slice is bathed in oxygenated artificial cerebral spinal fluid (aCSF) and not subject to alterations of the BBB. As such, the hypothesis being tested is that if the *in vivo* seizure phenotype in wild-type, tPA$^{-/-}$, and Nsp$^{-/-}$ mice is related to the BBB, then in an *ex vivo* slice preparation there should be no phenotypic difference between these mice. To test our hypothesis, brain slices from wild-type, tPA$^{-/-}$, and Nsp$^{-/-}$ mice were bathed in no

Mg^{2+}/high K^+ aCSF to generate synchronized population bursts. This method, which enhances conductance of NMDA receptors and lowers the neuronal firing threshold, is a well-established *in vitro* correlate of *in vivo* seizures. Synaptic transmission was assessed by field potential recordings in the CA1 and CA3 subfields of the hippocampus. Evoked responses in standard aCSF were used to generate input/output (I/O) curves as a measure of normal basal synaptic transmission, while a gap-free recording was used to measure the baseline field potential in standard aCSF and spontaneous, synchronized firing in no Mg^{2+}/high K^+ aCSF.

Our results demonstrate that with this model we are able to induce synchronized population bursts characteristic of *in vivo* seizure activity, and we are able to evaluate the neuronal component contributing to that activity. We find that the *ex vivo* "seizure-like" phenotype in brain slices from $Nsp^{-/-}$ and $tPA^{-/-}$ mice does not phenocopy the *in vivo* seizure behavior of $Nsp^{-/-}$ and $tPA^{-/-}$ mice. Interestingly, brain slices from $tPA^{-/-}$ mice appear to be in a more hyperexcitable state than wild-type or $Nsp^{-/-}$ mice, while brain slices from $Nsp^{-/-}$ mice appear to be in a more quiescent state than wild-type or $tPA^{-/-}$ mice. These data support the evidence demonstrating a significant BBB component to the *in vivo* seizure phenotype observed in $Nsp^{-/-}$ and $tPA^{-/-}$ mice.

3.3 Materials and Methods

3.3.1 Transgenic mice

3.3.1.1 Nsp^{BAC}-DsRED and tPA^{BAC}-Cer transgenic mice. Founder lines (519 and 552) for Nsp^{BAC}-DsRed transgenic mice were generated using BAC technology. To generate Nsp^{BAC}-DsRed transgenic mice, exon 9 of the neuroserpin gene, *Serpini1*, on a 222.141

kb BAC acquired from chori.org (RP23-300M7), was replaced with a DsRED fluorescent gene inserted into exon 9 of the neuroserpin gene (AJ001700.1) just prior to the coding sequence for the 13 residue vesicular targeting sequence (Ishigami et al., 2007) followed by a bovine growth hormone (BGH) polyadenylation signal sequence. The Nsp-DsRed fusion gene is under control of the endogenous regulatory elements contained in the *Serpini1* locus. BAC DNA integrity was verified by restriction enzyme analysis via pulse field gel electrophoresis and exon sequencing prior to pronuclear microinjection of supra-ovulated eggs from (C57BL/6 x SJL)F1/TAC female mice. Transgenic mice were genotyped by PCR using primers that were specific to a remnant of the sub-cloning PGKneo vector and the Nsp-DsRed fusion gene (FWD 5' – ACG GCG TGC TGA AGG GCG AGA TCT – 3', and REV 5' – CGT AGA ATG TTT CCT CTA CCT TAG C – 3'); and Nsp protein expression was confirmed by analysis of brain homogenates from the founder lines. After PCR analysis of the DsRED fusion gene confirmed stable, germline transmission in F1 pups two founder lines - lines 519 and 552 - were propagated; these mice have since been backcrossed at least 10 generations onto a C57BL/6J genetic background. However, only Nsp^{BAC}-DsRED transgenic mice from the F1 and F2 generations have been used for analysis in this thesis. Transgenic mice displayed normal gross anatomy and a Mendelian inheritance pattern. tPA^{BAC}-Cer transgenic mice that have a cerulean fluorescent gene fused the C-terminus of the tPA gene were described in detail previously (*See Chapter 2*) (Stevenson and Lawrence, 2018).

3.3.1.2 Transgenic mice for electrophysiological studies. For electrophysiological analysis a mixture of adult male and female tPA ($tPA^{-/-}$) (Carmeliet et al., 1993; Carmeliet et al., 1994) and neuroserpin ($Nsp^{-/-}$) mice (Madani et al., 2003), back-crossed at least 10 generations onto a C57BL/6J background, and their wild-type C57BL/6J controls were used (age: 8 – 20 wks). $Nsp^{-/-}$ mice were provided by Serguei Kozlov and Peter Sonderegger from the University of Zurich. Transgenic mice deficient for voltage-gated Na^+ channel β1 subunits ($Scn1b^{-/-}$), encoded by SCN1B and wild-type littermate controls were a kind gift from Lori Isom at the University of Michigan, Ann Arbor, USA (Chen et al., 2004). Electrophysiological experiments in $Scn1b^{-/-}$ and wild-type littermates were performed when mice were post-natal day P16-P17, prior to sex identification. All experiments were approved by the Institutional Animal Care and Use Committee at the University of Michigan, Ann Arbor, USA and the studies were conducted in accordance with the United States Public Health Service's Policy on Humane Care and Use of Laboratory Animals.

3.3.2 Protein expression analysis

3.3.2.1 Sample preparation. Total Nsp protein was analyzed using whole brain homogenates from Nsp^{BAC}-DsRED mice. Briefly, brains were harvested into ice-cold extraction buffer (0.4 M HEPES, 0.1 M NaCl, pH 7.4, 1% Triton X-100), homogenized for 1 min. (2 x 30 sec) and centrifuged at 10,000 x g for 10 min The supernatant was removed to a new, chilled 1.5 mL microcentrifuge tube and centrifuged again at 10,000 x g for 10 min. The supernatant was again removed to a new, chilled 1.5 mL microcentrifuge tube and used for ELISA assays.

3.3.2.2 Enzyme-linked immunosorbent assay (ELISA). An ELISA was performed to measure total Nsp levels from brain tissue extracts. Briefly, high-binding plates (Molecular Innovations, AVI-PLATE) were incubated with a rabbit anti-mNsp (2 µg/ml; HTmNs, Lawrence Lab) overnight at 4 °C in carbonate buffer (0.15 M Na2CO3, 0.35 M NaHCO3, pH 9.6). After which, the plate was washed 3 x 0.9% NaCl (0.05% Tween-20) and 200 uL of a blocking solution (PBS, 0.25% Bovine Serum Albumin (BSA), 0.05% Tween-20) was added to each well for 2 hrs at room temperature. The plate was again washed 3 x 0.9% NaCl (0.05% Tween-20) and 100 uL of brain extract samples/standards (diluted in blocking buffer) were loaded onto the plate and incubated for 2 hrs at room temperature. The plate was again washed 3 x 0.9% NaCl (0.05% Tween-20) and then 100 uL of sheep anti-mNsp-Biot (2 ug/mL; Molecular Innovations, SASMNSP-GF-HT-BIO) diluted in blocking buffer was added to each well for 1.5 hrs at room temperature. The plate was again washed 3 x 0.9% NaCl (0.05% Tween-20) and then 100 uL of sheep anti-HRP-conjugated secondary antibody (1:20,000) was diluted in blocking buffer and added to each well for 1 hr at room temperature. The plate was washed for a final time (3 x 0.9% NaCl (0.05% Tween-20)) After the final wash, 3,3',5,5'-Tetramethylbenzidine (TMB) substrate (Molecular Innovations, TMB) was added to each sample for 3 min at room temperature. H_2SO_4 (1 N) was then added and the plate read on a spectrophotometer at 450 nm.

3.3.2.3 Western blot. A Western blot was run to separate and detect endogenous Nsp protein and Nsp-DsRED protein in brain homogenates from Nsp^{BAC}-DsRED transgene positive and transgene negative mice. Briefly, samples, including 1 ng of recombinant

murine Nsp (mNsp) protein (Lawrence Lab) and brain homogenates from $Nsp^{-/-}$ mice, were diluted in 4X sample buffer (β-mercaptoethanol, BME), boiled for 10 min, and run on a 10% Tris gel (Bio-Rad, 4561033) for 10 min at 100 V and 40 min at 200 V. Protein was transferred overnight at 4 °C to a PVDF membrane. Blots was blocked for 1 hr (5% milk) at room temperature and then incubated with primary antibody rabbit anti-mNsp (2 µg/mL; Lawrence Lab) overnight at 4 °C in 1% BSA (0.1 % TBS-Tween 20). Membrane was then washed (3 x 0.1% TBS-Tween 20) 5 min per wash and incubated with the secondary antibody donkey anti-rabbit-HRP (1:10,000; Jackson ImmunoReserach, 711-036-152) in 0.5% milk (TBS, 0.1% Tween-20) for 1 hr at room temperature. Blots were then washed extensively in 0.1 % TBS-Tween 20 (3 x 10 min) with a final 5 min wash in TBS. Blots were then incubated with an enhanced chemiluminescence substrate (Pierce, 34080) and developed.

3.3.3 Immunofluorescence analysis

3.3.3.1 Sample preparation and antibodies. Mice were anesthetized with isoflurane and sacrificed by transcardiac perfusion for 3 min with PBS followed by perfusion for 5 min with 4% paraformaldehyde (PFA). Brains were harvested and post-fixed in 4% PFA for 1hr at 4 °C, then overnight in PBS. The brains were then moved to a 30% sucrose solution and kept at 4 °C till submerged. Subsequently, dorsal hippocampal sections (14 µm, bregma -1.5 to bregma -2.5) were cut coronally for immunofluorescence analysis of Nsp expression. Sections were permeabilized with 0.50% Triton X-100 (PBS) for 20 min at room temperature and blocked in 3% BSA (PBS) for 1 hr at room temperature. The sections were then incubated with primary antibodies in 2% BSA (PBS) overnight at

4 °C, followed by incubation with secondary antibodies in 2% BSA (PBS) for 1 hr at room temperature. When using biotin-conjugated primary antibodies and their respective streptavidin-conjugated secondary was used, a biotin-blocking kit was used to reduce background (ThermoFisher Scientific, E21390) and for amplification using the Tyramide SuperBoost Kit (ThermoFisher Scientific, B40932) detection protocols were followed according to the manufacturer's instructions.

The primary antibodies used were as follows: murine tissue plasminogen activator (Rabbit anti-mtPA, 12µg/mL; Molecular Innovations, ASMTPA-GF-HT; Lot# 914), RFP (Rabbit anti-RFP, 1:500; Sigma); podocalyxin (Goat anti-podocalyxin, 1:200; R and D); CD31 (Rat anti-mCD31, 1:100; BD Biosciences, 550274; Lot # 21055), somatostatin (Rat anti-SST, 1:100; Millipore, MAB354; Lot# 2885355, 3005269), Biotin-conjugated Goat anti-Chicken IgY H&L (1:100; abcam, ab6876). The secondary antibodies used were as follows: Donkey anti-Rat IgG (H+L) 594 (1:500; ThermoFisher Scientific, A-21209), Donkey anti-Rabbit IgG (H+L) 594 (1:500; ThermoFisher Scientific, A-21207), Tyramide-conjugated Alexa Fluor 488 (ThermoFisher Scientific, B40953), Donkey anti-Goat IgG (H+L) 488 (1:500; ThermoFisher Scientific, A-11055), Donkey anti-Rabbit IgG (H+L) 488 (1:500; ThermoFisher Scientific, A-21206). Nuclei were visualized with DAPI (4',6-diamidino-2-phenylindole, dihydrochloride; 1mg/mL). The sections were mounted using VectaShield anti-fade mounting medium (Vector Laboratories, H-1000).

3.3.3.2 Image acquisition, processing, and analysis. Widefield images (4x, 20x, or 40x objectives) were acquired on an inverted Nikon Te2000 microscope equipped with a

MicroPublisher 5.0 RTV color camera and a CoolSNAP HQ2 CCD camera or an inverted Ti Nikon microscope with an ANDOR Zyla sCMOS camera. Widefield images were initially acquired using MetaMorph Image Analysis software or Nikon's NIS-Elements Advanced Research software package. Further processing was done using the open source image processing package FIJI (Schindelin et al., 2012).

3.3.4 Electrophysiology

3.3.4.1 Slice preparation. Hippocampal slices were prepared and extracellular field potential recording methods were used similar to that previously described (Moore et al., 2011; Singer et al., 2011). Briefly, coronal brain slices (350 um) were cut on a vibratome under ice-cold (< 1 °C) oxygenated sucrose-based cutting solution containing the following (in mM): 2.8 KCl, 1.25 $MgCl_2$, 1.0 Mg_2O_4, 1.25 NaH_2PO_4, 1.25 $CaCl_2$, 206 sucrose, 26 $NaCHO_3$, 10 D-glucose, and 0.40 ascorbic acid. Slices were transferred to a holding chamber filled with aCSF containing the following (in mM): 124 NaCl, 2.8 KCl, 1 $MgSO_4$, 1.25 NaH_2PO_4, 2.5 $CaCl_2$, 26 $NaHCO_3$, 10 D-glucose, and 0.40 ascorbic acid at room temperature and remained there for at least 1 hr before being individually transferred to a submersion chamber and continuously perfused (~1.5 mL/min) with oxygenated aCSF heated to 31°C.

3.3.4.2 Basal synaptic transmission and synchronous activity recording. Extracellular field potential recordings (fEPSPs) were made using borosilicate glass-pipettes (Sutter Instruments) filled with aCSF. Pipettes were made on a P-97 Flaming-Brown pipette puller (Sutter Instruments) with a tip resistance ~ 1MΩ filled with artificial cerebral spinal

fluid (aCSF). All recordings were made using a differential amplifier (DP-301; Warner Instruments) and filtered at 1-3kHz. Recordings were digitized using a Molecular Devices 1440A Digidata A/D converter and stored on a Dell desktop computer running pClamp 10.0. Basal synaptic transmission was assessed by examining the input/output relationship in the CA1 and CA3 hippocampal subfields. In CA1, fEPSPs were evoked by stimulating the Schaffer collateral afferent fibers with bipolar electrodes, while fEPSPs in CA3 were evoked by stimulating the mossy fibers. Input/output curves were generated in aCSF by increasing the stimulation intensity (from 0 to 1.0 mA) and measuring the fEPSP slope (mV/ms) as a function of stimulus intensity (mA). Spontaneous, synchronous activity was induced by exchanging the normal aCSF perfusion with aCSF which contained 0 mmol/L Mg^{2+} and elevated (10 mmol/L) K^{+}. The number of synchronous events, the latency from the time of exchange until the first spontaneous high-frequency burst, the duration of the synchronous activity, the peak amplitude of high-frequency bursts, and the inter-event interval were recorded.

3.3.5 Statistical analysis

All recordings were analyzed off-line using Clampfit 10.4 (Axon Instruments). Sample size refers to the number of mice in the experiment, with 2-5 slices averaged per mouse. All statistical tests, including repeated measures ANOVA with Tukey's post-hoc comparison and log-rank (Mantel-Cox) tests, were performed in GraphPad Prism, version 7.0 (GraphPad Software, La Jolla, CA, USA), and a significance criterion of $p < 0.05$ was adopted. Log-rank (Mantel-Cox) statistical tests were performed on data presented in Kaplan-Meirer plots in order to account for mice that did not generalize and

develop synchronous activity during the experimental window. All other data is presented as the mean ± SEM.

3.4 Results

3.4.1 Both Nsp and tPA are highly expressed in the hippocampus in neurons and vascular- or vascular-associated cells

Previous *in situ* mRNA hybridization and immunohistochemical analysis has shown that both Nsp and tPA are highly expressed in neurons and vascular- or vascular-associated cells in the hippocampus (Hastings et al., 1997; Krueger et al., 1997; Yu et al., 2001; Teesalu et al., 2004; Fredriksson et al., 2015; Stevenson and Lawrence, 2018). In an effort to take advantage of the recent technological developments in immunofluorescence microscopy and employ those advancements to visualizing Nsp and tPA protein expression in the murine brain, two BAC transgenic mouse lines with DsRED and Cerulean fluorescent tags on Nsp and tPA, respectively, were generated. The generation and expression pattern of tPA protein in the tPA^{BAC}-Cer transgenic mouse is described in Chapter 2 (Stevenson and Lawrence, 2018). We report here for the first time on the Nsp^{BAC}-DsRED transgenic mice. A schematic diagram of the recombineering strategy used to insert the Exon 9-DsRED-Exon 9 construct into the BAC that houses the *Serpini1* locus is illustrated in Figure 3.1 A. ELISA analysis of brain homogenates from Nsp^{BAC}-DsRED (lines 519 and 552) transgene positive and transgene negative mice demonstrate increased murine Nsp (mNsp) protein expression, suggestive of increased copy number of the *Serpini1* gene (Figure 3.1 B). Representative western blot analysis of brain homogenates from Nsp^{BAC}-

DsRED line 552 demonstrates endogenous Nsp protein (~ 49 kDa) and Nsp-DsRED at a higher molecular weight (~ 75 kDA) due to the added mass of the DsRED protein (25 kDa) (Figure 3.1 C).

Immunofluorescence microscopic analysis of hippocampal section from Nsp^{BAC}-DsRED transgenic mice show that the Nsp protein fused with a DsRED fluorescent tag is appropriately targeted and appears to faithfully recapitulate previously reported endogenous expression patterns of Nsp in the adult murine brain (Hastings et al., 1997). In the hippocampus Nsp-DsRED is noticeable in hilar cells, CA1-CA3 pyramidal neurons, and in scattered, diffusely populated neurons of stratum radiatum and stratum oriens (Figure 3.2 and 3.3). In contrast, tPA-Cer is most highly expressed in the mossy fiber pathway in the hilus and stratum lucidum layer and, with antibody amplification, scattered somatostatin (SST) tPA-positive cell bodies are noticeable in stratum oriens (Figure 3.2 and 3.3). Both Nsp-DsRED and tPA-Cer, however, are present in vessel-associated cells, while tPA is also expressed by endothelial cells (Figure 3.2). These data show that Nsp and tPA are expressed in neurons, but also in vessel-associated cells. Therefore, it is unclear from the immunofluorescence localization of Nsp and tPA if the behavioral seizure phenotype exhibited by $Nsp^{-/-}$ ("seizure prone") and $tPA^{-/-}$ ("seizure resistant") mice is a direct result of the role that Nsp and tPA have on synaptic transmission or an indirect result of their role in regulating BBB permeability and extracellular homeostasis.

3.4.2 Mice deficient in Nsp, but not tPA, exhibit enhanced synaptic transmission in the hippocampal CA1 region

To begin to address the role of Nsp and tPA in regulating seizure progression, an electrophysiological approach was taken whereby synchronous (or "seizure-like") activity was induced in *ex vivo* brain slices from wild-type, $tPA^{-/-}$, and $Nsp^{-/-}$ mice. However, prior to measuring synchronous activity, basal synaptic transmission was assessed in the CA1 and CA3 region of the hippocampus. Schematic illustration of an *ex vivo* coronal hippocampal slice preparation for assessing basal synaptic transmission in the Schaffer collateral pathway of the CA1 region is presented in Figure 3.4 A. Representative traces of fEPSPs from stimulation of the Schaffer collateral-to-CA1 pyramidal neuron pathway illustrating the various aspects of CA1 synaptic transmission that can determine the shape of the curve is shown in Figure 3.4 B. Basal synaptic transmission was assessed in wild-type, $Nsp^{-/-}$, and $tPA^{-/-}$ mice by examining the input/output (I/O) curves (Figure 3.5). With increasing stimulation intensity of the Schaffer collateral pathway there is a corresponding increase in the slope and amplitude of the fEPSP in CA1 pyramidal neurons. Overlays of representative traces of the fEPSPs and the I/O curve illustrate this reciprocal relationship (Figure 3.5). The slope of the fEPSP, rather than the amplitude, was chosen as a measure of post-synaptic strength as negative feedback can sometimes dampen the amplitude. A repeated measures two-way ANOVA with a Tukey's post-hoc multiple comparison revealed that the slopes of the field potentials increased with Schaffer collateral stimulus intensity ($F_{(10,250)} = 254$, $p < 0.0001$) and that synaptic transmission in brain slices from $Nsp^{-/-}$ mice is significantly different from wild-type ($p < 0.0001$) and $tPA^{-/-}$ mice ($p = 0.0053$), but that the slope of the fEPSPs from $tPA^{-/-}$ mice is not significantly different from wild-type mice ($p = 0.7148$).

3.4.3 Mice deficient in either Nsp or tPA display deficits in basal synaptic transmission in the hippocampal CA3 region

Schematic illustration of an *ex vivo* coronal hippocampal slice preparation for assessing basal synaptic transmission in the mossy fiber-to-CA3 pathway is presented in Figure 3.4 C. Representative trace of a fEPSP from stimulation of the Mossy fiber-to-CA3 pyramidal neuron pathway illustrating the various aspects of CA3 synaptic transmission that can determine the shape of the curve is shown in Figure 3.4 D. Similar to the CA1 region, basal synaptic transmission was assessed by examining the I/O relationship (Figure 3.6). As with the Schaffer collateral pathway there is a corresponding increase in the slope of the fEPSP with incremental increases in stimulation intensity. Compiled representative traces from wild-type, $Nsp^{-/-}$, and $tPA^{-/-}$ overlaid from the fEPSPs at different stimulus intensities and the plotted I/O curve are shown in Figure 3.3. A repeated measures two-way ANOVA revealed that the slopes of the field potentials increased in mossy fiber stimulus intensity ($F_{(10,230)} = 220.1$, $p < 0.0001$). In contrast to the I/O curve from the CA1 region where brains slices from $Nsp^{-/-}$ mice exhibited enhanced synaptic transmission, a Tukey's post-hoc multiple comparison showed significant deficits in synaptic transmission between wild-type and $Nsp^{-/-}$ mice ($p = 0.0002$). Significant differences were also found in synaptic transmission between wild-type and $tPA^{-/-}$ mice ($p = 0.0161$), but not $Nsp^{-/-}$ and $tPA^{-/-}$ mice ($p = 0.2695$).

3.4.4 Ex vivo synchronous activity onset times in tPA$^{-/-}$ and Nsp$^{-/-}$ mice do not phenocopy in vivo seizure onset time

Despite significant differences in synaptic transmission between wild-type and Nsp$^{-/-}$ and Nsp$^{-/-}$ mice and tPA$^{-/-}$ mice, it was unclear if those differences would affect the progression of synchronous activity in an *ex vivo* model of seizures. Moreover, we wanted to test the hypothesis that if the *in vivo* seizure phenotype in wildtype, tPA$^{-/-}$, and Nsp$^{-/-}$ mice is related to the BBB, then in an *ex vivo* slice preparation there should be no phenotypic difference between these mice. To test our hypothesis, slices were bathed in no Mg^{2+}/high K^{+} aCSF to generate synchronized population bursts (Figure 3.7 and 3.8). This method, which enhances conductance of NMDA receptors and lowers the neuronal firing threshold, is a well-established *in vitro* correlate of *in vivo* seizures (Mody et al., 1987; Stanton et al., 1987; Zhang et al., 2012).

Mice deficient in tPA$^{-/-}$ have been consistently found, in different seizure models, to have a delayed behavior seizure onset time (Tsirka et al., 1995; Yepes et al., 2002; Pawlak et al., 2005; Fredriksson et al., 2015). In addition, wild-type mice and rats treated with Nsp and following intra-amgydala injections of kainic acid (KA) have been shown to have delayed seizure progression (Yepes et al., 2002), while Nsp$^{-/-}$ mice have an enhanced behavioral seizure onset time (Fredriksson et al., 2015).

In vivo electroencephalogram (EEG) analysis using an inter-hippocampal depth electrode revealed seizure onset times in wild-type, Nsp$^{-/-}$, and tPA$^{-/-}$ mice to correlate with their reported behavioral phenotype (Figure 3.9 A). As evidenced by the median time to seizure onset for each respective genotype, Nsp$^{-/-}$ mice (t = 39 min) progressed the quickest followed by wild-type mice (t = 65) and then tPA$^{-/-}$ mice (t = 100 min). Data

are presented as Kaplan-Meier plots and a log-rank (Mantel-Cox) statistical test was used to compare the distributions of wild-type (n = 7), $Nsp^{-/-}$ (n = 5), and $tPA^{-/-}$ (n = 5) mice. Statistically significant differences were found between wild-type mice and $Nsp^{-/-}$ mice (p = 0.0276), wild-type and $tPA^{-/-}$ mice (p = 0.0450), and $Nsp^{-/-}$ mice and $tPA^{-/-}$ mice (p = 0.0027).

In contrast, in the *ex vivo* "seizure-like" model, when perfused with the no Mg^{2+}/high K^{+} aCSF solution, brain slices from $tPA^{-/-}$ mice developed synchronous activity the quickest (t = 14), while brain slices from $Nsp^{-/-}$ mice were delayed in their synchronous activity onset times (t = 17) (Figure 3.9 B). The synchronous activity onset time for wild-type mice (t = 15) was in-between $tPA^{-/-}$ and $Nsp^{-/-}$ mice. A log-rank (Mantel Cox) statistical test found no significant difference between wild-type and $Nsp^{-/-}$ mice (p = 0.0572) or wild-type and $tPA^{-/-}$ mice (p = 0.2829), but a significant difference between $Nsp^{-/-}$ and $tPA^{-/-}$ mice (p = 0.0039). Previously, we reported there to be a statistically significant difference in synchronous activity onset time between wild-type and $tPA^{-/-}$ mice (Fredriksson et al., 2015). However, since that publication by Fredriksson et al. in 2015 we have increased our sample size for wild-type (n = 16), $Nsp^{-/-}$ (n = 14), and $tPA^{-/-}$ (n = 11) mice and now find no significant difference. These data demonstrate that the *in vivo* seizure phenotype observed in $Nsp^{-/-}$ and $tPA^{-/-}$ mice is not preserved in an *ex vivo* "seizure-like" model of synchronous activity. Moreover, the ex vivo "seizure-like" phenotype in $Nsp^{-/-}$ and $tPA^{-/-}$ mice is opposed to their *in vivo* seizure phenotype, suggesting that dysregulation of tPA activity at the BBB might be causal for the differences observed in the *in vivo* seizure phenotype between $Nsp^{-/-}$ and $tPA^{-/-}$ mice

To validate that our no Mg^{2+}/high K^{+} model is an *ex vivo* correlate of *in vivo* seizures, we induced synchronous activity in Scn1b$^{-/-}$ mice as a positive control (Figure 3.9 C). Scn1b$^{-/-}$ mice are deficient in the SCN1B gene, which encodes the voltage-gated sodium channel β1 subunit and plays and important in modulating neuronal excitability. Scn1b$^{-/-}$ mice display a severe neurological pathology that includes ataxia, spontaneous seizures by post-natal day 10, and premature death (Chen et al., 2004). Indeed, following perfusion of no Mg^{2+}/high K^{+} aCSF, Scn1b$^{-/-}$ mice (t = 12.2) developed synchronous activity at earlier time-points that their wild-type (t = 14.0) littermate controls. Statistical analysis using the log-rank (Mantel Cox) test revealed a significant difference between the genotypes (p = 0.0024). These data suggest that our *ex vivo* no Mg^{2+}/high K^{+} model is able to recapitulate the *in vivo* seizure phenotype. Given that the synchronous activity onset times from the brain slices of Nsp$^{-/-}$ mice and tPA$^{-/-}$ mice did not phenocopy the behavioral or EEG seizure induction times of Nsp$^{-/-}$ and tPA$^{-/-}$ mice *in vivo*, it reasons that Nsp and tPA are likely not acting to alter neuronal excitability and cause the phenotypic differences observed between these mice during seizure progression.

3.4.5 Ex vivo model of synchronous activity reveals hyperexcitable state in brain slices from tPA$^{-/-}$ mice, but a quiescent state in brain slices from Nsp$^{-/-}$ mice

In addition to examining the onset time of synchronous activity, we measured other parameters that might indicate if brain slices from Nsp$^{-/-}$ and tPA$^{-/-}$ mice are in a more hyperexcitable or quiescent state (Figure 3.10). For the temporal-related parameters that we measured – average frequency (events/min) and average inter-

event interval – wild-type, $Nsp^{-/-}$, and $tPA^{-/-}$ mice segregated according to their synchronous activity onset time (Figure 3.10 A and 3.10 B). Brain slices from $Nsp^{-/-}$ mice exhibited a more quiescent state; they had a slower frequency of events and a longer interval between events compared to wild-type and $tPA^{-/-}$ mice. In contrast, brain slices from $tPA^{-/-}$ mice exhibited a more hyperexcitable state; they had a faster frequency of events and a shorter interval between events compared to wild-type and $Nsp^{-/-}$ mice.

A one-way ANOVA revealed a statistical difference between genotypes ($F_{(2,38)} = 8.802$, $p = 0.0020$), with a Tukey's post-hoc multiple comparison showing a significant difference in the average frequency between wild-type and $tPA^{-/-}$ mice ($p = 0.0304$) and $Nsp^{-/-}$ and $tPA^{-/-}$ ($p = 0.0015$), but no significant difference between wild-type and $Nsp^{-/-}$ mice ($p = 0.3827$). Statistical analysis of the inter-event interval by one-way ANOVA also found a difference between genotypes ($F_{(2,38)} = 3.819$, $p= 0.0308$), but a Tukey's post-hoc multiple comparison only showed a significant difference between $Nsp^{-/-}$ and $tPA^{-/-}$ mice ($p = 0.0305$) and no difference between wild-type and $Nsp^{-/-}$ mice ($p = 0.1346$) and wild-type and $tPA^{-/-}$ mice ($p = 0.6492$). For both of these "seizure-like" parameters, though, the trend was for brain slices from $Nsp^{-/-}$ mice and $tPA^{-/-}$ to have divergent phenotypes, with $Nsp^{-/-}$ mice having a more quiescent phenotype and $tPA^{-/-}$ mice have a more hyperexcitable phenotype. Importantly, as with their synchronous activity onset times, when looking at average frequency of events and average inter-event interval, brain slices from $Nsp^{-/-}$ and $tPA^{-/-}$ mice exhibited an *ex vivo* "seizure-like" phenotype that differed from their *in vivo* seizure phenotype.

The average peak amplitude, however, did not show a similar trend to the temporal-related parameters (Figure 3.10 C). Rather than segregating in opposite

directions, synchronous events from $Nsp^{-/-}$ and $tPA^{-/-}$ mice both displayed peak amplitudes that were smaller than wild-type mice. A one-way ANOVA revealed a statistical difference between genotypes ($F_{(2,38)} = 6.898$, $p = 0.0028$), with a Tukey's post-hoc multiple comparison showing a significant difference between wild-type and $Nsp^{-/-}$ mice ($p = 0.0047$) and wild-type and $tPA^{-/-}$ mice ($p = 0.0487$), but no difference between $Nsp^{-/-}$ and $tPA^{-/-}$ mice ($p = 0.9518$).

3.5 Discussion

In the current study we dissected the neuronal component and the BBB component to the *in vivo* seizure phenotype of $Nsp^{-/-}$ and $tPA^{-/-}$ mice using an *ex vivo* "seizure-like" model of synchronous activity. We first demonstrated in newly generated Nsp^{BAC}-DsRED transgenic mice and tPA^{BAC}-Cer transgenic mice that Nsp and tPA are highly expressed in the hippocampus and that both are localized to neurons and vascular or vascular-associated cells. As previously reported, tPA-Cer protein is primarily expressed in the mossy fiber pathway of the hilus and stratum lucidum layer and in a scattered population of somatostatin (SST)-positive interneurons in stratum oriens, stratum pyramidale, and stratum radiatum (Sappino et al., 1993; Salles and Strickland, 2002; Louessard et al., 2016) (Stevenson and Lawrence, 2018). Further co-expression analysis revealed that the population of tPA- and SST-positive interneurons in stratum oriens are part of a subset of oriens-lacunosum molecular (O-LM) interneurons (Stevenson and Lawrence, 2018). OL-M interneurons have cells bodies that reside in stratum oriens and send GABAergic projections to the distal dendritic tuft and the proximal dendrites of CA1 pyramidal neurons (Klausberger, 2009).

Nsp-DsRED, in contrast, is expressed in hilar cells and in the pyramidal cell layer of hippocampal subfields CA1-CA3. These data are in agreement with previous immunohistochemical studies examining Nsp protein expression in the adult murine brain (Hastings et al., 1997; Teesalu et al., 2004) and demonstrate that the Nsp-DsRED fusion protein is appropriately targeted and faithfully recapitulates the endogenous expression pattern of Nsp. Interestingly, within the trisynaptic circuitry of the hippocampus, Nsp is largely expressed in the post-synaptic target cells of neurons expressing tPA. With respect to the mossy fibers of dentate granule cells, tPA is expressed in the giant mossy fiber boutons that synapse on the thorny dendritic excrescences of Nsp-expressing CA3 pyramidal neurons and hilar cells. And, tPA is pre-synaptically expressed in SST-positive OL-M interneurons, whose post-synaptic targets are Nsp-expressing CA1 pyramidal neurons. Nsp-DsRED cell bodies are also noticeable in stratum oriens and stratum radiatum, but it is of yet unknown if Nsp and tPA are co-expressed in these cells or if they are functionally linked.

It is also not known if the pre- and post-synaptic pairing of tPA and Nsp, respectively, is related to how this protease and protease-inhibitor are functioning. *In vitro* biochemical analysis demonstrates that tPA rapidly and efficiently reacts with Nsp, but also that the Nsp/tPA complex is unstable and dissociates within minutes, resulting in the complete cleavage of Nsp and release of active tPA (Hastings et al., 1997; Barker-Carlson et al., 2002; Makarova et al., 2003). Moreover, both Nsp and the Nsp/tPA complex have been shown to be internalized via a low-density lipoprotein (LDL) receptor-related protein 1 (LRP1) mediated mechanism in cultured primary neurons (Makarova et al., 2003). However, while internalized Nsp is sorted to the

lysosome for degradation, the Nsp/tPA complex is not similarly trafficked and degradation of the complex is significantly attenuated. It is not clear what purpose the internalized Nsp/tPA complex is serving. As LRP1 is reported to function as an endocytic signaling receptor (Strickland et al., 2014), it's possible that the Nsp/tPA complex is functioning in that capacity, but further studies are needed to address that question. Crossing the Nsp^{BAC}-DsRED and tPA^{BAC}-Cer transgenic mice would help to begin to address the subcellular localization and interaction of these two proteins at the mossy fiber-to-CA3 synapse and OL-M interneuron-to-CA1 synapse.

Immunofluorescence analysis of hippocampal sections from Nsp^{BAC}-DsRED and tPA^{BAC}-Cer transgenic mice also demonstrated that Nsp and tPA are proximally localized to directly act on blood vessels (Fredriksson et al., 2015). Nsp and tPA were previously identified in a subset perivascular interneurons that express the vasoactive markers SST and vasoactive intestinal peptide (VIP), respectively. In our hands, however, we were not able to confirm that tPA and VIP are co-expressed in the same interneuron population. It is unclear why we were not able to replicate the immunofluorescence co-expression studies by Fredriksson and colleagues (2015). Nonetheless, in tPA^{BAC}-Cer transgenic mice we do find both vascular and perivascular tPA protein, and in the Nsp^{BAC}-DsRED mice there is a population of DsRED-positive perivascular cells that are as yet still unidentified. Cumulatively, these immunofluorescence data indicate that both Nsp and tPA are proximally localized to influence neuronal excitability and/or BBB permeability and effectuate the observed phenotypic differences in seizure severity in $Nsp^{-/-}$ and $tPA^{-/-}$ mice.

As the immunofluorescence data is inconclusive, we took a more physiological functional approach to dissect the neuronal and/or BBB component to the in vivo seizure phenotype in $Nsp^{-/-}$ and $tPA^{-/-}$ mice. Prior to examining the *ex vivo* "seizure-like" synchronous activity in brain slice from wild-type, $Nsp^{-/-}$, and $tPA^{-/-}$ mice, however, we wanted to test slice health and to assess whether there were any differences in basal synaptic transmission between the genotypes. Interestingly, we found that there were significant differences in synaptic efficacy in CA1 between wild-type and $Nsp^{-/-}$ mice and $Nsp^{-/-}$ and $tPA^{-/-}$ mice. In the Schaffer collateral-to-CA1 pathway $Nsp^{-/-}$ mice exhibited enhanced basal synaptic transmission, while the I/O curves were not statistically different between wild-type and $tPA^{-/-}$ mice.

Though there was no statistical difference in synaptic transmission between wild-type and $tPA^{-/-}$ mice, the shape of the I/O curve from $tPA^{-/-}$ mice appears to plateau at higher stimulus intensities. It's possible that in the $tPA^{-/-}$ mice there are fewer fibers to recruit, resulting in fewer synapses and a diminished fEPSP slope, though further experiments would need to be done to investigate whether this plateau is significant and, if so, if a pre- or post-synaptic mechanism is responsible. With respect to the significant difference in basal synaptic transmission between wild-type and $Nsp^{-/-}$ mice, it is not clear if the enhanced synaptic efficacy in $Nsp^{-/-}$ mice is due to some direct effect of Nsp or some indirect effect from loss of inhibition over tPA activity. For, transgenic mice that overexpress tPA have been reported to have an increase in paired-pulse facilitation in the Schaffer collateral-to-CA1 pathway in stratum radiatum. However, when paired-pulse facilitation was examined in the Schaffer collateral pathway of $Nsp^{-/-}$ mice, compared to wild-type controls, no significant difference was observed (Reumann et al.,

2017). Therefore, further studies need to be done to reconcile Nsp's reported effects in synaptic transmission and synaptic plasticity studies, especially as a small sample size (6 slices from 3 wild-type mice and 7 slices from 3 $Nsp^{-/-}$ mice) was used in the paired-pulse experiments with Nsp deficient mice.

Previously, Frey et al. (1996) reported $tPA^{-/-}$ mice to be under enhanced GABAergic transmission in the hippocampal CA1 region. When assessing synaptic transmission in the Schaffer collateral-to-CA1 pathway, Frey et al. (1996) found that a larger EPSP was needed to evoke a pop-spike of similar magnitude in the $tPA^{-/-}$ mice. In addition, compared to wild-type mice, $tPA^{-/-}$ mice were reported to have a significantly reduced paired-pulse facilitation of the second pop-spike. When GABAergic transmission was blocked with the $GABA_A$ blocker bicuculine, however, the pop-spike in $tPA^{-/-}$ mice showed a significant increase in facilitation. As we did not examine all the same parameters as Frey et al. (1996) it is unclear if our data does not agree. However, it is important to note that the genetic background of the $tPA^{-/-}$ mice and control mice used by Frey and colleagues was not reported. Therefore, it is not known if the differences in basal synaptic transmission between our experiments and those by Frey et al. (1996) are biologically related to tPA, experimental, or due to some strain modifying genes.

We also assessed synaptic transmission in the mossy fiber-to-CA3 pathway prior to inducing synchronous activity with our no Mg^{2+}/high K^+ aCSF solution. In contrast to the CA1 region, both $Nsp^{-/-}$ and $tPA^{-/-}$ exhibited decreased synaptic efficacy in the mossy fiber-to-CA3 pathway. $Nsp^{-/-}$ and $tPA^{-/-}$ mice were not significantly different from each other though. As the I/O curves from $Nsp^{-/-}$ and $tPA^{-/-}$ mice did not oppose one

another, it is unclear if the loss of tPA regulation and loss of tPA activity acutely affect basal synaptic transmission or if there is some confounding developmental factor contributing to decreased synaptic efficacy in both the $Nsp^{-/-}$ and $tPA^{-/-}$ mice. Interestingly, similar to the I/O curve in the CA1 region of stratum radiatum, there is a plateau in the I/O curve at higher stimulus intensities in brain slices from $tPA^{-/-}$ mice. Again, this plateau could be the result of fewer fibers, but further experiments are needed to elucidate the pre- or post-synaptic mechanism for the decreased slope of the fEPSP at higher stimulus intensities.

Despite significant differences between wild-type and $Nsp^{-/-}$ mice and wild-type and $tPA^{-/-}$ in basal synaptic transmission, it was unclear if these differences would affect the development of synchronous activity in our *ex vivo* no Mg^{2+}/high K^{+} model. As there were significant differences between $Nsp^{-/-}$ and $tPA^{-/-}$ mice in all the temporal "seizure-like" parameters we measured while brain slices were being perfused with the no Mg^{2+}/high K^{+} solution, basal synaptic transmission doesn't appear to correlate with the propensity for a brain slice to develop synchronous activity. The decreased peak amplitudes in brain slices from both $Nsp^{-/-}$ and $tPA^{-/-}$ mice, however, did correlate with their deficits in basal synaptic transmission in the mossy fiber-to-CA3 pyramidal cell pathway. Therefore, while synaptic efficacy might not indicate anything about onset to synchronous activity, it might be indicative of the peak amplitude of synchronous events.

Importantly, though, the ex vivo "seizure-like" phenotype in brain slices $Nsp^{-/-}$ and $tPA^{-/-}$ mice was opposed to their *in vivo* behavioral and EEG seizure phenotype. Indeed, in the temporal "seizure-like" parameters we assessed $tPA^{-/-}$ mice appeared to be in a more hyperexcitable state, while $Nsp^{-/-}$ mice appeared to be in a more quiescent state.

We validated that our *ex vivo* model was able to detect phenotypic differences in *in vivo* seizure behavior using the Scn1b$^{-/-}$ transgenic mice that develop spontaneous seizures around post-natal day P10 (Chen et al., 2004). These data strongly indicate that the *in vivo* seizure phenotype observed in Nsp$^{-/-}$ and tPA$^{-/-}$ mice is not related to the role Nsp and/or tPA may be having on neuronal excitability.

Rather, in conjunction with our data demonstrating a correlation between BBB permeability and seizure severity in Nsp$^{-/-}$ and tPA$^{-/-}$ mice (Fredriksson et al., 2015), the lack of an *ex vivo* "seizure-like" phenotype suggests that there is a significant BBB component to seizure progression in Nsp$^{-/-}$ and tPA$^{-/-}$ mice. Indeed, using a combination of *in vitro* and *in vivo* approaches, we have demonstrated that tPA's actions on the BBB appear to be mediated through tPA-catalzyed activation of latent platelet-derived growth factor-CC (PDGF-CC) and subsequent binding of active PDGF-CC to its receptor, PDGFRα, a tyrosine kinase receptor (Fredriksson et al., 2004; Su et al., 2008). Immunohistochemical analysis has shown that tPA, Nsp, PDGF-CC, and the PDGFRα are expressed by perivascular cells (Su et al., 2008; Fredriksson et al., 2015), with the α-receptor being specifically localized to astrocytes (Su et al., 2017).

With pharmacologic and genetic blockade of the PDGFRα activation we further demonstrated the importance of the tPA/PDGF-CC/PDGFRα signaling cascade in regulating BBB permeability and seizure (Fredriksson et al., 2015). Conditional ablation of the PDGFRα in perivascular astrocytes significantly delayed time to seizure generalization. And, consistent with tPA being an upstream activator of PDGFRα signaling, treatment with the tyrosine kinase inhibitor Imatinib had no effect on seizure onset or generalization in tPA$^{-/-}$ mice, but it significantly delayed seizure progression in

Nsp$^{-/-}$ and wild-type mice. Together, these data results strongly support a mechanism whereby activation of the tPA/PDGF-C/PDGFRα signaling pathway induces opening of the BBB and contributes to seizure progression.

References

Barker-Carlson K, Lawrence DA, Schwartz BS (2002) Acyl-enzyme complexes between tissue-type plasminogen activator and neuroserpin are short-lived in vitro. J Biol Chem 277:46852-46857.

Berg AT, Berkovic SF, Brodie MJ, Buchhalter J, Cross JH, van Emde Boas W, Engel J, French J, Glauser TA, Mathern GW, Moshe SL, Nordli D, Plouin P, Scheffer IE (2010) Revised terminology and concepts for organization of seizures and epilepsies: report of the ILAE Commission on Classification and Terminology, 2005-2009. Epilepsia 51:676-685.

Carmeliet P, Kieckens L, Schoonjans L, Ream B, van Nuffelen A, Prendergast G, Cole M, Bronson R, Collen D, Mulligan RC (1993) Plasminogen activator inhibitor-1 gene-deficient mice. I. Generation by homologous recombination and characterization. J Clin Invest 92:2746-2755.

Carmeliet P, Schoonjans L, Kieckens L, Ream B, Degen J, Bronson R, De Vos R, van den Oord JJ, Collen D, Mulligan RC (1994) Physiological consequences of loss of plasminogen activator gene function in mice. Nature 368:419-424.

Chen C, Westenbroek RE, Xu X, Edwards CA, Sorenson DR, Chen Y, McEwen DP, O'Malley HA, Bharucha V, Meadows LS, Knudsen GA, Vilaythong A, Noebels JL, Saunders TL, Scheuer T, Shrager P, Catterall WA, Isom LL (2004) Mice lacking sodium channel beta1 subunits display defects in neuronal excitability, sodium channel expression, and nodal architecture. J Neurosci 24:4030-4042.

Daneman R (2012) The blood-brain barrier in health and disease. Ann Neurol 72:648-672.

Fredriksson L, Li H, Fieber C, Li X, Eriksson U (2004) Tissue plasminogen activator is a potent activator of PDGF-CC. EMBO J 23:3793-3802.

Fredriksson L, Stevenson TK, Su EJ, Ragsdale M, Moore S, Craciun S, Schielke GP, Murphy GG, Lawrence DA (2015) Identification of a neurovascular signaling pathway regulating seizures in mice. Ann Clin Transl Neurol 2:722-738.

Friedman A, Kaufer D, Heinemann U (2009) Blood-brain barrier breakdown-inducing astrocytic transformation: novel targets for the prevention of epilepsy. Epilepsy Res 85:142-149.

Hastings GA, Coleman TA, Haudenschild CC, Stefansson S, Smith EP, Barthlow R, Cherry S, Sandkvist M, Lawrence DA (1997) Neuroserpin, a brain-associated inhibitor of tissue plasminogen activator is localized primarily in neurons. Implications for the regulation of motor learning and neuronal survival. J Biol Chem 272:33062-33067.

Herman ST (2002) Epilepsy after brain insult: targeting epileptogenesis. Neurology 59:S21-26.

Ishigami S, Sandkvist M, Tsui F, Moore E, Coleman TA, Lawrence DA (2007) Identification of a novel targeting sequence for regulated secretion in the serine protease inhibitor neuroserpin. Biochem J 402:25-34.

Klausberger T (2009) GABAergic interneurons targeting dendrites of pyramidal cells in the CA1 area of the hippocampus. Eur J Neurosci 30:947-957.

Krueger SR, Ghisu GP, Cinelli P, Gschwend TP, Osterwalder T, Wolfer DP, Sonderegger P (1997) Expression of neuroserpin, an inhibitor of tissue plasminogen activator, in the developing and adult nervous system of the mouse. J Neurosci 17:8984-8996.

Lascano AM, Korff CM, Picard F (2016) Seizures and Epilepsies due to Channelopathies and Neurotransmitter Receptor Dysfunction: A Parallel between Genetic and Immune Aspects. Mol Syndromol 7:197-209.

Laxer KD, Trinka E, Hirsch LJ, Cendes F, Langfitt J, Delanty N, Resnick T, Benbadis SR (2014) The consequences of refractory epilepsy and its treatment. Epilepsy Behav 37:59-70.

Louessard M, Lacroix A, Martineau M, Mondielli G, Montagne A, Lesept F, Lambolez B, Cauli B, Mothet JP, Vivien D, Maubert E (2016) Tissue Plasminogen Activator Expression Is Restricted to Subsets of Excitatory Pyramidal Glutamatergic Neurons. Mol Neurobiol 53:5000-5012.

Madani R, Kozlov S, Akhmedov A, Cinelli P, Kinter J, Lipp HP, Sonderegger P, Wolfer DP (2003) Impaired explorative behavior and neophobia in genetically modified mice lacking or overexpressing the extracellular serine protease inhibitor neuroserpin. Mol Cell Neurosci 23:473-494.

Magiorkinis E, Sidiropoulou K, Diamantis A (2010) Hallmarks in the history of epilepsy: epilepsy in antiquity. Epilepsy Behav 17:103-108.

Makarova A, Mikhailenko I, Bugge TH, List K, Lawrence DA, Strickland DK (2003) The low density lipoprotein receptor-related protein modulates protease activity in the brain by mediating the cellular internalization of both neuroserpin and neuroserpin-tissue-type plasminogen activator complexes. J Biol Chem 278:50250-50258.

Mody I, Lambert JD, Heinemann U (1987) Low extracellular magnesium induces epileptiform activity and spreading depression in rat hippocampal slices. J Neurophysiol 57:869-888.

Moore SJ, Throesch BT, Murphy GG (2011) Of mice and intrinsic excitability: genetic background affects the size of the postburst afterhyperpolarization in CA1 pyramidal neurons. J Neurophysiol 106:1570-1580.

Oby E, Janigro D (2006) The blood-brain barrier and epilepsy. Epilepsia 47:1761-1774.

Pawlak R, Melchor JP, Matys T, Skrzypiec AE, Strickland S (2005) Ethanol-withdrawal seizures are controlled by tissue plasminogen activator via modulation of NR2B-containing NMDA receptors. Proc Natl Acad Sci U S A 102:443-448.

Qian Z, Gilbert ME, Colicos MA, Kandel ER, Kuhl D (1993) Tissue-plasminogen activator is induced as an immediate-early gene during seizure, kindling and long-term potentiation. Nature 361:453-457.

Reumann R, Vierk R, Zhou L, Gries F, Kraus V, Mienert J, Romswinkel E, Morellini F, Ferrer I, Nicolini C, Fahnestock M, Rune G, Glatzel M, Galliciotti G (2017) The serine protease inhibitor neuroserpin is required for normal synaptic plasticity and regulates learning and social behavior. Learn Mem 24:650-659.

Rogove AD, Siao C, Keyt B, Strickland S, Tsirka SE (1999) Activation of microglia reveals a non-proteolytic cytokine function for tissue plasminogen activator in the central nervous system. J Cell Sci 112 (Pt 22):4007-4016.

Salles FJ, Strickland S (2002) Localization and regulation of the tissue plasminogen activator-plasmin system in the hippocampus. J Neurosci 22:2125-2134.

Sappino AP, Madani R, Huarte J, Belin D, Kiss JZ, Wohlwend A, Vassalli JD (1993) Extracellular proteolysis in the adult murine brain. J Clin Invest 92:679-685.

Shorvon SD (2011) The etiologic classification of epilepsy. Epilepsia 52:1052-1057.

Singer BH, Gamelli AE, Fuller CL, Temme SJ, Parent JM, Murphy GG (2011) Compensatory network changes in the dentate gyrus restore long-term potentiation following ablation of neurogenesis in young-adult mice. Proc Natl Acad Sci U S A 108:5437-5442.

Stanton PK, Jones RS, Mody I, Heinemann U (1987) Epileptiform activity induced by lowering extracellular [Mg2+] in combined hippocampal-entorhinal cortex slices: modulation by receptors for norepinephrine and N-methyl-D-aspartate. Epilepsy Res 1:53-62.

Stevenson TK and Lawrence AL (2018) Characerization of tissue plasminogen activator expression and trafficking in the adult murine brain. eNeuro (in press).

Strickland DK, Au DT, Cunfer P, Muratoglu SC (2014) Low-density lipoprotein receptor-related protein-1: role in the regulation of vascular integrity. Arterioscler Thromb Vasc Biol 34:487-498.

Su EJ, Fredriksson L, Geyer M, Folestad E, Cale J, Andrae J, Gao Y, Pietras K, Mann K, Yepes M, Strickland DK, Betsholtz C, Eriksson U, Lawrence DA (2008) Activation of PDGF-CC by tissue plasminogen activator impairs blood-brain barrier integrity during ischemic stroke. Nat Med 14:731-737.

Su EJ, Cao C, Fredriksson L, Nilsson I, Stefanitsch C, Stevenson TK, Zhao J, Ragsdale M, Sun YY, Yepes M, Kuan CY, Eriksson U, Strickland DK, Lawrence DA, Zhang L (2017) Microglial-mediated PDGF-CC activation increases cerebrovascular permeability during ischemic stroke. Acta Neuropathol 134:585-604.

Su EJ, Fredriksson L, Kanzawa M, Moore S, Folestad E, Stevenson TK, Nilsson I, Sashindranath M, Schielke GP, Warnock M, Ragsdale M, Mann K, Lawrence AL, Medcalf RL, Eriksson U, Murphy GG, Lawrence DA (2015) Imatinib treatment reduces brain injury in a murine model of traumatic brain injury. Frontiers in cellular neuroscience 9:385.

Teesalu T, Kulla A, Simisker A, Siren V, Lawrence DA, Asser T, Vaheri A (2004) Tissue plasminogen activator and neuroserpin are widely expressed in the human central nervous system. Thromb Haemost 92:358-368.

Tsirka SE, Gualandris A, Amaral DG, Strickland S (1995) Excitotoxin-induced neuronal degeneration and seizure are mediated by tissue plasminogen activator. Nature 377:340-344.

Yepes M, Sandkvist M, Moore EG, Bugge TH, Strickland DK, Lawrence DA (2003) Tissue-type plasminogen activator induces opening of the blood-brain barrier via the LDL receptor-related protein. J Clin Invest 112:1533-1540.

Yepes M, Sandkvist M, Coleman TA, Moore E, Wu JY, Mitola D, Bugge TH, Lawrence DA (2002) Regulation of seizure spreading by neuroserpin and tissue-type plasminogen activator is plasminogen-independent. J Clin Invest 109:1571-1578.

Yu H, Schleuning WD, Michl M, Liberatore G, Tan SS, Medcalf RL (2001) Control elements between -9.5 and -3.0 kb in the human tissue-type plasminogen activator gene promoter direct spatial and inducible expression to the murine brain. Eur J Neurosci 14:799-808.

Zhang ZJ, Koifman J, Shin DS, Ye H, Florez CM, Zhang L, Valiante TA, Carlen PL (2012) Transition to seizure: ictal discharge is preceded by exhausted presynaptic GABA release in the hippocampal CA3 region. J Neurosci 32:2499-2512.

Figure 3.1

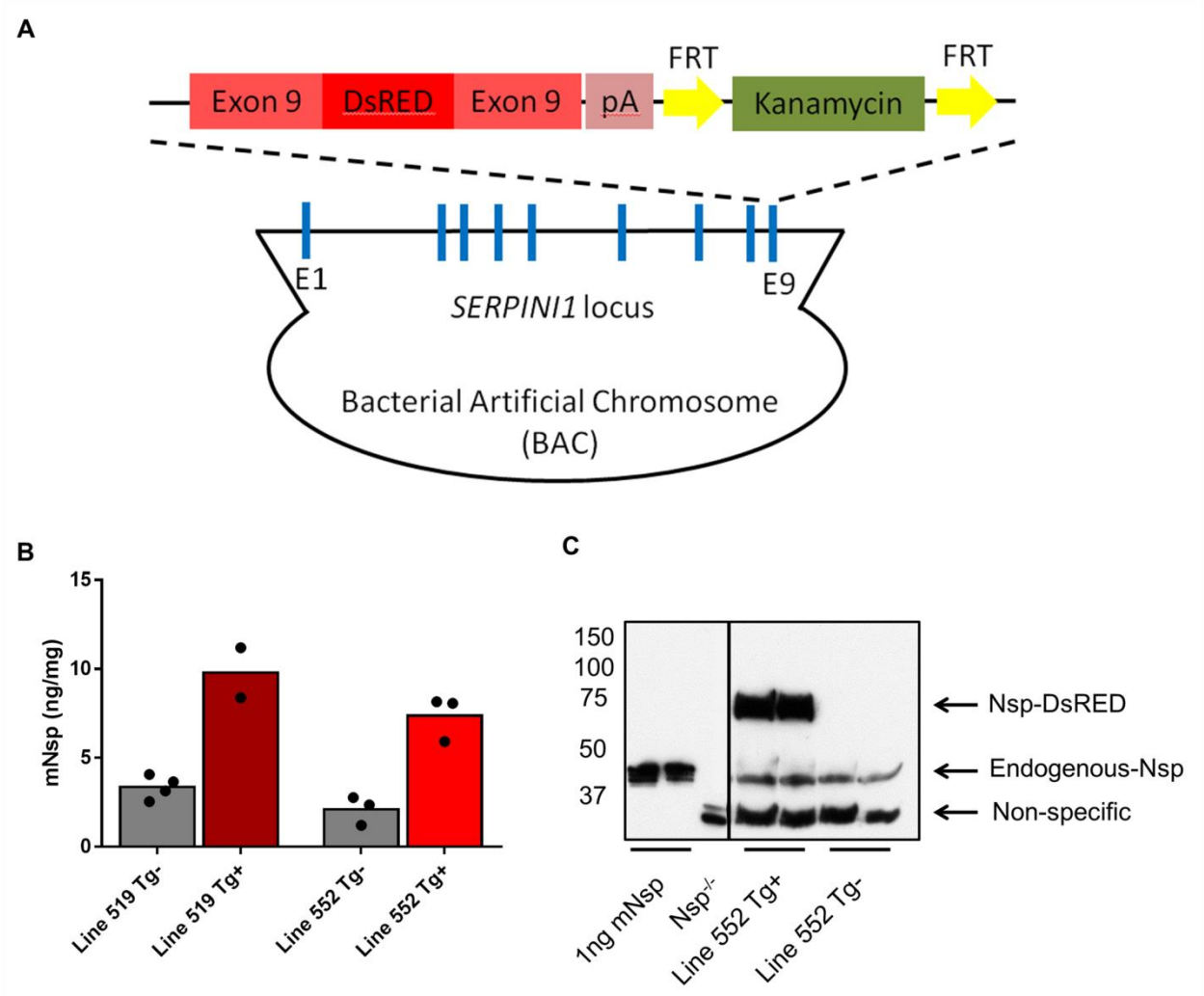
A
Exon 9
DsRED
Exon 9
pA
FRT
Kanamycin
FRT
E1
E9
SERPINI1 locus
Bacterial Artificial Chromosome
(BAC)
B
mNsp (ng/mg)
15
10
5
0
Line 519 Tg-
Line 519 Tg+
Line 552 Tg-
Line 552 Tg+
C
150
100
75
50
37
Nsp-DsRED
Endogenous-Nsp
Non-specific
1ng mNsp
Nsp-/-
Line 552 Tg+
Line 552 Tg-

Figure 3.1. Generation of Nsp^{BAC}–DsRED transgenic reporter mice and protein expression analysis. (A) Diagram of the BAC recombineering strategy used to insert the fluorescent DsRED gene. Before pronuclear injection, the kanamycin cassette was removed by *Flp* recombinase. (B) An ELISA assay was performed to quantify the concentration of mNsp (ng/mg) in the Nsp^{BAC}–DsRED founder mice, lines 519 and 552. Brains from transgene positive and transgene negative adult mice of lines 519 and 552 were harvested and homogenized for detection by ELISA. Increased levels of mNsp in both lines demonstrate the presence and insertion of at least one copy of the Nsp-DsRED BAC into the mouse genome. Data is presented as the mean. (C) Western blot of brain homogenates from Nsp^{BAC}-DsRED line 552 were probed for murine Nsp (mNsp; 2µg/mL). Purified recombinant mNsp (1 ng) was run as a positive control for endogenous Nsp (~45kDa) and a brain homogenate sample from a Nsp$^{-/-}$ mouse was run as a negative control. The ~75kDa band for transgene positive mice reflects the added molecular weight of the DsRED tag (~25kDa).

Figure 3.2

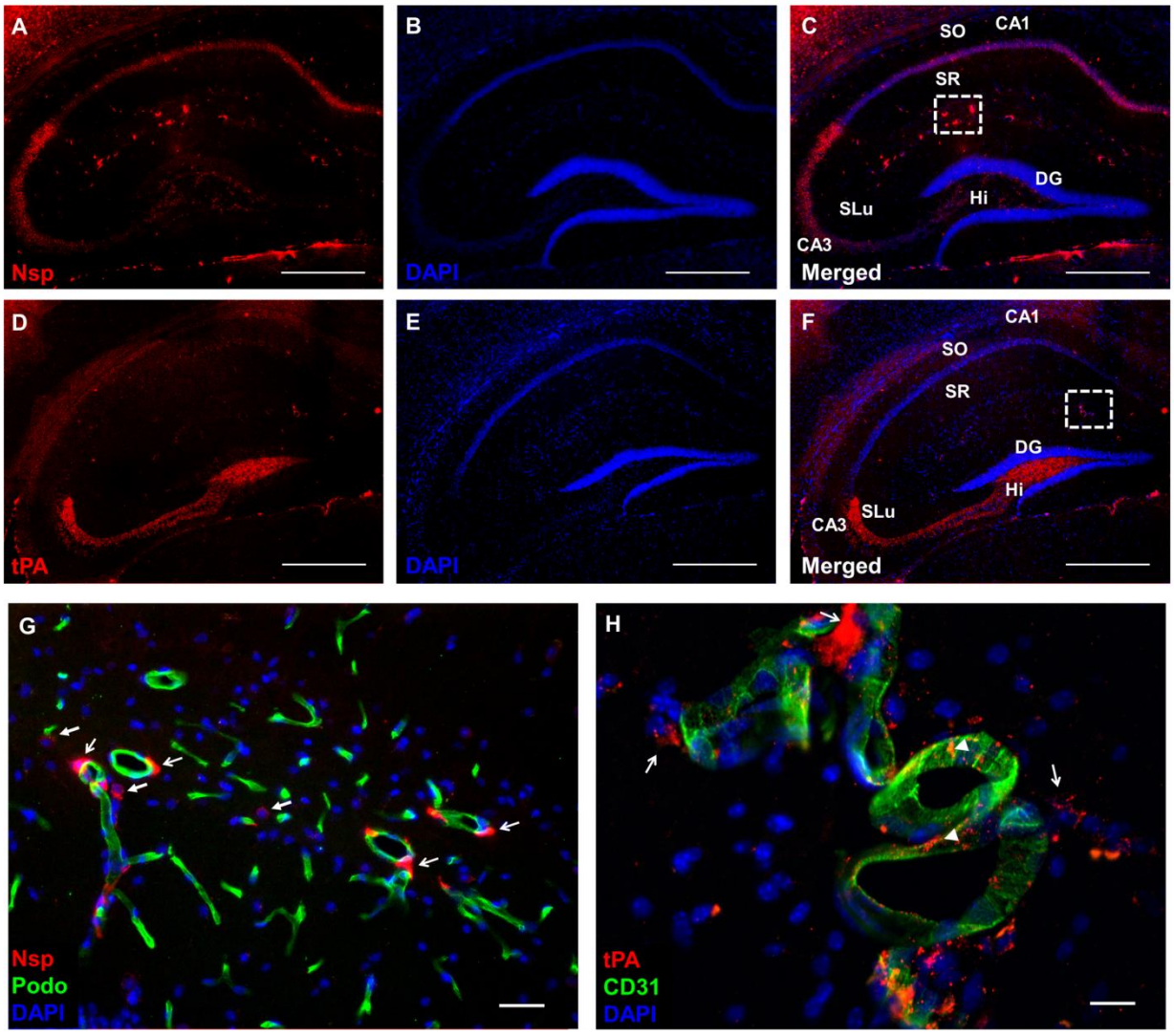
A
Nsp
B
DAPI
C
SO
CA1
SR
DG
Hi
SLu
CA3
Merged
D
tPA
E
DAPI
F
CA1
SO
SR
DG
Hi
SLu
CA3
Merged
G
Nsp
Podo
DAPI
H
tPA
CD31
DAPI

Figure 3.2. Nsp and tPA are both highly expressed in neurons and vascular or vascular-associated cells in the hippocampus. Representative widefield (4x) immunofluorescent hippocampal images from Nsp^{BAC}–DsRED (A – C) and tPA^{BAC}-Cer (D – F) transgenic mice. tPA-Cer signal has been pseudocolored red. (A - C) Intense Nsp-DsRED signal was detected in the hippocampus of transgene positive Nsp^{BAC}–DsRED mice, specifically in the CA1-CA3 pyramidal cell layer, in the hilus, and near blood vessels. To enhance the DsRED signal, an anti-RFP primary antibody was used. (D – F) Cerulean signal in tPA^{BAC}-Cer transgenic mice is prominently seen in the mossy fiber pathway in the hilus and stratum lucidum layer, and in blood vessels. To enhance the Cer signal, an anti-mtPA primary antibody was used. tPA-Cer signal has been pseudocolored red. (C, F) White, dotted boxes outlining blood vessels in the hippocampal fissure of Nsp^{BAC}-DsRED and tPA^{BAC}-Cer transgenic mice are shown in magnification in panels G (20x) and H (40x). Blood vessels in panel G are stained for the endothelial cell marker Podocalyxin (green), while blood vessels in panel H are stained or the endothelial cell marker CD-31 (green). (G) Nsp-DsRED signal is apparent in perivascular cells (open arrows), while scattered Nsp-DsRED positive cells are also present in stratum radiatum (closed arrows). (H) tPA-Cer signal is apparent in the endothelial cell compartment (arrowheads) and in cells surrounding blood vessels (open arrows). All nuclei were visualized with the nuclear stain DAPI. Abbreviations: SLu – stratum lucidum; Hi – hilus; DG – dentate gyrus; SR – stratum radiatum; SO – stratum oriens. Scale bars: A - F, 500 µm; G, 50 µm; H, 25 µm.

Figure 3.3

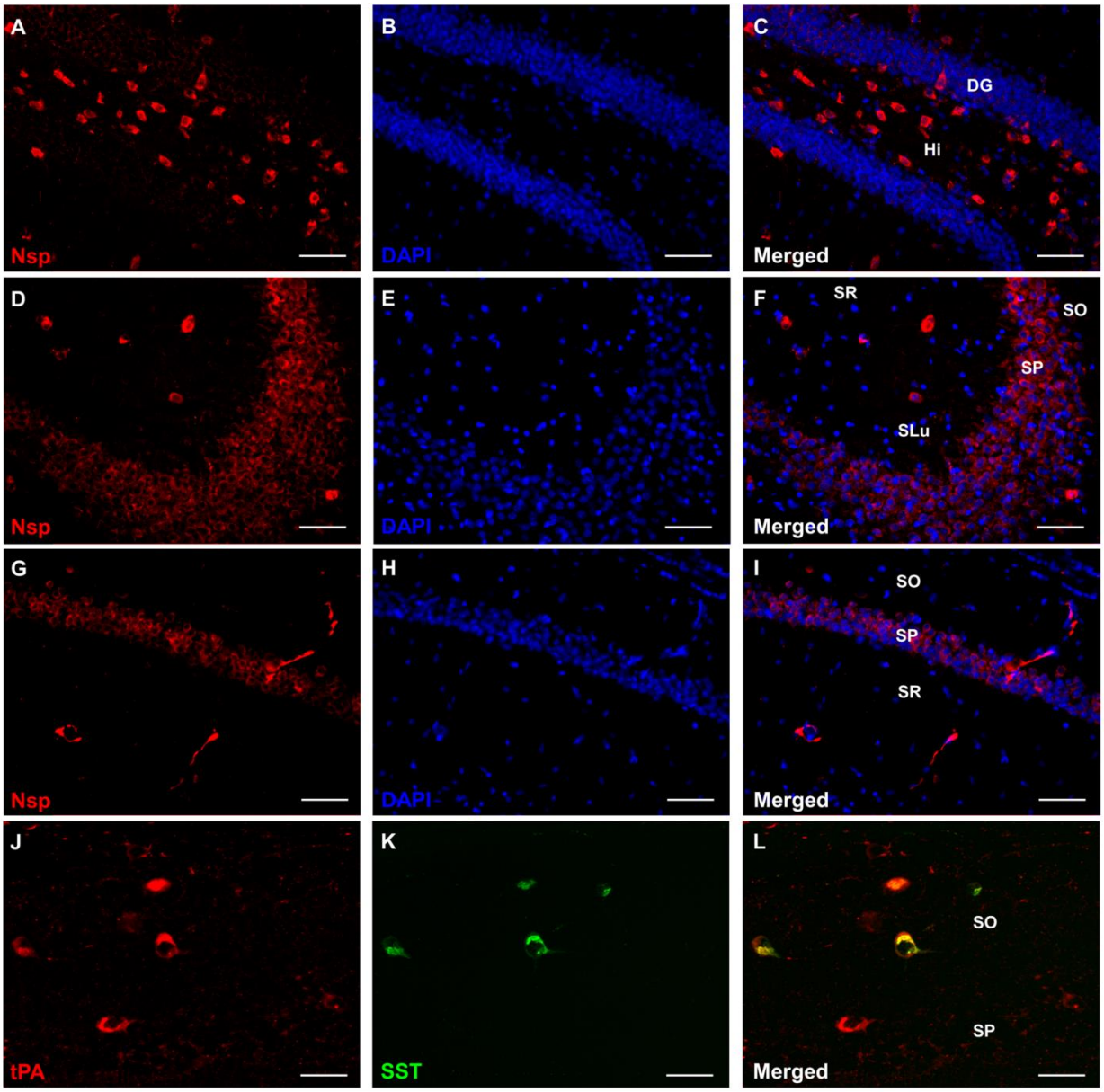
A
Nsp
B
DAPI
C
DG
Hi
Merged
D
Nsp
E
DAPI
F
SR
SO
SP
SLu
Merged
G
Nsp
H
DAPI
I
SO
SP
SR
Merged
J
tPA
K
SST
L
SO
SP
Merged

Figure 3.4. Expression pattern of Nsp and tPA in the hippocampus of adult murine mice. Representative immunofluorescent images (20x) from Nsp^{BAC}–DsRED **(A – I)** and tPA^{BAC}-Cer **(J – L)** transgenic mice. Nsp (*red*) is localized to cell bodies in the hilus **(A – C)**, CA3 pyramidal cell layer **(D – F)**, CA1 pyramidal cell layer **(G – I)**, and in scattered cell bodies in stratum radiatum and stratum oriens **(F – I)**. As previously reported, tPA-positive cell bodies (red) are present in stratum oriens **(J – L)** and represent a sub-population of interneurons that are somatostatin (SST)-positive (green) and belong to a family of oriens-lacunosum molecular (OL-M) interneurons. tPA-Cer signal has been pseudocolored red. All nuclei were visualized with the nuclear stain DAPI. Abbreviations: SLu – stratum lucidum; Hi – hilus; DG – dentate gyrus; SR – stratum radiatum; SP – stratum pyrmidale; SO – stratum oriens. Scale bars: A – L, 25 µm.

Figure 3.4

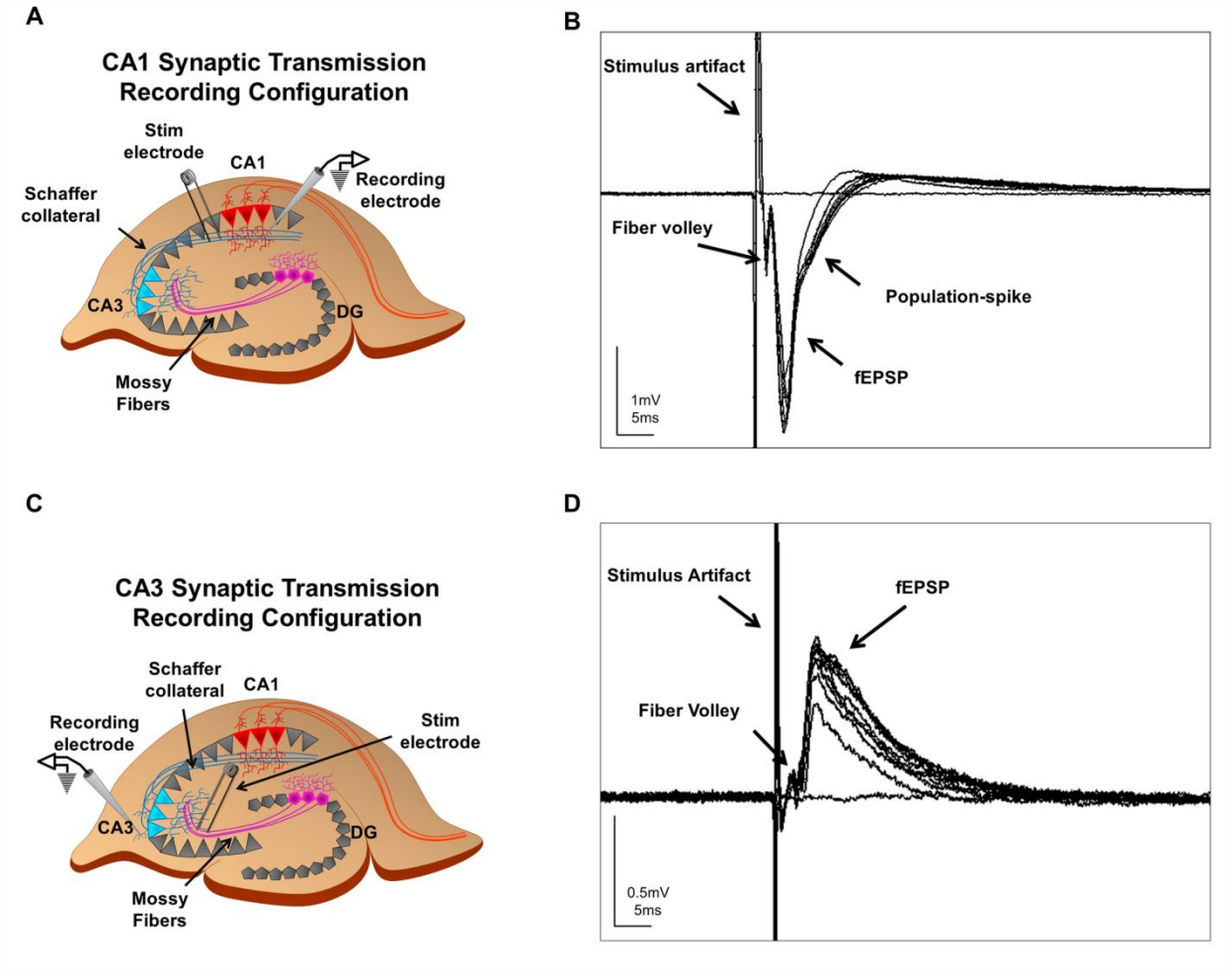
A
CA1 Synaptic Transmission
Recording Configuration
Stim
electrode
CA1
Recording
electrode
Schaffer
collateral
CA3
DG
Mossy
Fibers
B
Stimulus artifact
Fiber volley
Population-spike
fEPSP
1mV
5ms
C
CA3 Synaptic Transmission
Recording Configuration
Schaffer
collateral
CA1
Recording
electrode
Stim
electrode
CA3
DG
Mossy
Fibers
D
Stimulus Artifact
fEPSP
Fiber Volley
0.5mV
5ms

Figure 3.4. Electrophysiological field potential recording configuration for measuring synaptic transmission and synchronous activity in the CA1 and CA3 regions of the hippocampus. (A) Evoked responses from CA1 and **(C)** CA3 hippocampal subfields in standard artificial cerebral spinal fluid (aCSF) were used to generate input/output (I/O) curves as a measure of normal basal synaptic transmission. **(A,B)** For CA1 synaptic transmission recordings, Schaffer collateral axons in stratum radiatum are stimulated using a bipolar electrode to evoke a excitatory post-synaptic response in the CA1 pyramidal neurons, which is recorded by an electrode in stratum radiatum as the field excitatory post-synaptic potential (fEPSP). When recording, it is common to detect a stimulus artifact and the fiber volley, which represents the action potentials generated from the Schaffer collaterals. If the EPSP is strong enough to depolarize the CA1 neurons to threshold, it is also possible to detect a population spike ("pop-spike"), which is due to the action potentials from CA1 neurons. **(C, D)** A similar recording configuration is used to assess synaptic transmission in CA3. Bipolar stimulating electrodes are placed in the mossy fiber pathway and mossy fibers are stimulated to evoke an excitatory post-synaptic response in the CA3 pyramidal neurons, which is detected by the recording electrode in the stratum oriens layer as a fEPSP. In the CA3 recording configuration it is also possible to detect fiber volleys – or actions potentials from the mossy fibers.

Figure 3.5

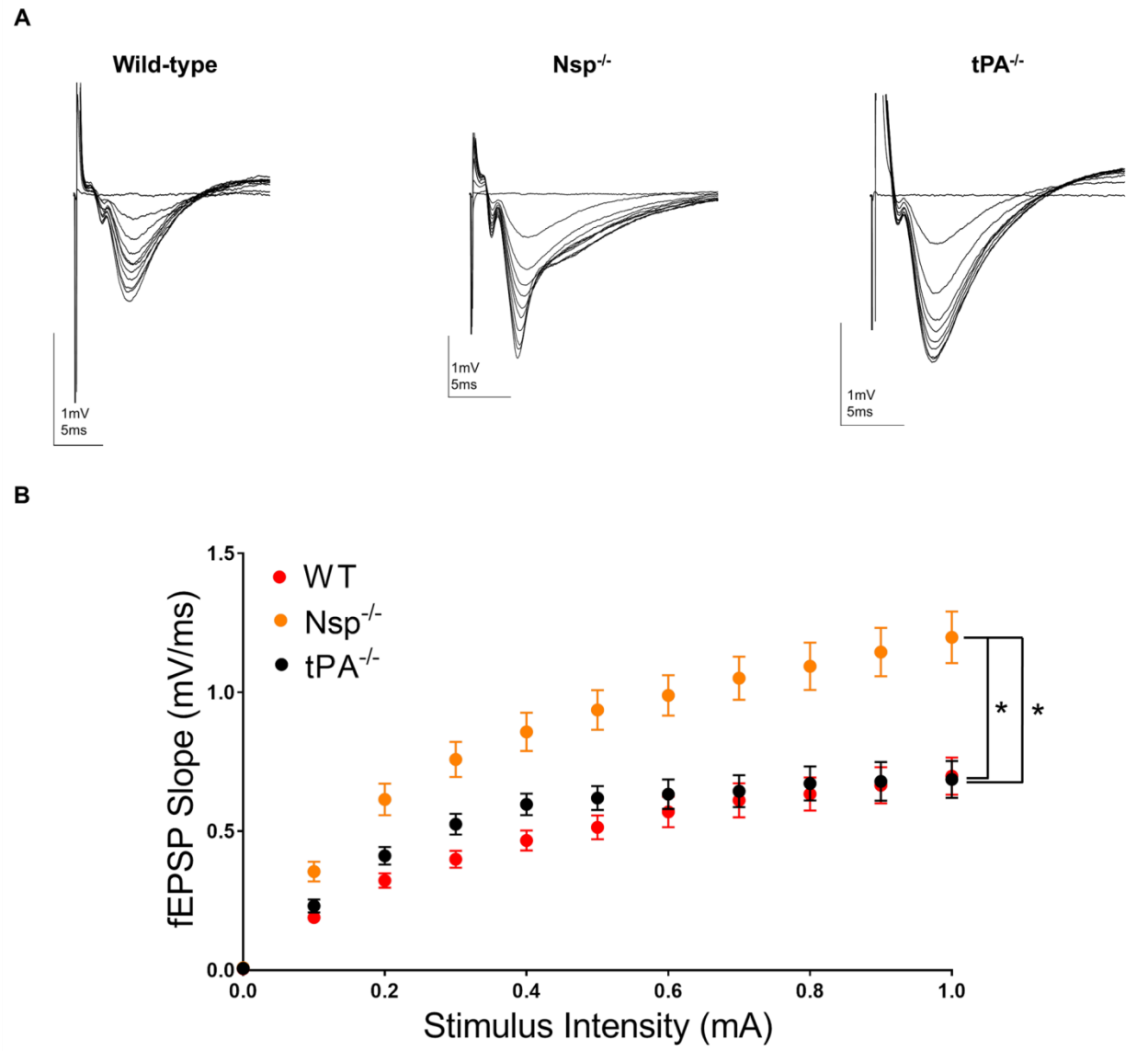
A
Wild-type
Nsp-/-
tPA-/-
1mV
5ms
1mV
5ms
1mV
5ms
B
WT
Nsp-/-
tPA-/-
fEPSP Slope (mV/ms)
Stimulus Intensity (mA)
0.0
0.5
1.0
1.5
0.0
0.2
0.4
0.6
0.8
1.0
*
*

Figure 3.5. Brain slices from Nsp$^{-/-}$ mice, but not tPA$^{-/-}$ mice, demonstrate enhanced synaptic efficacy compared to wild-type mice in the CA1 hippocampal subfield. (A) Compiled, representative traces of field excitatory post-synaptic potentials (fEPSPs) from the hippocampal stratum radiatum lamina of wild-type, Nsp$^{-/-}$, and tPA$^{-/-}$ mice. **(B)** Input/output curve of fEPSP slope (mV/ms) plotted as a function of increasing stimulus intensity, from 0 to 1.0 mA in 0.1 mA increments. Basal synaptic transmission was significantly different in brain slices from Nsp$^{-/-}$ mice (38 slices from 11 mice) compared to wild-type mice (32 slices from 11 mice) and tPA$^{-/-}$ mice (17 slices from 6 mice), but not between wild-type and tPA$^{-/-}$ mice. Brain slices from all mice displayed significant increases in the slope of the fEPSP with increasing stimulus intensity. Data are presented as mean ± SEM. * $p < 0.05$.

Figure 3.6

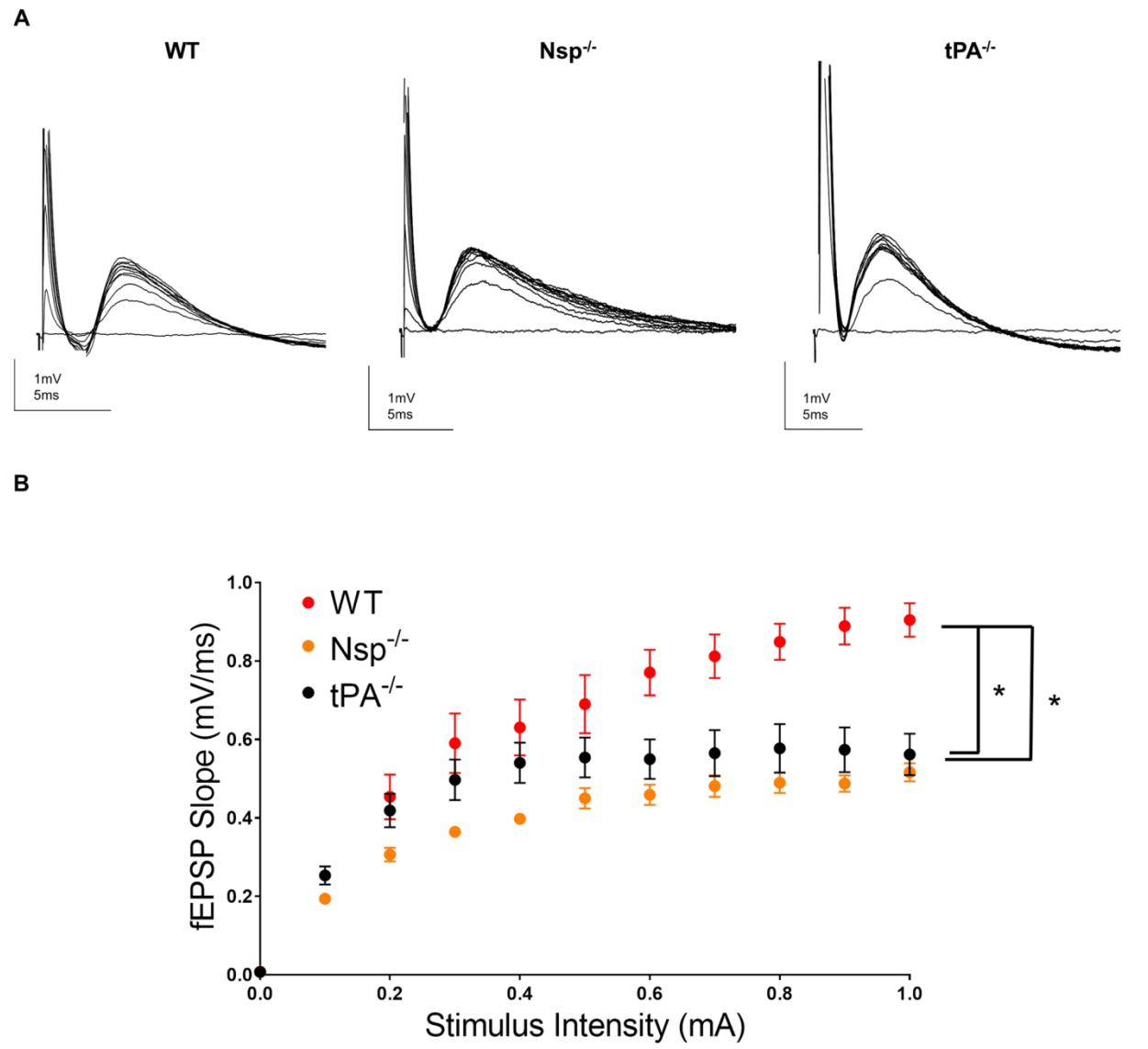
A
WT
Nsp-/-
tPA-/-
1mV
5ms
1mV
5ms
1mV
5ms
B
WT
Nsp-/-
tPA-/-
fEPSP Slope (mV/ms)
Stimulus Intensity (mA)
0.0
0.2
0.4
0.6
0.8
1.0
*
*

Figure 3.6. Brain slices from both Nsp$^{-/-}$ and tPA$^{-/-}$ mice exhibit decreased synaptic efficacy compared to brain slices from wild-type mice in the CA3 hippocampal subfield. (A) Compiled, representative traces of field excitatory post-synaptic potentials (fEPSPs) from the hippocampal stratum oriens lamina of wild-type, Nsp$^{-/-}$, and tPA$^{-/-}$ mice. **(B)** Input/output curve of fEPSP slope (mV/ms) plotted as a function of increasing stimulus intensity, from 0 to 1.0 mA in 0.1 mA increments. Basal synaptic transmission was significantly different in brain slices from wild-type mice (30 slices from 9 mice) compared to Nsp$^{-/-}$ mice (28 slices from 9 mice) and tPA$^{-/-}$ mice (25 slices from 8 mice), but not between Nsp$^{-/-}$ and tPA$^{-/-}$ mice. Brain slices from all mice displayed significant increases in the slope of the fEPSP with increasing stimulus intensity. Data are presented as mean ± SEM. * $p < 0.05$.

Figure 3.7

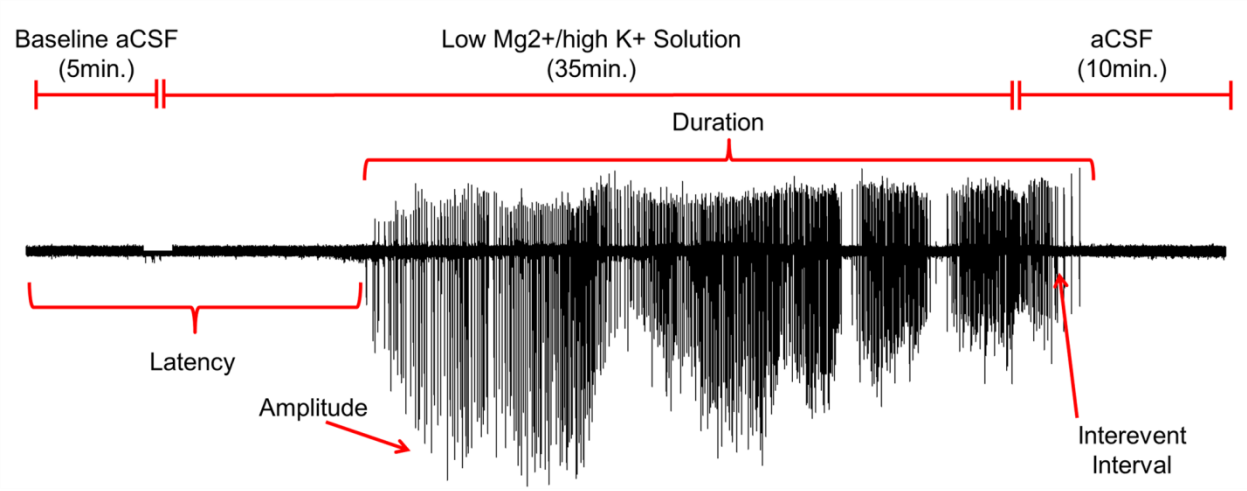
Baseline aCSF
(5min.)
Low Mg2+/high K+ Solution
(35min.)
aCSF
(10min.)
Duration
Latency
Amplitude
Interevent
Interval

Figure 3.7. Representative trace of an electrophysiological field potential recording used to assess synchronous activity in the CA3 region of hippocampal brain slices. Continuous recordings in CA3 were used to measure the baseline field potential in standard aCSF and synchronized firing in no Mg^{2+}/high K^{+} aCSF. Baseline field potentials were recorded for 5 min. before the no Mg^{2+}/high K^{+} solution was washed in to the recording chamber. Synchronous activity was recorded in the no Mg^{2+}/high K^{+} solution for 35 min before standard aCSF was washed back in to the chamber. This method, which enhances conductance of NMDA receptors and depolarizes the neurons, is a well-established *in vitro* correlate of *in vivo* seizures. Different parameters, including latency to synchronous activity, duration, number of events, peak amplitude, and inter-event interval, were measured to assess the hyperexcitable state of brain slices from wild-type, $Nsp^{-/-}$, and $tPA^{-/-}$ mice.

Figure 3.8

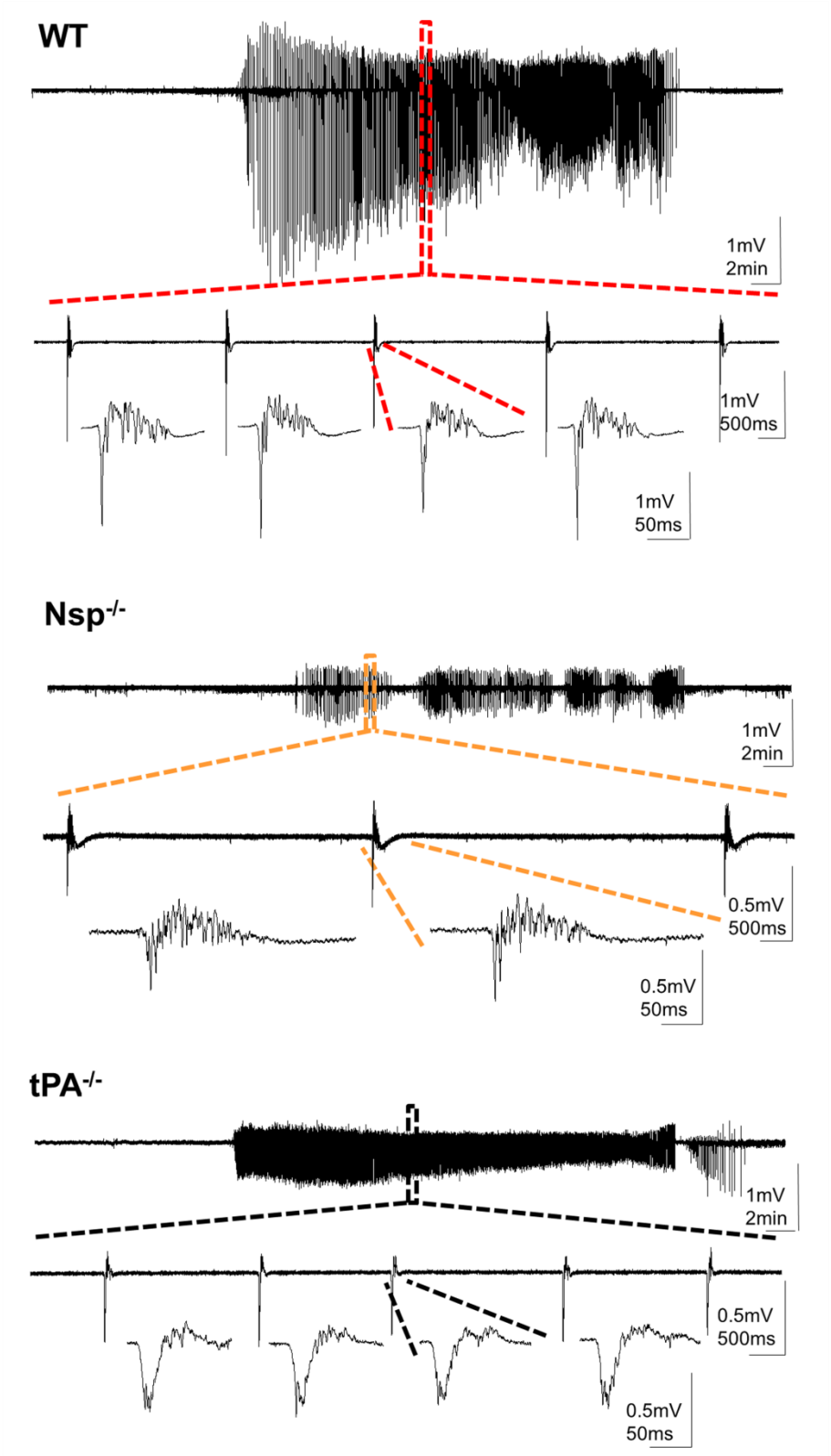
WT
1mV
2min
1mV
500ms
1mV
50ms
Nsp-/-
1mV
2min
0.5mV
500ms
0.5mV
50ms
tPA-/-
1mV
2min
0.5mV
500ms
0.5mV
50ms

Figure 3.8. Representative tracings of synchronous activity in no Mg^{2+}/high K^{+} aCSF from the CA3 region of wild-type, $Ns^{-/-}$ and $tPA^{-/-}$ mice. An example of a high-frequency burst/event is magnified from each trace. Each trace is representative of gap-free recordings from WT (n = 16), $Nsp^{-/-}$ (n = 14), and $tPA^{-/-}$ (n = 11) mice. Differences in onset time to synchronous activity and amplitude are apparent.

Figure 3.9

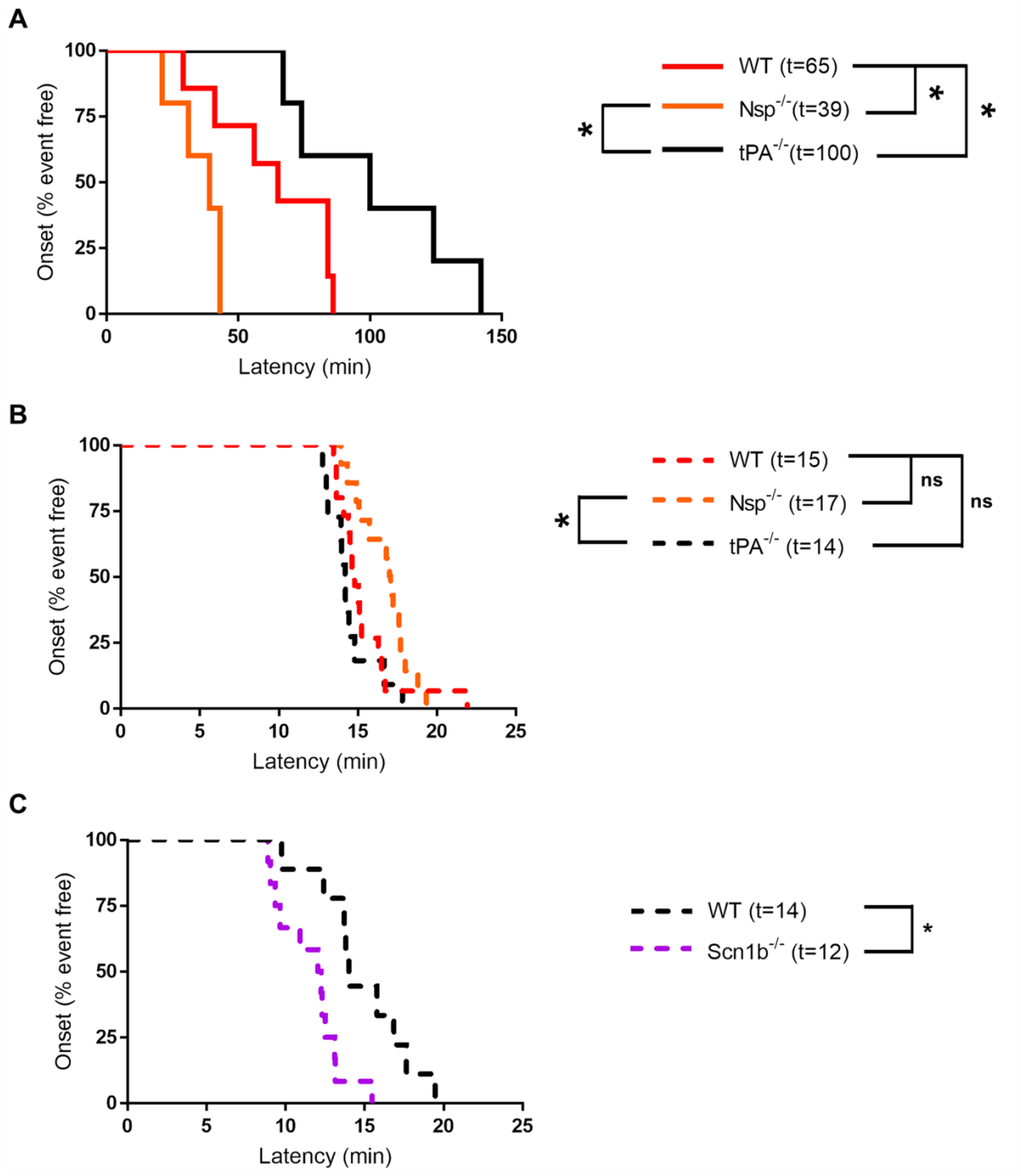
A
100
75
50
25
0
Onset (% event free)
0
50
100
150
Latency (min)
WT (t=65)
Nsp-/-(t=39)
tPA-/-(t=100)
*
*
*
B
100
75
50
25
0
Onset (% event free)
0
5
10
15
20
25
Latency (min)
WT (t=15)
Nsp-/- (t=17)
tPA-/- (t=14)
*
ns
ns
C
100
75
50
25
0
Onset (% event free)
0
5
10
15
20
25
Latency (min)
WT (t=14)
Scn1b-/- (t=12)
*

Figure 3.9. *Ex vivo* "seizure-like" activity in brain slices from Nsp$^{-/-}$ and tPA$^{-/-}$ mice does not match the *in vivo* seizure phenotype. Data are presented in Kaplan-Meier plots and median time (t = min) to electrographic event is indicated in the figure. (A) An inter-hippocampal depth electrode recorded the onset of electroencephalographic (EEG) seizure activity following intra-amygdala injections of kainic acid (KA) in wild-type (n = 7), Nsp$^{-/-}$ (n = 5), and tPA$^{-/-}$ (n = 5) mice. Electrographic seizure activity develops earliest in the Nsp$^{-/-}$ (t = 39 min) and latest in the tPA$^{-/-}$ mice (t = 100 min), while wild-type mice (t = 65 min) are in-between. Log-rank (Mantel Cox) statistical analysis revealed significant differences between wild-type and Nsp$^{-/-}$ mice, wild-type and tPA$^{-/-}$ mice, and Nsp$^{-/-}$ and tPA$^{-/-}$ mice. The EEG recordings correlate with the clinical scoring of seizure behavior (Fredriksson et al., 2015). (B) Onset to synchronous activity was measured from extracellular field potential recordings in the stratrum oriens layer of the CA3 region of wild-type (n = 16), Nsp$^{-/-}$ (n = 14), and tPA$^{-/-}$ (n = 11) mice. Synchronous activity, or "seizure-like" activity, was induced by exchanging normal aCSF for a no Mg^{2+}/high K^{+} aCSF solution. Log-rank (Mantel Cox) statistical analysis revealed no significant differences between wild-type and Nsp$^{-/-}$ mice or wild-type and tPA$^{-/-}$ mice. Significant differences, however, were found between Nsp$^{-/-}$ and tPA$^{-/-}$ mice. In contrast to the *in vivo* seizure phenotype, brain slices from tPA$^{-/-}$ mice (t = 14 min) developed synchronous activity more quickly than Nsp$^{-/-}$ mice (t = 17 min), while brain slices from wild-type mice are in-between (t = 15 min). (C) No Mg^{2+}/high K^{+} model of synchronous activity was validated in a transgenic mouse model (Scn1b$^{-/-}$) that develops spontaneous seizures (Chen et al., 2004). Scn1b$^{-/-}$ mice (n = 4; t = 12 min) develop synchronous activity more quickly than their wild-type littermate controls (n = 3; t = 14 min). * $p < 0.05$; ns = not significant.

Figure 3.10

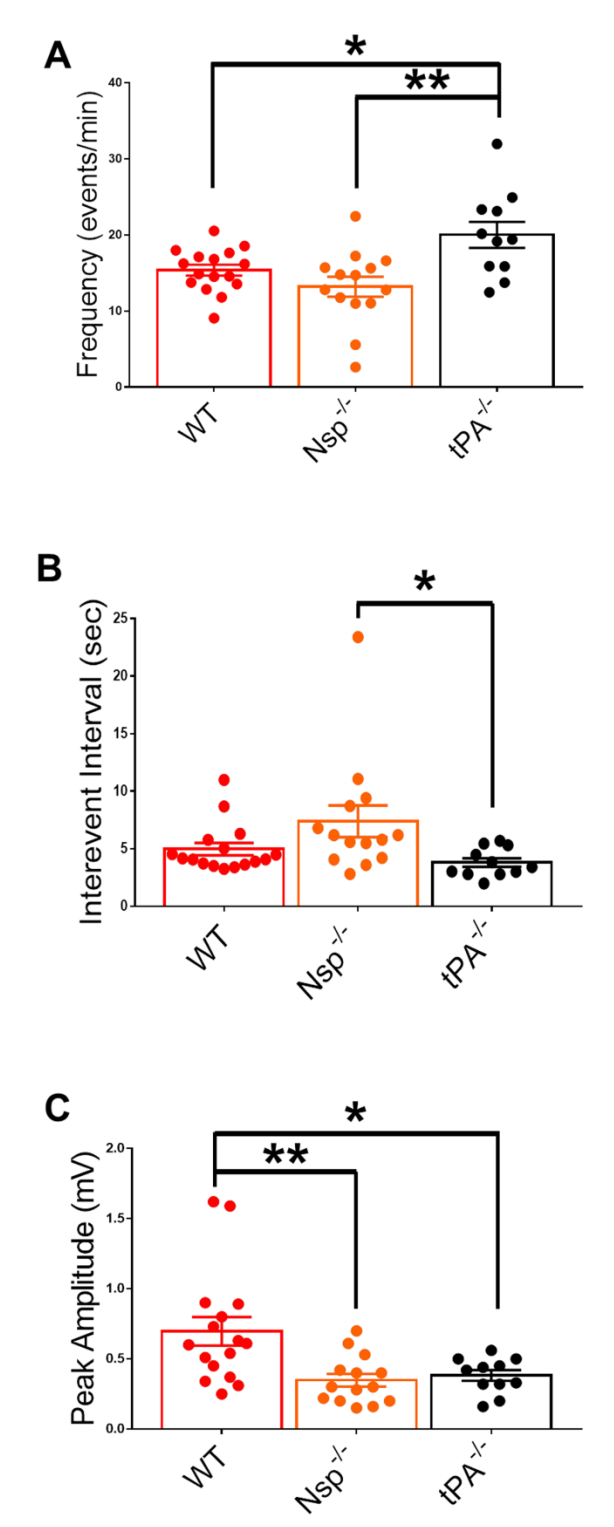
A
*
**
Frequency (events/min)
0
10
20
30
40
WT
Nsp -/-
tPA -/-
B
*
Interevent Interval (sec)
0
5
10
15
20
25
WT
Nsp -/-
tPA -/-
C
*
**
Peak Amplitude (mV)
0.0
0.5
1.0
1.5
2.0
WT
Nsp -/-
tPA -/-

Figure 3.10. No Mg^{2+}/high K^{+} model of synchronous activity reveal brain slices from $tPA^{-/-}$ mice to be in a hyperexcitable state and brain slices from $Nsp^{-/-}$ mice to be in a quiescent state. Temporal parameters of synchronous activity, including frequency (events/min) and inter-event interval (sec), demonstrate that brain slices from $Nsp^{-/-}$ and $tPA^{-/-}$ mice have divergent phenotypes. Brain slices in $tPA^{-/-}$ mice (n = 11) appear to be more hyperexcitable, while brain slices from $Nsp^{-/-}$ mice (n = 14) appear to be more quiescent. Wild-type mice (n = 16) have a more intermediate phenotype. **(A – B)** Mice deficient in tPA have a faster frequency of events/min and a shorter inter-event interval, while $Nsp^{-/-}$ mice have a slower frequency of events/min and a longer inter-event interval. **(C)** Both $Nsp^{-/-}$ and $tPA^{-/-}$ mice, however, have short peak amplitudes (mV) than wild-type mice. * $p < 0.05$ and ** $p < 0.005$.

CHAPTER 4

Cerebrovascular morphometry and network connectivity characteristics in wild-type and tPA-deficient mice: Implications for blood flow regulation and pathophysiology

4.1 Abstract

The serine protease tissue-plasminogen activator (tPA), classically known for the role that it plays in fibrinolysis, is also expressed on the abluminal side of the vasculature in the central nervous system (CNS). Parenchymal brain tPA has been implicated in a variety of neuropathological processes, including stroke, seizure progression, and traumatic brain injury. In addition to these pathological roles for tPA, a physiological one was reported when $tPA^{-/-}$ (Carmeliet-$tPA^{-/-}$) mice were found to have an attenuated functional hyperemia response following whisker-barrel stimulation. Recently, however, $tPA^{-/-}$ mice have been shown to harbor “passenger mutations” from the original 129/sv embryonic stem (ES) cells flanking the tPA gene and to have developmental differences in cerebrovascular and cerebroventricular morphometry and molecular composition.

To understand whether some strain-dependent modifier genes or the observed vascular developmental difference associated with tPA deficiency can account for the diminished functional hyperemia observed in $tPA^{-/-}$ mice, we performed a detailed analysis of the vasculature in wild-type, Carmeliet-$tPA^{-/-}$, and in the recently established

Szabo-tPA$^{-/-}$ mice. The Szabo-tPA$^{-/-}$ mice are a new line of tPA deficient mice that were generated using zinc-finger nuclease genome editing on a pure C57BL/6J genetic background. Cerebrovascular morphometry and density statistics were gathered from each of the three genotypes using SeeDeepBrain (SeeDB) clear brain technology and an enhanced vascular visualization method. This approach allowed for a more extensive analysis of vascular morphometry – including measurements of correlated vessel diameter and length, vascular density, and vertex degree – which is not possible with conventional immunofluorescence and microscopy techniques.

With our more extensive analysis we are able to confirm that Carmeliet-tPA$^{-/-}$ mice have a denser capillary bed than both wild-type mice and Szabo-tPA$^{-/-}$ mice, however, we did not find any differences in vessel diameter, as was previously reported. In our analysis of network connectivity, we also found there to be a significant difference between wild-type and Carmeliet-tPA$^{-/-}$ mice in branch vertex degree. Carmeliet-tPA$^{-/-}$ mice have fewer vessels that branch with vertex degree 3, but more vessels that branch with vertex degree 4. It is not clear if this statistical difference with respect to vertex degree has a biological effect. We do find, though, that there is a correlation between vascular density and blood flow, since Carmeliet-tPA$^{-/-}$ mice had an elevated basal Doppler flux, compared to wild-type and Szabo-tPA$^{-/-}$ mice. Baseline Doppler flux in Szabo-tPA$^{-/-}$ mice was not statistically different than wild-type mice

These data suggest that some strain-dependent genes are responsible for the elevated blood flow phenotype in Carmeliet-tPA$^{-/-}$ mice. Furthermore, it raises questions about how the cerebrovascular architecture can influence blood flow at rest and in response to a neural stimulus. For, if the brains of Carmeliet-tPA$^{-/-}$ mice are already at

an elevated level of perfusion, then it's conceivable that they don't require the same increase in blood flow to meet the metabolic demands of the tissue when there is an increase in neural activity. Our results begin to help address these questions by providing important vascular statistics on vessel morphometry, density, and connectivity. These data are critical for establishing networks to take a statistical modeling approach to calculate blood flow at a steady-state and when there is a transient change.

4.2 Introduction

Tissue plasminogen activator (tPA), encoded by the *PLAT* gene, is a serine protease that is expressed by vascular endothelial cells and is classically known for its role in promoting fibrinolysis. However, in contrast to its role in fibrinolysis, in the central nervous system (CNS), where tPA is expressed by neurons (*See Chapter 2*) (Sappino et al., 1993; Yu et al., 2001; Salles and Strickland, 2002; Fredriksson et al., 2015; Louessard et al., 2016), many *in vivo* studies using tPA deficient mice ($tPA^{-/-}$) have demonstrated that tPA can have harmful effects in the CNS (Tsirka et al., 1995; Tsirka et al., 1996; Tsirka et al., 1997; Rogove and Tsirka, 1998; Wang et al., 1998; Yepes et al., 2002; Yepes et al., 2003; Su et al., 2008; Su et al., 2015; Su et al., 2017). In these studies, tPA has been shown to promote excitotoxicity, neurodegeneration, and loss of blood-brain barrier (BBB) integrity in models of stroke, seizure, and traumatic brain injury. Complicating the narrative of tPA primarily being an effector molecule during pathological events, however, was a study demonstrating, *in vivo,* a physiological role for tPA in the CNS (Park et al., 2008). Compared to wild-type controls, mice lacking tPA ($tPA^{-/-}$) were shown to have significant deficits in neurovascular coupling (data

schematically recreated in Figure 4.1). The diverse and disparate *in vivo* roles of tPA in the CNS have led to two predominant hypotheses: 1) tPA is a pleiotropic mediator with compartmentalized actions (Stevenson and Lawrence, 2018), and 2) the functions attributed to tPA are an indirect result of tPA's effects on BBB permeability, and in turn, loss of extracellular homeostasis (Fredriksson et al., 2017).

Recently, though, two reports have raised questions about studies that used $tPA^{-/-}$ mice as a model for the effects of acute tPA loss in physiological and pathological events (Stefanitsch et al., 2015; Szabo et al., 2016). With new $tPA^{-/-}$ mice, herein called Szabo-$tPA^{-/-}$, that were generated using zinc-finger nuclease technology on a pure C57BL/6J background, Szabo et al. (2016) demonstrated that the original $tPA^{-/-}$ mice (herein called Carmeliet-$tPA^{-/-}$) harbor ~20 Mbp of DNA flanking the *Plat* allele that is from the 129/Sv embryonic stem (ES) cell genomic DNA. This ~20 Mbp region of DNA contains variants that are potential "passenger mutations" which may affect the expression or activity of genes not related to tPA, including genes reported to have neurologic function, such as ARHGEF18 (neurite retraction) and MCF2L (formation and stabilization of glutamatergic synapses). In a second study, Stefanitsch et al. (2015) showed that the Carmeliet-$tPA^{-/-}$ mice have an aberrant cerebrovascular architecture. Though no gross anatomical differences in neuronal patterning in brains from adult Carmeliet $tPA^{-/-}$ mice had been previously observed (Carmeliet et al., 1994; Frey et al., 1996; Huang et al., 1996), Stefanitsch et al. (2015) found significant differences in the morphology and molecular composition of cerebral vessels from Carmeliet-$tPA^{-/-}$ mice. Compared to their wild-type littermate controls, Carmeliet-$tPA^{-/-}$ mice were shown to have an increase in small-diameter capillaries (< 10 μm) and a decrease in larger-

diameter, smooth muscle-covered (> 15 µm) vessels (Figure 4.2 A and B); enhanced expression of ERG (ETS related gene) and ZO-1 (zona occludin-1), a marker of vascular integrity and a tight-junction protein, respectively; and decreased expression of the PDGFRα, a tyrosine receptor implicated in neurovascular signaling.

To determine if 129/Sv "passenger mutations" and/or developmental loss of tPA is/are responsible for the aberrant cerebrovascular architecture, a more exhaustive analysis of vessel morphometry was undertaken in wild-type mice and in both the original Carmeliet-tPA$^{-/-}$ mice and the Szabo-tPA$^{-/-}$ mice. Using an enhanced vascular visualization method, coupled with SeeDeepBrain (SeeDB) clearing, we were able to sample from an extensive area of the mouse brain and gather statistics on the correlated diameter and length distributions, branch density, and branching vertex degree. Our results confirm the finding from Stefanitsch et al. (2015) that Carmeliet-tPA$^{-/-}$ mice have a denser capillary network than wild-type mice. We also extend upon that result by showing that this difference in capillary density appears to be due to some strain modifying genes as the pure C57BL/6J Szabo-tPA$^{-/-}$ mice were not statistically different than wild-type mice. Importantly, we report that the calculated vascular density in each of the genotypes appears to correlate with their respective basal cerebral blood flow. Carmeliet-tPA$^{-/-}$ mice had a significantly elevated baseline laser speckle intensity signal compared to either wild-type or Szabo-tPA$^{-/-}$ mice.

These data, therefore, will provide important insights into how the cerebrovasculature architecture can affect blood flow regulation, which has specific implications for the role attributed to tPA in neurovascular coupling (Park et al., 2008), but also more general implications for other neurological pathologies, like Alzheimer's

disease, that have been reported to have an altered morphology and 3D architecture (Meyer et al., 2008).

4.3 Materials and Methods

4.3.1 Tomato lectin and gelatin cast

A modified protocol (Tsai et al., 2009) was used to fluorescently label the cerebrovasculature in the murine brain. First, mice were given a 100 µl tail-vein injection of either DyLight® 488 *Lycopersicon Esculentum* (Tomato) Lectin (Vector Laboratories; DL-1174) or DyLight® 594 *Lycopersicon Esculentum* (Tomato) Lectin (Vector Laboratories; DL-1177) before isofluorane induction (4%). Prior to injection, the tomato lectin dye was dialyzed with PBS to remove the sodium azide preservative. The tomato lectin dye circulated for 10 min before the mouse was cardiac-perfused with, in sequential order, warmed 0.9% NaCl with Heparin (20 U) for 2 min, 4% paraformaldehyde (PFA) for 2 min, and fluorophore-gelatin for 3 min, all at a perfusion rate of 7 mL/min. Following perfusion, the mouse was chilled on a bed of ice for 30 min to solidify the gelatin solution; after which, the brain was carefully removed and post-fixed overnight in 4% PFA. The brain was rinsed in PBS before being coronally sectioned into 1 mm slabs and cleared using the SeeDeepBrain (SeeDB) method (Ke et al., 2013; Ke and Imai, 2014).

The fluorophore-gelatin solution contained porcine skin gelatin type A (Sigma; G1890) and Albumin-fluorescein isothiocyanate (FITC) conjugate (Sigma; A9771) or Dextran-rhodamine B isothiocyanate conjugate (Sigma; R9379) and was prepared by bringing a 2% gelatin solution in PBS to a boil before cooling it to 50 °C, at which point

Albumin-fluorescein isothiocyanante or Dextran-rhodamine B isothiocyanante was added to achieve a final concentration of 0.1% (w/v). The fluorophore-gelatin solution was then filtered through filter paper (Whatman; grade 3) pre-moistened with PBS, and cooled and maintained at 40°C till perfusion.

4.3.2 SeeDeepBrain "SeeDB" optical clearing

"SeeDB", a water-based optical clearing approach, was employed to allow for greater depth visualization of the fluorescently-labeled vascular network (Ke et al., 2013; Ke and Imai, 2014). SeeDB clearing is a non-toxic clearing method that reduces light scatter by incrementally changing the aqueous solution of the tissue to a saturated fructose solution which has a refractive index of 1.490 and is, therefore, closer to the refractive index of fixed tissue. Following PFA fixation and sectioning, 1 mm thick slabs of tissue were placed in a 20% fructose solution (w/v; fructose dissolved in distilled water) for 4-8 hrs, a 40% fructose solution for 4-8 hrs, a 60% fructose solution for 4-8hrs, an 80% fructose solution for 12hrs, a 100% solution for 12 hrs, and finally, in SeeDB for 24-48hrs. SeeDB is a saturated fructose solution comprised of 20.25 g of fructose in 5 mL of distilled water. To reduce browning of tissue and autofluorescence, the 20%-100% fructose solutions contained 0.5% α-thiolglycerol and the SeeDB solution contained 2.0% α-thiolglycerol. All incubations were done at room temperature on a rotating shaker.

4.3.3 Image acquisition, processing, and analysis

After “SeeDB” clearing, images were acquired using a Leica SP5X 2-Photon laser scanning microscope with a Coherent “Chameleon” 2-photon laser (800 nm excitation). The SP5X microscope is equipped with an acousto-optical beam splitter (AOBS) and hybrid detectors. Emitted light was gathered between 498-600 nm for DyLight® 488 /FITC dyes or 604-700 nm for DyLight® 594/Rhodamine B dyes. Images (512 pixels x 512 pixels or 1024 pixels x 2014 pixels) were acquired using a dry 10x objective or a 20x multi-immersion objective at a scanning rate of 200Hz, with a line averaging of 2 per axial position. Z-stacks were collected at 1 µm increments, ranging in total thickness from 100 µm (10x) to 250 µm (20x). Image processing was done using the open source image processing package FIJI (Schindelin et al., 2012). A manual threshold was set so that all values in the bottom 4% of pixel intensities in the image were converted to zero. The threshold was applied evenly across the images and equally for all genotypes. Two-photon confocal images are presented as either maximum intensity projections or 3D volumetric maximum projections using FIJI’s 3D viewer (Schmid et al., 2010).

The Matlab-based Volumetric Image Data Analysis (VIDA) software program was used to generate a centerline mask over the vascular network from which vessel diameter, vessel length, and connectivity data was gathered. The VIDA suite was developed by the Kleinfeld Lab at the University of California – San Diego and is a freely available shared technology. The raw data extracted from the VIDA was further processed and analyzed using custom-written Matlab and Mathematica scripts. The

Mathematica program was written by Dr. Randy C. Stevenson, an applied physicist consulting for the University of Michigan.

4.3.4 Laser speckle contrast imaging

Laser speckle contrast imaging (LSCI) was used to measure cerebral blood flow in the cortical surface of wild-type (n = 10), Carmeliet-tPA$^{-/-}$ (n = 9), and Szabo-tPA$^{-/-}$ (n = 9) mice. Mice were anesthetized with chloral hydrate (450 mg/kg) and maintained on isoflurane (3%) for the measurements. Flux measurements were gathered using a portable Laser Speckle device (MoorFLPI, Moor Instruments) connected to a dell laptop computer equipped with real-time data acquisition software (MoorFLPI software version 2.01, Moor Instruments). In the present study, an image sampling rate of 0.13 Hz with an exposure time of 20 ms was used, with the final frame being used for quantification. All CBF flux measurements were obtained within a 17.44 mm x 13.4 mm region, but four regions of interest (ROIs) from that larger area were selected to quantify flux. The four ROIs (~ 1mm^2) approximately correspond to the barrel cortex at bregma -0.5 and -2.0.

4.3.5 Mutant Mice

For vessel morphometry analysis a mixture of adult (age: 15 to 25 wks) male and female Carmeliet-tPA$^{-/-}$ (Carmeliet et al., 1993; Carmeliet et al., 1994) were used. Carmeliet-tPA$^{-/-}$ mice have been back-crossed at least 10 generation onto a C57BL/6J background. Similarly, a mixture of adult (age: 15 to 21 wks) male and female Szabo-tPA$^{-/-}$ (Szabo et al., 2016) mice and their wild-type littermate controls were also used for

vessel morphometry analysis. Szabo-tPA$^{-/-}$ mice were generated using zinc-finger nuclease technology on a pure C57BL/6J background. For LSCI, age- and sex-matched adult (age: 10 to 12 wks) C57BL/6J wild-type, Carmeliet-tPA$^{-/-}$, and Szabo-tPA$^{-/-}$ male were used. All experiments were approved by the Institutional Animal Care and Use Committee at the University of Michigan, Ann Arbor, USA and the studies were conducted in accordance with the United States Public Health Service's Policy on Humane Care and Use of Laboratory Animals.

4.3.6 Statistical Analysis

All statistical tests, including one-way ANOVA with Tukey's post-hoc comparison, were performed in GraphPad Prism, version 7.0 (GraphPad Software, La Jolla, CA, USA), and a significance criterion of $p < 0.05$ was adopted. All data are presented as the mean ± standard error of the mean (SEM) or mean ± standard deviation (SD), and indicated as such in the figure text. Vessel diameter and length data are given out to the thousandths place, but given the resolution of the data, the accuracy of the values is likely only to the tenths place. Graphs were generated in either GraphPad Prism or Mathematica, version 11.0 (Wolfram Research, Champaign, IL, USA).

4.4 Results

4.4.1 Vessel diameter distributions from the adult murine brain are lognormally distributed

Stefanitsch et al. (2016) published the original observation that Carmeliet-tPA$^{-/-}$ mice (n = 5) have more small-diameter capillary-sized vessels (< ~10 μm) and fewer

large-diameter (> ~15 μm) arteriole- or artery-sized vessels compared to wild-type littermate controls (n = 5). These data were acquired from CD-31 and α-smooth muscle actin (ASMA)-stained 50 μm free-float vibratome coronal sections. CD-31 is an endothelial cell marker that detects all blood vessels, while ASMA is a mural (smooth muscle cells and pericytes) cell marker and detects arterioles and arteries.

We plotted the raw CD-31 and ASMA vessel diameter distributions from Stefanitsch et al. (2016) (the primary data was kindly provided by Dr. Linda Fredriksson of the Karolinska Institute, Stockholm Sweden) in separate histograms (Figure 4.2 A and B) and noticed that both distributions had a left skew, with Carmeliet-tPA$^{-/-}$ mice having an increased number of small-diameter vessels and a decreased number of large-diameter vessels compared to wild-type mice. The skewness of the histogram and the all-positive nature of the data indicated that vessel diameter may be lognormally distributed. Therefore, we replotted the CD-31 and ASMA vessel diameter data from both wild-type and Carmeliet-tPA$^{-/-}$ mice as normalized numerical probability densities and fit the data to a lognormal distribution (Figure 4.3 A and B) using the non-linear fitting function in Mathematica. The lognormal fit parameters for the CD-31 and ASMA datasets are given in Table 4.1 and Table 4.2, respectively, as well as the estimated mean, mode (peak value), and standard deviation. These quantities were calculated from the formulas provided in Table 4.3. For a normal distribution, the mean and the mode are the same value; this is only true for the lognormal distribution if the fitting parameter σ vanishes, which is a degenerate case. The mean diameter of CD-31-stained vessels from wild-type mice is 6.140 μm, while Carmeliet-tPA$^{-/-}$ mice have a smaller mean vessel diameter of 4.623 μm. Similarly, the mean diameter of ASMA-

stained vessels from wild-type mice is 21.325 µm, while Carmeliet-tPA$^{-/-}$ mice have a smaller mean diameter of 14.334 µm.

A comparison of different probability distribution functions revealed the lognormal distribution to be a good model for the numerical diameter data (Figure 4.4). Compared to the normal and Weibull probability distribution functions, the lognormal distribution function had the best fit to the numerical diameter data, with a R^2 of 0.9876. The R^2 values, fitting parameters, and functional form for the normal, Weibull, and lognormal distributions are given in Table 4.4.

4.4.2 Double labeling of vasculature allows for enhanced visualization of small and large vessels in the murine brain and quantification of vessel morphometry and network connectivity

The original analysis of vessel morphometry by Stefanitsch et al. (2016) was limited in sample size and quantification of different parameters that provide insight into vascular architecture and connectivity. Therefore, to gather more informative vessel morphometry statistics and sample from a larger volume of tissue we employed SeeDeepBrain (SeeDB) clearing, an enhanced vascular visualization method, and sophisticated computational programs to analyze the cerebrovasculature in wild-type, Carmeliet-tPA$^{-/-}$, and Szabo-tPA$^{-/-}$ mice.

A singular vascular labeling approach, using only a tomato-lectin-conjugated fluorophore, was initially taken to gather vessel morphometry statistics (Figure 4.5 A and C). Tomato-lectin, which is a glycoprotein from the *lycopersicon esculentum* (tomato) plant, intercalates into the endothelial glycocalyx and when conjugated to a

fluorophore brightly labels the vasculature. Though this approach is sufficient for vascular visualization, it is not adequate for automated quantification of vessel morphometry, as the tomato-lectin dye does not fill the vessel lumen; even capillaries of ~7 μm appeared as "hollow" and the Volumetric Image Data Analysis (VIDA) Matlab-based software suite detected the endothelial walls separated by the lumen as two separate vessels.

To overcome this experimental obstacle a double labeling approach was taken. Using a modified version of the protocol described by Tsai et al. (2009), we labeled the vasculature with both a tomato-lectin conjugated fluorophore and a fluorophore-gelatin cast. The less viscous tomato-lectin dye efficiently labels the smaller vessels, while the more viscous gelatin solution fills the lumen of larger vessels. The enhanced visualization of larger vessels is appreciable when comparing the single labeling approach (Figure 4.5 A) with the double labeling approach (Figure 4.5 B) in 10x max-projection images (1476 μm x 1476 μm x 100 μm) of the cortex and dorsal hippocampus at bregma -2.0. Magnified 3D volumetric images are shown (Figure 4.5 C, D) to more clearly illustrate the difference in labeling approach.

After implementing this double labeling approach we were able to analyze vessel morphometry and network connectivity using the VIDA suite and a custom Mathematica program. Two 20x images (738 μm x 738 μm x 250 μm) were acquired from the barrel cortex at bregma -0.5 and -2.0 (Figure 4.6 A) in SeeDB-cleared 1 mm thick (*see Methods and Materials section for full description of SeeDB clearing*) coronal slices from wild-type, Carmeliet-tPA$^{-/-}$, and Szabo-tPA$^{-/-}$ mice. The y-direction of the image (738 μm) spans from cortical layer 1 to approximately cortical layer 5. A representative 20x 3D

volumetric image and a magnified region (200 µm x 200 µm x 100 µm) is shown in Figure 4.6 A and B, respectively. The Matlab-based VIDA suite program used to process the image and extract vessel statistics is described in detail in Tsai et al. (2009). Briefly, a centerline mask comprised of individual vertices is generated over the entire 3D vascular network (Figure 4.6 C). Each vertex is associated with an XYZ coordinate in the 3D volumetric image. The radius of the vessel is extrapolated from the centerline at each vertex. The median of radii for all the vertices in a branch was chosen to represent the radius of the entire branch. Junction points demarcate branching points between vessels (Figure 4.6 D and E). An example volumetric vessel branch comprised of 30 bulbar segments between two junction points is shown (Figure 4.6 F). The length of the vessel is calculated by measuring the length between two contiguous vertices and then summing those segment lengths (Figure 4.6 G).

4.4.3 Vessel diameter and length distributions do not vary between wild-type mice and mice deficient in tPA

In contrast to the vessel diameter distributions from wild-type and Carmeliet-tPA$^{-/-}$ mice reported by Stefanitsch et al. (2016), with our more extensive analytical approach we did not detect any difference in the mean or the mode of vessel diameter distributions. When vessel branch diameters from all samples (n = 8) per genotype were aggregated and fit to a lognormal function (Figure 4.7 A), the distributions from all three genotypes appeared to overlay one another. The fit parameters for the lognormal distribution, mean, mode, and standard deviation are presented in Table 4.5. When the mean (Figure 4.7 B) and mode (Figure 4.7 C) from the lognormal fit data for each of the

samples (n = 8) was compiled per genotype and a one-way ANOVA was performed, no statistical difference was detected (mean: $F_{(2,21)} = 0.1137$, $p = 0.8930$; mode: ($F_{(2,21)} = 0.1792$, $p = 0.8372$). These data suggest that the differences between wild-type and Carmeliet-tPA$^{-/-}$ mice in mean vessel diameter first reported by Stefanitsch et al. (2016) are possibly a result of small sample size (see *Discussion*).

With our approach we were also able to gather statistics on vessel length. And, similar to the vessel diameter distributions, we did not detect any difference in vessel length distributions between wild-type, Carmeliet-tPA$^{-/-}$, and Szabo-tPA$^{-/-}$ mice. Vessel length also appeared to be lognormally distributed, therefore, vessel length distributions from all samples (n=8) per genotype were aggregated and fit to a lognormal function (Figure 4.8). The lognormal fits to the numerical length data, along with the mean, mode, and standard deviation, are presented numerically in Table 4.6. In addition, the mean and mode from the lognormal fit data for each of the samples (n = 8) was compiled per genotype and a one-way ANOVA was performed. No statistical difference was detected in the mean ($F_{(2,21)} = 1.906$, $p = 0.1736$) or the mode ($F_{(2,21)} = 2.237$, $p = 0.1316$) across genotypes, though both the Carmeliet-tPA$^{-/-}$ and the Szabo-tPA$^{-/-}$ mice show a trend toward shorter branch lengths.

4.4.4 Joint probability distribution reveals vessel diameter and length to be negatively correlated in the barrel cortex of wild-type mice and mice deficient in tPA

To determine if there exists a correlation between vessel diameter and length, a vessel's diameter and it's corresponding length were gathered from the VIDA suite when analyzing vascular morphometry in wild-type, Carmeliet-tPA$^{-/-}$, and Szabo-tPA$^{-/-}$

mice. The numerical diameter-length correlated datasets from all samples (n = 8) per genotype were aggregated and fit to a joint bivariate lognormal probability density function (Figure 4.9). The lognormal fit parameters for diameter and length and the correlation coefficients are given in Table 4.7 and the functional form for the joint bivariate lognormal distribution is given in Table 4.8. From the joint bivariate lognormal distribution for diameter and length we find there to be a weakly negative correlation for vessel diameter and length. We observed this correlation for wild-type (ρ = -0.276), Carmeliet-tPA$^{-/-}$ (ρ = -0.219), and Szabo-tPA$^{-/-}$ (ρ = -0.252) mice. The negative correlation probably results in part from the apparent flow conductance through a blood vessel branch. In the mid-19th century, Jean Poiseuille was the first to model steady-state flow in a cylindrical tube. Poiseuille showed that the flow (Q) is linearly related to the change in pressure (P) across the length (l) of a tube of radius (r) through the conductance (G) by:

$$Q = G\,P; \quad G = \left(\frac{\pi\, r^4}{8\,\mu_a\, l}\right),$$

where μ_a is the apparent viscosity. Thus, our negatively correlated vessel diameter and length data are in agreement with the inverse relationship seen for diameter and length in the expression for flow conductance. It is unclear what the biological significance is of there being a weak negative correlation for vessel diameter and length. To the best of our knowledge, though, we are the first to report on the lognormal distribution being a good model for cortical capillary vessel diameter and length, and on the weakly negative correlation of these two random variables.

4.4.5 Capillary density in the barrel cortex is increased in Carmeliet-tPA$^{-/-}$ mice in relation to wild-type mice

Though the techniques employed by Stefanitsch et al. (2016) did not enable volumetric vascular density to be quantified, the increased number of small-diameter-CD-31-stained vessels and small-diameter-ASMA-stained vessels in Carmeliet-tPA$^{-/-}$ mice suggested that the Carmeliet-tPA$^{-/-}$ mice had a denser vascular bed. Branch number (per mm^3), therefore, was calculated from all samples (n = 8) per genotype (Figure 4.10) from 20x 3D volumetric images. These images (738 µm x 738 µm x 250 µm; Δz = 1 µm) comprise approximately cortical layers 1- 5. Our analysis of vascular density, therefore, is over multiple cortical layers; we have yet to quantify differences in density as a function of cortical depth. From our own preliminary observations, however, and from previous reports (Blinder et al., 2013) there does appear to be a correlation between the cell density of a cortical layer and the corresponding vascular density of that cortical layer. A one-way ANOVA of the average vascular density between genotypes revealed a statistical difference ($F_{(2,21)} = 4.845$, $p = 0.0186$), with a Tukey's post-hoc multiple comparison showing a significant difference in the mean branch density between wild-type and Carmeliet-tPA$^{-/-}$ mice ($p = 0.0140$), but not wild-type and Szabo-tPA$^{-/-}$ mice ($p = 0.2990$) or Carmeliet-tPA$^{-/-}$ and Szabo-tPA$^{-/-}$ mice ($p = 0.2736$). This increase in vascular density is largely a product of an increase in capillary density, as over ~ 98% of the vessels are less than 7 µm *(see PDF in Figure 4.7*). The difference in density is appreciable from 20x 3D volumetric images (738 µm , 738 µm x 250 µm) of the barrel cortex in wild-type, Carmeliet-tPA$^{-/-}$, and Szabo-tPA$^{-/-}$ mice (Figure 4.10).

4.4.6 Carmeliet-tPA$^{-/-}$ mice have a different branching pattern than wild-type mice

An analysis of network connectivity in wild-type, Carmeliet-tPA$^{-/-}$, and Szabo-tPA$^{-/-}$ mice revealed Carmeliet-tPA$^{-/-}$ mice to have a different branching pattern. The vascular network from each of the samples (n = 8) per genotype was analyzed for vessels that branch with a vertex degree 1-5. The network topology graph (Figure 4.11 E) illustrates the relative connectivity relationship between branches and their respective vertex degree in color (1, red; 2, orange; 3, green; 4, blue; 5, purple). Vertex degrees of 1, 2 and 5 are largely an artifact of an edge-effect from the image, as seen in the network graph with red, orange, and purple circles occupying the periphery. The vast majority (~ 95%) of vessels branch with a vertex degree of 3, as indicated by the green solid circles. Approximately ~5% of the vessels branch with a vertex degree of 4, as indicated by the blue solid circles. Representative magnified images of small-diameter sized vessels (Figure 4.11 A) and large-diameter sized vessels (Figure 4.11 B) demonstrate that vertices of degree 3 (open arrows) and 4 (closed arrows) can be observed in both small and large vessels. A one-way ANOVA revealed there to be a significant difference among genotypes for branches with vertices of degree 3 ($F_{(2,21)}$ = 6.374, p = 0.0069) and degree 4 ($F_{(2,21)}$ = 4.297, p = 0.0273). A Tukey's post-hoc multiple comparisons test was performed and significant differences were found between wild-type and Carmeliet-tPA$^{-/-}$ mice for vertex degree 3 (p = 0.0054) and 4 (p = 0.0225) within the same volume of cortical tissue. No significant differences were found between wild-type and Szabo-tPA$^{-/-}$ mice (p = 0.0927) or Carmeliet-tPA$^{-/-}$ and Szabo-tPA$^{-/-}$ (p = 0.3979) mice for vertex degree 3. Similarly, no significant differences were found between wild-type and Szabo-tPA$^{-/-}$ mice (p = 0.1808) or Carmeliet-tPA$^{-/-}$ and

Szabo-tPA$^{-/-}$ ($p = 0.5518$) mice for vertex degree 4. It is unclear how, if at all, this statistical difference in vertex degree is related to biological function.

4.4.7 Carmeliet-tPA$^{-/-}$ mice, but not Szabo-tPA$^{-/-}$ mice, have an elevated basal level of cerebral blood flow in the cortical surface

To determine if these observed changes in vascular density and connectivity might influence cerebral blood flow, laser speckle contrast imaging (LSCI) was used to characterize basal blood flow in wild-type ($n = 10$), Carmeliet-tPA$^{-/-}$ ($n = 9$), and Szabo-tPA$^{-/-}$ ($n = 9$) mice. Four regions of interest (~ 1 mm^2) were selected, whose midline was around bregma -0.5 and -2.0 and whose medial/lateral orientation ranged from ±1.5 to ± 2.5, to measure basal blood flow. These anatomical regions approximately correspond to the regions that were analyzed for vascular morphometry and density.

Representative images of basal cerebral blood flow are shown, with Carmeliet-tPA$^{-/-}$ mice clearly having an elevated signal across the cortical surface (Figure 4.12 A). This difference is appreciable in a histogram plot of the basal speckle signal showing that wild-type and Szabo-tPA$^{-/-}$ mice have a similar laser speckle distribution and that Carmeliet-tPA$^{-/-}$ mice have a rightward shift to higher intensity values (Figure 4.12 B). A one-way ANOVA found a significant difference ($F_{(2,25)} = 18.96$, $p < 0.0001$) with a Tukey's post-hoc multiple comparisons test revealing a statistically significant difference between wild-type and Carmeliet-tPA$^{-/-}$ mice ($p < 0.0001$) and Carmeliet-tPA$^{-/-}$ and Szabo-tPA$^{-/-}$ mice ($p < 0.0001$), but no statistical difference between wild-type and Szabo-tPA$^{-/-}$ mice ($p = 0.9949$) (Figure 4.12 C).

From LSCI it is possible to infer relative spatial and temporal differences in blood flow, but not absolute measurements of blood flow velocity (Briers et al., 2013). As such, we are not able to make definitive statements about whether a difference in the LSCI signal between genotypes is due to a difference in velocity or a difference in density. However, given that we do not observe a difference in capillary vessel diameter and length distributions between genotypes and given that the LSCIs were acquired under comparable physiological conditions, the mean of the velocity distribution is likely to be approximately equal. These data, therefore, indicate that there may be a correlation between an increase in vascular density and the intensity of the laser speckle signal. Indeed, linear regression analysis shows a weak linear relationship (R^2 = 0.7724) between vascular density and the laser speckle signal (Figure 4.12 D).

4.5 Discussion

Of particular interest in the original report by Stefanitsch et al. (2016) that demonstrated Carmeliet-tPA$^{-/-}$ mice to have an altered cerebrovascular architecture was the shift in vessel diameter distributions, with Carmeliet-tPA$^{-/-}$ mice having an increased number of smaller-diameter capillaries and a decreased number of larger, smooth-muscle covered arterioles and arteries compared to wild-type mice. These data suggested that Carmeliet-tPA$^{-/-}$ mice have a denser capillary bed. The implications for this result were two-fold: 1) it demonstrated that Carmeliet-tPA$^{-/-}$ have a possible developmental phenotype and that 2) functions attributed to acute loss of tPA are potentially the result of some developmental artifact. Whether the putative developmental phenotype is due to constitutive loss of tPA or some other modifying

genes is unclear, as another report published soon after showed Carmeliet-tPA$^{-/-}$ mice to have “passenger mutations” from the 129/Sv ES cells used to generate the knockout mice (Szabo et al., 2016).

Given that functions attributed to tPA – including BBB regulation, neurodegeneration, seizure progression, and neurovascular coupling – were derived from studies using the Carmeliet-tPA$^{-/-}$ mice, the observation that Carmeliet-tPA$^{-/-}$ mice have increased capillary number is consequential. This is especially true for the attenuated functional hyperemia response or the decreased stroke volume seen in Carmeliet-tPA$^{-/-}$ mice. It’s plausible, for example, that an elevated baseline level of perfusion from a denser capillary bed reduces the need for the same increase in blood flow to meet the metabolic demands of the tissue during heightened neural activity. Similarly, during stroke, an increased capillary density might help to preserve more tissue in the penumbra, resulting in a small infarct volume. We have since induced stroke in wild-type and Szabo-tPA$^{-/-}$ mice using a photothrombotic middle cerebral artery occlusion model and find that Szabo-tPA$^{-/-}$ mice, like the Carmeliet-tPA$^{-/-}$ mice, have smaller infarct volumes (Su and Lawrence, personal communication) Nonetheless, given the significance of these confounding interpretations for tPA’s role in neurovascular coupling, it was imperative that the results from Stefanitsch et al. (2015) be confirmed.

Accordingly, the data presented in this study both confirm and contradict the findings that Stefanitsch et al. (2015) originally published. Consistent with what was previously suggested by the Stefanitsch data, we find that the vascular capillary density in the barrel cortex of Carmeliet-tPA$^{-/-}$ mice is significantly increased compared to wild-

type and Szabo-tPA$^{-/-}$ mice. Moreover, while the Szabo-tPA$^{-/-}$ mice had a trend toward elevated capillary density, it was not statistically different than wild-type or Carmeliet-tPA$^{-/-}$ mice. We also find that there is a trend for Carmeliet-tPA$^{-/-}$ mice to have shorter capillary vessel lengths, which is in agreement with vessels branching more frequently, resulting in an increased density. And, that Carmeliet-tPA$^{-/-}$ mice have significantly fewer vessels that branch with vertex degree 3 (~1% decrease), but significantly more vessels that branch with vertex degree 4 (~1% increase); though it is unclear if this difference in vertex degree is biologically significant. Nonetheless, we find that the increase in capillary density appears to correlate to some degree with an elevation in basal cerebral blood flow. These data give weight to the possibility that the brains of Carmeliet-tPA$^{-/-}$ mice are more highly perfused and might not have the same metabolic demands with heightened neuronal activity.

In contrast to the differences in vessel diameter distributions reported by Stefanitsch et al. (2015), however, we did not find any difference in the mean or mode of the lognormal fits to the diameter distribution data between wild-type, Carmeliet-tPA$^{-/-}$, and Szabo-tPA$^{-/-}$ mice. This difference between studies is likely due to an error in sampling. We analyzed ~20x more vessels. The CD-31-stained vessel diameter statistics gathered by Stefanitsch et al. (2015) were from five wild-type and five Carmeliet-tPA$^{-/-}$ mice and combined for a total of 1342 and 1518 vessels, respectively; on the other hand, we analyzed a total of 22,326 and 28,024 vessels from four wild-type and four Carmeliet-tPA$^{-/-}$ mice, respectively (25,222 vessels were analyzed from the Szabo-tPA$^{-/-}$ mice). It is not possible for us to comment on the different diameter distributions between wild-type and Carmeliet-tPA$^{-/-}$ mice that were reported for larger-

smooth muscle covered vessels. Our method did not distinguish between arterioles and arteries and venuoles and veins. Therefore, a more exhaustive analysis that examines the distribution of smooth-muscle covered vessels is still needed. Cumulatively, though, these data suggest that there might be an interaction between constitutive loss of tPA and some strain-modifying gene leading to differences in vascular density.

Strain-dependent differences in vascularization have been reported (Chan et al., 2004; Chalothorn et al., 2007; Ward et al., 2007; Kang et al., 2015). Interestingly, in one study, it was reported that in a sub-strain of 129 inbred mice (129S3/SvIM) there was an increase in vessel surface area and density compared to C57BL/6J mice. Though there is wide genetic variation within the 129 “family” (Simpson et al., 1997) and a direct correlation can’t be drawn between the enhanced vascularization reported in the corneal limbus of 129S3/SvIM mice and the increased vascular density in the Carmeliet-tPA$^{-/-}$ mice (which have remnant 129/Sv DNA), this study, in addition to others, demonstrates that there are significant differences in vascularization between mouse strains that might complicate interpretation of some measured variables. Moreover, in one of the studies looking at angiogenesis in the cortex across strains under normoxia and hypoxia conditions, different mouse strains – CD1, 129/Sv, C57BL/6, and Balb/c – had differing levels of increased vascularization in response to hypoxia (Ward et al., 2007). Unlike CD1, 129/Sv, and C57BL/6 mouse strains, the Balb/c mice did not show a significant difference in vessel area between normoxic and hypoxic conditions. The Balb/c mice, however, appeared to have an increased baseline level of vascularization compared to the other strains. It’s possible, therefore, that similar to our speculation about the attenuated functional hyperemia response reported in the Carmeliet-tPA$^{-/-}$

mice, when there is already an elevated level of basal perfusion from an increase in vessel density there is less metabolic demand for an increase in blood flow.

If not some strain-modifying genes from the 129/Sv remnant DNA, then how might constitutive loss of tPA increase vascular density? Superficially, there is more evidence to suggest that the absence of tPA would result in hypovascularization rather than hypervascularization. Pro-hepatocyte growth factor (pro-HGF) has been shown to be cleaved by tPA into its mitogenic active two-chain form (Mars et al., 1993). HGF, though originally described in hepatocytes, is highly expressed in the brain (Jung et al., 1994) and acts as a pleiotropic mediator of cell proliferation and differentiation, neuronal outgrowth and chemoattraction, and survival (Maina and Klein, 1999). HGF is also an pro-angiogenic factor, and in brain tumors high expression of HGF or its receptor c-met strongly correlate with tumor growth and angiogenesis, while inhibition of HGF or c-met decrease tumor growth and angiogenesis. In keeping with tPA being associated with angiogenesis, activation of the sonic hedgehog (Shh) signaling pathway was shown to upregulate tPA and induce capillary-like tube formation in primary mouse brain endothelial cells (MBEC) (Teng et al., 2012). In addition, the pro-angiogenic factors VEGF (vascular endothelial growth factor) and Ang1 (angiopoietin 1) were found to be significantly downregulated in MBECs cultured from tPA deficient mice and MBECs lacking tPA had impaired tube formation. Therefore, these data suggest that loss of tPA would decrease pro-growth signaling cascades that support vessel sprouting, which in turn, would seem to suggest a hypovascularization phenotype *in vivo*.

Similarly, tPA has also been shown to increase Wnt-LRP5/6-GSK3β-β-catenin signaling via tPA-induced release of Wnt7a from the extracellular matrix of cultured

neural progenitor cells and direct tPA binding to LRP5/6 (Lee et al., 2014). Activation of the β-catenin signaling pathway has been shown to be critical for vasculogenesis and BBB differentiation in the CNS (Quaegebeur et al., 2011). Thus, if Carmeliet-tPA$^{-/-}$ mice were found to have a reduced vascular density, altered β-catenin signaling would be a likely avenue to explore as a possible molecular mechanism. However, as Carmeliet-tPA$^{-/-}$ mice have a denser vasculature, it seems unlikely that activation of the Wnt-LRP5/6-GSK3β-β-catenin is responsible. Indeed, beyond the report published by Stefanitsch et al. (2015) and our own results, we are not able to find any study linking loss of tPA and angiogenesis or vasculogenesis. It is also unclear if the observed difference in vascular density in the Carmeliet-tPA$^{-/-}$ mice is due to differences in chronic or acute loss of tPA and/or changes in angiogenesis or vasculogenesis. As such, future experiments should control for these variables and examine the temporal development of blood vessels.

It also became apparent to us that a rigorous analysis of cerebrovascular architecture would have implications beyond answering a very specific question about the Carmeliet-tPA$^{-/-}$ transgenic mice. For, altered vascular morphology and 3D architecture have been reported in mouse models of Alzheimer's disease (Meyer et al., 2008; Bennett et al., 2018) and it has been shown that cerebral hypoperfusion precedes cognitive decline (Ruitenberg et al., 2005); though it is still not clear how an altered vascular network affects blood flow regulation. A modeling approach that incorporates vascular morphometry and connectivity statistics to calculate blood flow, therefore, would be beneficial in both the basic science and clinical setting. To this end, we have gathered statistics on correlated vessel diameter and length, vascular density, and

branching vertex degree. Moreover, we have established that the lognormal distribution is a good model for cerebral vessel diameter and length, and that there is a weak negative correlation between vessel diameter and length. These characteristics are critical for establishing a vascular network and they lay the groundwork for a statistical modeling approach to calculate blood flow, given a model for the flow resistance of each branch.

Acknowledgements

We would like to thank and acknowledge the assistance provided by Dr. Philbert Tsai of Dr. David Kleinfeld's lab at the University of California, San Diego in running the VIDA suite Matlab program to gather diameter-length measurements from 3D images of the cerebrovasculature; Dr. Randy Stevenson for his expertise in applied physics and mathematical modeling, and for his work in writing the Mathematica programs to analyze the vascular network statistics; Dr. Enming Su for his technical assistance in gathering blood flow measurements; Dr. Linda Fredriksson for sharing the raw vessel diameter data from wild-type and Carmeliet-tPA$^{-/-}$ mice, and Dr. Geoffrey Murphy for sharing his workstation for computational analysis.

References

Bennett RE, Robbins AB, Hu M, Cao X, Betensky RA, Clark T, Das S, Hyman BT (2018) Tau induces blood vessel abnormalities and angiogenesis-related gene expression in P301L transgenic mice and human Alzheimer's disease. Proc Natl Acad Sci U S A 115:E1289-E1298.

Blinder P, Tsai PS, Kaufhold JP, Knutsen PM, Suhl H, Kleinfeld D (2013) The cortical angiome: an interconnected vascular network with noncolumnar patterns of blood flow. Nat Neurosci 16:889-897.

Briers D, Duncan DD, Hirst E, Kirkpatrick SJ, Larsson M, Steenbergen W, Stromberg T, Thompson OB (2013) Laser speckle contrast imaging: theoretical and practical limitations. J Biomed Opt 18:066018.

Carmeliet P, Kieckens L, Schoonjans L, Ream B, van Nuffelen A, Prendergast G, Cole M, Bronson R, Collen D, Mulligan RC (1993) Plasminogen activator inhibitor-1 gene-deficient mice. I. Generation by homologous recombination and characterization. J Clin Invest 92:2746-2755.

Carmeliet P, Schoonjans L, Kieckens L, Ream B, Degen J, Bronson R, De Vos R, van den Oord JJ, Collen D, Mulligan RC (1994) Physiological consequences of loss of plasminogen activator gene function in mice. Nature 368:419-424.

Chalothorn D, Clayton JA, Zhang H, Pomp D, Faber JE (2007) Collateral density, remodeling, and VEGF-A expression differ widely between mouse strains. Physiol Genomics 30:179-191.

Chan CK, Pham LN, Chinn C, Spee C, Ryan SJ, Akhurst RJ, Hinton DR (2004) Mouse strain-dependent heterogeneity of resting limbal vasculature. Invest Ophthalmol Vis Sci 45:441-447.

Fredriksson L, Lawrence DA, Medcalf RL (2017) tPA Modulation of the Blood-Brain Barrier: A Unifying Explanation for the Pleiotropic Effects of tPA in the CNS. Semin Thromb Hemost 43:154-168.

Fredriksson L, Stevenson TK, Su EJ, Ragsdale M, Moore S, Craciun S, Schielke GP, Murphy GG, Lawrence DA (2015) Identification of a neurovascular signaling pathway regulating seizures in mice. Ann Clin Transl Neurol 2:722-738.

Frey U, Muller M, Kuhl D (1996) A different form of long-lasting potentiation revealed in tissue plasminogen activator mutant mice. J Neurosci 16:2057-2063.

Huang YY, Bach ME, Lipp HP, Zhuo M, Wolfer DP, Hawkins RD, Schoonjans L, Kandel ER, Godfraind JM, Mulligan R, Collen D, Carmeliet P (1996) Mice lacking the gene encoding tissue-type plasminogen activator show a selective interference

with late-phase long-term potentiation in both Schaffer collateral and mossy fiber pathways. Proc Natl Acad Sci U S A 93:8699-8704.

Jung W, Castren E, Odenthal M, Vande Woude GF, Ishii T, Dienes HP, Lindholm D, Schirmacher P (1994) Expression and functional interaction of hepatocyte growth factor-scatter factor and its receptor c-met in mammalian brain. J Cell Biol 126:485-494.

Kang HM, Sohn I, Kim S, Kim D, Jung J, Jeong JW, Park C (2015) Optical measurement of mouse strain differences in cerebral blood flow using indocyanine green. J Cereb Blood Flow Metab 35:912-916.

Ke MT, Imai T (2014) Optical clearing of fixed brain samples using SeeDB. Curr Protoc Neurosci 66:Unit 2 22.

Ke MT, Fujimoto S, Imai T (2013) SeeDB: a simple and morphology-preserving optical clearing agent for neuronal circuit reconstruction. Nat Neurosci 16:1154-1161.

Lee SH, Ko HM, Kwon KJ, Lee J, Han SH, Han DW, Cheong JH, Ryu JH, Shin CY (2014) tPA regulates neurite outgrowth by phosphorylation of LRP5/6 in neural progenitor cells. Mol Neurobiol 49:199-215.

Louessard M, Lacroix A, Martineau M, Mondielli G, Montagne A, Lesept F, Lambolez B, Cauli B, Mothet JP, Vivien D, Maubert E (2016) Tissue Plasminogen Activator Expression Is Restricted to Subsets of Excitatory Pyramidal Glutamatergic Neurons. Mol Neurobiol 53:5000-5012.

Maina F, Klein R (1999) Hepatocyte growth factor, a versatile signal for developing neurons. Nat Neurosci 2:213-217.

Mars WM, Zarnegar R, Michalopoulos GK (1993) Activation of hepatocyte growth factor by the plasminogen activators uPA and tPA. Am J Pathol 143:949-958.

Meyer EP, Ulmann-Schuler A, Staufenbiel M, Krucker T (2008) Altered morphology and 3D architecture of brain vasculature in a mouse model for Alzheimer's disease. Proc Natl Acad Sci U S A 105:3587-3592.

Park L, Gallo EF, Anrather J, Wang G, Norris EH, Paul J, Strickland S, Iadecola C (2008) Key role of tissue plasminogen activator in neurovascular coupling. Proc Natl Acad Sci U S A 105:1073-1078.

Quaegebeur A, Lange C, Carmeliet P (2011) The neurovascular link in health and disease: molecular mechanisms and therapeutic implications. Neuron 71:406-424.

Rogove AD, Tsirka SE (1998) Neurotoxic responses by microglia elicited by excitotoxic injury in the mouse hippocampus. Curr Biol 8:19-25.

Ruitenberg A, den Heijer T, Bakker SL, van Swieten JC, Koudstaal PJ, Hofman A, Breteler MM (2005) Cerebral hypoperfusion and clinical onset of dementia: the Rotterdam Study. Ann Neurol 57:789-794.

Salles FJ, Strickland S (2002) Localization and regulation of the tissue plasminogen activator-plasmin system in the hippocampus. J Neurosci 22:2125-2134.

Sappino AP, Madani R, Huarte J, Belin D, Kiss JZ, Wohlwend A, Vassalli JD (1993) Extracellular proteolysis in the adult murine brain. J Clin Invest 92:679-685.

Simpson EM, Linder CC, Sargent EE, Davisson MT, Mobraaten LE, Sharp JJ (1997) Genetic variation among 129 substrains and its importance for targeted mutagenesis in mice. Nat Genet 16:19-27.

Stefanitsch C, Lawrence AL, Olverling A, Nilsson I, Fredriksson L (2015) tPA Deficiency in Mice Leads to Rearrangement in the Cerebrovascular Tree and Cerebroventricular Malformations. Frontiers in cellular neuroscience 9:456.

Su EJ, Fredriksson L, Geyer M, Folestad E, Cale J, Andrae J, Gao Y, Pietras K, Mann K, Yepes M, Strickland DK, Betsholtz C, Eriksson U, Lawrence DA (2008) Activation of PDGF-CC by tissue plasminogen activator impairs blood-brain barrier integrity during ischemic stroke. Nat Med 14:731-737.

Su EJ, Cao C, Fredriksson L, Nilsson I, Stefanitsch C, Stevenson TK, Zhao J, Ragsdale M, Sun YY, Yepes M, Kuan CY, Eriksson U, Strickland DK, Lawrence DA, Zhang L (2017) Microglial-mediated PDGF-CC activation increases cerebrovascular permeability during ischemic stroke. Acta Neuropathol 134:585-604.

Su EJ, Fredriksson L, Kanzawa M, Moore S, Folestad E, Stevenson TK, Nilsson I, Sashindranath M, Schielke GP, Warnock M, Ragsdale M, Mann K, Lawrence AL, Medcalf RL, Eriksson U, Murphy GG, Lawrence DA (2015) Imatinib treatment reduces brain injury in a murine model of traumatic brain injury. Frontiers in cellular neuroscience 9:385.

Szabo R, Samson AL, Lawrence DA, Medcalf RL, Bugge TH (2016) Passenger mutations and aberrant gene expression in congenic tissue plasminogen activator-deficient mouse strains. J Thromb Haemost 14:1618-1628.

Teng H, Chopp M, Hozeska-Solgot A, Shen L, Lu M, Tang C, Zhang ZG (2012) Tissue plasminogen activator and plasminogen activator inhibitor 1 contribute to sonic hedgehog-induced in vitro cerebral angiogenesis. PLoS One 7:e33444.

Tsai PS, Kaufhold JP, Blinder P, Friedman B, Drew PJ, Karten HJ, Lyden PD, Kleinfeld D (2009) Correlations of neuronal and microvascular densities in murine cortex revealed by direct counting and colocalization of nuclei and vessels. J Neurosci 29:14553-14570.

Tsirka SE, Rogove AD, Strickland S (1996) Neuronal cell death and tPA. Nature 384:123-124.

Tsirka SE, Gualandris A, Amaral DG, Strickland S (1995) Excitotoxin-induced neuronal degeneration and seizure are mediated by tissue plasminogen activator. Nature 377:340-344.

Tsirka SE, Rogove AD, Bugge TH, Degen JL, Strickland S (1997) An extracellular proteolytic cascade promotes neuronal degeneration in the mouse hippocampus. J Neurosci 17:543-552.

Wang YF, Tsirka SE, Strickland S, Stieg PE, Soriano SG, Lipton SA (1998) Tissue plasminogen activator (tPA) increases neuronal damage after focal cerebral ischemia in wild-type and tPA-deficient mice. Nat Med 4:228-231.

Ward NL, Moore E, Noon K, Spassil N, Keenan E, Ivanco TL, LaManna JC (2007) Cerebral angiogenic factors, angiogenesis, and physiological response to chronic hypoxia differ among four commonly used mouse strains. J Appl Physiol (1985) 102:1927-1935.

Yepes M, Sandkvist M, Moore EG, Bugge TH, Strickland DK, Lawrence DA (2003) Tissue-type plasminogen activator induces opening of the blood-brain barrier via the LDL receptor-related protein. J Clin Invest 112:1533-1540.

Yepes M, Sandkvist M, Coleman TA, Moore E, Wu JY, Mitola D, Bugge TH, Lawrence DA (2002) Regulation of seizure spreading by neuroserpin and tissue-type plasminogen activator is plasminogen-independent. J Clin Invest 109:1571-1578.

Yu H, Schleuning WD, Michl M, Liberatore G, Tan SS, Medcalf RL (2001) Control elements between -9.5 and -3.0 kb in the human tissue-type plasminogen activator gene promoter direct spatial and inducible expression to the murine brain. Eur J Neurosci 14:799-808.

Figure 4.1

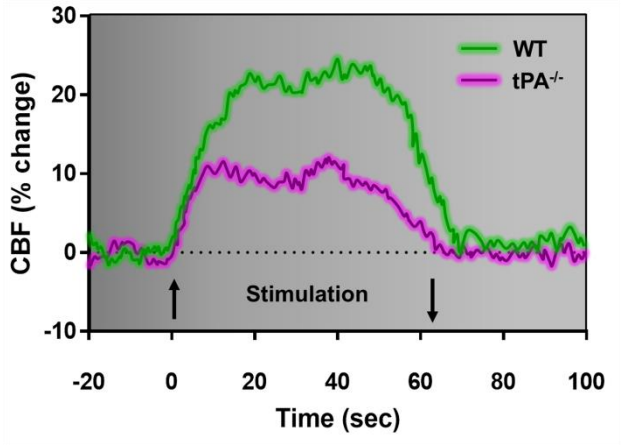
30
20
10
0
-10
CBF (% change)
WT
tPA-/-
Stimulation
-20
0
20
40
60
80
100
Time (sec)

Figure 4.1. Illustrative rendering of cerebral blood flow response in barrel cortex following whisker stimulation in wild-type and Carmeliet-tPA$^{-/-}$ mice from Park et al. (2008). Mice deficient in tPA (purple) have diminished functional hyperemia compared to wild-type mice (green) following activation of the barrel cortex from whisker stimulation. This attenuation appeared to be specific to the hemodynamic response that accompanies increased neural activity, as the cerebrovascular in Carmeliet-tPA$^{-/-}$ mice responded normally to stimuli that increase blood flow via smooth muscle relaxation and endothelial cell vasodilation. Figure recreated and modified from Park et al. (2008).

Figure 4.2

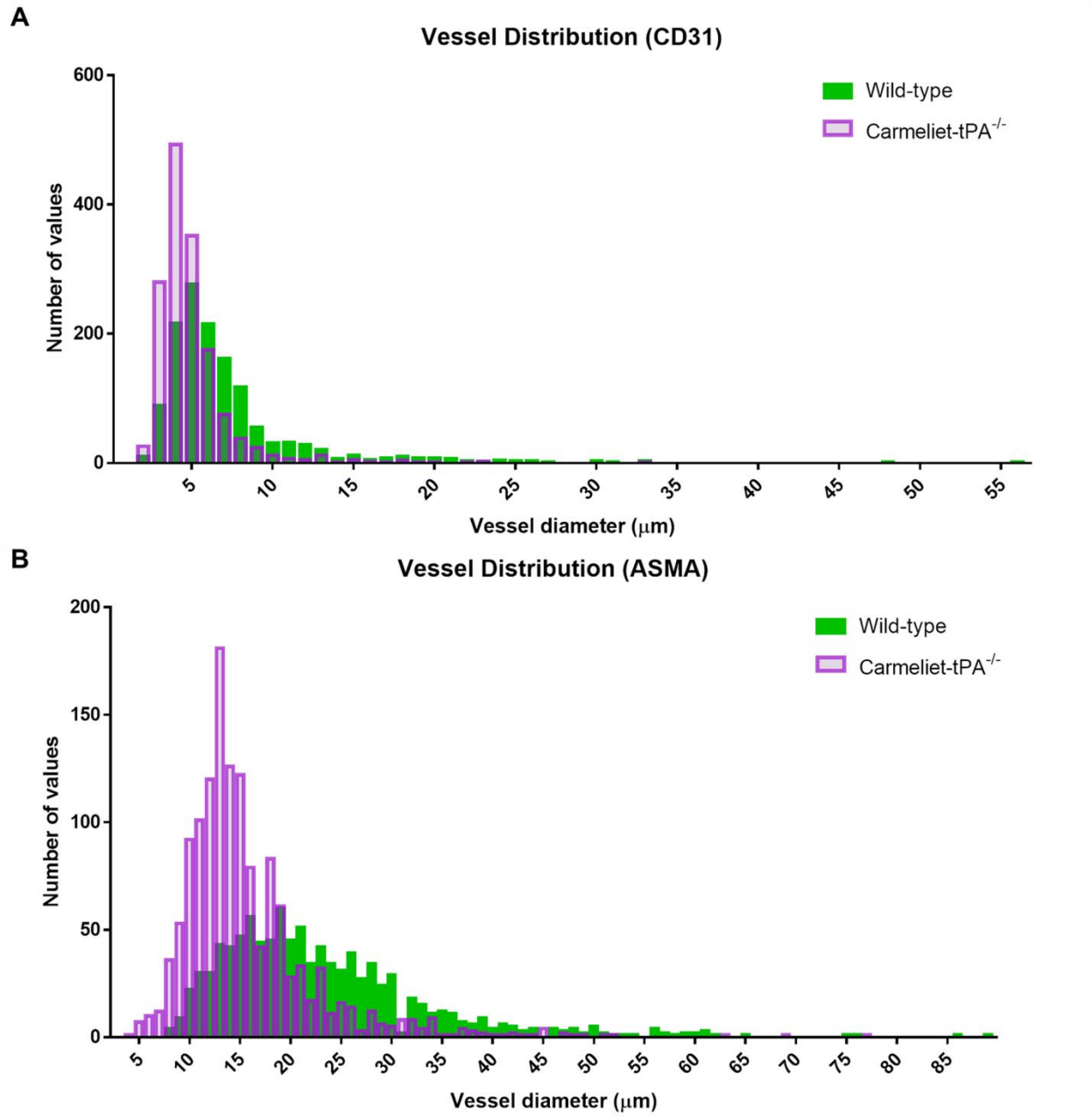
A
Vessel Distribution (CD31)
Wild-type
Carmeliet-tPA-/-
Number of values
600
400
200
0
5
10
15
20
25
30
35
40
45
50
55
Vessel diameter (μm)
B
Vessel Distribution (ASMA)
Wild-type
Carmeliet-tPA-/-
Number of values
200
150
100
50
0
5
10
15
20
25
30
35
40
45
50
55
60
65
70
75
80
85
Vessel diameter (μm)

Figure 4.2. Cerebral blood vessel diameter distributions from wild-type and Carmeliet-tPA$^{-/-}$ mice. Immunofluorescence analysis of blood vessels diameters from wild-type (n = 5) and Carmeliet-tPA$^{-/-}$ (n = 5) mice acquired by confocal microscopy using the endothelial cell marker CD-31 and the smooth muscle marker α-smooth muscle actin (ASMA). CD-31 detects all blood vessels, while ASMA detects arterioles and arteries. **(A)** Histogram plot of CD-31 stained vessel diameters shows Carmeliet-tPA$^{-/-}$ mice to have a left skew, which is indicative of having an increased number of small diameter capillaries and a decreased number of larger diameter blood vessels. **(B)** This trend is also appreciable when arterioles and arteries were specifically analyzed using the ASMA stain; a greater number of small diameter arterioles and a fewer number of large diameter arterioles are detected in the Carmeliet-tPA$^{-/-}$ mice compared to wild-type mice. Data was collected from stainings repeated four independent times of 50 µm free-float coronal sections from the cortex and hippocampus at bregma -1.5. Raw data from Stefanitsch et al. (2015) was re-graphed using GraphPad Prism 7.0.

Figure 4.3

Table 4.1 Lognormal fit parameters for CD-31 vessel diameter distribution data

Genotype	μ	σ	Mode (μm)	Mean (μm)	SD (μm)
Wild-type	1.795	0.363	5.041	6.140	2.301
Carmeliet-tPA$^{-/-}$	1.487	0.296	4.054	4.623	1.400

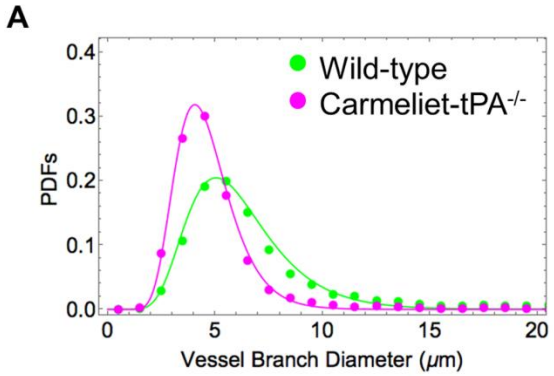

Table 4.2 Lognormal fit parameters for ASMA vessel diameter distribution data

Genotype	μ	σ	Mode (μm)	Mean (μm)	SD (μm)
Wild-type	2.993	0.365	17.454	21.325	8.061
Carmeliet-tPA$^{-/-}$	2.625	0.273	12.814	14.334	3.992

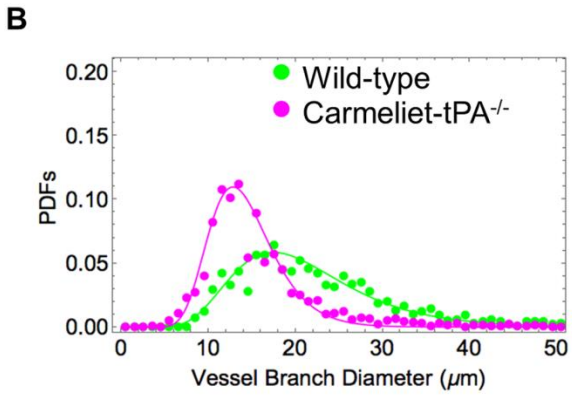

Table 4.3 Estimates for mean, mode, and standard deviation from lognormal fitting parameters (μ, σ)

Mean	Mode	Standard devidation
$e^{\left(\mu+\frac{\sigma^2}{2}\right)}$	$e^{(\mu-\sigma^2)}$	$\sqrt{\left[e^{\sigma^2}-1\right]e^{(2\mu+\sigma^2)}}$

Figure 4.3. Cerebral blood vessel CD31 and ASMA diameter distributions from wild-type and Carmeliet-tPA$^{-/-}$ mice are lognormally distributed. A lognormal distribution was fit to both the CD-31 **(A)** and ASMA **(B)** numerical diameter distributions for wild-type and Carmeliet-tPA$^{-/-}$ mice. The lognormal fit parameters and the mean, mode, and standard deviation of the fitted lognormal distribution is given, respectively, for the CD-31 and ASMA diameter distributions in **Table 4.1** and **Table 4.2**. The estimates for the mean, mode, and standard deviation were calculated from the formulas given in **Table 4.3**. Both the mean and mode for Carmeliet-tPA$^{-/-}$ mice are smaller than wild-type mice in the CD-31 dataset and the ASAM dataset. Data is plotted as the vessel branch diameter as a function of the probability density function (PDF). Raw data from Stefanitsch et al. (2015) was re-graphed and fit to a lognormal function using Mathematica.

Figure 4.4

Table 4.4 Comparison of the goodness-of-fit for three skewed statistical models

Distribution	R^2	Fitting Parameters	Functional Form
Normal	0.9358	μ = 4.06, σ = 1.94	$p_N(x;\mu,\sigma) = \frac{e^{-\frac{(x-\mu)^2}{2\sigma^2}}}{\sqrt{2\pi}\,\sigma}, -\infty < x < +\infty$
Weibull	0.9524	α = 2.36, β = 4.88	$p_W(x;\alpha,\beta) = \frac{\beta}{\alpha}\left(\frac{x}{\alpha}\right)^{\beta-1} e^{-(x/\alpha)^{\beta}}, x \geq 0$
Lognormal	0.9876	μ = 1.47, σ = 0.50	$p_{LN}(x;\mu,\sigma) = \frac{e^{-\frac{(ln(x)-\mu)^2}{2\sigma^2}}}{\sqrt{2\pi}\,x\,\sigma}, x > 0$

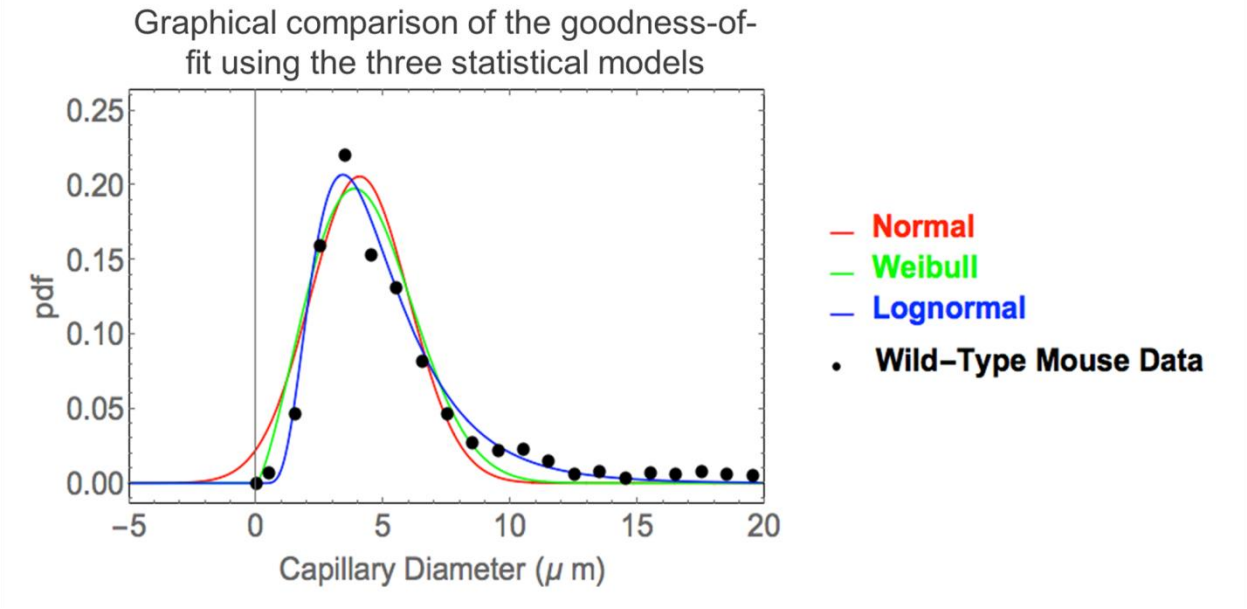

Figure 4.4. Vessel diameter data is lognormally distributed. A comparison of three different probability distribution functions revealed the best model for the vessel diameter data to be the lognormal distribution. Compared to the normal and Weibull probability distribution functions, the lognormal distribution function had the best fit to the numerical vessel diameter distribution, as indicated by the R^2 values given in **Table 4.4**. A representative numerical distribution from a wild-type mouse is shown, as are the representative fits for each of the respective distribution models. The functional forms of the distribution models are also provided in **Table 4.4**.

Figure 4.5

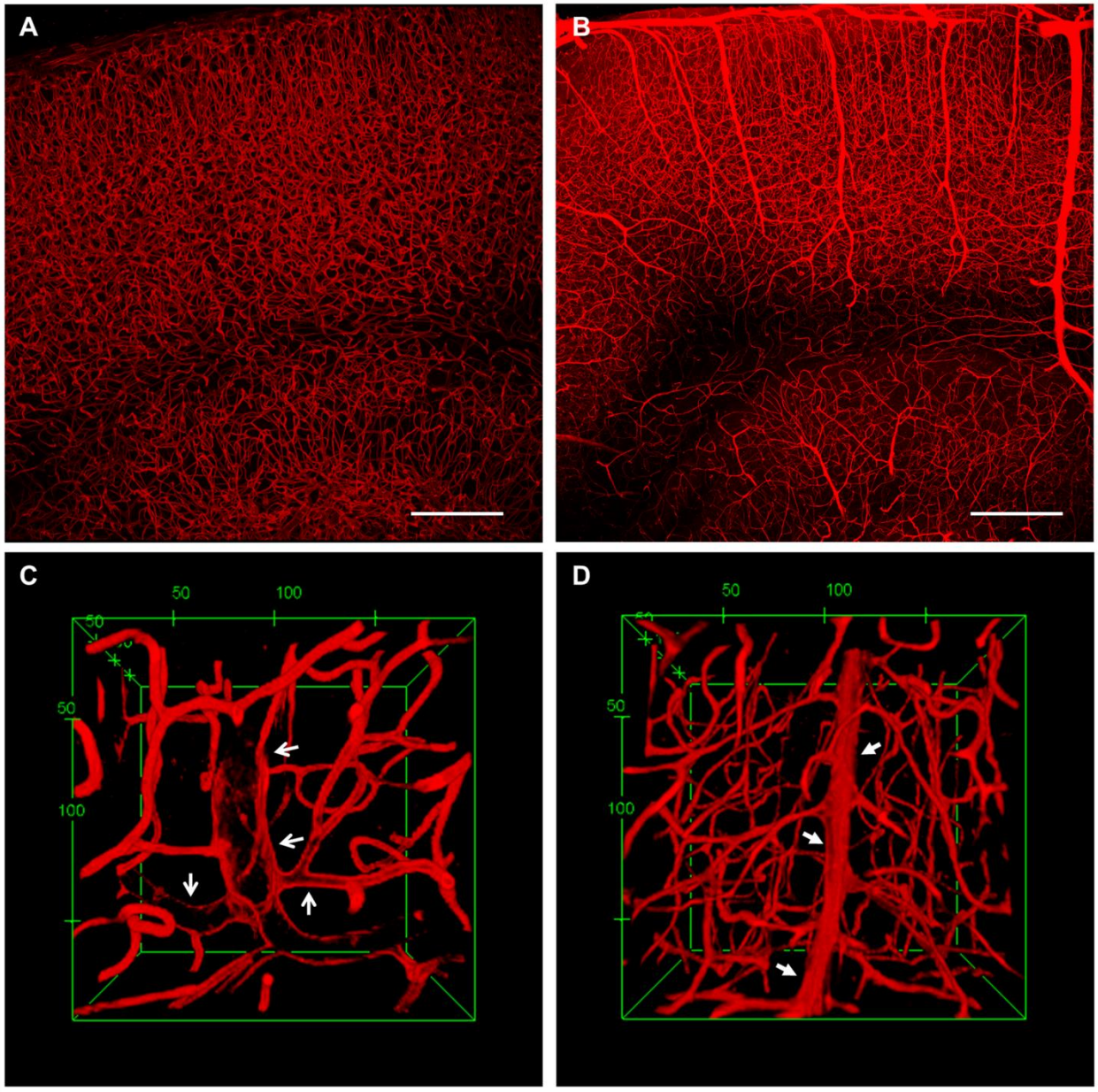

Figure 4.5. Enhanced vascular visualization with SeeDeepBrain clearing and tomato-lectin/gelatin-fluorophore cast. (A and B) Representative 10x images (1476 µm x 1476 µm x 100 µm; Δz = 1 µm) from coronal sections (bregma -2.0) of wild-type mice demonstrating the enhanced vascular visualization of larger vessels with a double-labeling approach. Coronal sections (1 mm slabs) were cleared using SeeDeepBrain (SeeDB). SeeDB is a water-based optical clearing approach that reduces light scatter by incrementally changing the aqueous solution of the tissue to a saturated fructose solution. **(A and C)** Labeling alone with a tomato-lectin conjugated fluorophore does not sufficiently detect large vessels. Open arrows indicate unfilled vessels. Tomato-lectin (from *Lycopersicon esculentum*) is a glycoprotein that intercalates into the endothelial glycocalyx. **(B and D)** A double labeling approach using a tomato-lectin-conjugated fluorophore and a gelatin-fluorophore cast was taken to visualize both large and small vessels. Closed arrows indicate filled vessels. 10x image in panel B has been psuedocolored red. Following tail-vein injection of either DyLight 594-labeled tomato-lectin or DyLight 488-labeled tomato-lectin, mice were cardiac perfused with a 2% gelatin solution containing 0.1% Rhodamine B Isothiocyanate-Dextran or 0.1% Fluorescein-isothiocyanate Albumin, respectively (See detailed protocol described in *Materials and Methods*). Scale bars: A and B, 250 µm; C and D, image scale in µm.

Figure 4.6

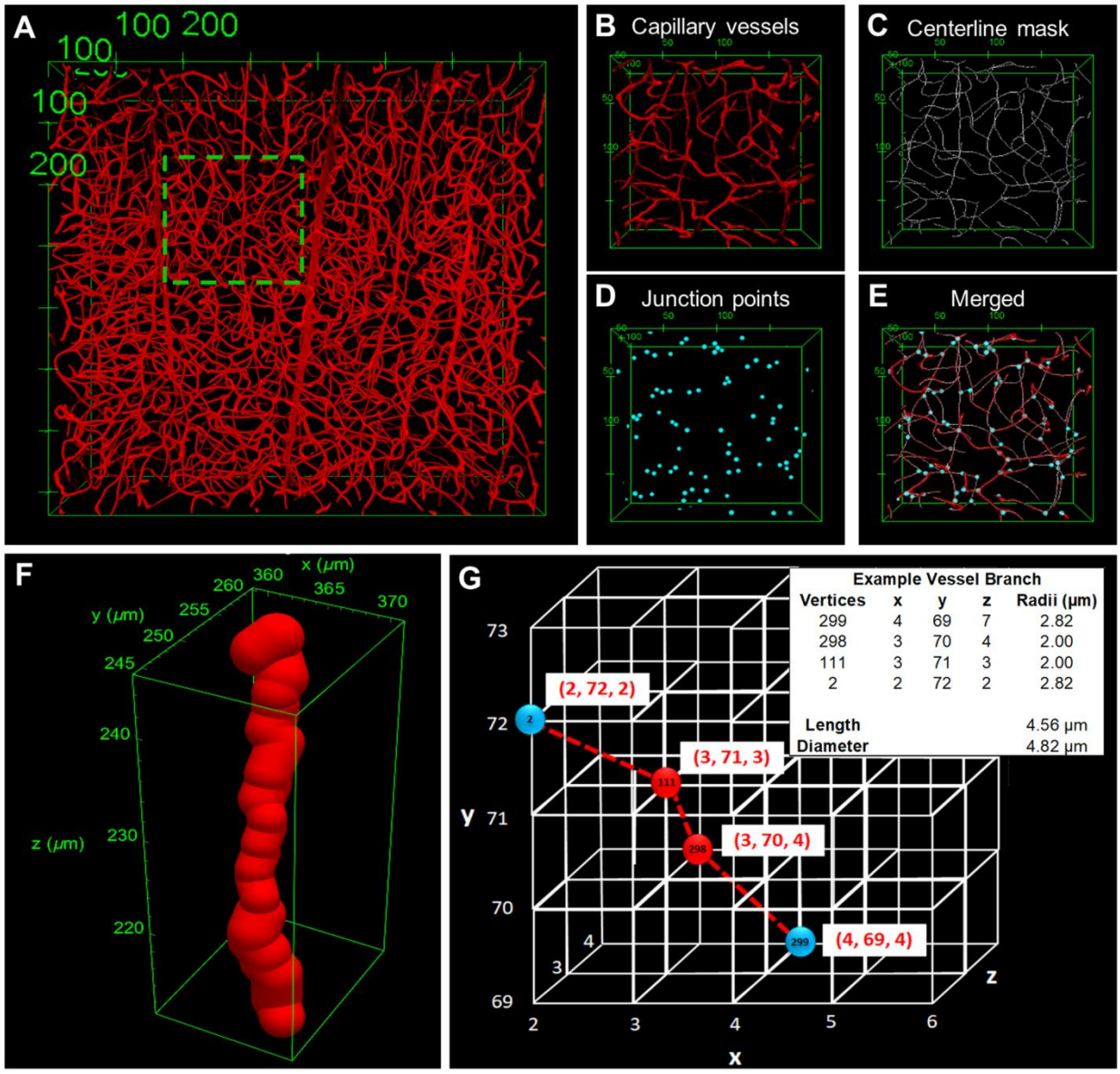
A
100 200
100
100
200
B Capillary vessels
C Centerline mask
D Junction points
E Merged
F
x (μm)
360
260
365
370
y (μm)
255
250
245
240
z (μm)
230
220
G
Example Vessel Branch
Vertices x y z Radii (μm)
299 4 69 7 2.82
298 3 70 4 2.00
111 3 71 3 2.00
2 2 72 2 2.82
Length 4.56 μm
Diameter 4.82 μm
(2, 72, 2)
(3, 71, 3)
(3, 70, 4)
(4, 69, 4)
73
72
y 71
70
69
2
3
4
5
6
x
z

Figure 4.6. Acquiring blood vessel statistics using the Matlab-based software suite, Volumetric Image Data Analysis (VIDA), and a custom written Mathematica program. (A) Representative 3D volumetric 20x image (738 µm x 738 µm x 250 µm; Δz = 1 µm) from the barrel cortex of a wild-type mouse, yielding a tissue volume of approximately 0.14 mm^3. Two 20x images were acquired per mouse (n = 4). **(B – G)** VIDA suite and a custom written Mathematica program were used to gather correlated diameter-length statistics from the 3D tissue sections. VIDA was written and developed by the Kleinfeld Lab and a full description of the Matlab-based VIDA software suit is given in Tsai et al. (2009) and the Mathematica program was written by Dr. Randy C. Stevenson (University of Michigan consultant). **(B)** Representative magnified volume of capillary vessels. **(C)** Centerline mask comprising vertices over the entire 3D vascular network. Each vertex is associated with an XYZ coordinate and a radius is extrapolated at that XYZ coordinate (see panel G). **(D)** Junction points (cyan balls) demarcating the branching points of vessels. **(E)** Merged volumetric image demonstrating centerline mask and junction points overlaying vascular network. **(F)** Representative vessel branch made up of 30 segments. A segment connects two contiguous vertices within a vessel branch. A vessel branch is defined as the set of vertices between two junction points. **(G)** Schematic illustration showing a representative vessel branch comprised of four vertices (2, 111, 298 and 299) and three segments between two junction points (cyan balls). The median of the individual radii for all the vertices in a vessel branch was chosen to represent the radius of the entire vessel branch. The length between vertices was calculated and summed for all the segments in a vessel branch to determine the total length of a vessel branch. Image scale in µm.

Figure 4.7

Table 4.5 Lognormal fit parameters for vessel diameter distribution data

Genotype	μ	σ	Mode (μm)	Mean (μm)	SD (μm)
Wild-type	1.458	0.214	4.103	4.395	0.951
Carmeliet-tPA$^{-/-}$	1.428	0.237	3.942	4.228	1.030
Szabo-tPA$^{-/-}$	1.448	0.231	4.033	4.367	1.021

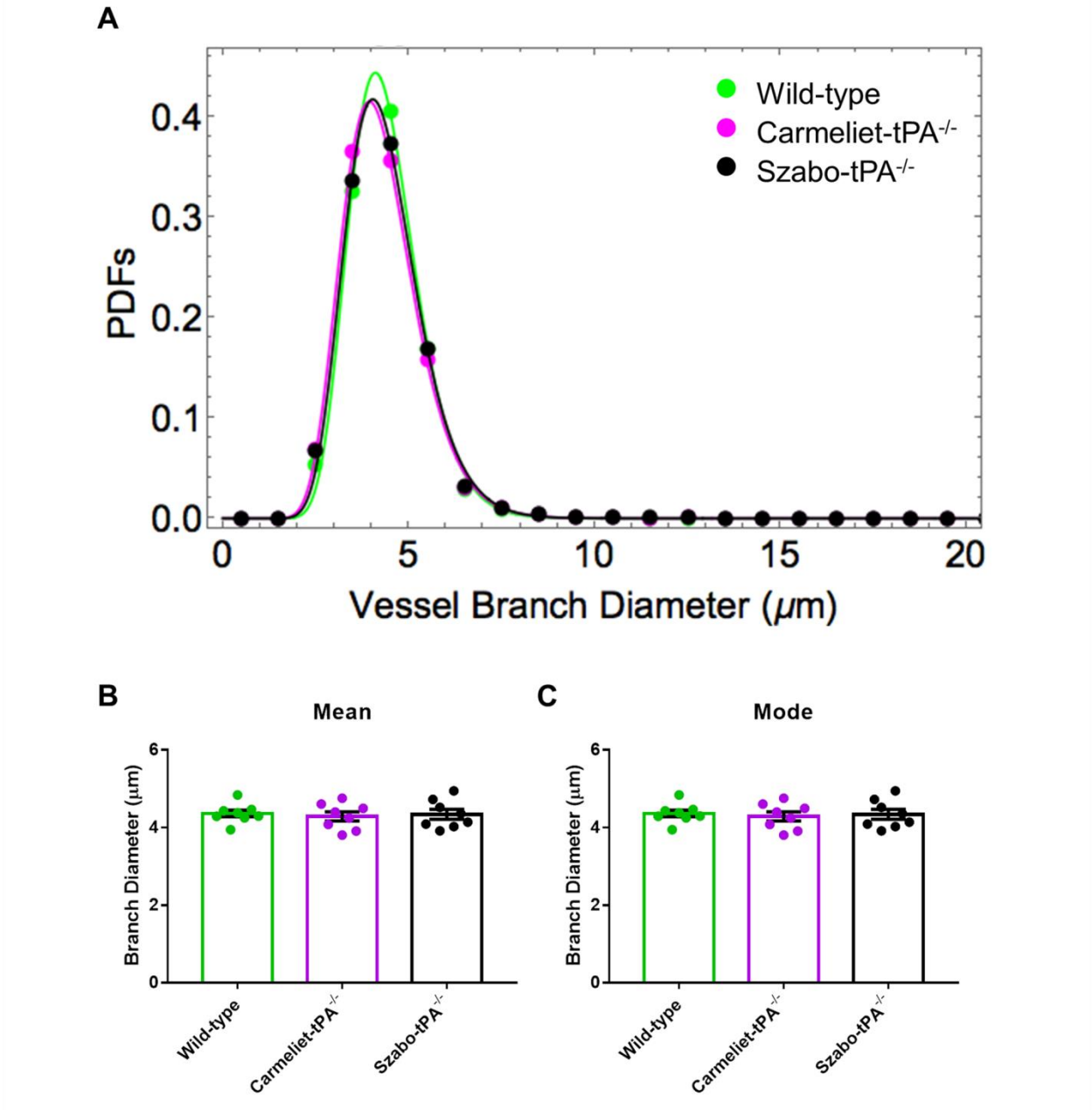

Figure 4.7. Vessel diameter distributions do not vary between wild-type mice and mice deficient in tPA. (A) Vessel branch diameter (μm) datasets from all samples (n = 8) per genotype were aggregated and plotted. Solid circles represent the numerical diameter data and the solid lines represent the lognormal fit to the diameter data. Lognormal fit parameters for the vessel diameter distribution are given in the corresponding **Table 4.5**. The mean **(B)** and mode **(C)** from the lognormal fit data for each of the samples (n = 8) was compiled per genotype and a one-way ANOVA was performed. No statistical difference was detected in the mean or mode across genotypes. **(B and C)** Data are presented as mean ± SEM.

Figure 4.8

Table 4.6 Lognormal fit parameters for vessel length distribution data

Genotype	μ	σ	Mode (μm)	Mean (μm)	SD (μm)
Wild-type	3.676	0.857	18.941	56.974	3517.870
Carmeliet-tPA$^{-/-}$	3.590	0.840	17.887	51.556	2725.290
Szabo-tPA$^{-/-}$	3.614	0.846	18.160	53.076	2941.520

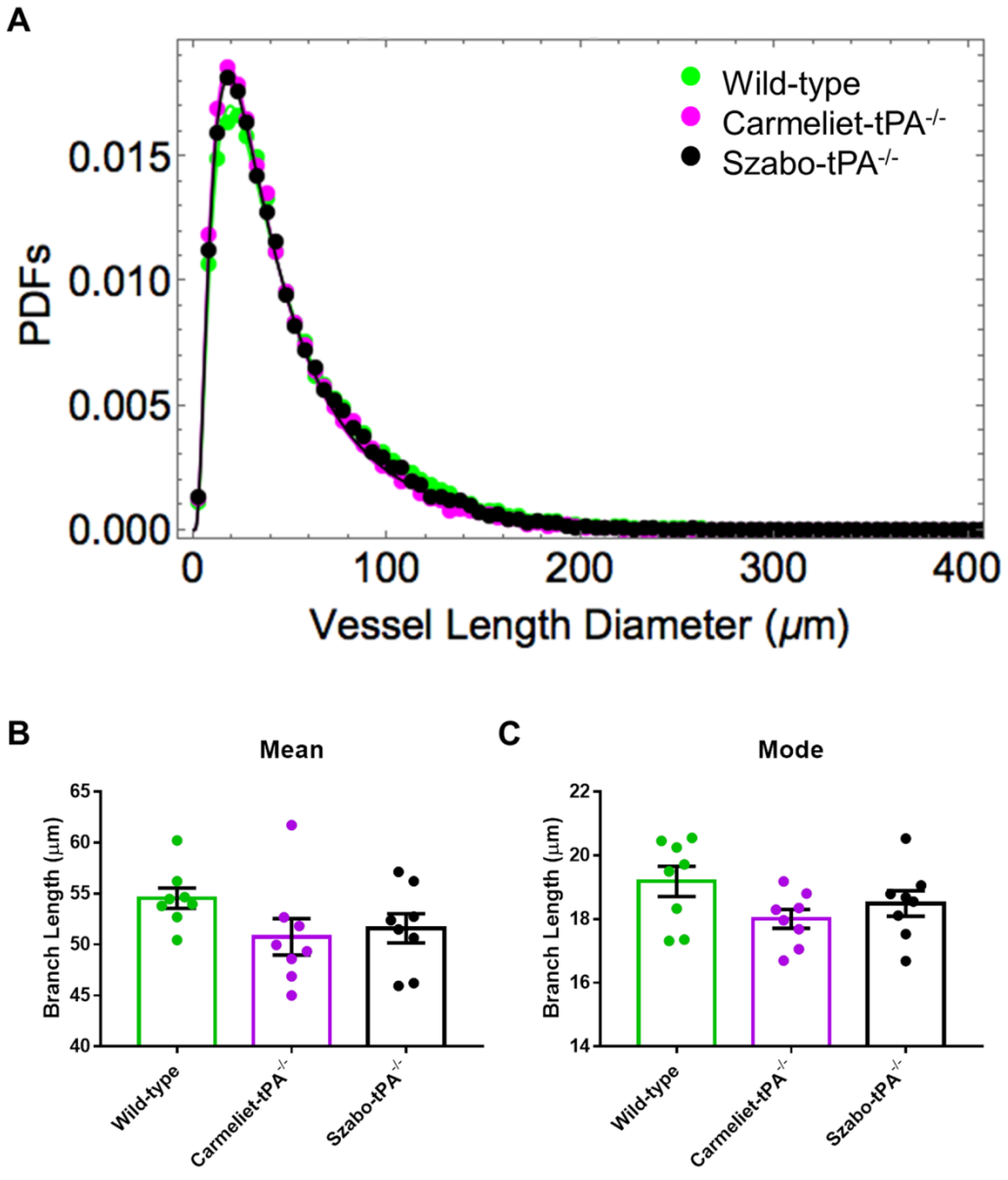

Figure 4.8. Vessel length distributions do not vary between wild-type mice and mice deficient in tPA. (A) Vessel length (µm) datasets from all samples (n = 8) per genotype were aggregated and plotted. Solid circles represent the numerical length data and the solid lines represent the lognormal fit to the length data. Lognormal fit parameters for the vessel length distribution are given in the corresponding **Table 4.6**. The mean **(B)** and mode **(C)** from the lognormal fit data for each of the samples (n = 8) was compiled per genotype and a one-way ANOVA was performed. No statistical difference was detected in the mean or mode across genotypes, though both the Carmeliet-tPA$^{-/-}$ and the Szabo-tPA$^{-/-}$ mice show a trend toward shorter branch lengths. **(B and C)** Data are presented as mean ± SEM.

Figure 4.9

Table 4.7 Parameters and correlation for the fitted joint bivariate lognormal distribution of diameter and length

Genotype	μ_D	σ_D	μ_L	σ_L	ρ_{DL}
Wild-type	1.458	0.214	3.676	0.214	-0.276
Carmeliet-tPA$^{-/-}$	1.428	0.237	3.590	0.237	-0.219
Szabo-tPA$^{-/-}$	1.448	0.231	3.614	0.231	-0.252

Table 4.8 Joint bivariate lognormal probability density function

Functional form and correlation matrix

$$p(x, y; \Sigma) \frac{e^{-\frac{(\text{Log}[y]-\mu_2)^2 \sigma_1^2 - 2\rho(\text{Log}[x]-\mu_1)(\text{Log}[y]-\mu_2)\sigma_1\sigma_2 + (\text{Log}[x]-\mu_1)^2\sigma_2^2}{2(1-\rho^2)\sigma_1^2\sigma_2^2}}}{2\pi x y \sqrt{(1-\rho^2)}}, \Sigma = \begin{pmatrix} \sigma_1^2 & \rho\sigma_1\sigma_2 \\ \rho\sigma_1\sigma_2 & \sigma_2^2 \end{pmatrix}$$

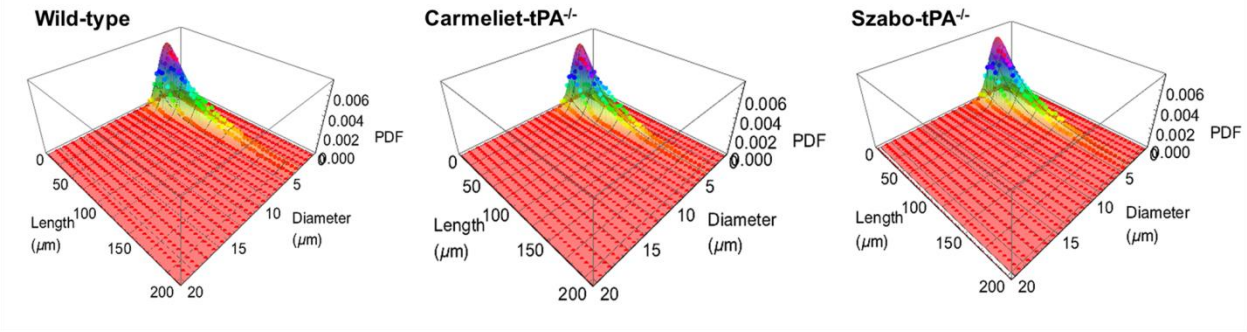

Figure 4.9. Joint probability distribution reveals vessel diameter and length to be weakly negatively correlated in the barrel cortex of wild-type mice and mice deficient in tPA. Correlated vessel diameter and length datasets from all samples (n = 8) per genotype were aggregated and plotted. Solid circles represent the correlated diameter-length numerical data and the transparent color overlay represents the lognormal fit to the diameter-length data. Lognormal fit parameters for diameter and length and the correlation for the joint bivariate lognormal probability density function are given in the corresponding **Table 4.7**. The μ and σ fit parameters for diameter and length were obtained from their respective univariate diameter and length distributions (*see Figure 4.7 for diameter and Figure 4.8 for length*). The correlation coefficient (ρ) was obtained by fitting the joint bivariate lognormal distribution to the joint bivariate numerical data. Functional form of the joint bivariate lognormal probability density function and correlation matrix (∑) is given in **Table 4.8**. For wild-type, Carmeliet-tPA$^{-/-}$ mice, and Szabo-tPA$^{-/-}$ mice a weakly negative correlation is found for diameter and length for blood vessels in the barrel cortex.

Figure 4.10

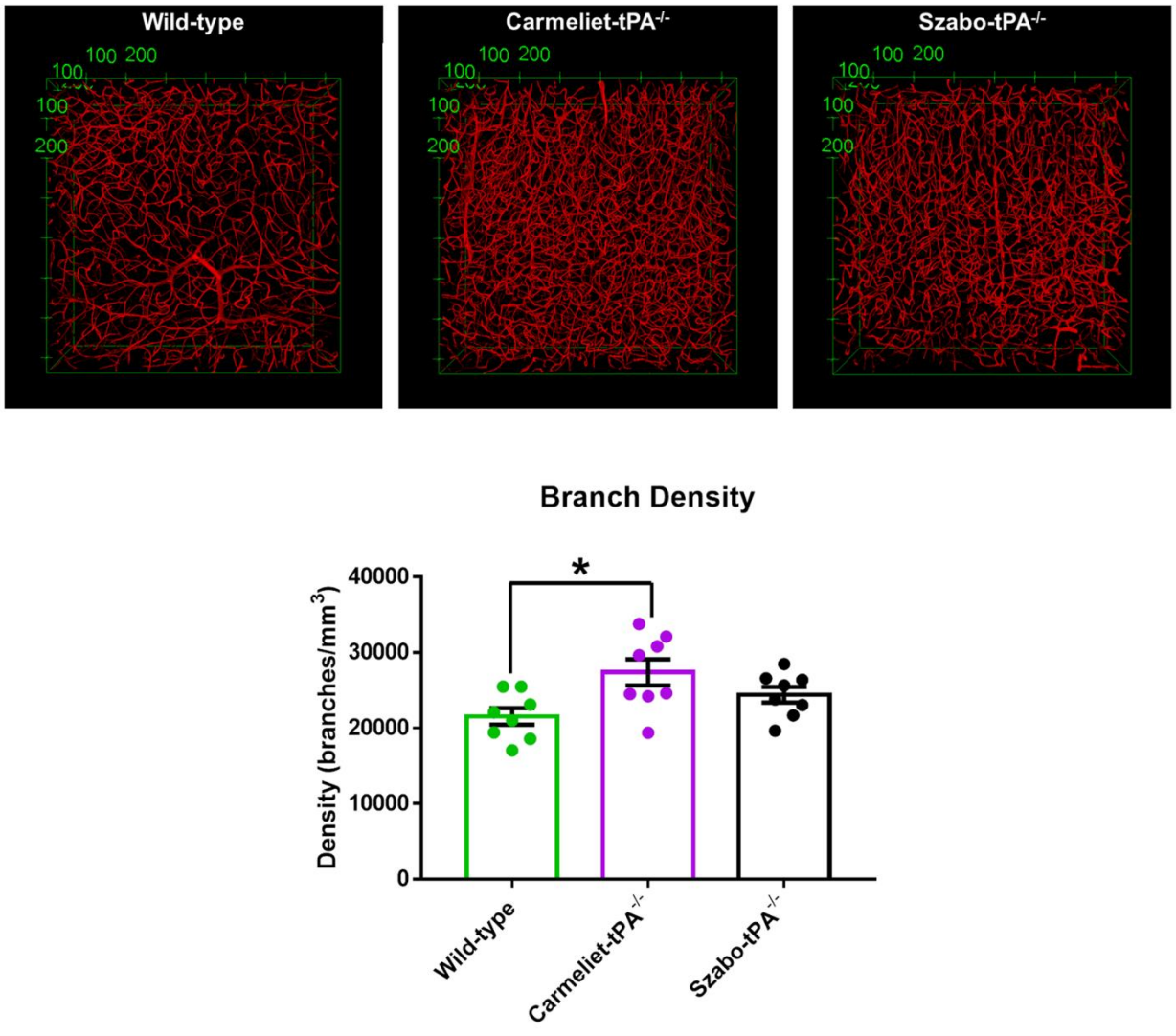
Wild-type
Carmeliet-tPA-/-
Szabo-tPA-/-
100 200
100
100
200
Branch Density
Density (branches/mm3)
40000
30000
20000
10000
0
*
Wild-type
Carmeliet-tPA-/-
Szabo-tPA-/-

Figure 4.10. Carmeliet-tPA$^{-/-}$ mice, but not Szabo-tPA$^{-/-}$ mice, have a more dense capillary bed than wild-type mice. Representative volumetric 20x images (738 µm x 738 µm x 250 µm; Δz = 1 µm) from the barrel cortex of wild-type, Carmeliet-tPA$^{-/-}$, and Szabo-tPA$^{-/-}$ mice illustrate the differences in vascular density. In the y-direction, these images comprise approximately cortical layers 1- 5. Vessel density (#/mm^3) datasets from all samples (n = 8) per genotype were aggregated and a one-way ANOVA with a Tukey's post-hoc multiple comparisons test was performed. Carmeliet-tPA$^{-/-}$ mice were found to have an increased vascular density compared to wild-type mice, but not Szabo-tPA$^{-/-}$ mice, in the barrel cortex. The increase in vascular density is largely a product of an increase in capillary density, as over ~ 98% of the vessels are less than 7 µm (*see PDF in Figure 4.7*). Data are presented as mean ± SEM. * $p < 0.05$.

Figure 4.11

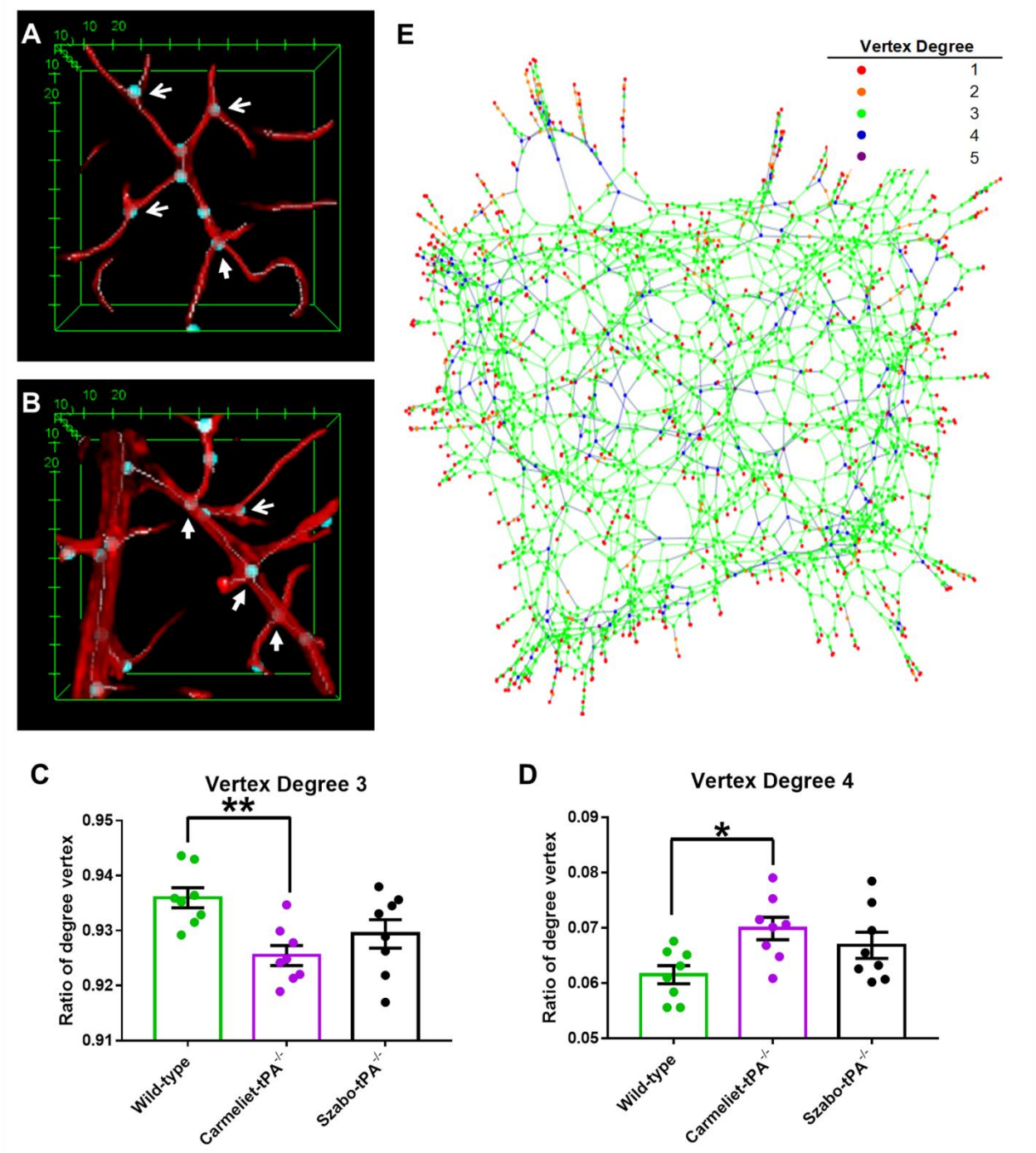
A
B
E
Vertex Degree
1
2
3
4
5
C
Vertex Degree 3
**
Ratio of degree vertex
0.95
0.94
0.93
0.92
0.91
Wild-type
Carmeliet-tPA-/-
Szabo-tPA-/-
D
Vertex Degree 4
*
Ratio of degree vertex
0.09
0.08
0.07
0.06
0.05
Wild-type
Carmeliet-tPA-/-
Szabo-tPA-/-

Figure 4.11. Vessel branching pattern differs between wild-type and Carmeliet-tPA$^{-/-}$ mice, but not Szabo-tPA$^{-/-}$ mice. (A and B) Representative 3D volumetric images illustrating vessels that branch with vertex degree 3 (open arrows) and vertex degree 4 (closed arrows). White lines represent the centerline mask and the cyan balls represent the junction points. Both smaller, capillary-sized vessels **(A)** and larger, arteriole-sized vessels **(B)** were observed to have vertices of degree 3 and 4. **(C and D)** An analysis of vessel network characteristics revealed a difference in branching pattern, with Carmeliet-tPA$^{-/-}$ mice having fewer vessels that branch with a vertex degree 3 **(C)**, but more vessels that branch with a vertex degree 4 within the same volume of cortical tissue **(D)**. The ratio of vertices with degree 3 and degree 4 was calculated by separately dividing the number of 3 degree vertices and 4 degree vertices for each sample (n = 8) per genotype by the total of 3 and 4 degree vertices. **(E)** Network graph showing connectivity of branches and vertices of degree 1 to 5. Statistics were gathered for vertices of degree 1, 2, and 5, but these vertex degrees were largely an artifact of an edge-effect from the image and not included in the analysis. A one-way ANOVA with a Tukey's post-hoc multiple comparisons test was performed and the difference in vertex degree 3 and 4 between wild-type and Carmeliet-tPA$^{-/-}$ mice was found to be significant. Data are presented as mean ± SEM. * $p < 0.05$ and ** $p < 0.005$.

Figure 4.12

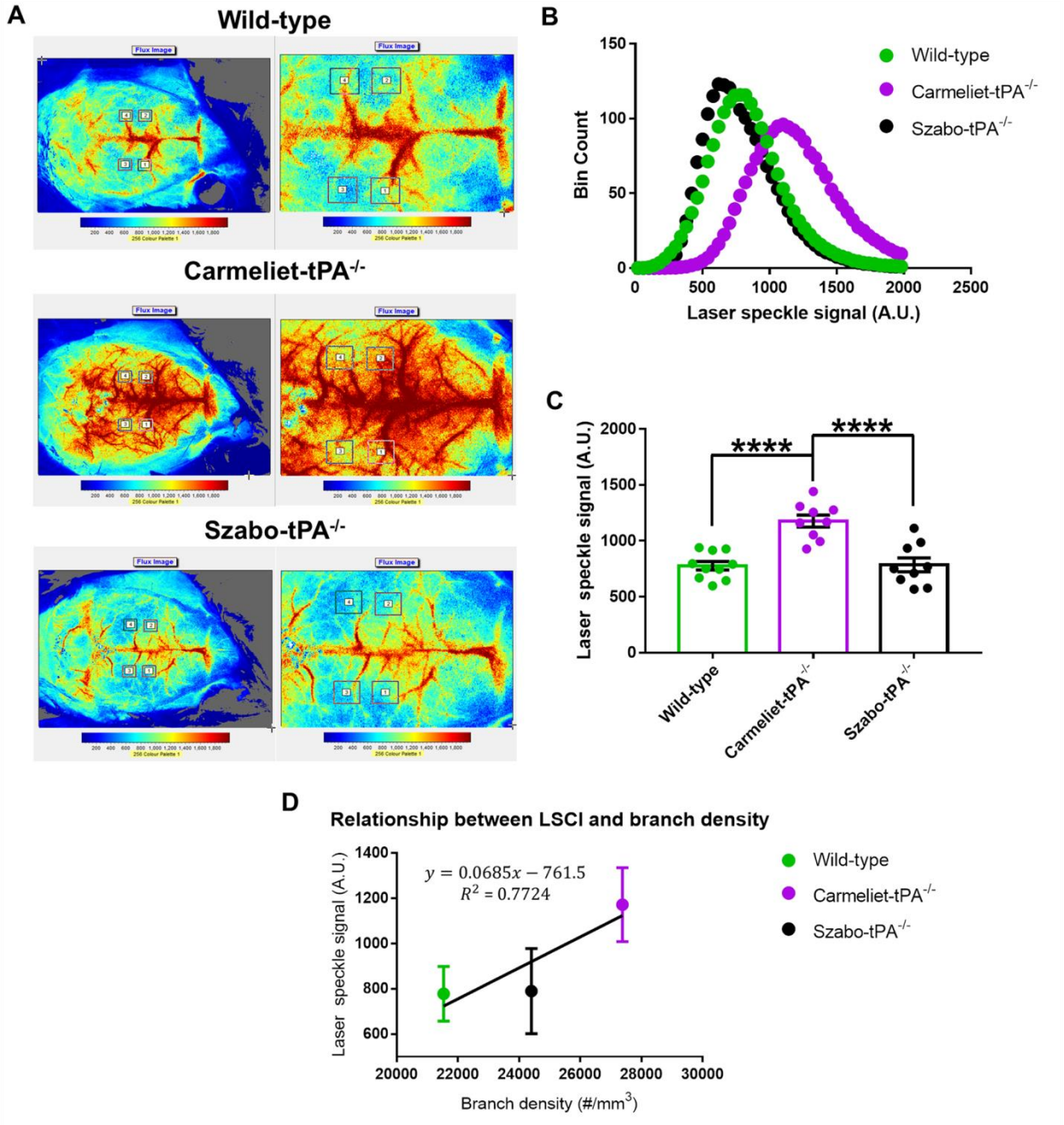
A
Wild-type
Carmeliet-tPA-/-
Szabo-tPA-/-
B
Wild-type
Carmeliet-tPA-/-
Szabo-tPA-/-
Bin Count
Laser speckle signal (A.U.)
C
Laser speckle signal (A.U.)
****
****
Wild-type
Carmeliet-tPA-/-
Szabo-tPA-/-
D
Relationship between LSCI and branch density
y = 0.0685x − 761.5
R2 = 0.7724
Laser speckle signal (A.U.)
Branch density (#/mm3)
Wild-type
Carmeliet-tPA-/-
Szabo-tPA-/-

Figure 4.12. Elevated level of basal blood flow in Carmeliet-tPA$^{-/-}$ mice correlates with increased vascular density. Laser speckle contrast imaging (LSCI) was used to characterize the baseline blood flow in wild-type (n = 10), Carmeliet-tPA$^{-/-}$ (n = 9), and Szabo-tPA$^{-/-}$ (n = 9) mice through the skull over the entire cortical surface. **(A)** Representative images of basal cerebral blood flow from each of the genotypes shows Carmeliet-tPA$^{-/-}$ mice to have a heightened level of blood flow over the cortical area not populated by large vessels. Red color-coded areas indicate high flux, while blue areas indicate low flux. Four regions of interest (1 mm^2) were selected whose midline was around bregma -0.5 and -2.0 and whose medial/lateral orientation ranged from ±1.5 to ± 2.5 to measure blood flow. These anatomical regions approximately correspond to the regions that were analyzed for vascular morphometry and density. **(B)** Histogram plot of the laser speckle intensity signal averaged from each of the four ROIs for each of the three genotypes. Wild-type, Carmeliet-tPA$^{-/-}$, and Szabo-tPA$^{-/-}$ mice each display similarly shaped distribution curves; however, the distribution curve for the Carmeliet-tPA$^{-/-}$ mice has a marked rightward shift toward higher laser speckle intensity values. **(C)** Bar graph of the mean laser speckle intensity signal averaged from each of the four ROIs per mouse for each of the three genotypes. A one-way ANOVA with a Tukey's post-hoc multiple comparisons test was performed and a statistically significant difference was found between wild-type and Carmeliet-tPA$^{-/-}$ mice and Carmeliet-tPA$^{-/-}$ and Szabo-tPA$^{-/-}$ mice, but not wild-type and Szabo-tPA$^{-/-}$ mice. **(D)** Plot of LSCI signal as a function of vessel branch density. Linear regression analysis revealed a weak linear relationship (R^2 = 0.7724) between vessel branch density and basal blood flow. Data in bar graphs are presented as mean ± SEM. Data in XY plot are presented as mean ± SD. **** $p < 0.0001$.

Chapter 5

Discussion

5.1 Summary

The work presented in this dissertation provides a detailed characterization of tPA expression in the adult murine brain, with more specific focus on tPA's cellular and subcellular localization and function in the hippocampus. Using newly generated transgenic reporter mice – PlatβGAL and tPA^{BAC}-Cer – we show that tPA is primarily trafficked away from its site of synthesis to nerve fibers in limbic and limbic-associated brain structures. This uncoupling is most apparent in the hippocampus where tPA-βGAL expression is present in the granule cell layer of the dentate gyrus, but tPA-Cer is localized to the mossy fibers, the axonal projections of the dentate granule cells. We also observed this differential expression pattern in the amygdala and globus pallidus of the basal ganglia. In an *ex vivo* slice preparation we examined the effect of tPA loss on basal synaptic transmission in the CA1 and CA3 subfields and on the propensity for the neural network in the CA3 region to develop synchronous activity. With this *ex vivo* model of "seizure-like" activity we were able to dissect the BBB component from the *in vivo* seizure phenotype and determine that the "seizure-resistance" observed in $tPA^{-/-}$ mice is likely a result of improved barrier function, not tPA's role in modulating synaptic transmission. Lastly, we extend upon previous evidence showing Carmeliet-$tPA^{-/-}$ mice to have an aberrant cerebrovascular architecture using sophisticated imaging and

analytical tools. A more rigorous examination of vascular morphometry and connectivity revealed that the increased vascular density in Carmeliet-tPA$^{-/-}$ mice is possibly a compounded result of constitutive loss of tPA and/or some strain-dependent modifier genes. Cumulatively, though, our results suggest that tPA is likely a pleiotropic mediator in the central nervous system whose actions are highly temporally and spatially compartmentalized.

5.1.1 Regional expression pattern of tPA in the adult murine brain

Early gross anatomical *in situ* analysis of tPA mRNA expression and activity suggested a disconnect between where tPA is synthesized and where it is trafficked in the adult murine brain (Sappino et al., 1993). However, this study was never followed-up by a detailed characterization of tPA expression in the mouse brain employing more advanced genetic tools and microscopic imaging analysis. Rather, studies examining a limited brain region or cell-type that expresses tPA or studies heavily dependent on *in vitro* cell cultures have been used to over-generalize about how tPA is functioning in the entirety of the central nervous system (Wu et al., 2015; Louessard et al., 2016). Accordingly, we utilized novel transgenic reporter mice – PlatβGAL and tPA^{BAC}-Cer – and high resolution confocal microscopy to address these shortcomings. With these mice we have confirmed the previously reported observation that tPA mRNA and protein are differentially expressed in the hippocampus; in addition, we demonstrate for the first time that this dichotomy exists in the amygdala and globus palidus of the basal ganglia as well. Moreover, the work presented in this thesis describes for the first time new regional localizations of tPA in the adult murine brain, including the paraventricular

nucleus of the thalamus, the periaqueductal gray, and the parabrachial nucleus. These previously unrecognized regions of tPA expression, that are primarily restricted to the limbic system or limbic-associated brain structures, will be informative in understanding how tPA is involved in modulating information flow within or between these anatomical substrates to influence brain function.

5.1.1.2 Amygdala

Previous studies have demonstrated a role for tPA in the amygdala in different models of neuronal plasticity (Koob et al., 1998; Vyas et al., 2002). Mice deficient in tPA have been found to be resistant to stress-induced anxiety (Matys and Strickland, 2003; Pawlak et al., 2003) and ethanol withdrawal seizures (Pawlak et al., 2005). In addition, in wild-type mice both an increase in anxiety following chronic restraint and ethanol withdrawal correlated with an increase in tPA activity in the centromedial amygdala, but not the basolateral amygdala. Our observation that tPA-Cer fluorescence is exclusively expressed in the centromedial nucleus of the amygdala, not the basolateral nucleus, is in agreement those results. When compared to the PlatβGAL mice, however, a more informative, though complex, picture of tPA's function in amygdala circuitry emerges. As tPA-βGAL was detected in both the basolateral and centromedial nuclei and neurons in the basolateral nucleus send projections to the centromedial nucleus, it's possible that the tPA-Cer in the centromedial nucleus is trafficked tPA from basolateral nerve projections. We also find, however, tPA-Cer fluorescence in the bed nucleus of the stria terminalis, the paraventricular nucleus of the thalamus, periaqueductal gray, and parabrachial nucleus – anatomical substrates of the centromedial amygdala (Janak and

Tye, 2015; Babaev et al., 2018). Therefore, it's also possible that the tPA-Cer in the centromedial amygdala is trafficked tPA in afferent/efferent nerve fibers to/from these brain regions. Moreover, each of these regions has been previously shown to modulate different aspects of fear and anxiety (Penzo et al., 2015; Tasan et al., 2016).

Specifically, the neuropeptide NPY is expressed in the bed nucleus of the stria terminalis, the paraventricular nucleus of the thalamus, periaqueductal gray, and parabrachial nucleus (as well as the cortex, hippocampus, basal ganglia, hypothalamus, and locus coeruleus) and it has been implicated in being an important molecule modulating neurotransmission among and between these regions (Tasan et al., 2016). Given the highly coincident expression pattern between these two peptides/proteins it's intriguing to speculate that they may be functioning to effectuate similar outcomes, though possibly through different spatial and temporal pathways. For, biophysical analysis of tPA and NPY release from adrenal chromaffin cells has shown tPA and NPY to be expressed in separate chromaffin cell subpopulations and to have different mobility and discharge rates. NPY was found to dissipate from the fusion site within ~200ms, while tPA's dissipation rate was much slower, lasting over many seconds (Weiss et al., 2014b; Weiss et al., 2014a; Bohannon et al., 2017). The physiological implications of slower discharge are unclear, though delayed release suggests that tPA may be modifying the initial signaling in some way. It may be of interest, therefore, for future studies examining tPA's expression and function in the amygdala and its associated brain regions to focus on whether or not tPA has a modulatory effect on NPY signaling.

5.1.1.3 Basal ganglia

In this dissertation we also report, for the first time, on tPA expression in the external (GPe) and internal (GPi) globus pallidus nuclei of the basal ganglia. And, similar to there being a differential expression pattern in the hippocampus and amygdala, the dichotomy between somatic tPA/β-Gal and trafficked tPA-Cer is appreciable when comparing tPA expression in the PlatβGAL and tPA^{BAC}-Cer transgenic mice. In the PlatβGAL reporter mice, β-Gal staining is present in the caudate/putamen (neostriatum) but absent in both the GPe and GPi. Contrastingly, in the tPA^{BAC}-Cer fusion mice, tPA-Cer fluorescence is absent in caudate/putamen but present in the GPe, GPi, and substantia nigra pars reticulata (SNr). The GPi and SNr are embryologically and functionally equivalent anatomical structures (Purves et al., 2001), as they are the output nuclei of the basal ganglia.

Given what is known about basal ganglia circuitry, it's likely that the observed tPA-Cer is expressed in nerve fibers that are part of the direct loop through the basal ganglia, not the indirect loop (Gilman and Newman, 2002; Jahanshahi et al., 2015). In the direct loop, GABAergic neurons from caudate/putamen project through the GPe to the GPi or through the strionigral fibers to the SNr (Purves et al., 2001). Both the GPi and SNr send GABAergic projections to the thalamus. The direct loop is known to increase thalamocortical excitation and it is important for the selection of desired behaviors.

Though there are no functional studies on how tPA may influence the output nuclei of the basal ganglia, the effects of tPA loss have been examined in the corticalstriatal pathway and in the mesolimbic dopamine system (Centonze et al., 2002;

Nagai et al., 2004). In the corticalstriatal pathway, deficits in LTP were found in $tPA^{-/-}$ mice compared to wild-type mice (Centonze et al., 2002). As dopamine treatment did not induce a membrane depolarization in striatal interneurons from $tPA^{-/-}$ mice, but previous studies had shown the necessity for dopamine in neostriatal LTP (Kerr and Wickens, 2001), it was thought that tPA was modulating dopaminergic signaling, and synaptic transmission in turn. These experiments, however, were done using a whole-cell recording configuration, not field potentials; moreover, only 9 cells from wild-type mice and 11 cells from $tPA^{-/-}$ mice were recorded from in the neostriatum (caudate/putamen). Given our tPA localization data showing no tPA-βGAL or tPA-Cer expression in caudate/putamen and the small recording sample size, these whole-cell electrophysiological experiments should be repeated using transgenic mice that enable tPA-expressing cell bodies to be identified.

Nonetheless, evidence for tPA-mediated modulation of dopaminergic signaling can be found in the ventral striatum/nucleus accumbens (Nagai et al., 2004). Morphine-induced drug dependency was used to study tPA's effects on activity-dependent synaptic plasticity in the mesolimbic dopaminergic system. Morphine is known to increase dopaminergic neurotransmission to ventral striatum by acting on μ-opioid receptors in the ventral tegmental area. Following morphine injection, wild-type mice were found to have increased mRNA and protein expression of somatic tPA in ventral striatum. This increase in tPA appears to have functional implications for the rewarding effects of morphine since $tPA^{-/-}$ mice displayed reductions in the conditioned place preference task. The conditioned place preference test measures the amount of time a mouse spends in a compartment that it associates with morphine treatment vs a

compartment that it associates with vehicle treatment. Subsequent *in vivo* microdialysis measurements revealed $tPA^{-/-}$ mice to have significantly reduced dopamine levels in ventral striatum following morphine treatment. These results suggest that tPA plays a role in regulating dopamine release and in modulating dopaminergic communication in the mesolimbic system.

We, however, do not detect tPA-βGAL in ventral striatum; and while we do find tPA-βGAL puncta in the ventral tegmental area of the midbrain, in our serial coronal sections from tPA^{BAC}-Cer mice we do not readily see any tPA-Cer puncta in the ventral tegmental area or ventral striatum. This discrepancy in tPA localization to ventral striatum may be due to the fact that all of our analysis was on basal tPA expression levels, while the study by Nagai et al. (2004) observed tPA after morphine treatment. Nonetheless, given the accumulating evidence demonstrating a role for the basal ganglia in augmenting motivational behavior (Ikemoto et al., 2015), it is intriguing to speculate that tPA from the GPe, GPi, and SNr, not ventral striatum, may be responsible for modulating the rewarding effect of morphine in wild-type mice.

5.1.2 Functional implications of tPA expression in the hippocampus

Since tPA was found to be an immediate-early gene in the hippocampus following activity-dependent events (Qian et al., 1993), it has been shown to modulate numerous neurological processes including synaptic plasticity and neurovascular coupling, as well as neurodegeneration and BBB permeability (Carroll et al., 1994; Tsirka et al., 1995; Frey et al., 1996; Huang et al., 1996; Tsirka et al., 1997; Baranes et al., 1998; Rogove et al., 1999; Yepes et al., 2003; Pang et al., 2004; Park et al., 2008;

Su et al., 2008; Su et al., 2017). Many of the functional conclusions drawn about tPA activity, however, were performed prior to a detailed description of tPA's protein localization and have not been affirmed by high-resolution, imaging analysis. This is especially confounding in the case of tPA, as we have shown that there is a differential expression pattern between where tPA is synthesized and where it is trafficked in the hippocampus, amygdala, and basal ganglia.

5.1.2.1 CA1 hippocampal subfield – basal synaptic transmission

Indeed, early electrophysiological studies on tPA's role in L-LTP in the Schaffer collateral-to-CA1 pyramidal cell pathway presumed a post-synaptic release mechanism for tPA's effects (Huang et al., 1996; Zhuo et al., 2000). These models were likely based on *in situ* mRNA expression analysis showing tPA in the CA1 to CA3 pyramidal cells (Qian et al., 1993; Sappino et al., 1993). In our tPA^{BAC}-Cer fusion reporter mouse, however, we do not detect tPA-protein in the CA1 pyramidal cells, even with GFP-Tyramide amplification, which is in agreement with what others have reported using traditional immunohistochemistry (Salles and Strickland, 2002; Louessard et al., 2016). And, while we do occasionally see cerulean puncta in stratum radiatum, the linear tract-like orientation and appearance suggest that these puncta are in axonal processes, not the distal dendritic trees of the CA1 pyramidal neurons. In keeping with this interpretation, we found tPA-positive cells in the stratum oriens/alveus lamina that share an immunocytochemical profile with somatostatin (SST)/oriens-lacunosum moleculare (O-LM) interneurons, whose cell bodies reside in stratum oriens and send axonal projections to stratum lacunosum-moleculare.

In support of our imaging studies demonstrating a limited role for tPA post-synaptic to Schaffer collaterals we found no difference in basal synaptic transmission (slope of field EPSP vs stimulus intensity) between wild-type and $tPA^{-/-}$ mice in the Schaffer collateral-to-CA1 pyramidal cell pathway. Despite not seeing a statistical difference, however, there did appear to be a difference in the shape of the I/O curves between wild-type and $tPA^{-/-}$ mice; at higher stimulus intensities the I/O curve from $tPA^{-/-}$ mice plateaued. It's possible, therefore, that in the $tPA^{-/-}$ mice there are intrinsically fewer fibers to recruit, resulting in fewer synapses and a diminished fEPSP slope. Future experiments would need to be done to investigate whether this plateau is biologically significant and, if so, if a pre- or post-synaptic mechanism is responsible.

Our results, however, do not necessarily contradict previous studies that have attributed a role for tPA in modulating L-LTP. For, while we did not detect tPA-Cer protein expression in the apical dendrites of CA1 pyramidal neurons, there is *in vitro* evidence to suggest that tPA protein can be rapidly synthesized from tPA mRNA that is present in dendrites and polyadenylated after glutamate stimulation (Shin et al., 2004). Glutamate-induced polyadenylation of tPA mRNA and tPA protein synthesis were both dependent on specific activation of the metabotropic glutamate receptor (mGluR1) type 1. In this study, glutamate was also found to stimulate the release of tPA from cultured primary hippocampal neurons. This result is in agreement with previous reports demonstrating tPA to be localized to dense-core vesicles and targeted to a regulated secretory pathway that can be rapidly activated to release tPA (Gualandris et al., 1996; Parmer et al., 1997; Lochner et al., 2008; Scalettar et al., 2012). Therefore, it's plausible

that our inability to detect tPA-Cer in CA1 pyramidal cell dendrites was due the translational regulation of tPA protein, which is kept at a low basal level.

Interestingly, we found tPA-Cer positive cells in stratum oriens to co-express mGluR1a, which is highly expressed in SST/O-LM interneurons. Though our analysis of mGluR1a expression focused on somatic localization, previous imaging studies demonstrated mGluRs to be tightly localized to a region surrounding the post-synaptic specialization (Lujan et al., 1997; Takumi et al., 1999). It is unclear if a similar mechanism of rapid mGluR-dependent tPA protein synthesis and release is occurring somatically in SST/O-LM interneurons; for, dense core granule fusion can occur at the cell body, as well as in axonal boutons and dendrites (Huang and Neher, 1996; Trueta et al., 2012). More broadly, it is also unclear why tPA appears to be differentially localized to the soma or axonal processes in the hippocampus. It's possible that inhibitory and excitatory neurons possess different molecular machinery to traffick dense core vesicles (Ramirez-Franco et al., 2016) or that the difference in hippocampal sub-regional expression (stratum oriens lamina vs stratum lucidum lamina) of tPA results in differential trafficking. Evidence for this tightly regulated, regional specification of dense core trafficking to either dendrites or axons can be found for the neuropeptide NPY (Ramamoorthy et al., 2011).

The tPA^{BAC}-Cer fusion reporter mice we generated, therefore, are not only important for answering specific questions related to how tPA is functioning in CNS physiology and pathology, these mice also provide an important tool to interrogate questions related to dense core trafficking, docking, and release. Understanding these basic biological processes at a microscopic level is important for understanding how the

brain works at a macroscopic level, for neuropeptides are critical molecules regulating a range of functions from metabolism and reproduction to behavior as well as learning and memory (Billington and Levine, 1992; Garrison et al., 2012; Borbely et al., 2013; Kormos and Gaszner, 2013; Walker and McGlone, 2013).

5.1.2.2 CA3 hippocampal subfield – basal synaptic transmission

Though the identification of tPA in a sparse population of SST/O-LM interneurons in the hippocampus is a novel finding, the most concentrated and intense tPA-Cer signal in the mouse brain is the mossy fiber pathway. As immunohistochemistry and *in situ* zymography have shown high levels of tPA in the mossy fiber pathway, the fact that we see tPA-Cer fluorescence in the mossy fibers is an important indication that the tPA-Cer protein from the BAC is being appropriately targeted. These previous studies, however, only generally described tPA expression in the mossy fiber pathway; tPA's specific compartmentalization was not examined. Taking advantage of the tPA-Cer fusion construct in this dissertation we report for the first time on tPA's subcellular localization to giant mossy fiber boutons (MFBs) in stratum lucidum of the hippocampal CA3 region. MFBs synapse with hilar mossy cells and the apical dendritic spines or "thorny excrescences" of CA3 pyramidal cells (Frotscher et al., 1994; Acsady et al., 1998). Electrophysiological studies have shown mossy fiber-to-CA3 pyramidal cell synapses to have marked paired-pulse facilitation and NMDAR-independent LTP (Salin et al., 1996; Henze et al., 2000; Toth et al., 2000; Nicoll and Schmitz, 2005).

The specific localization of tPA-Cer puncta to giant MFBs suggests that it may have a role in regulating synaptic efficacy at the mossy fiber-to-CA3 pyramidal cell

synapse. Consistent with this model, we found tPA$^{-/-}$ mice to have a decrease in basal synaptic transmission in CA3 compared to wild-type mice. And, similar to what we observed in the CA1 hippocampal subfield, there was an attenuation in the slope of the I/O curve at higher stimulation intensities. When basal synaptic transmission in *ex vivo* slices from Nsp$^{-/-}$ mice was assessed, we found Nsp$^{-/-}$ mice, like tPA$^{-/-}$ mice, to have a decreased post-synaptic response at similar stimulation intensities compared to wild-type mice. There was no significant difference between Nsp$^{-/-}$ and tPA$^{-/-}$ mice. This finding was unexpected. As Nsp is a specific inhibitor of tPA in the central nervous system (Hastings et al., 1997; Barker-Carlson et al., 2002; Fredriksson et al., 2015), it was thought that unregulated tPA activity would result in the opposite phenotype. This segregation between loss of tPA activity and enhanced tPA activity has been seen with respect to LTP, with tPA$^{-/-}$ mice showing deficits in LTP and tPA overexpressing mice showing enhancements (Huang et al., 1996; Baranes et al., 1998; Madani et al., 1999). Though further experiments are needed to address the underlying mechanisms for these deficits, we can think of a few plausible explanations: 1) Even though Nsp is expressed in CA3 pyramidal cells, it is not targeted to the CA3 dendrites to act locally and inhibit tPA activity; or 2) Nsp and tPA may modulate synaptic transmission at the mossy fiber-to-CA3 synapse through independent pathways. Nsp in the CA3 pyramidal cells may affect synaptic transmission post-synaptically, while tPA in the mossy fibers may affect synaptic transmission pre-synaptically.

5.1.2.3 CA3 hippocampal subfield – synchronous activity

Though $Nsp^{-/-}$ and $tPA^{-/-}$ mice do not display any differences in basal synaptic transmission at the mossy fiber-to-CA3 synapse they do have differences in their propensity to develop synchronous activity. A no Mg^{2+}/high K^{+} model was used to assess synchronous or "seizure-like" activity in *ex vivo* hippocampal brain slices. With this approach, we were able to dissect the BBB component from the *in vivo* seizure phenotype observed in "seizure-prone" $Nsp^{-/-}$ mice and "seizure-resistant" $tPA^{-/-}$ mice. Despite having similar I/O curves, in all the temporal parameters we measured in our model (latency to synchronous activity, frequency of events, and inter-event interval), brain slices from $tPA^{-/-}$ mice were more hyperexcitable than $Nsp^{-/-}$ mice. This *ex vivo* phenotype is opposed to the *in vivo* phenotype observed for both $tPA^{-/-}$ and $Nsp^{-/-}$ mice. The average amplitude of high-frequency bursting events, however, did not segregate by genotype like the temporal synchronous activity parameters. For both $tPA^{-/-}$ and $Nsp^{-/-}$ mice, average amplitude of events were smaller compared to wild-type mice, which is consistent with basal synaptic transmission being decreased in both $Nps^{-/-}$ and $tPA^{-/-}$ mice. These results suggest that there are different mechanisms governing the synaptic strength vs latency to/frequency of firing in $tPA^{-/-}$ and $Nsp^{-/-}$ mice. They also indicate that there might be differences in the neuronal network outside the mossy fiber-to-CA3 synapse that are altering the development and rate of synchronous activity in $tPA^{-/-}$ and $Nsp^{-/-}$ mice. Moreover, when placed in the context of our *in vivo* data showing a correlation between latency to seizure activity and BBB permeability, these *ex vivo* results indirectly support a model whereby tPA-mediated control of vascular integrity dictates seizure progression.

5.1.3 Cerebrovascular morphometry and network connectivity

In addition to tPA's role in regulating BBB permeability, a role for parenchymal brain tPA in mediating physiological vascular responses has been observed. In neurovascular coupling experiments, tPA$^{-/-}$ mice were found to have an attenuated functional hyperemia response compared to wild-type mice (Park et al., 2008). Recently, though, tPA$^{-/-}$ mice were shown to harbor "passenger mutations" from the original 129/Sv embryonic stem (ES) cells flanking the tPA gene (Szabo et al., 2016) and to have developmental differences in cerebrovascular and cerebroventricular morphometry and molecular composition (Stefanitsch et al., 2015). It is unclear if some strain-modifying genes from the remnant 129/Sv DNA or some developmental difference from constitutive loss of tPA are responsible for the aberrant cerebrovascular architecture. Moreover, it is unclear how the cerebrovascular architecture might be influencing blood flow at rest and in response to a neural stimulus. To help begin to address these questions, we undertook a more extensive analysis of vessel morphometry and network connectivity in wild-type mice and in both the Carmeliet-tPA$^{-/-}$ mice and Szabo-tPA$^{-/-}$ mice. Understanding how these parameters influence blood flow has implications beyond basic science research, as an aberrant vasculature has been observed in mouse models of Alzheimer's disease and diminished blood flow has been found to precede cognitive decline in Alzheimer's patients (Ruitenberg et al., 2005; Meyer et al., 2008; Bennett et al., 2018).

In this dissertation, our analysis of the vasculature in wild-type, Carmeliet-tPA$^{-/-}$, and Szabo-tPA$^{-/-}$ confirms that the vascular capillary density in the barrel cortex of Carmeliet-tPA$^{-/-}$ mice is significantly increased compared to wild-type. While the

capillary density in Szabo-tPA$^{-/-}$ mice trends upward, it was not statistically different than wild-type or Carmeliet-tPA$^{-/-}$ mice. Moreover, the trend that we observed in Carmeliet-tPA$^{-/-}$ mice toward a decrease in blood vessel length is consistent with blood vessels branching more frequently, giving rise to a dense capillary bed. Compared to wild-type mice, Carmeliet-tPA$^{-/-}$ mice also have significantly fewer vessels that branch with vertex degree 3 (~1% decrease), but significantly more vessels that branch with vertex degree 4 (~1% increase), given the same volume of cortical tissue. It is unclear, though, if this difference in vertex degree is biologically significant.

We also noticed from the joint bivariate lognormal distribution of correlated diameter and length that vessel diameter and length are weakly, negatively correlated. Though we initially thought that vessel diameter and length would be positively correlated, the inverse relationship that we observe for correlated diameter and length can be found in Poiseuille's Law. Poiseuille's Law is a physical law that models steady-state conductance flow in a cylindrical tube. Poiseuille showed that flow (Q) is linearly related to a change in pressure (P) across the length (l) of a tube of radius (r) through its conductance (G) by:

$$Q = G\,P; \quad G = \left(\frac{\pi\, r^4}{8\,\mu_a\, l}\right),$$

where μ_a is the apparent viscosity. Our negatively correlated vessel diameter and length data, therefore, are in agreement with the expression for flow conductance that Poiseuille experimentally derived over 175 years ago.

Though we didn't find there to be a difference in the correlated diameters and lengths between genotypes, of the various vasculature characteristics that we did examine, the most striking was vascular density. Moreover, when we used laser speckle contrast imaging (LSCI) to measure basal cerebral blood flow in the cortical surface of wild-type, Carmeliet-tPA$^{-/-}$, and Szabo-tPA$^{-/-}$ mice, there appeared to be a correlation in the laser speckle signal and vascular density. Mice with less dense capillary beds – wild-type and Szabo-tPA$^{-/-}$ mice – had lower levels of speckle signal, while the Carmeliet-tPA$^{-/-}$ mice with the denser capillary bed and the highest speckle intensity signal. Linear regression analysis revealed there to be a slight linear correlation between vascular density and the intensity of the laser speckle signal. While further studies still need to be performed using littermate controls for the Carmeliet-tPA$^{-/-}$ mice, these results don't discount the possibility that the reported functional hyperemia deficits in Carmeliet-tPA$^{-/-}$ mice might be the result of an altered vasculature morphometry and architecture.

5.2 Limitations and future directions

Though the work we present in this dissertation substantively advances our understanding of tPA's localization and function in the central nervous system, this research is not without limitations. In addition, our findings raise further questions that necessitate future experiments. The following is an attempt to summarize where improvements can be made and where the direction of this research should head.

5.2.1 Determining the regional connectivity of tPA-expressing brain regions

Though our side-by-side analysis of PlatβGAL and tPA^{BAC}-Cer transgenic reporter mice provides a more informative profile of tPA localization in the adult murine brain, future experiments are needed to interrogate many of the putative anatomical connections that we propose for regions expressing tPA. To more directly determine if the tPA-Cer we detect in the centromedial nucleus of the amygdala is from axonal projections in the basolateral nucleus, a neurotoxic agent could be injected into the basolateral nucleus (Maren, 1999). If tPA-Cer expression decreases in the centromedial nucleus, this would suggest that the tPA-Cer protein is being trafficked from the basolateral nucleus. Similarly, to test if the tPA-Cer we see in the GPe, GPi, and SNr is coming from axonal projections in caudate/putamen, neurotoxic lesions can be made in caudate/putamen (Guevara et al., 2002) and changes in cerulean fluorescence can be assessed in the GPe, GPi, and SNr. Unilateral injections of the neurotoxic agent into either the basolateral amygdala or caudate/putamen would also allow for the contralateral side to be used as a paired control of changes in tPA-Cer fluorescence.

5.2.2 Generating cell-type specific conditional tPA knockout mice

While the $tPA^{-/-}$ mice have been an indispensable tool to study tPA's physiological and pathological functions *in vivo*, these global knockout mice are not without their disadvantages and shortcomings. Though initial anatomical analysis of $tPA^{-/-}$ mice did not uncover any gross abnormalities (Carmeliet et al., 1994; Frey et al., 1996; Huang et al., 1996), subsequent studies have found $tPA^{-/-}$ mice to have a cerebrovascular and cerebroventricular developmental phenotype (Wang et al., 2011;

Stefanitsch et al., 2015). In addition to these confounding developmental variables, the original tPA$^{-/-}$ mice have remnant 129/Sv ES cell DNA (Szabo et al., 2016). Recognizing the influence of strain (Flurkey et al., 2009), new tPA$^{-/-}$ mice were generated using zinc-finger nucleases. Importantly, these mice are on a pure C57BL/6J background and they do not have any of the “passenger mutations” found in the original tPA$^{-/-}$ mice (Szabo et al., 2016).

However, these Szabo-tPA$^{-/-}$ mice do not help to address possible compensatory changes (Kreiner, 2015) in neuronal function that arise from constitutive loss of tPA. We cannot account for more subtle, even localized changes in protein expression, neuronal/glial patterning, and network connectivity that may be altered with global, embryonic deletion of tPA. Indeed, it is still unclear how a denser capillary network and enlarged cerebroventricles could be affecting physiological functions in the adult mouse, let alone neural and/or glial development. As such, in order to investigate the acute loss of tPA in distinct brain structures on synaptic physiology and behavior, a cell-type specific conditional knock-out mouse is needed.

Cell-type specific conditional deletion of tPA in certain brain structures can be accomplished by delivering an adeno-associated viral vector containing a Cre recombinase (Rohlmann et al., 1996) that is driven by a neuronal specific promoter, like calcium/calmodulin-dependent protein kinase II α (CaMKIIα), to transgenic mice that have the second exon of tPA gene flanked by LoxP sites (Stefanelli et al., 2016; Todd et al., 2018). An even more informative transgenic mouse strategy would be to engineer a transgenic mouse whose reporter gene expression is dependent on Cre-mediated excision of the tPA gene (Schnutgen et al., 2003; Schnutgen et al., 2005). These mice

would not only allow for site- and time-specific conditional ablation of the tPA gene, but they would permit the visualization and monitoring of cells that no longer express tPA. Specifically, for example, with these mice an electrophysiological profile of tPA-expressing neurons could be generated, as could a regional map of tPA's physical and functional connectivity.

5.2.3 Determining the role of tPA in amygdala- and basal ganglia-associated brain structures

With these transgenic mice, a CaMKII-Cre virus can be separately injected into the centromedial amygdala, periaqueductal gray, parabrachial nucleus, or the paraventricular nucleus of the thalamus, and the contribution of tPA activity in/from each of these regions to amygdala function can be independently assessed. As the periaqueductal gray (Deng et al., 2016), the parabrachial nucleus (Sato et al., 2015), and the paraventricular nucleus of the thalamus (Bhatnagar et al., 2003) have all been reported to play a role in stress and fear, it would be informative to understand the individual role, or collective role, tPA from these regions may be playing in amygdala function.

One way for amygdala function to be examined is through behavioral paradigms that involve fear learning. Previous groups have performed fear conditioning experiments on $tPA^{-/-}$ mice, but the results have been variable. One group reported no difference in percent time freezing in the context (unconditioned stimulus; US) or tone (conditioned stimulus; CS) test between male wild-type and $tPA^{-/-}$, but when female wild-type and $tPA^{-/-}$ mice were analyzed, female $tPA^{-/-}$ mice had an enhanced freezing

response to both the US and CS (Huang et al., 1996). Another group, however, found male tPA$^{-/-}$ mice to have an attenuated freezing response to the US, but an enhanced freezing response to the CS (Calabresi et al., 2000). Wild-type mice in these experiments, however, did not appear to learn to associate the tone with the unconditioned stimulus, so it is difficult to make comparative statements about the effect of tPA in these studies. In addition, for both of these studies the genetic background of the tPA$^{-/-}$ mice is not reported. Since strain differences have been observed in fear conditioning (Temme et al., 2014), it is important to repeat these experiments with the appropriate controls.

While behavioral assessments of tPA$^{-/-}$ mice in fear conditioning experiments have been variable across labs, mice deficient in tPA have been consistently found to have deficits in active or passive avoidance tasks (Huang et al., 1996; Calabresi et al., 2000; Pawlak et al., 2002). These data suggest that tPA$^{-/-}$ mice have deficits in acquisition or working memory to aversive or associative learning. Given the behavioral data demonstrating tPA$^{-/-}$ mice to have diminished stress-induced anxiety (Pawlak et al., 2003; Matys et al., 2004), however, the impairments observed in tPA$^{-/-}$ mice in avoidance tasks might be due to tPA's effects on stress-induced neuronal plasticity in the amygdala (Bennur et al., 2007) and not any effect of tPA on hippocampal-dependent learning and memory. Future studies, therefore, that employ task-independent stressors to test learning and memory (Moore et al., 2013) would be informative in discriminating between tPA's role in stress versus learning and memory.

Active avoidance tasks have also been shown to depend on striatal (caudate/putamen) (Vecsei and Beal, 1991) and dopaminergic signaling in the

mesolimbic and nigrostriatal pathway (Koob et al., 1984). Given our recent data demonstrating tPA-Cer expression in the basal ganglia and earlier studies showing $tPA^{-/-}$ mice to have decreased dopamine levels and dopamine receptor expression (Centonze et al., 2002; Nagai et al., 2004), specific deletion of tPA from the globus palldius followed by behavioral analysis in active avoidance tasks would be informative in determining if pallidal tPA has a role in the observed deficits in active avoidance.

5.2.4 Determining tPA's role in hippocampal synaptic plasticity

Neuronal specific deletion of tPA in the hippocampus would also be important for following-up on the differences in basal synaptic transmission that we observed in the mossy fiber-to-CA3 pathway. Given that the attenuation in the I/O curve at higher stimulus intensities in $tPA^{-/-}$ mice in both the CA1 and CA3 region might have been due to a developmental decrease in fiber number or synapses, a cell-type specific conditional knock-out of tPA would allow us circumvent that putative experimental confounder and directly test the effect of acute tPA loss. If we are able to confirm that there is a decrease in basal synaptic transmission in these conditional $tPA^{-/-}$ mice, then further experiments dissecting whether tPA is acting pre- or post-synaptically would be beneficial in elucidating its mechanism of action. It's important to keep in mind, though, that tPA is stored in dense core vesicles (DCV) (Lochner et al., 2008; Scalettar et al., 2012), not synaptic vesicles, and that traditional experimental paradigms used to assess pre- or post-synaptic determinants of synaptic strength might need to be adjusted to what is known about the release properties of DCVs (Voets et al., 1999).

5.2.5 Dissecting the molecular machinery of dense core vesicle trafficking and release

Indeed, there is still much we don't know about DCV trafficking and release (Nurrish, 2014). Moreover, what we do know is derived from studies using primary neuroendocrine cells or PC12 cells, which are an immortalized cell line from the pheochromocytoma of a rat adrenal medulla (Hoover et al., 2014). Therefore, the tPA^{BAC}-Cer transgenic fusion reporter mice are an ideal tool to study basic DCV neurobiology. Instead of neuroendocrine and adrenal gland cells, tPA^{BAC}-Cer mice can be used to study the molecular machinery that targets DCVs to axons vs dendrites or that is crucial for DCV priming and docking in primary neuronal cultures. For example, live-cell imaging can be used to follow tPA-Cer puncta as it is trafficked; and given that we see tPA-Cer in giant mossy fiber boutons *in vivo*, and not *en passant* or filipodial extensions, these experiments can help inform about the machinery and signaling pathways that regulate tPA's spatial distribution (Bharat et al., 2017). More specific questions about tPA release in neurons could also be addressed. Does tPA release from neurons have the same release kinetics as tPA from adrenal chromaffin cells (Weiss et al., 2014b; Weiss et al., 2014a)? If not, what is causing the difference? What might be the physiological reason and implications? The tPA^{BAC}-Cer transgenic mice will be a useful *in vitro* tool for addressing these, and other, questions.

5.2.6 Chronic vs acute effect of tPA loss on vasculogenesis and angiogenesis

As our data suggest that there may be a strain-independent effect of tPA on vascular density, it is important to determine if this effect is from acute or chronic loss of tPA, and if tPA is either directly or indirectly affecting vasculogenesis (*de novo*) or

angiogenesis (from a pre-existing vessel), or both. A conditional global tPA knockout mouse - tPA^{CreERT} - ($tPA^{flox/flox}$ mouse crossed with a tamoxifen inducible Cre transgenic mouse (Metzger and Chambon, 2001; Feil et al., 2009) would be informative in differentiating between these potential mechanisms. Accordingly, vascular density, along with other vascular morphometry and network connectivity characters, can be assessed in adult mouse models of acute tPA (tPA^{CreERT}) and chronic tPA (Szabo-$tPA^{-/-}$) loss. In addition, it would be important to examine these vascular characteristics at earlier time-points. If changes in vascular density and/or other parameters are observed during early embryonic development in Szabo-$tPA^{-/-}$ mice, it would suggest that tPA is either directly (or indirectly through compensatory changes) involved in vasculogenesis. Conversely, if changes in vascular density and/or other parameters are observed in adult Szabo-$tPA^{-/-}$ mice, than these data would support a model where tPA has more of a role in angiogenesis.

5.2.7 Controlling for environmental factors with littermate controls

In addition to the importance of controlling for strain, it is important to control for environment as well. This is especially true for vascular patterning as differences in cerebral angiogenesis have been reported in the barrel, auditory, and motor cortices of mice exposed to chronic stimulation from whisker tickle, noise, or motor activity (Whiteus et al., 2014). Using littermate controls help to mitigate some of the variability within the same genotypic cohort (Holmdahl and Malissen, 2012). In our analysis of vascular morphometry and connectivity, the Szabo-$tPA^{-/-}$ mice were compared with their wild-type littermate controls. However, the Carmeliet-$tPA^{-/-}$ mice, though analyzed at the

same time, they were not compared with their respective wild-type littermate controls. Therefore, these experiments need to be repeated with the appropriate controls.

5.2.8 Gathering vessel morphometry statistics on smooth-muscle covered vessel

Though our method of collecting vascular morphometry statistics is more informative than traditional immunofluorescence techniques, it is limited in its ability to differentiate between arteries and arterioles and veins and venuoles. Being able to distinguish between these blood vessel types is important since a difference in the numerical diameter distribution for smooth-muscle covered vessels between wild-type and Carmeliet-tPA$^{-/-}$ mice was reported by Stefanitsch et al. (2015). Therefore, future experiments should involve wild-type and tPA deficient mice that have been crossed with transgenic mice expressing a fluorescent protein in smooth muscle cells (Armstrong et al., 2010). While we didn't detect a difference in the diameter of all blood vessels between these genotypes, it's possible that differences in the diameter and number of smooth-muscle covered vessels exist. As smooth-muscle covered arterioles have been shown to be critical regulators of blood flow, integrating neural activity with the proportional functional hyperemia response (Hill et al., 2015), it is important to determine if this population of blood vessels is different in wild-type, Carmeliet-tPA$^{-/-}$, and Szabo-tPA$^{-/-}$ mice using more sophisticated analytical tools.

5.2.9 Modeling blood flow

With the vascular data we have gathered we can begin to address questions beyond how tPA may or may not be functioning to alter the vascular architecture. By

taking a modeling approach, for example, we can incorporate our vascular morphometry statistics and network connectivity data to assess how changes in the vasculature affect blood flow. There is some correlative evidence to suggest that an altered vascular morphology has functional implications for blood flow regulation. In models of Alzheimer's disease, mice are reported to have an altered vascular morphology and 3D architecture (Meyer et al., 2008; Bennett et al., 2018), and in the clinical setting, patients with Alzheimer's disease present with hypoperfusion (Ruitenberg et al., 2005). The data we have gathered on vessel diameter and length, vascular density, and branching vertex degree, therefore, will be critical for establishing a vascular network, and for laying the groundwork for a statistical modeling approach to calculate blood flow, given a model for the flow resistance of each branch.

5.3 Concluding remarks

In summary, in this dissertation we provide a primer on the regional, cellular, and subcellular localization of tPA in the central nervous system. These data are important for informing our understanding of tPA function, especially given the differential expression pattern we observe for tPA in the hippocampus, amygdala, basal ganglia, and associated brain structures, demonstrating that tPA can act far from its site of synthesis. In particular, we examined the effect of tPA loss in the mossy fiber pathway of the hippocampus and found $tPA^{-/-}$ mice to have significant deficits in basal synaptic transmission and to be more hyperexcitable than $Nsp^{-/-}$ mice. This *ex vivo* synchronous-activity "seizure-like" phenotype for $tPA^{-/-}$ and $Nsp^{-/-}$ mice is opposed to the *in vivo* seizure phenotype for both genotypes. Therefore, while tPA may be playing a role in

modulating synaptic transmission, *in vivo*, the more dominant role for tPA appears to be in BBB regulation. Lastly, in our extensive analysis of vascular morphometry and network connectivity we find that the increased vascular density in Carmeliet-tPA$^{-/-}$ mice may be due to some additive effect of strain-dependent modifier genes and constitutive loss of tPA. Cumulatively, this dissertation provides evidence for tPA being a pleiotropic mediator in the central nervous system whose actions are highly temporally and spatially restricted. Moreover, the genetic mouse models and analytical tools we developed will not only help answer basic science questions related to tPA and DCV neurobiology, but they can be translated to the clinical realm to further our understanding of how the cerebrovasculature affects blood flow and the pathology of neurodegenerative diseases, like Alzheimer.

References

Acsady L, Kamondi A, Sik A, Freund T, Buzsaki G (1998) GABAergic cells are the major postsynaptic targets of mossy fibers in the rat hippocampus. J Neurosci 18:3386-3403.

Armstrong JJ, Larina IV, Dickinson ME, Zimmer WE, Hirschi KK (2010) Characterization of bacterial artificial chromosome transgenic mice expressing mCherry fluorescent protein substituted for the murine smooth muscle alpha-actin gene. Genesis 48:457-463.

Babaev O, Piletti Chatain C, Krueger-Burg D (2018) Inhibition in the amygdala anxiety circuitry. Exp Mol Med 50:18.

Baranes D, Lederfein D, Huang YY, Chen M, Bailey CH, Kandel ER (1998) Tissue plasminogen activator contributes to the late phase of LTP and to synaptic growth in the hippocampal mossy fiber pathway. Neuron 21:813-825.

Barker-Carlson K, Lawrence DA, Schwartz BS (2002) Acyl-enzyme complexes between tissue-type plasminogen activator and neuroserpin are short-lived in vitro. J Biol Chem 277:46852-46857.

Bennett RE, Robbins AB, Hu M, Cao X, Betensky RA, Clark T, Das S, Hyman BT (2018) Tau induces blood vessel abnormalities and angiogenesis-related gene expression in P301L transgenic mice and human Alzheimer's disease. Proc Natl Acad Sci U S A 115:E1289-E1298.

Bennur S, Shankaranarayana Rao BS, Pawlak R, Strickland S, McEwen BS, Chattarji S (2007) Stress-induced spine loss in the medial amygdala is mediated by tissue-plasminogen activator. Neuroscience 144:8-16.

Bharat V, Siebrecht M, Burk K, Ahmed S, Reissner C, Kohansal-Nodehi M, Steubler V, Zweckstetter M, Ting JT, Dean C (2017) Capture of Dense Core Vesicles at Synapses by JNK-Dependent Phosphorylation of Synaptotagmin-4. Cell Rep 21:2118-2133.

Bhatnagar S, Huber R, Lazar E, Pych L, Vining C (2003) Chronic stress alters behavior in the conditioned defensive burying test: role of the posterior paraventricular thalamus. Pharmacol Biochem Behav 76:343-349.

Billington CJ, Levine AS (1992) Hypothalamic neuropeptide Y regulation of feeding and energy metabolism. Curr Opin Neurobiol 2:847-851.

Bohannon KP, Bittner MA, Lawrence DA, Axelrod D, Holz RW (2017) Slow fusion pore expansion creates a unique reaction chamber for co-packaged cargo. J Gen Physiol 149:921-934.

Borbely E, Scheich B, Helyes Z (2013) Neuropeptides in learning and memory. Neuropeptides 47:439-450.

Calabresi P, Napolitano M, Centonze D, Marfia GA, Gubellini P, Teule MA, Berretta N, Bernardi G, Frati L, Tolu M, Gulino A (2000) Tissue plasminogen activator controls multiple forms of synaptic plasticity and memory. Eur J Neurosci 12:1002-1012.

Carmeliet P, Schoonjans L, Kieckens L, Ream B, Degen J, Bronson R, De Vos R, van den Oord JJ, Collen D, Mulligan RC (1994) Physiological consequences of loss of plasminogen activator gene function in mice. Nature 368:419-424.

Carroll PM, Tsirka SE, Richards WG, Frohman MA, Strickland S (1994) The mouse tissue plasminogen activator gene 5' flanking region directs appropriate expression in development and a seizure-enhanced response in the CNS. Development 120:3173-3183.

Centonze D, Napolitano M, Saulle E, Gubellini P, Picconi B, Martorana A, Pisani A, Gulino A, Bernardi G, Calabresi P (2002) Tissue plasminogen activator is required for corticostriatal long-term potentiation. Eur J Neurosci 16:713-721.

Deng H, Xiao X, Wang Z (2016) Periaqueductal Gray Neuronal Activities Underlie Different Aspects of Defensive Behaviors. J Neurosci 36:7580-7588.

Feil S, Valtcheva N, Feil R (2009) Inducible Cre mice. Methods Mol Biol 530:343-363.

Flurkey K, Currer JM, Leiter EH, Witham B (2009) The Jackson Laboratory Handbook on Genetically Standardized Mice, Sixth Edition, Sixth Edition Edition. Bar Harbor, ME 04609 USA: The Jackson Laboratory.

Fredriksson L, Stevenson TK, Su EJ, Ragsdale M, Moore S, Craciun S, Schielke GP, Murphy GG, Lawrence DA (2015) Identification of a neurovascular signaling pathway regulating seizures in mice. Ann Clin Transl Neurol 2:722-738.

Frey U, Muller M, Kuhl D (1996) A different form of long-lasting potentiation revealed in tissue plasminogen activator mutant mice. J Neurosci 16:2057-2063.

Frotscher M, Soriano E, Misgeld U (1994) Divergence of hippocampal mossy fibers. Synapse 16:148-160.

Garrison JL, Macosko EZ, Bernstein S, Pokala N, Albrecht DR, Bargmann CI (2012) Oxytocin/vasopressin-related peptides have an ancient role in reproductive behavior. Science 338:540-543.

Gilman S, Newman S (2002) Manter and Gatz's Essentials of Clinical Neuroanatomy and Neurophysiology, 10th edition Edition. Philadelphia, PA: F.A. Davis Company.

Gualandris A, Jones TE, Strickland S, Tsirka SE (1996) Membrane depolarization induces calcium-dependent secretion of tissue plasminogen activator. J Neurosci 16:2220-2225.

Guevara BH, Torrico F, Hoffmann IS, Cubeddu LX (2002) Lesion of caudate-putamen interneurons with kainic acid alters dopamine and serotonin metabolism in the olfactory tubercle of the rat. Cell Mol Neurobiol 22:835-844.

Hastings GA, Coleman TA, Haudenschild CC, Stefansson S, Smith EP, Barthlow R, Cherry S, Sandkvist M, Lawrence DA (1997) Neuroserpin, a brain-associated inhibitor of tissue plasminogen activator is localized primarily in neurons. Implications for the regulation of motor learning and neuronal survival. J Biol Chem 272:33062-33067.

Henze DA, Urban NN, Barrionuevo G (2000) The multifarious hippocampal mossy fiber pathway: a review. Neuroscience 98:407-427.

Hill RA, Tong L, Yuan P, Murikinati S, Gupta S, Grutzendler J (2015) Regional Blood Flow in the Normal and Ischemic Brain Is Controlled by Arteriolar Smooth Muscle Cell Contractility and Not by Capillary Pericytes. Neuron 87:95-110.

Holmdahl R, Malissen B (2012) The need for littermate controls. Eur J Immunol 42:45-47.

Hoover CM, Edwards SL, Yu SC, Kittelmann M, Richmond JE, Eimer S, Yorks RM, Miller KG (2014) A novel CaM kinase II pathway controls the location of neuropeptide release from Caenorhabditis elegans motor neurons. Genetics 196:745-765.

Huang LY, Neher E (1996) Ca(2+)-dependent exocytosis in the somata of dorsal root ganglion neurons. Neuron 17:135-145.

Huang YY, Bach ME, Lipp HP, Zhuo M, Wolfer DP, Hawkins RD, Schoonjans L, Kandel ER, Godfraind JM, Mulligan R, Collen D, Carmeliet P (1996) Mice lacking the gene encoding tissue-type plasminogen activator show a selective interference with late-phase long-term potentiation in both Schaffer collateral and mossy fiber pathways. Proc Natl Acad Sci U S A 93:8699-8704.

Ikemoto S, Yang C, Tan A (2015) Basal ganglia circuit loops, dopamine and motivation: A review and enquiry. Behav Brain Res 290:17-31.

Jahanshahi M, Obeso I, Rothwell JC, Obeso JA (2015) A fronto-striato-subthalamic-pallidal network for goal-directed and habitual inhibition. Nat Rev Neurosci 16:719-732.

Janak PH, Tye KM (2015) From circuits to behaviour in the amygdala. Nature 517:284-292.

Kerr JN, Wickens JR (2001) Dopamine D-1/D-5 receptor activation is required for long-term potentiation in the rat neostriatum in vitro. J Neurophysiol 85:117-124.

Koob GF, Simon H, Herman JP, Le Moal M (1984) Neuroleptic-like disruption of the conditioned avoidance response requires destruction of both the mesolimbic and nigrostriatal dopamine systems. Brain Res 303:319-329.

Koob GF, Roberts AJ, Schulteis G, Parsons LH, Heyser CJ, Hyytia P, Merlo-Pich E, Weiss F (1998) Neurocircuitry targets in ethanol reward and dependence. Alcohol Clin Exp Res 22:3-9.

Kormos V, Gaszner B (2013) Role of neuropeptides in anxiety, stress, and depression: from animals to humans. Neuropeptides 47:401-419.

Kreiner G (2015) Compensatory mechanisms in genetic models of neurodegeneration: are the mice better than humans? Frontiers in cellular neuroscience 9:56.

Lochner JE, Spangler E, Chavarha M, Jacobs C, McAllister K, Schuttner LC, Scalettar BA (2008) Efficient copackaging and cotransport yields postsynaptic colocalization of neuromodulators associated with synaptic plasticity. Dev Neurobiol 68:1243-1256.

Louessard M, Lacroix A, Martineau M, Mondielli G, Montagne A, Lesept F, Lambolez B, Cauli B, Mothet JP, Vivien D, Maubert E (2016) Tissue Plasminogen Activator Expression Is Restricted to Subsets of Excitatory Pyramidal Glutamatergic Neurons. Mol Neurobiol 53:5000-5012.

Lujan R, Roberts JD, Shigemoto R, Ohishi H, Somogyi P (1997) Differential plasma membrane distribution of metabotropic glutamate receptors mGluR1 alpha, mGluR2 and mGluR5, relative to neurotransmitter release sites. J Chem Neuroanat 13:219-241.

Madani R, Hulo S, Toni N, Madani H, Steimer T, Muller D, Vassalli JD (1999) Enhanced hippocampal long-term potentiation and learning by increased neuronal expression of tissue-type plasminogen activator in transgenic mice. EMBO J 18:3007-3012.

Maren S (1999) Neurotoxic basolateral amygdala lesions impair learning and memory but not the performance of conditional fear in rats. J Neurosci 19:8696-8703.

Matys T, Strickland S (2003) Tissue plasminogen activator and NMDA receptor cleavage. Nat Med 9:371-372; author reply 372-373.

Matys T, Pawlak R, Matys E, Pavlides C, McEwen BS, Strickland S (2004) Tissue plasminogen activator promotes the effects of corticotropin-releasing factor on the amygdala and anxiety-like behavior. Proc Natl Acad Sci U S A 101:16345-16350.

Metzger D, Chambon P (2001) Site- and time-specific gene targeting in the mouse. Methods 24:71-80.

Meyer EP, Ulmann-Schuler A, Staufenbiel M, Krucker T (2008) Altered morphology and 3D architecture of brain vasculature in a mouse model for Alzheimer's disease. Proc Natl Acad Sci U S A 105:3587-3592.

Moore SJ, Deshpande K, Stinnett GS, Seasholtz AF, Murphy GG (2013) Conversion of short-term to long-term memory in the novel object recognition paradigm. Neurobiol Learn Mem 105:174-185.

Nagai T, Yamada K, Yoshimura M, Ishikawa K, Miyamoto Y, Hashimoto K, Noda Y, Nitta A, Nabeshima T (2004) The tissue plasminogen activator-plasmin system participates in the rewarding effect of morphine by regulating dopamine release. Proc Natl Acad Sci U S A 101:3650-3655.

Nicoll RA, Schmitz D (2005) Synaptic plasticity at hippocampal mossy fibre synapses. Nat Rev Neurosci 6:863-876.

Nurrish S (2014) Dense core vesicle release: controlling the where as well as the when. Genetics 196:601-604.

Pang PT, Teng HK, Zaitsev E, Woo NT, Sakata K, Zhen S, Teng KK, Yung WH, Hempstead BL, Lu B (2004) Cleavage of proBDNF by tPA/plasmin is essential for long-term hippocampal plasticity. Science 306:487-491.

Park L, Gallo EF, Anrather J, Wang G, Norris EH, Paul J, Strickland S, Iadecola C (2008) Key role of tissue plasminogen activator in neurovascular coupling. Proc Natl Acad Sci U S A 105:1073-1078.

Parmer RJ, Mahata M, Mahata S, Sebald MT, O'Connor DT, Miles LA (1997) Tissue plasminogen activator (t-PA) is targeted to the regulated secretory pathway. Catecholamine storage vesicles as a reservoir for the rapid release of t-PA. J Biol Chem 272:1976-1982.

Pawlak R, Magarinos AM, Melchor J, McEwen B, Strickland S (2003) Tissue plasminogen activator in the amygdala is critical for stress-induced anxiety-like behavior. Nat Neurosci 6:168-174.

Pawlak R, Melchor JP, Matys T, Skrzypiec AE, Strickland S (2005) Ethanol-withdrawal seizures are controlled by tissue plasminogen activator via modulation of NR2B-containing NMDA receptors. Proc Natl Acad Sci U S A 102:443-448.

Pawlak R, Nagai N, Urano T, Napiorkowska-Pawlak D, Ihara H, Takada Y, Collen D, Takada A (2002) Rapid, specific and active site-catalyzed effect of tissue-plasminogen activator on hippocampus-dependent learning in mice. Neuroscience 113:995-1001.

Penzo MA, Robert V, Tucciarone J, De Bundel D, Wang M, Van Aelst L, Darvas M, Parada LF, Palmiter RD, He M, Huang ZJ, Li B (2015) The paraventricular thalamus controls a central amygdala fear circuit. Nature 519:455-459.

Purves D, Augustine G, Fitzpatrick D, Katz L, LaMantia A, McNamara J, Williams S (2001) Modulation of movement by the basal ganglia, 2nd edition Edition. Sunderland, MA: : Sinauer Associates.

Qian Z, Gilbert ME, Colicos MA, Kandel ER, Kuhl D (1993) Tissue-plasminogen activator is induced as an immediate-early gene during seizure, kindling and long-term potentiation. Nature 361:453-457.

Ramamoorthy P, Wang Q, Whim MD (2011) Cell type-dependent trafficking of neuropeptide Y-containing dense core granules in CNS neurons. J Neurosci 31:14783-14788.

Ramirez-Franco JJ, Munoz-Cuevas FJ, Lujan R, Jurado S (2016) Excitatory and Inhibitory Neurons in the Hippocampus Exhibit Molecularly Distinct Large Dense Core Vesicles. Frontiers in cellular neuroscience 10:202.

Rogove AD, Siao C, Keyt B, Strickland S, Tsirka SE (1999) Activation of microglia reveals a non-proteolytic cytokine function for tissue plasminogen activator in the central nervous system. J Cell Sci 112 (Pt 22):4007-4016.

Rohlmann A, Gotthardt M, Willnow TE, Hammer RE, Herz J (1996) Sustained somatic gene inactivation by viral transfer of Cre recombinase. Nat Biotechnol 14:1562-1565.

Ruitenberg A, den Heijer T, Bakker SL, van Swieten JC, Koudstaal PJ, Hofman A, Breteler MM (2005) Cerebral hypoperfusion and clinical onset of dementia: the Rotterdam Study. Ann Neurol 57:789-794.

Salin PA, Scanziani M, Malenka RC, Nicoll RA (1996) Distinct short-term plasticity at two excitatory synapses in the hippocampus. Proc Natl Acad Sci U S A 93:13304-13309.

Salles FJ, Strickland S (2002) Localization and regulation of the tissue plasminogen activator-plasmin system in the hippocampus. J Neurosci 22:2125-2134.

Sappino AP, Madani R, Huarte J, Belin D, Kiss JZ, Wohlwend A, Vassalli JD (1993) Extracellular proteolysis in the adult murine brain. J Clin Invest 92:679-685.

Sato M, Ito M, Nagase M, Sugimura YK, Takahashi Y, Watabe AM, Kato F (2015) The lateral parabrachial nucleus is actively involved in the acquisition of fear memory in mice. Mol Brain 8:22.

Scalettar BA, Jacobs C, Fulwiler A, Prahl L, Simon A, Hilken L, Lochner JE (2012) Hindered submicron mobility and long-term storage of presynaptic dense-core granules revealed by single-particle tracking. Dev Neurobiol 72:1181-1195.

Schnutgen F, Doerflinger N, Calleja C, Wendling O, Chambon P, Ghyselinck NB (2003) A directional strategy for monitoring Cre-mediated recombination at the cellular level in the mouse. Nat Biotechnol 21:562-565.

Schnutgen F, De-Zolt S, Van Sloun P, Hollatz M, Floss T, Hansen J, Altschmied J, Seisenberger C, Ghyselinck NB, Ruiz P, Chambon P, Wurst W, von Melchner H (2005) Genomewide production of multipurpose alleles for the functional analysis of the mouse genome. Proc Natl Acad Sci U S A 102:7221-7226.

Shin CY, Kundel M, Wells DG (2004) Rapid, activity-induced increase in tissue plasminogen activator is mediated by metabotropic glutamate receptor-dependent mRNA translation. J Neurosci 24:9425-9433.

Stefanelli T, Bertollini C, Luscher C, Muller D, Mendez P (2016) Hippocampal Somatostatin Interneurons Control the Size of Neuronal Memory Ensembles. Neuron 89:1074-1085.

Stefanitsch C, Lawrence AL, Olverling A, Nilsson I, Fredriksson L (2015) tPA Deficiency in Mice Leads to Rearrangement in the Cerebrovascular Tree and Cerebroventricular Malformations. Frontiers in cellular neuroscience 9:456.

Su EJ, Fredriksson L, Geyer M, Folestad E, Cale J, Andrae J, Gao Y, Pietras K, Mann K, Yepes M, Strickland DK, Betsholtz C, Eriksson U, Lawrence DA (2008) Activation of PDGF-CC by tissue plasminogen activator impairs blood-brain barrier integrity during ischemic stroke. Nat Med 14:731-737.

Su EJ, Cao C, Fredriksson L, Nilsson I, Stefanitsch C, Stevenson TK, Zhao J, Ragsdale M, Sun YY, Yepes M, Kuan CY, Eriksson U, Strickland DK, Lawrence DA, Zhang L (2017) Microglial-mediated PDGF-CC activation increases cerebrovascular permeability during ischemic stroke. Acta Neuropathol 134:585-604.

Szabo R, Samson AL, Lawrence DA, Medcalf RL, Bugge TH (2016) Passenger mutations and aberrant gene expression in congenic tissue plasminogen activator-deficient mouse strains. J Thromb Haemost 14:1618-1628.

Takumi Y, Ramirez-Leon V, Laake P, Rinvik E, Ottersen OP (1999) Different modes of expression of AMPA and NMDA receptors in hippocampal synapses. Nat Neurosci 2:618-624.

Tasan RO, Verma D, Wood J, Lach G, Hormer B, de Lima TC, Herzog H, Sperk G (2016) The role of Neuropeptide Y in fear conditioning and extinction. Neuropeptides 55:111-126.

Temme SJ, Bell RZ, Pahumi R, Murphy GG (2014) Comparison of inbred mouse substrains reveals segregation of maladaptive fear phenotypes. Front Behav Neurosci 8:282.

Todd WD, Fenselau H, Wang JL, Zhang R, Machado NL, Venner A, Broadhurst RY, Kaur S, Lynagh T, Olson DP, Lowell BB, Fuller PM, Saper CB (2018) A hypothalamic circuit for the circadian control of aggression. Nat Neurosci 21:717-724.

Toth K, Suares G, Lawrence JJ, Philips-Tansey E, McBain CJ (2000) Differential mechanisms of transmission at three types of mossy fiber synapse. J Neurosci 20:8279-8289.

Trueta C, Kuffler DP, De-Miguel FF (2012) Cycling of dense core vesicles involved in somatic exocytosis of serotonin by leech neurons. Front Physiol 3:175.

Tsirka SE, Gualandris A, Amaral DG, Strickland S (1995) Excitotoxin-induced neuronal degeneration and seizure are mediated by tissue plasminogen activator. Nature 377:340-344.

Tsirka SE, Rogove AD, Bugge TH, Degen JL, Strickland S (1997) An extracellular proteolytic cascade promotes neuronal degeneration in the mouse hippocampus. J Neurosci 17:543-552.

Vecsei L, Beal MF (1991) Comparative behavioral and neurochemical studies with striatal kainic acid- or quinolinic acid-lesioned rats. Pharmacol Biochem Behav 39:473-478.

Voets T, Neher E, Moser T (1999) Mechanisms underlying phasic and sustained secretion in chromaffin cells from mouse adrenal slices. Neuron 23:607-615.

Vyas A, Mitra R, Shankaranarayana Rao BS, Chattarji S (2002) Chronic stress induces contrasting patterns of dendritic remodeling in hippocampal and amygdaloid neurons. J Neurosci 22:6810-6818.

Walker SC, McGlone FP (2013) The social brain: neurobiological basis of affiliative behaviours and psychological well-being. Neuropeptides 47:379-393.

Wang TW, Zhang H, Gyetko MR, Parent JM (2011) Hepatocyte growth factor acts as a mitogen and chemoattractant for postnatal subventricular zone-olfactory bulb neurogenesis. Mol Cell Neurosci 48:38-50.

Weiss AN, Bittner MA, Holz RW, Axelrod D (2014a) Protein mobility within secretory granules. Biophys J 107:16-25.

Weiss AN, Anantharam A, Bittner MA, Axelrod D, Holz RW (2014b) Lumenal protein within secretory granules affects fusion pore expansion. Biophys J 107:26-33.

Whiteus C, Freitas C, Grutzendler J (2014) Perturbed neural activity disrupts cerebral angiogenesis during a postnatal critical period. Nature 505:407-411.

Wu F, Torre E, Cuellar-Giraldo D, Cheng L, Yi H, Bichler EK, Garcia PS, Yepes M (2015) Tissue-type plasminogen activator triggers the synaptic vesicle cycle in cerebral cortical neurons. J Cereb Blood Flow Metab 35:1966-1976.

Yepes M, Sandkvist M, Moore EG, Bugge TH, Strickland DK, Lawrence DA (2003) Tissue-type plasminogen activator induces opening of the blood-brain barrier via the LDL receptor-related protein. J Clin Invest 112:1533-1540.

Zhuo M, Holtzman DM, Li Y, Osaka H, DeMaro J, Jacquin M, Bu G (2000) Role of tissue plasminogen activator receptor LRP in hippocampal long-term potentiation. J Neurosci 20:542-549.